

**AN EVALUATION OF WIND ENERGY POTENTIAL FOR
POWER GENERATION IN MOZAMBIQUE**

by

JONAS NOMBORA ZUCULE

Submitted in fulfillment of the requirement for the degree of Master of Science in the School of
Environmental Sciences

University of KwaZulu-Natal

Durban, 2012

ABSTRACT

Wind energy is a continuous, clean source of energy that can be harnessed for electricity generation or water pumping. The geographic location of Mozambique, and the long coastline renders the country a good wind energy potential that could potentially be exploited for water pumping or electrical power systems that have social and economic benefits and thereby contribute to a reduction in unsustainable practices of wood biomass burning which is the main source of energy in rural villages and high density suburbs of the main cities of the country.

This study is focused on evaluating the potential of harnessing wind energy for electrical power generation in Mozambique using the Wind Atlas Analysis and Application Programme (WA^sP) model. The study characterises wind speed patterns and wind frequency distributions at selected meteorological stations based on hourly observations, and models the available wind energy in coastal and interior areas. Meteorological parameters such as wind speed data from nearby meteorological stations and wind turbine characteristics were used as inputs into the model. To effectively harness wind energy, mean annual wind speeds should at least be 3 ms^{-1} . For this reason only sites satisfying this criterion were selected. The spatial selection criteria considered a fair distribution of candidate sites such that coastal areas of the southern, northern and the interior Niassa and Nampula provinces were covered.

The results of the WA^sP model simulations, indicate that there is sufficient wind energy resource in both interior and coastal areas, which varies with height a.g.l., and that can be exploited for pumping water and generating electricity in small or medium electrical power systems, particularly the coastal areas of Ponta de Ouro, Mavelane, and Tofinho where the mean annual wind speed is above 5.0 ms^{-1} at the 10 m level and about 8.0 ms^{-1} at the highest levels (50 - 60 m a.g.l.) and interior area of Lichinga (mean annual wind speed of about 6 ms^{-1} at the same highest levels). The lowest wind energy potential (mean annual wind speed of about 4.0 ms^{-1}) is found in the Nampula area.

Dedication

To my family, Ermelinda S. Chambe and Suchy A. Zucule, for your tireless and endless love. You are my inspiration.

Preface

The whole thesis, unless specifically indicated to the contrary in the text, is the researcher's own work, and has not been submitted in part, or as a whole, to any other University. The research work was carried out in the School of Environmental Sciences, University of KwaZulu-Natal, under the supervision of Professor Roseanne Diab over the period 2009 to 2010.

Signature

Supervisor:.....

Date:

Student:

Date:

DECLARATION OF PLAGIARISM

I, declare that

1. The reaserch reported in this thesis, except where otherwise indicated, is my original research.
2. This thesis has not been submitted for any degree or examination at any other university.
3. This thesis does not contain other persons' data, picture graphs or other information, unless specifically acknowledged as being sourced from other persons.
4. This thesis does not contain other persons' writing unless specifically acknowleged as being sourced from other researchers. Where other written sources have been quoted, then:
 - a Their words have been re-written but the general information attributed to them has been referenced;
 - b Where their exact words have been used, then their writing has been placed in italics and inside quotation marks, and referenced.
5. This thesis does not contain text, graphs or tables copied and pasted from the Internet, unless specifically acknowledged, with the source being detailed in the thesis and in the References sections.

Signed:

Acknowledgements

My appreciation for the successful completion of this research project goes first to my supervisor Professor Roseanne Diab for her candid and consistent encouragement, comments, suggestions and assistance throughout the process of my research. My appreciation also goes to Professor Fethi Ahmed, for his encouragement, suggestions and direction during the research process. Their guidance and input have shaped my academic skills in the research field.

To the Swedish International Development Agency (SIDA) funding programme goes my appreciation for supporting all my studies.

My gratitude also to the Eduardo Mondlane University, particularly Professor Boaventura C. Cuamba, for the opportunity given to me to be part of the Energy Science and Technology Research Program in Mozambique (ESTRP). I am also academically indebted to the Director of the National Institute of Meteorology for his encouragement and for giving me an opportunity to realize a dream.

My appreciation is also extended to Anuradha Mohan, James White from Vestas A/S, Linda Sloka and Tom Lambert from Mistaya Engineering Inc., Berit C. Larsen from Risø DTU and Mike Childs from Global Mapper Software LLC for their technical support so that the data analysis and modelling could be performed successfully.

To my friends and colleagues at the National Institute of Meteorology, Eduardo Mondlane University and the School of Environmental Sciences, University of KwaZulu-Natal, in particular Daniel M., Gilbeto M., Herminio T., Marcelino M., Célia A., Manuel M., Elmah M., Zola I., Geoffrey S., Liphaletsa K., and Solomon T. for their

friendship and willingness to share their skills with me, which was the stepping-stone for my success in this project.

TABLE OF CONTENTS

CHAPTER ONE: INTRODUCTION	1
1.1 Background to the study	1
1.2 Problem statement	3
1.3 Rationale for the study	4
1.4 Aim and objectives of the study	5
1.5 The study areas	6
1.5.1 Location	6
1.5.2 Topography	7
1.5.3 Climate	11
1.5.4 Population	14
1.5.5 Electricity access	15
1.6 Structure of the thesis	19
1.7 Summary	19
CHAPTER TWO: LITERATURE REVIEW	20
2.1 Introduction	20
2.2 Wind as a source of energy	20
2.3 The available and extractable energy from the wind	23
2.4 The wind and energy potential prediction models	26
2.5 The effect of topography, surface roughness on the wind speed	30
2.5.1 The effect of the terrain	30
2.5.2 The effect of surface roughness	31
2.5.3 The effect of obstacles	35
2.5.4 The effect of local winds	37

2.6	Numerical modelling of wind energy	37
2.6.1	Background to the WA ^s P model.....	40
2.6.3	Application of WA ^s P model in wind energy assessment	51
2.7	Summary.....	52
CHAPTER THREE: DATA AND RESEARCH METHODOLOGY		54
3.1	Data.....	54
3.1.1	Introduction	54
3.1.2	Wind data and data quality.....	54
3.1.3	Wind observations.....	60
3.1.4	Meteorological station selection criteria for modelling.....	63
3.1.5	Summary	63
3.2	Research methodology	64
3.2.1	Introduction	64
3.2.2	Technique of wind energy assessment	64
3.2.3	Summary	71
CHAPTER FOUR: RESULTS AND DISCUSSION.....		73
4.1	Introduction	73
4.2	Results for Mavelane	74
4.2.1	Observed wind data.....	74
4.2.2	Wind atlas data at Mavalane	75
4.2.3	Predicted wind climate for the Mavalane area	77
4.2.4	Wind resource maps	83
4.3	Results for Ponta de Ouro.....	84
4.3.1	Observed wind data.....	84
4.3.2	Wind atlas data at Ponta de Ouro	85
4.3.3	Predicted wind climate for the Ponta de Ouro area.....	87

4.3.4	Wind resource maps	92
4.4	Results for Tofinho	94
4.4.1	Observed wind data	94
4.4.2	Wind atlas data at Tofinho	95
4.4.3	Predicted wind climate for the Tofinho area	97
4.4.4	Wind resource maps	101
4.5	Results for Vilankulo	102
4.5.1	Observed wind data	102
4.5.2	Wind atlas data at Vilankulo	104
4.5.3	Predicted wind climate for the Vilankulo area	105
4.5.4	Wind resource maps	110
4.6	Results for Pemba	113
4.6.1	Observed wind data	113
4.6.2	Wind atlas data at Pemba	114
4.6.3	Predicted wind climate for the Pemba area	116
4.6.4	Wind resource maps	121
4.7	Results for Nampula	122
4.7.1	Observed wind data	122
4.7.2	Wind atlas data at Nampula	124
4.7.3	Predicted wind climate for the Nampula area	125
4.7.4	Wind resource maps	130
4.8	Results for Lichinga	133
4.8.1	Observed wind data	133
4.8.2	Wind atlas data at Lichinga	134
4.8.3	Predicted wind climate for the Lichinga area	136
4.8.4	Wind resource maps	141
4.9	General discussion	143

4.10	Summary.....	145
CHAPTER FIVE: CONCLUSION		146
5.1	Summary.....	146
5.2	Limitations of the study	147
5.3	Recommendations	147
REFERENCES		150
APPENDICES		160
APPENDIX A	Roughness length and terrain surface characteristics used for modelling...	161
APPENDIX B	Coordinates of the meteorological station and predicted sites	162
APPENDIX C	Obstacle description	163
APPENDIX D	Roughness description.....	166
APPENDIX E	The wind speed and Weibull-k frequency distribution	171

LIST OF FIGURES

1. 1:	Map showing provinces of Mozambique.	6
1. 2:	Digital elevation model representing the topography of the study areas.	8
1. 3:	Topography of Mozambique	10
1. 4a:	The climatic zones.	12
1. 5:	The mean and extreme position of the ITCZ over Southern Africa.	13
1. 6:	Inhabitants per square kilometer.	15
1. 7:	The EDM power transmission lines throughout the country.	18
2. 1:	Ideal air flow through a wind turbine.	24
2. 2:	Acceleration of air flow over a hill.	31
2. 3:	The atmospheric boundary layer shear profile.	31
2. 4:	The surface roughness and the change of wind speed with height.	32
2. 5:	The effect of trees and buildings on the air flow.	36
2. 6:	The wind atlas methodology.	43
2. 7:	Ideal flow with a change of roughness class with the height.	44
3. 1:	Geographic location of stations collecting wind data.	57
3. 2a:	Anemography and anemometer.	57
3. 3:	Mean diurnal wind speeds for Class 1 meteorological stations.	61
3. 4:	Mean monthly wind speeds for Class 1 meteorological stations.	62
3. 5:	A schematic representation of the WA ^S P modeling methodology.	66
3. 6:	A typical Google Earth image used for roughness classification.	67
3. 7:	A typical Google Earth image used for obstacles collection.	68
3. 8:	The Vestas V52 power curve.	69

4. 1:	Observed wind rose and wind speed frequency distribution at Mavalane.	74
4. 2:	Wind speed frequency distribution and speed by sector at Mavalane.....	75
4. 3:	Regional wind climate of Mavalane meteorological station.	77
4. 4:	Map showing the location of the turbine sites in the Mavalane area.	78
4. 5:	Predicted mean wind speed and available wind energy in the Mavalane area.....	79
4. 6:	Predicted wind rose and speed frequency distribution in the Mavalane area.....	80
4. 7:	Predicted wind speed frequency distribution in the Mavalane area.	81
4. 8:	The extractable wind energy in the Mavalane area.	81
4. 9:	Extractable wind energy by azimuth sector at site 2 in the Mavalane area.....	82
4. 10:	Extractable energy rose and frequency distribution in the Mavalane area.....	82
4. 11:	Wind and energy resource maps in the Mavalane area.	83
4. 12:	Observed wind rose and speed frequency distribution at Ponta de Ouro	84
4. 13:	Wind speed frequency distribution and speed by sector at Ponta de Ouro.	85
4. 14:	Regional wind climate of Ponta de Ouro meteorological station.....	86
4. 15:	Map showing the location of the turbine sites in the Ponta de Ouro area.	87
4. 16:	Predicted mean wind speed and available wind energy in the Ponta de Ouro area.	88
4. 17:	Predicted wind rose and speed frequency distribution in the Ponta de Ouro area.	89
4. 18:	Predicted wind speed frequency distribution in the Ponta de Ouro area.....	89
4. 19:	The extractable wind energy in the Ponta de Ouro area.....	90
4. 20:	Extractable average wind energy by azimuth sector in the Ponta de Ouro area.	91
4. 21:	Extractable energy rose and frequency distribution in the Ponta de Ouro area.	91
4. 22:	Wind speed resource map in the Ponta de Ouro area.....	92
4. 23:	Wind energy resource map in the Ponta de Ouro area.	93
4. 24:	Observed wind rose and wind speed frequency distribution at Tofinho	94

4. 25: Wind speed frequency distribution speed by sector at Tofinho.	95
4. 26: Regional wind climate of Tofinho meteorological station.	96
4. 27: Map showing the location of the turbine sites in the Tofinho area.	97
4. 28: Predicted mean wind speed and available wind energy in the Tifinho area.....	98
4. 29: Predicted wind rose and speed frequency distribution in the Tofinho area.....	99
4. 30: Predicted wind speed frequency distribution in the Tofinho area.	99
4. 31: The extractable wind energy in the Tofinho area.	100
4. 32: Extractable average wind energy by azimuth sector in the Tofinho area.....	101
4. 33: Extractable energy rose and frequency distribution in the Tofinho area.....	101
4. 34: Wind speed and energy resource maps in the Tofinho area.	102
4. 35: Observed wind rose and wind speed frequency distribution at Vilankulo.	103
4. 36: Wind speed frequency distribution and speed by sector at Vilankulo.	103
4. 37: Regional wind climate of Vilankulo meteorological station.	105
4. 38: Map showing the location of the potential turbine sites in the Vilankulo area.	106
4. 39: Predicted mean wind speed and available wind energy in the Vilankulo area.....	107
4. 40: Predicted wind rose and speed frequency distribution in the Vilankulo area.	108
4. 41: Predicted wind speed frequency distribution in the Vilankulo area.	108
4. 42: The extractable wind energy at potential turbine sites in the Vilankulo area.....	109
4. 43: Extractable average wind energy by azimuth sector in the Vilankulo area.....	110
4. 44: Extractable energy rose and frequency distribution in the Vilankulo area.....	110
4. 45: Wind speed resource map in the Vilankulo area.	111
4. 46: Wind energy resource map in the Vilankulo area.	112
4. 47: Observed wind rose and wind speed frequency distribution at Pemba.	113
4. 48: Wind speed frequency distribution and wind speed by sector at Pemba.....	114

4. 49: Regional wind climate of Pemba meteorological station.	115
4. 50: Map showing the location of the potential turbine sites in the Pemba area.	116
4. 51: Predicted mean wind speed and available wind energy in the Pemba area.	117
4. 52: Predicted wind rose and speed frequency distribution in the Pemba area.	118
4. 53: Predicted wind speed frequency distribution in the Pemba area.	119
4. 54: The extractable wind energy at three potential turbine sites in the Pemba area.	119
4. 55: Extractable average wind energy by azimuth sector in the Pemba area.	120
4. 56: Extractable energy rose and frequency distribution in the Pemba area.	120
4. 57: Wind speed resource map in the Pemba area.	121
4. 58: Wind energy resource map in the Pemba area.	122
4. 59: Observed wind rose and wind speed frequency distribution at Nampula.	123
4. 60: Wind speed frequency distribution and speed by sector at Nampula.	123
4. 61: Regional wind climate of Nampula meteorological station.	125
4. 62: Map showing the location of the potential turbine sites in the Nampula area.	126
4. 63: Predicted mean wind speed and available wind energy in the Nampula area.	127
4. 64: Predicted wind rose and speed frequency distribution in the Nampula area.	128
4. 65: Predicted wind speed frequency distribution in the Nampula area.	128
4. 66: The extractable wind energy at potential turbine sites in the Nampula area.	129
4. 67: Extractable average wind energy by azimuth sector in the Nampula area.	130
4. 68: Extractable energy rose and frequency distribution in the Nampula area.	130
4. 69: Wind speed resource map in the Nampula area.	131
4. 70: Wind energy resource map in the Nampula area.	132
4. 71: Observed wind rose and speed frequency distribution at Lichinga.	133
4. 72: Wind speed frequency distribution and mean wind speed by sector at Lichinga.	134

4. 73: Regional wind climate of Lichinga meteorological station.....	135
4. 74: Map showing the location of the potential sites in the Lichinga area.	136
4. 75: Predicted mean wind speed and available wind energy in the Lichinga area.	137
4. 76: Predicted wind rose and speed frequency distribution in the Lichinga area.	138
4. 77: Predicted wind speed frequency distribution in the Lichinga area.....	139
4. 78: The extractable wind energy at potential sites in the Lichinga area.....	139
4. 79: Extractable average wind energy by azimuth sector in the Lichinga area.	140
4. 80: Extractable energy rose and frequency distribution in the Lichinga area.	140
4. 81: Wind speed resource map in the Lichinga area.	141
4. 82: Wind energy resource map in the Lichinga area.	142

LIST OF PLATES

1. 1:	Ponta de Ouro dunes showing topography typical of all the coastal zones ...	9
3. 1:	Ponta do Ouro meteorological mast looking towards the east.....	56
3. 2:	Mavalane anemometer viewed towards the east.....	58
3. 3:	Inhambane and Vilankulo meteorological stations.	59

LIST OF TABLES

2. 1:	Classes of wind power density at 10 and 50 m.....	26
2. 2:	Typical values of surface roughness length z_0 and power law exponent α	35
2. 3:	Roughness length and surface characteristics	45
2. 4:	Porosity of obstacles	46
3. 1:	Meteorological stations that collect hourly wind speed.	55
3. 2:	Summary statistics of wind speed of the synoptic stations.	60
3. 3:	Specifications and performance of V52-850 kW wind turbine.....	70
4. 1:	Wind atlas data at Mavalane.....	76
4. 2:	Wind atlas data at Ponta de Ouro	86
4. 3:	Wind atlas data at Tofinho	96
4. 4:	Wind atlas data at Vilankulo	104
4. 5:	Wind atlas data at Pemba	115
4. 6:	Wind atlas data at Nampula.....	124
4. 7:	Wind atlas data at Lichinga	135

LIST OF ABBREVIATIONS AND ACRONYMS

ABL	Atmospheric Boundary Layer
AEP	Annual Energy Production
AWS	Automatic Weather Station
BZ-model	Bessel Expansion on a Zooming Grid model
CAB	Congo Air Boundary
COE	Cost of Energy
CTA	Confederação das Associações Economicas de Moçambique
DEM	Digital Elevation Model
DINAGECA	Direção Nacional de Geografia e Cadastro
DNER	Direção Nacional de Energia Novas e Renovaveis
DPA	Direção Provincial de Agricultura
EDM	Eletricidade de Moçambique
ENM	Editora Nacional de Moçambique
FUNAE	Fundo Nacional de Energia
GDP	Gross Domestic Product
GovM	Government of Mozambique
GWh	Gigawatt hour
HCB	Higroelectrica de Cahora Bassa
Hz	Hertz
IMF	International Monetary Fund
INAM	Instituto Nacional de Meteorologia
INE	Instituto Nacional de Estatistica
ITCZ	Intertropical Convergence Zone
KAMM	Kalsruhe Atmospheric Mesoscale Model
kw	Kilowatt
KWh	Kilowatt hour
Mcell	Moçambique Celular
MDGs	Milennium Development Goals
ME	Ministerio de Energia

MINED	Ministerio da Educaão
MM4	Fourth-Generation NCAR/Pennsylvania State Mesoscale Model
MM5	Fifth-Generation NCAR/Pennsylvania State Mesoscale Model
MW	Megawatt
MWh	Megawatt hour
NAP	National Academy Press
NGO	Non-governmental Organization
NOABL	Numerical Objective Analysis of Boundary Layer
OWC	Observed wind climate
PBL	Planetary Boundary Layer
PDF	Probability Distribution Function
PWC	Predicted wind climate
RPM	Rotation Per Minute
RWC	Regional wind climate
SADC	Southern Africa Development Community
SBL	Surface Boundary Layer
SIDA	Swedish International Development Agency
TDM	Telecomunicaões de Moambique
TSR	Tip-speed ratio
UEM	Universidade Eduardo Mondlane
USA	United States of America
UTM	Universal Transverse Mercator
VCS	Vestas Converter System
WADS	Wind atlas data set
WA ^s P	Wind Atlas Analysis and Application Program
WECS	Wind Energy Conversion System
WINDS	Wind-field interpolation by non-divergent schemes
WMO	World Meteorological Organization

CHAPTER ONE

INTRODUCTION

1.1 Background to the study

Energy is available as two different alternatives; non-renewable (coal, oil, natural gas) and renewable (solar, wind, hydro, wave, biomass) sources (Sahin, 2004). Wind energy has played a long and important role in the history of civilization. It has been used to sail ships, grind grain and pump water (Ahmed and Abouzeid, 2001; Gipe, 2004; Erdogdu, 2008). Since 1891, when “Dane Poul LaCour” (Sahin, 2004; Erdogdu, 2008) succeeded in generating electricity from wind, wind energy has become a promising alternative to oil, mainly because it is continuous and does not cause environmental contamination. However, the popularity of using the energy of the wind has always fluctuated and the interest in wind energy, particularly wind turbines, declined with the fall of fuel prices after World War II (Erdogdu, 2008).

The energy crisis in 1973 that led to the first oil price shock (Ackermann and Söder, 2002; Sahin, 2004), associated with the limited supply of fossil fuels and their well-known negative environmental impacts raised the interest in renewable energy resources for electricity generation. Wind energy is one of the clean, sustainable and environmentally-friendly alternative energy sources that is currently experiencing increasing development worldwide.

Mozambique is a developing country, with an economy that is highly dependent on the agricultural sector, which provides direct and indirect employment or livelihoods for about 80% of the economically active population, and which contributes roughly 30% of the Gross Domestic Product (GDP) (O’Brien and Vogel, 2003). The country is energy rich; it has 39 rivers emptying into Indian Ocean, unexploited biomass (about 7 Exajoules of biofuels), solar energy (about 1.49 million GWh) that could be used for both on-and off-grid application, geothermal resources (about 25 MW of exploitable power) and adequate wind energy (an average wind speed of 6 - 7 ms^{-1}) (Hankins, 2009). The country is aware of the need to promote sustainable development by using

environmentally-friendly alternative energy resources. This awareness is clearly stated in the Mozambican Poverty Reduction Strategy, PARPA II (GovM, 2006a; IMF, 2007).

With an area of 799 380 km² (INE, 1998) and 20 million inhabitants (ENM, 2009), Mozambique is primarily dependent on hydro-power from the Cahora Bassa dam (Hankins, 2009) that produces 13 105 022 MWh (ME, 2007). Other sources include small hydro, thermal and natural gas power stations, which together contribute only 1.5% of the total 13 284 910 MWh (ME, 2007) produced in the country.

This quantity of energy produced, coupled with a limited national utility power grid that only had about 302 218 households connected to it in 2005 (ME, 2007), point to an unsatisfactory situation in terms of meeting electricity demands, particularly in the rural areas where more than 70% of the population lives (INE, 1998).

The shortage of power supplies leads to the massive consumption of fuel wood (wood and charcoal) which is the main source (about 96%) of the renewable energy consumed in the country (ME, 2007). This consumption contributes negatively to deforestation and destruction of biodiversity.

Wind energy is a clean and readily available renewable energy resource that is widely utilized worldwide, yet its exploitation is very limited in Mozambique (Hankins, 2009; Chambal, 2010). The location of the country, along the south-eastern coast of southern Africa, its long coastline, the second longest in Africa (Hankins, 2009), and some highlands in the interior region, consisting of open terrain, are conditions favorable for the existence of a good wind resource.

Fraenkel *et al.* (1993) state that in the 1980s the first attempt to exploit wind energy for water-pumping had been established in the south of the country, under the support of the Dutch government programme of wind energy for developing countries.

Recently, in an effort to promote the exploitation and use of wind energy for electrical power production, a study was undertaken to assess the possibility of installing large-scale wind farms at two locations in the south of the country (Ponta de Ouro and Tofinho). This assessment indicated an average wind speed of 6 - 7 ms⁻¹ at a 20 m hub

height. It was concluded that electricity could be generated at a cost of 9 US¢/kWh (DNER, 2008; Hankins, 2009).

Against this background, a more widespread investigation of the wind energy resource and wind energy potential in Mozambique is a strategically good starting point to promote the exploitation of wind energy, and therefore the promotion of sustainable development for the country.

1.2 Problem statement

Mozambique, like most under-developed countries, is a country in which the electrical utility, which provides 7.8% (ME, 2007; Mulder and Tembe, 2008) of the 20 million inhabitants with electricity, falls far short of meeting the national demand for energy, particularly in rural communities where most of the country's population lives. This level of accessibility to electricity and the lowest per capita use of electricity in the world (about 50 kWh/capita/annum) (Hankins, 2009) retard the socio-economic development of the country, particularly in the rural areas.

The rural areas of the county are typically infrastructurally poor. There is very limited access to communication, roads and income generation activities because of little economic activity (Hankins, 2009). Greater access to electricity could boost local industry, trade and the ability to process agricultural products and therefore contribute to poverty reduction (GovM, 2005b).

The apparently significant expansion of the utility grid countrywide between 2003 and 2005, which was an increase of about 50%, 30% and 15% for the Southern, Central and Northern regions (ME, 2007) respectively, is insignificant when considered in the context of the total population (20 million inhabitants). The increase in electrification represented only an additional 129 000 households connected to the utility grid, giving a total of about 302 000 households connected up to 2005 (ME, 2007).

The total power production of Mozambique is 13 284 910 MWh (ME, 2007), with hydro-power from the Cahora Bassa dam being the major source of electricity,

producing 98.6% of the total electricity generated (ME, 2007). However, hydro-power cannot be the sole source of power. Despite all the advantages that it has, it is well known that hydro-power stations require specific locations with special characteristics and that large hydro-power schemes have an irreversible negative impact on the environment (Esteves, 2004).

For these reasons and because the country is energy rich in viable green energy sources, investigations into the utilization of mini and micro-hydro-power stations, as well as other clean renewable energy sources such as solar and wind power, should be undertaken to satisfy the energy demands of the country in the medium- and short-term.

In the light of the Millennium Development Goals (MDGs), the energy policy and electrification system of the Mozambican Government are directed to rural areas to ensure sustainable development through the use of green energy (GovM, 2006a; Hankins, 2009). This is the justification for the introduction of solar off-grid energy schemes, which comprise 4% of the total renewable energy produced (ME, 2007), and which are used to supply power to rural hospitals (health clinics), schools, government offices, street lightning and off-grid tourist hotels (Hankins, 2009), as well as for water pumping and grinding activities in rural communities.

Firewood and charcoal represent the major sources of renewable energy, comprising 92% and 4% of the total respectively (ME, 2007). Wind power is still an unknown and unexploited energy resource in the country (ME, 2007; Hankins, 2009).

1.3 Rationale for the study

An evaluation of the wind resource and wind energy potential in Mozambique through the production of a wind atlas and maps of the wind resource using observed and modelled wind data can promote the exploitation of wind energy either for water-pumping or electrical power production for on-grid or off-grid wind power applications.

In addition, evaluation of the wind and energy resource potential can help either in planning wind measurements and data collection for the specific purpose of installing wind turbines or checking wind speed measurements that have been recorded at local weather stations.

A wind energy potential map can also stimulate wind energy projects and promote the exploitation of the wind for different applications, such as electricity generation, water pumping for irrigation and livestock rearing, and cereal grinding. It can also become a tool to help decision-makers seek potential investors in this unexploited field. All these have the potential to bring prosperity and raise the standard of living due to improved educational facilities and public health benefits, as well as improve opportunities in the agricultural sector and promote local enterprises and the development of rural infrastructure.

1.4 Aim and objectives of the study

This project aims to undertake an evaluation of the wind energy potential for electrical power generation in Mozambique by using a modeling technique.

The specific objectives of the study are:

1. To characterize the wind speed patterns based on hourly observed wind data at meteorological stations; and
2. To model the wind power availability in two selected areas using a numerical model that uses wind speed data from individual sites and wind turbine characteristics to provide a spatial representation of wind power which enables the identification of potential sites with high mean annual wind speeds sufficient for electricity generation.

1.5 The study areas

1.5.1 Location

Mozambique is located on the south-eastern side of the southern African subcontinent, between latitudes $10^{\circ} 27' S$ and $26^{\circ} 52' S$ and longitudes $30^{\circ} 12' E$ and $40^{\circ} 52' E$ (INE, 1998), and has a long coastline of about 2 515 km (INE, 1998; O'Brien and Vogel, 2003). It is expected to possess a good wind resource potential that can be harnessed for energy purposes. Figure 1.1 illustrates the administrative areas or provinces of Mozambique.

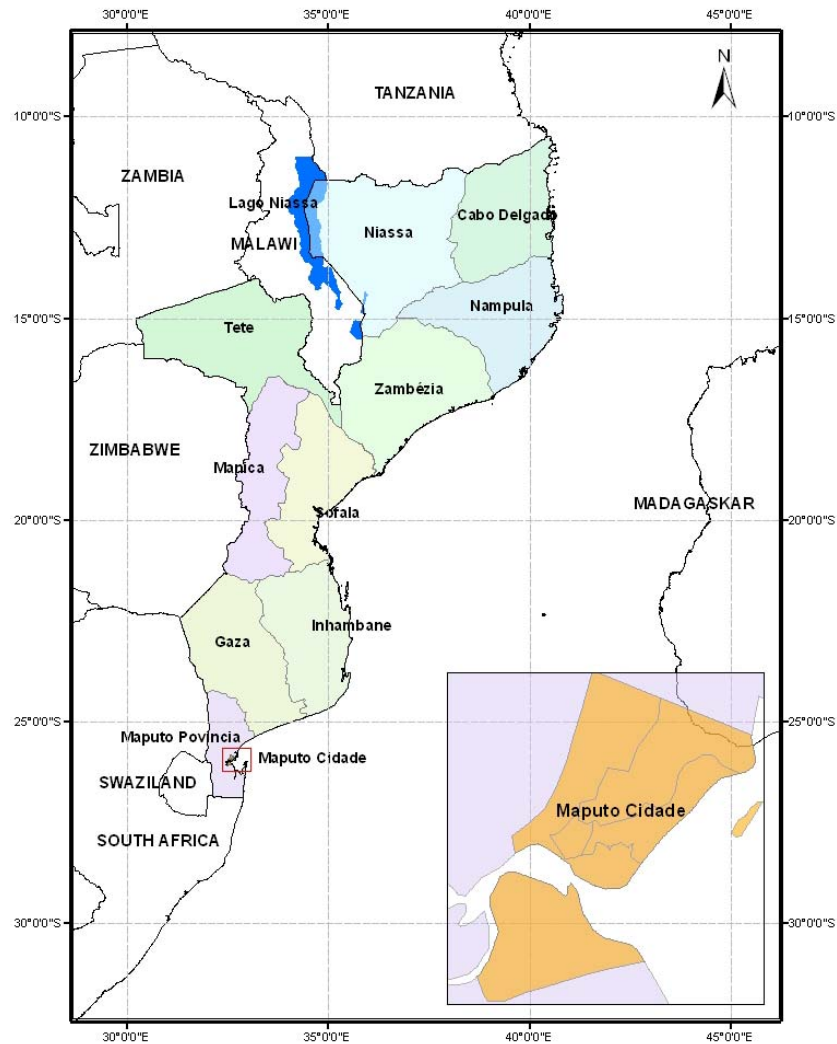


Figure 1. 1: Map showing provinces of Mozambique.

The study areas selected are the coastal zones of the southern and northern regions of Mozambique and the interior areas of Nampula and Niassa provinces. The southern coastal area lies between latitudes $21^{\circ} 45' S$ and $26^{\circ} 52' S$ and longitudes $32^{\circ} 27' E$ and $36^{\circ} E$, from Ponta de Ouro to Vilankulo; the northern coastal area lies between latitudes $11^{\circ} 59' S$ and $15^{\circ} 32' S$ and longitudes $40^{\circ} 12' E$ and $40^{\circ} 33' E$, from Mossuril to Macomia. The interior area comprises the districts of Lichinga, between latitudes $12^{\circ} 59' S$ and $14^{\circ} 00' S$ and longitudes $35^{\circ} 00' E$ and $35^{\circ} 59' E$, and Nampula between latitudes $15^{\circ} 00' S$ and $15^{\circ} 25' S$ and longitudes $39^{\circ} 00' E$ and $39^{\circ} 47' E$ (Fig. 1.2).

In general, coastal areas are characterized by more frequent strong winds than interior areas. This contrast is related to the thermal effect and the low roughness of the water surface in coastal areas. Wind speed diminishes rapidly about 3 km away from the shore line (Gipe, 2004) when the roughness of the inland surface changes more significantly.

1.5.2 Topography

The coastal plain lies at an elevation of less than 200 m. The interior province of Nampula is between 100 - 500 m altitude and Lichinga is between 1 000 - 1 500 m altitude (ENM, 2009). The coastal plain is characterized by dunes and open lands, while low grasses and small dispersed bushes are the typical vegetation.

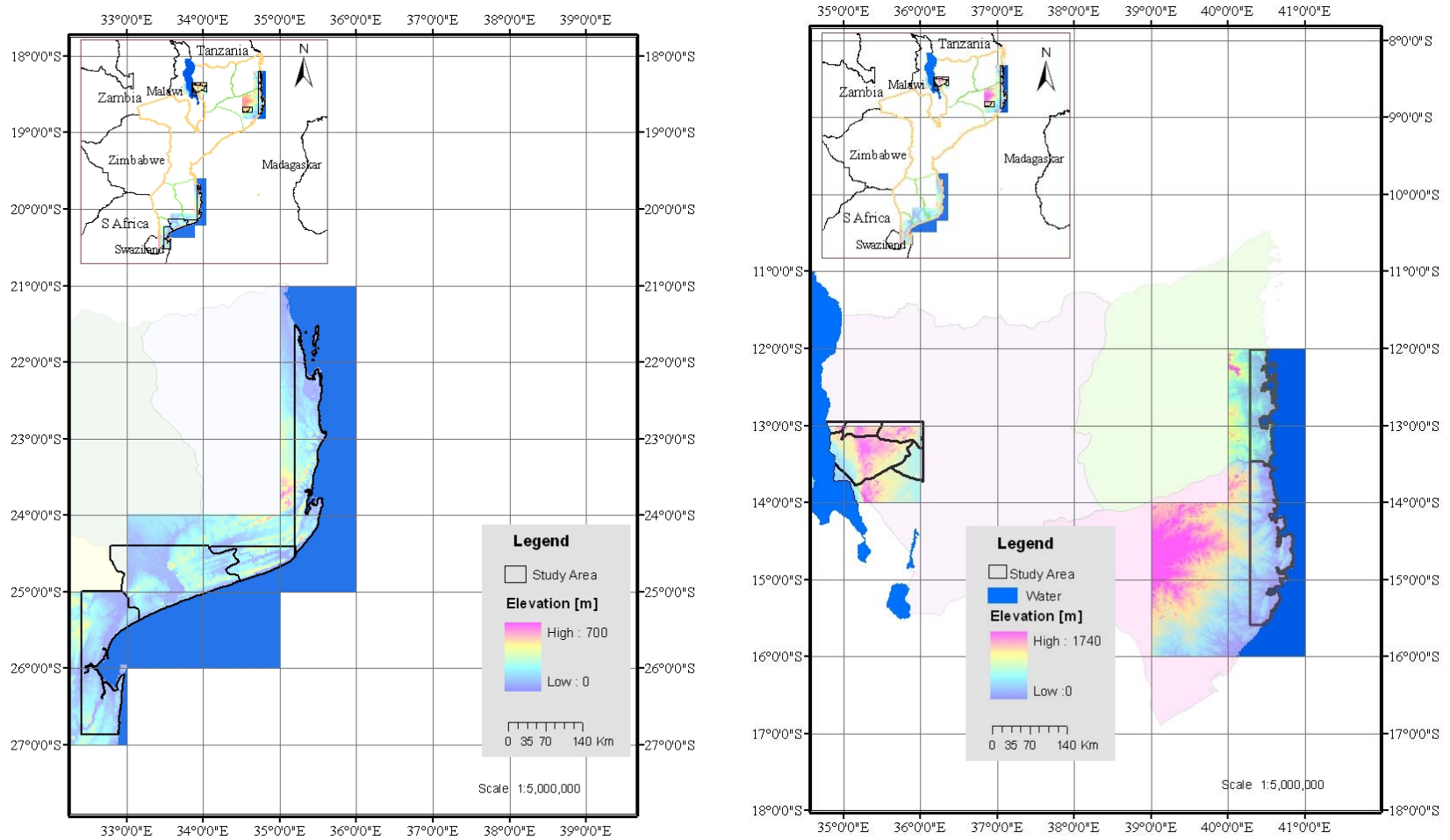


Figure 1. 2: Digital elevation model representing the topography of the coastal and interior study areas.

Some isolated hilly areas of less than 200 m elevation are sparsely situated throughout the coastal plain, but these features are very characteristic of the hinterland area, particularly to the south of Maputo near the Swaziland and KwaZulu-Natal borders, where elevations reach about 800 m (ENM, 2009). Plate 1.1 illustrates the typical topography of the coastal areas.



Plate 1. 1: Ponta de Ouro dunes showing topography typical of all the coastal zones [Source: DNER, 2008; Photo by Riso].

In the interior, the flat terrain is dominated by open areas with low grass and dispersed bushes. Mountainous areas, with elevations above 1 500 m (ENM, 2009), are characteristic of the north-west of Niassa province, north and north-west of Tete (Angonia), the Alta Zambézia in the Zambézia province and the western part of Manica province close to the Zimbabwe border. Figure 1.3 illustrates the topography of Mozambique.

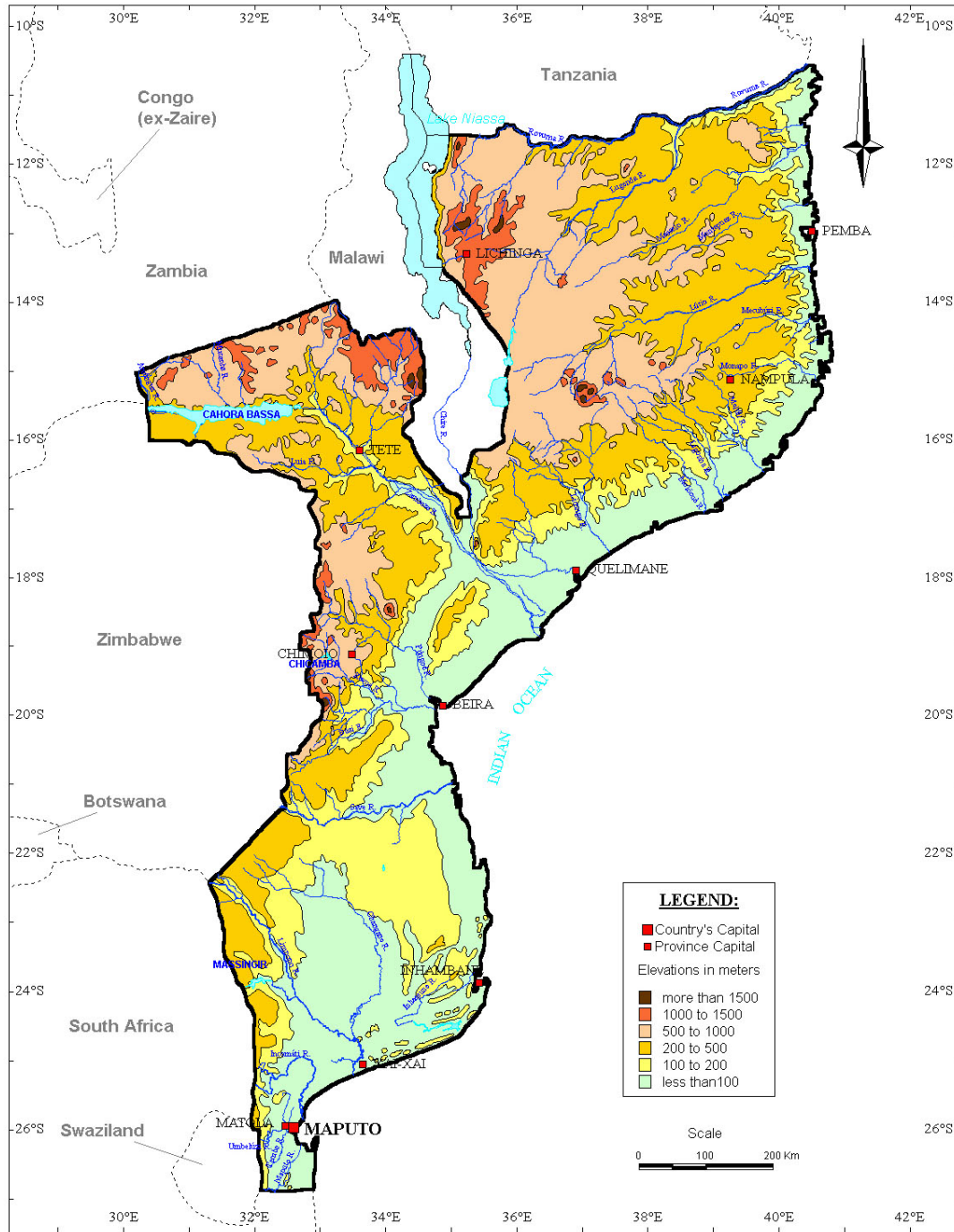


Figure 1. 3: Topography of Mozambique [Source: MINED, 1986].

1.5.3 Climate

According to the Köppen classification scheme (Faria and Gonçalves, 1968; MINED, 1986; Matos and Ramalho, 1989; O'Brien and Vogel, 2003, ENM, 2009), the climate of Mozambique is tropical savanna, with four main climate zones, namely: A_w (tropical and humid), B_s (tropical and dry), C_w (higher altitude) and B_s (tropical semi-arid) (Fig. 1.4 a).

Two typical climate seasons characterize Mozambique: the warm and rainy summer, which extends from November to April, and the dry and cooler winter from May to October (O'Brien and Vogel, 2003). The annual mean temperature and rainfall (Fig. 1.4b and 1.4c) vary from the northern to the southern region and from the coast to the highlands in the interior of the country. The coastal plain has a tropical and humid climate with a mean temperature of about 24°C in the southern region and 25°C in the northern regions (Fig. 1.4 a and 1.4b).

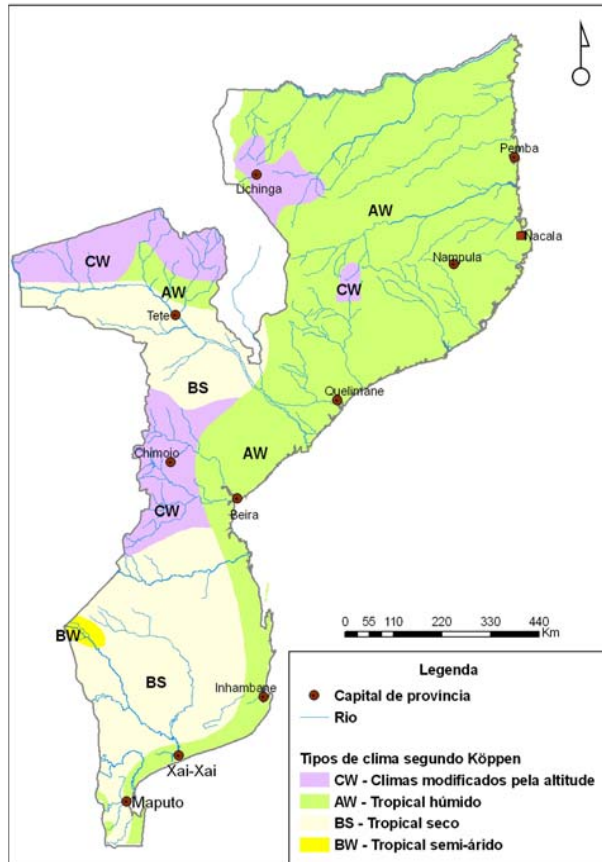


Figure 1. 4a: The climatic zones [Source: MINED, 1986].

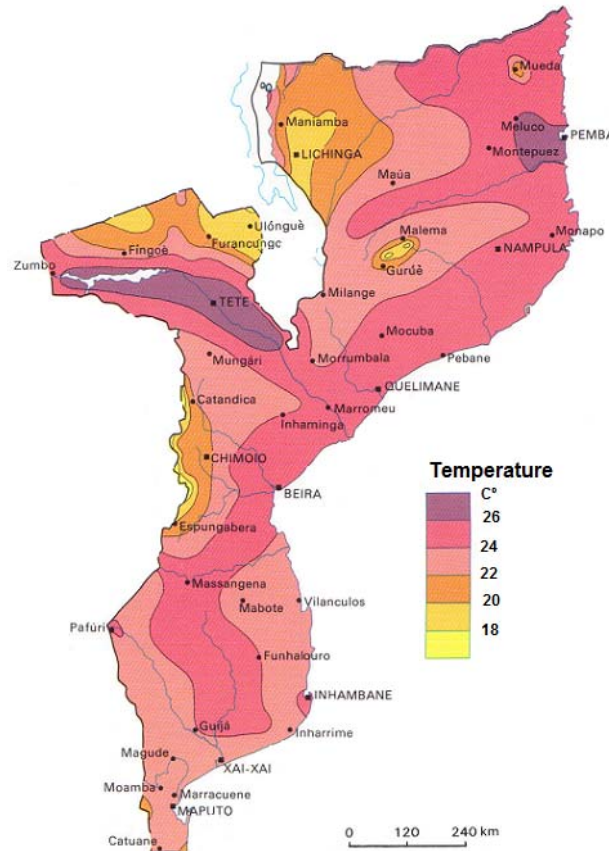


Figure 1.4b: Annual mean temperatures [Source: MINED, 1986].

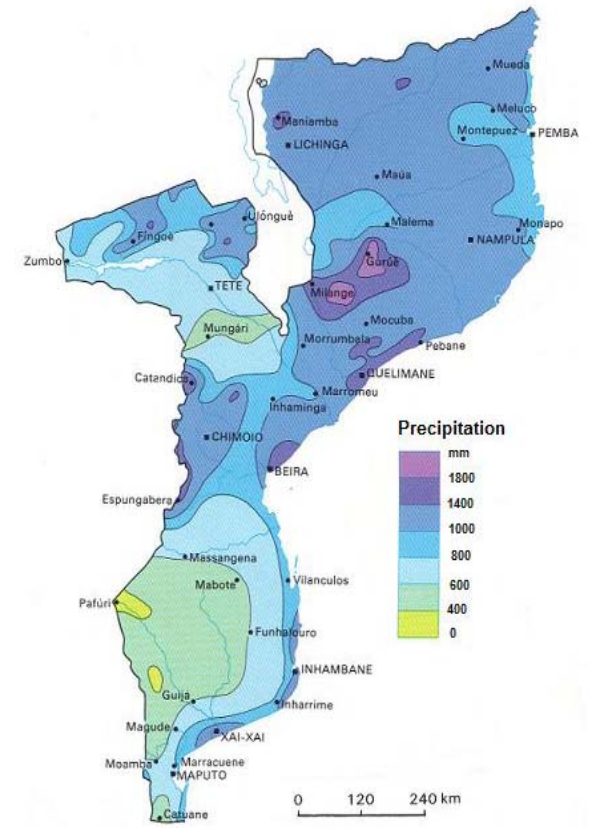


Figure 1.4c: Annual mean precipitation [Source: MINED, 1986].

The wind regime in summer is predominantly of a south-easterly or southerly flow in the southern region (Da Mata, 1962; Martyn, 1992) and north-north-east (NNE) in the northern region (Da Mata, 1962) (Fig. 1.5).

In the southern region, the wind regime is a consequence of the south-east trade winds from the Indian Ocean High (Martyn, 1992), while the northern region is influenced by the north-east Monsoon from Somalia and east Africa (Hastenrath, 1985; Martyn, 1992).

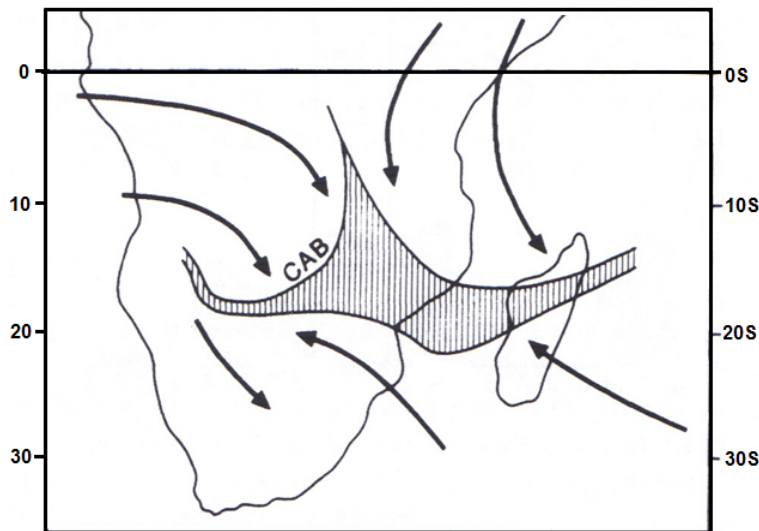


Figure 1. 5: The mean and extreme position of the ITCZ over Southern Africa from December to January and the Congo Air Boundary (CAB) [Source: Martyn, 1992; McGregor and Nieuwolt, 1998].

In winter, the Intertropical Convergence Zone (ITCZ) is situated in the Northern Hemisphere and the whole of south-eastern Africa comes under the influence of the permanent Indian Ocean High centered over 30° S (Ayoade, 1983; Wells, 1986; Martyn, 1992), which dominates the general circulation of the Southern Hemisphere (Wells, 1986; Tyson and Preston-Whyte, 2000).

In view of this pressure distribution over south-eastern Africa, throughout the country either north of 15° S or south of 21° S latitude and as well as in between this belt, the wind

regime is predominantly south-easterly (SE) or easterly winds (Da Mata, 1962). This wind regime is a consequence of the permanent Indian Ocean high centred over 30°S (Martyn, 1992) associated with the presence of the winter South African High over the subcontinent (Van Heerden and Hurry, 1987; Martyn, 1992).

1.5.4 Population

The vast geographical extent of Mozambique, 799 380 km² (INE, 1998) and low population density of about 25.7 inhabitants/km² (ENM, 2009) hampers accessibility of rural communities to conventional energy (about 8% with access to electricity) (ME, 2007; Mulder and Tembe, 2008; Hankins, 2009). Electrification of sparsely population rural areas is difficult and not cost-effective (Mulder and Tembe, 2008; Hankins, 2009). The coastal areas of the country are relatively more populated than the interior areas (Fig. 1.6).

The province of Niassa, one of the study areas in the northern region, is the most extensive (8 689 467km²) and least populated province of the country (9.13 inhabitants/km²) (ENM, 2009). Most of the population is close to Lago Niassa (Fig. 1.6). Maputo (Maputo Cidade), one of the study areas in the south, has the smallest area and is the most populated province (about 3 664 inhabitants/km²), while Nampula (49.96 inhabitants/km²) in the northern region is the second most populated province of the country (ENM, 2009).

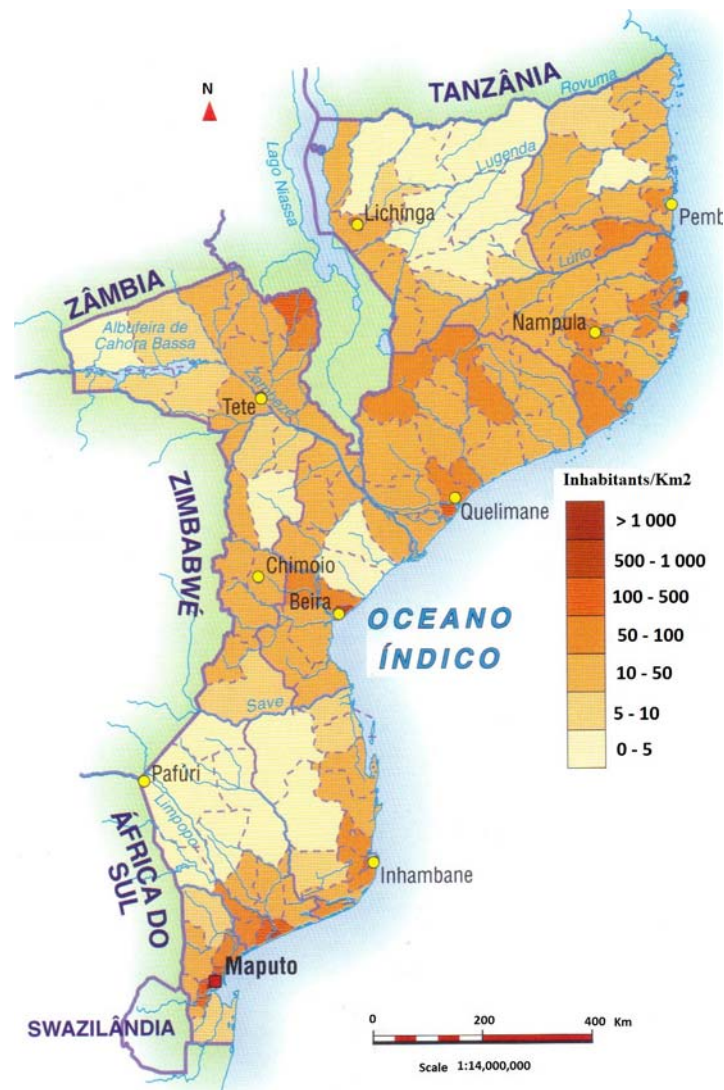


Figure 1. 6: Inhabitants per square kilometer [Source: ENM, 2009].

1.5.5 Electricity access

A lack of access to modern energy by most rural communities throughout the country hampers productive activities, most of which are dependent on electricity, and prevents most of the poor households from increasing their income. According to Mulder and Tembe

(2008) and Hankins (2009), more than 80% of Mozambique's population is off-grid and relies on traditional wood and charcoal biomass resources for all of their energy needs.

The electricity accessibility for all provinces in 2008, was still below 8% (Mulder and Tembe, 2008; Hankins, 2009). Exceptions include Maputo Cidade (the country's capital with 61.4% access), Maputo Provincia (about 33.6% access), Gaza (15.5%) and Sofala (12.4%) (Hankins, 2009). The province of Tete, where the hydro-power scheme of Cahora Bassa is located, had only 6% electricity accessibility in 2008, while Zambézia, the fourth most populated province, had the least electricity accessibility, with only 4.7% access (Hankins, 2009).

In order to reduce these asymmetries that are found country-wide, one of the objectives of Mozambique's Poverty Reduction Strategy (GovM, 2005b) for the energy sector is to improve the provision of energy to households through its electrification master plan that is being implemented by Electricidade de Moçambique (EDM) (Mozambique's electricity utility) to expand the existing national grid fed by hydro-power from Cahora Bassa (Mulder and Tembe, 2008).

In the southern region of the country, despite the operational 110 kV transmission line from Xai-Xai (Gaza province) substation to Lindela (Inhambane province) (Fig. 1.7), many rural communities, schools, and hospitals less than 5 km away from this corridor do not have access to electricity. This scenario is similar across the country and is a consequence of the sparsely populated rural areas and the vast geographical area that make the distribution of commercial energy to these communities expensive (Hankins, 2009).

Figure 1.7 illustrates the EDM transmission power lines throughout the country fed by hydro-power from Cahora Bassa where the operational transmission lines are shown in solid lines and planned ones in dotted lines. Apart from this main grid, there are numerous off-grid back-up generators which operate in regional capitals country-wide. One such isolated gas-fired mini-grid operates in the rural areas of Inhambane province, namely Nova

Mambone, Inhassoro and Vilankulo, which supplies electricity to other small rural villages, *viz.* Mapinhane, Mabote and Maimelane (DNER, 2008).

Different initiatives are being undertaken in order to provide decentralized off-grid power to community centres with common facilities, *viz.* local enterprises, schools, training and health centers, by using renewable energy sources such as solar photovoltaic (Hankins, 2009). Utilization of wind energy for power generation is also being planned (DNER, 2008; Hankins, 2009).

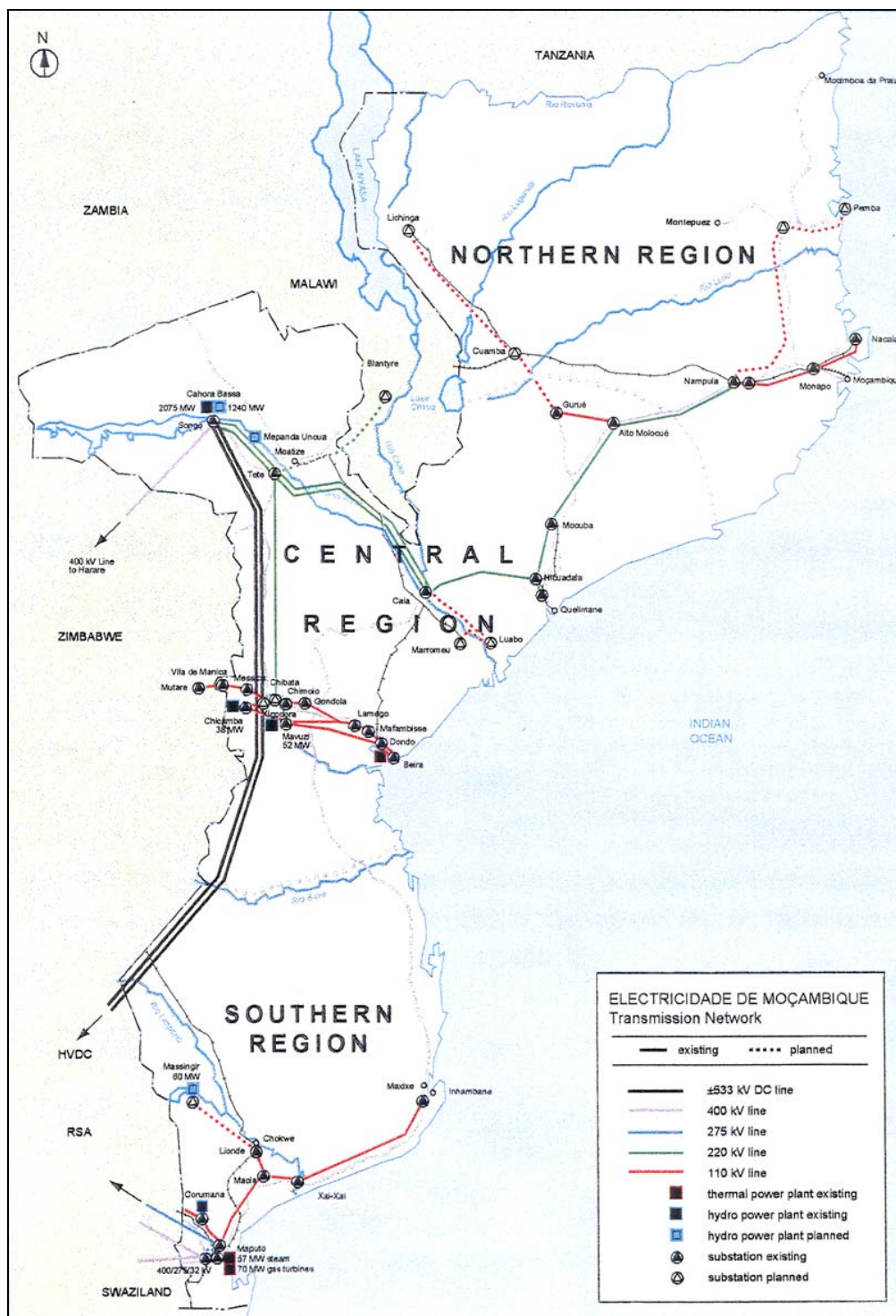


Figure 1. 7: The EDM power transmission lines throughout the country [Source: EDM, 2007].

1.6 Structure of the thesis

This thesis is divided into five chapters. Chapter One is an introduction to the study, where the problem, justification, the aim and objectives of the study are outlined. Chapter Two is devoted to a theoretical discussion and literature review about harnessing wind for energy applications, while Chapter Three characterizes the meteorological data sets and describes the methodological procedures that were used in the study. In Chapter Four, the wind energy resources in the selected study areas are predicted and mapped and Chapter Five summarizes the results from the previous chapters, draws conclusions and makes general recommendations for future investigations.

1.7 Summary

This chapter has provided the background concerning the need to exploit the wind as a continuous and clean energy source for electricity generation.

In this regard, based on energy statistics from previous studies, it has been highlighted that the lack of electricity affects the majority of the country's population who have no access to utility services. This fact leads to the massive consumption of wood biomass and charcoal as the main sources of energy, a practice that is environmentally unfriendly as it degrades the natural vegetation and furthermore, during combustion emits air pollutants which are harmful to human health.

It was therefore stressed that an evaluation of the wind resource and wind energy potential could contribute to and promote the exploitation of this continuous clean source of energy to generate electricity. This could contribute to the national electricity grid and could boost local industry, trade and create employment and improve the life of the local communities by providing them with access to improved education and health facilities, thus contributing to poverty reduction in line with Mozambique's Poverty Reduction Strategy.

CHAPTER TWO

LITERATURE REVIEW

2.1 Introduction

Wind as source of energy is well established source (Wortman, 1983). It is an abundant, clean, sustainable and environmentally-friendly alternative energy source. It has been used throughout human civilization for different purposes.

In various parts of the world, wind has been widely used as an energy source for milling grain, pumping water and for electrical power production. During World Wars I and II it was used to overcome energy shortages (Wortman, 1983; Sahin, 2004; Erdogdu, 2008). In Mozambique, the Gaza Province Agricultural Department (DPA) installed fifty small wind pumps per year in the mid-1980s for purposes of ground water extraction. This project was supported by the Dutch government programme of wind energy for developing countries (Fraenkel *et al.*, 1993). The project was interrupted by the unrest in the country.

This chapter discusses the wind as a source of energy and provides a background on the techniques to estimate the available and extractable wind energy. It also highlights some benefits of wind energy, and discusses wind energy prediction models used to assess the wind energy resource. The different factors determining the amount of energy which can be harnessed at particular sites are also highlighted.

2.2 Wind as a source of energy

Wind energy, comes from solar energy like most other energy sources (Cheremisinoff, 1978; Twidell and Weir, 2006; Erdogdu, 2008). Wind as a source of energy was used to

sail ships, to mill grain and to pump water (Cheremisinoff, 1978; Fraenkel *et al.*, 1993; Ahmed and Abouzeid, 2001; Sahin, 2004; Erdogdu, 2008). Wind has also always played an essential role in agriculture and forestry, acting as a pollination agent for grain crops and several commercially-valuable timber species.

As far back as 5000 years ago, the ancient Egyptians used wind energy to propel boats (Fraenkel *et al.*, 1993; Wortman, 1983; Erdogdu, 2008). Different authors describe the crude versions of drag-type vertical axis windmill machines that may have existed as early as 2 000 B.C. in Babylonia and China (Cheremisinoff, 1978; Wortman, 1983). Fraenkel *et al.* (1993) refer to Seistan, a province on the border of Iran and Afghanistan, that was famous for using wind to run mill-stones and to draw water from wells.

The aforementioned archaic windmill technology has spread and developed. The literature describes the introduction of windmills into Europe by the Arabs through the Iberian Peninsula during the Muslim expansion in the year 750 BC (Fraenkel *et al.*, 1993). It is also stated that by 1096-1191, during the time of the Crusaders, the use of windmills was well established and they spread throughout Europe (Fraenkel *et al.*, 1993; Wortman, 1983). In the 1500s, the Spanish explorers and settlers introduced windmills to the Americas (Cheremisinoff, 1978).

Wind as a source of energy from which electricity can be generated is attributed to the work of Dane Poul LaCour, in 1891, who built the first wind turbine and began the generation of electricity from wind (Sahin, 2004; Erdogdu, 2008). Since that time, the Wind Energy Conversion System (WECS) technology has developed significantly. During World Wars I and II, Danish engineers improved the technology to overcome the energy shortages (Sahin, 2004; Erdogdu, 2008), and thereafter the utilization of the energy from the WECS became widespread worldwide.

However, according to Sahin (2004), the interest in large-scale wind turbines declined after World War II, so that small-scale wind turbines received greater interest as power systems in remote areas. Furthermore, the oil crisis in the early 1970s (Freris, 1990; Fraenkel *et al.*,

1993; Walker and Jenkins, 1997; Sahin, 2004; Twidell and Weir, 2006; Erdogdu, 2008;) heightened the interest in the WECS and from then onwards, financial support for research in, and the development of, wind energy increased rapidly from the early 1980s in the USA and Europe (Sahin, 2004).

Recent times however, have seen the rapid evolution of wind turbine technology, which is spurred on by the threat of global warming, making wind energy a promising alternative to oil, mainly because it cannot be depleted. Wind turbines can be installed quickly in isolated villages or rural sites, with or without connections to the utility services, thus reducing financing costs and providing flexibility in meeting the increasing demand for energy (NAP, 1991; Twidell and Weir, 2006; Gipe, 2004). Wind turbines can also coexist with other land uses (NAP, 1991). The cost of energy (COE) from wind power plants is economically competitive now with some conventional energy generation sources (NAP, 1991). Environmentally, wind power systems are benign, being free of gaseous emissions, particulates and radioactive by-products. However, some negative impacts such as television signal interference and very specific impacts related to land use and soil degradation and aesthetics do exist (WMO, 1981).

Wind energy for electrical applications in small or large wind energy systems can be placed in three major categories, namely, interconnected alternate current (*a.c.*), non-interconnected *a.c.* or direct current (*d.c.*) and remote *d.c.* (WMO, 1981).

Gipe (2004) has stated that a hybrid station using both solar and wind energy is a good option, in particular in rural areas where there is a shortage of power. This is because such a station offers greater reliability than separate wind or solar technology and is more cost-effective, particularly for developing countries such as Mozambique. In addition, Gipe (2004) contends that such a remote power system would permit the use of less costly components than if the system depended on only one power source, and it could also lower the cost of a remote power system.

2.3 The available and extractable energy from the wind

The solar radiation which heats the earth, produces large-scale motion of the atmosphere, causing regions of unequal heating over land and oceans. This creates a pressure gradient which results in air mass movement from high pressure to low pressure, namely, the wind.

The wind energy is a result of the wind motion and is called kinetic energy (Fraenkel *et al.*, 1993). The power P due to the kinetic energy of the wind is proportional to the volume of air passing through an area A [m] in a unit time t [s] with velocity v , and physically is $P = 1/2\rho Av^3$; where ρ is the air density (about 1.225 kgm^{-3}) (Jamil *et al.*, 1995; Walker and Jenkins, 1997; Ackermann and Söder, 2002; Sahin, 2004; Gipe, 2004; Mortensen *et al.*, 2007).

The air density depends on altitude and meteorological conditions, air pressure and temperature, both being functions of height above sea level (a.s.l.) (Fraenkel *et al.*, 1993; Jamil *et al.*, 1995; Walker and Jenkins, 1997; Ackermann and Söder, 2002; Gipe, 2004).

The WECS makes use of this kinetic energy by slowing down the wind to remove the unaffected inflow kinetic energy (v_0), converting it into rotational energy in the spinning rotor A_1 , (Fig. 2.1), where A_0 and A_2 are upstream and downstream respectively, of the rotor (Fraenkel *et al.*, 1993; Ackermann and Söder, 2002; Twidell and Weir, 2006).

Wortman (1983) and Ackermann and Söder (2002) have stated that the wind power in the incoming wind flux A_0 is not extracted completely by the wind turbine A_1 . On the contrary, the air mass would be stopped completely in the intercepting rotor area, causing the congestion of the cross-sectional area for the following air masses.

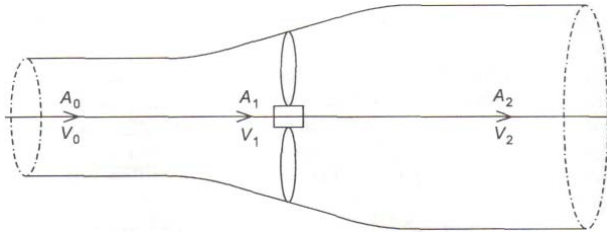


Figure 2. 1: Ideal air flow through a wind turbine [Source: Walker and Jenkins, 1997].

Therefore, the optimum (maximum) theoretical amount of wind energy that can be extracted from unaffected inflow by the rotor (WMO, 1981; Ackermann and Söder, 2002; Twidell and Weir, 2006) is given as:

$$P = \frac{1}{2} C_p \rho A v^3 \quad (2.1)$$

where A is the swept area, v the mean wind speed and $C_p = 4a(1-a)^2$. The constant C_p is the dimensionless power coefficient or Betz limit (WMO, 1981; Fraenkel *et al.*, 1993; Wortman, 1983; Walker and Jenkins, 1997; Ackermann and Söder, 2002; Gipe, 2004; Twidell and Weir, 2006) which can be derived from Newton's second law (Wortman, 1983; Walker and Jenkins, 1997; Twidell and Weir, 2006) and a is the downstream velocity factor or wind speed ratio (Walker and Jenkins, 1997; Twidell and Weir, 2006), and describes the ratio of upstream to downstream wind speeds (Walker and Jenkins, 1997). The differentiation of C_p with respect to a , shows C_p to be a maximum when the speed ratio a is $1/3$ (Wortman, 1983; Walker and Jenkins, 1997; Twidell and Weir, 2006; Gipe, 2004), which is about $C_p = 16/27 = 59\%$.

Twidell and Weir (2006) have shown that the Betz limit itself does not reveal anything about the dynamic rotational state of a turbine that is necessary to reach the criterion of maximum efficiency. So, the dimensionless characteristic for dynamic matching is the tip-speed-ratio (TSR), λ_0 , which is related to the blade-tip radius R , speed of the oncoming

wind v_0 and the angular velocity Ω (Twidell and Weir, 2006) and represents the impact of unavoidable swirl losses (Ackermann and Söder, 2002; Sahin, 2004). It is defined as:

$$\lambda_0 = \frac{\Omega R}{V_0} \approx \frac{4\pi}{n} \quad (2.2)$$

and n is the number of turbine blades.

Another most important wind energy characteristic for wind energy resource evaluation, is the mean power density (or available wind energy) P [Wm^{-2}]. The mean power density, $P = 1/2\rho v^3$ (Troen and Petersen, 1989; Souza and Granja, 1997; Twidell and Weir, 2006) and according to Hennessey (1977), it is the instantaneous power density available (available wind energy) in a flow of air through a unit cross-sectional area normal to the flow.

According to Gipe (2004), the power density can be calculated in two ways, *viz.* the sum of the series of power density calculations for each wind speed and its frequency of occurrence (the number of hours per year the wind blows at that speed) for the site distribution of wind speeds, or by using the average wind speed and the appropriate cube factor.

The power density is affected by changes in air density when sites differ markedly from those at standard sea-level conditions. Table 2.1 gives the classification of wind power density at 10 m and 50 m a.g.l. according to the WMO (1981).

Table 2. 1: Classes of wind power density at 10 and 50 m¹ a.g.l. [After: WMO, 1981].

Wind power class	Description	10 m		50 m	
		Wind power density (Wattsm ⁻²)	Wind speed (ms ⁻¹)	Wind power density (Wattsm ⁻²)	Wind speed (ms ⁻¹)
1	Poor	0 - 100	0.0 - 4.4	0 - 200	0.0 -5.6
2	Marginal	100 - 150	4.4 - 5.1	200 - 300	5.6 -6.4
3	Fair	150 - 200	5.1 - 5.6	300 - 400	6.4 -7.0
4	Good	200 - 250	5.6 - 6.0	400 - 500	7.0 -7.5
5	Excellent	250 - 300	6.0 - 6.4	500 - 600	7.5 -8.0
6	Outstanding	300 - 400	6.4 - 7.0	600 - 800	8.0 -11.9
7	Superb	400 - 1000	7.0 - 9.4	800 - 2000	>11.9

2.4 The wind and energy potential prediction models

According to Mortensen *et al.* (2007), a regional assessment of wind and energy resources over a large area, should predict the mean wind speed and total annual energy production (extractable wind energy) for a specific wind turbine at a particular site. A good regional wind energy resource assessment is therefore sensitive to the available wind speed probability distribution for a given location for a given period of time, and this information can help to choose an appropriate WECS.

Besides the lognormal probability distribution function (PDF) (Justus *et al.*, 1976; Garcia *et al.*, 1998; Zaharim *et al.*, 2009b), the Weibull and Rayleigh PDFs are the most widely used PDFs to describe the wind speed for WECS applications (Justus *et al.*, 1976; Doran and Verholec, 1978; Takle and Brown, 1978; Tuller and Brett, 1984; Jamil *et al.*, 1995; Souza and Granja, 1997; Garcia *et al.*, 1998; Lun and Lam, 2000; Gipe, 2004; Twidell and Weir, 2006; Leite and Filho, 2006; Hrayshat, 2007). The Weibull distribution is a two parameter function, and was named after the Swedish physicist W. Weibull, who applied it in the 1930s to study material strength (Lun and Lam, 2000). Recently, it has been used for

¹ Vertical extrapolation of wind based on 1/7 power law.

energy applications because it gives a better fit to experimental data at a wider range of sites than the Rayleigh distribution (Hennessey, 1977; Lun and Lam, 2000; Gipe, 2004; Zaharim *et al.*, 2009a).

The Weibull probability distribution function (PDF) according to Twidell and Weir (2006) is expressed as,

$$F(v)dv = \left(\frac{k}{c}\right)\left(\frac{v}{c}\right)^{k-1} \exp\left[-\left(\frac{v}{c}\right)^k\right] dv \quad (2.3)$$

where $F(v)$ is the PDF which gives the frequency of occurrence of a given wind speed v [ms^{-1}], \exp is the base e exponential function, k is a dimensionless shape factor that describes the form of the distribution and c [ms^{-1}] is the scale factor. The relation between the parameters c and k is given by the mean wind speed, $V_{\text{avg}}=c\Gamma(1+1/k)$ (Souza and Granja, 1997; Justus *et al.*, 1976; Jaramillo and Borja, 2004; Leite and Filho, 2006).

The shape factor k has a value of about 2 in the mid-latitudes and is relatively higher in the trade winds belt and areas of monsoon winds (about 3.5) (Knecht, 2004). It is inversely related to the variance, σ^2 , of the mean wind speed, and Γ is the gamma function and is the continuous function defined for positive real numbers t (Gronau, 2003; Jaramillo and Borja, 2004; Vinh and Ngoc, 2009),

$$\Gamma(t) = \int_0^{\infty} e^{-x} x^{t-1} dx \quad (2.4)$$

and the Gamma function satisfies $\Gamma(1)=1$ and $\Gamma(t+1)=t\Gamma(t)$.

For $k > 1$ the maximum (modal value) lies at $v > 0$, while the function decreases for $0 < k = 1$. The Weibull PDF shows different distribution properties according to the change in the k value (Sahin, 2004):

- $k = 1$ exponential probability distribution function;
- $k = 2$ Rayleigh probability distribution function; and
- $k = 3.6$ the Weibull PDF appears as an approximate of a gaussian PDF.

The parameter, c , varies with height in accordance with the power law $c/c_0 = (z/z_0)^n$ (Justus *et al.*, 1976; Doran and Verholek, 1978); where the exponent n is averaged to 0.23 and standard deviation of 0.03 (Justus *et al.*, 1976) and is closely related to the mean wind speed (Justus *et al.*, 1976).

Takle and Brown (1978) state that for data sets with a high probability of calm winds and low c , the Weibull function is not likely to provide a good fit to the data.

For $k=2$, the Weibull function becomes the Rayleigh function as noted above (Freris, 1990; Jamil *et al.*, 1995; Gipe, 2004; Twidell and Weir, 2006), also called the Chi-square distribution (Twidell and Weir, 2006) where π is a constant (3.14) and V_{avg} is the average wind speed.

$$F(v) = \frac{\pi v}{2V_{avg}^2} \exp \left[-\frac{\pi}{4} \left(\frac{v}{V_{avg}} \right)^2 \right] \quad (2.5)$$

The Rayleigh function according to Twidell and Weir (2006) is useful for a preliminary analysis of wind power potential in areas where the only available data are either maps, showing the interpolated curves of mean wind speed, or where only the average wind speed is known.

Special care should be taken because the power density calculated from the Rayleigh distribution function, for a given average wind speed, according to Gipe (2004) is almost twice that derived from the average wind speed alone, and it also overestimates the potential generation at trade wind sites.

The Weibull PDF model is the basic underlying assumption of the WA^SP method and is used to describe the measured directional wind speed distributions and generates outputs of Weibull wind speed distributions in 12 directional sectors (Lange and Højstrup, 2001; Bowen and Mortensen, 2004). For short time series, this procedure introduces an error due to the deviations of the measured distribution from the Weibull curves (Lange and Højstrup, 2001).

The specific sites where the turbines are frequently sited, are usually different from meteorological stations, even though a way of using the climatic wind data recorded at meteorological stations is needed to predict the wind climate at a turbine site. The rising interest in new and renewable energy sources towards the end of 20th century, especially wind energy for electricity production, has led to different models being developed for this specific area.

One of the most widely used models, to evaluate the wind resource estimations is the Wind Atlas Analysis and Application Programme (WA^SP) (Dube, 1994; Abdeladim *et al.*, 1996; Lange and Højstrup, 2001; Ackermann and Söder, 2002; Esteves, 2004; Bowen and Mortensen, 2004; Mortensen *et al.*, 2003; Migoya *et al.*, 2007; Narayana, 2008; DNER, 2008; Palma *et al.*, 2008), which is the standard method for wind resource prediction inland and offshore (Lange and Højstrup, 2001; Sahin, 2004; Esteves, 2004).

The WA^SP model is a computer code (Mortensen *et al.*, 1991; Palma *et al.*, 2008) and does a horizontal and vertical extrapolation of wind data taking into account the effect of obstacles, shelter and terrain height variation to produce a wind climate or regional wind climate (RWC) (Troen and Petersen, 1989; Mortensen *et al.*, 1991; Mortensen *et al.*, 2007; Migoya *et al.*, 2007). It also estimates the wind climate, the average annual energy production (AEP) at a turbine site, and it also maps the wind and energy resources.

2.5 The effect of topography, surface roughness and obstacles on the wind speed

2.5.1 The effect of the terrain

The air flow and the amount of available power from the wind are strongly influenced by the local terrain characteristics (Wortman, 1983; Petersen *et al.*, 1997). Therefore, a good knowledge of the terrain and its effect on the wind is important to the wind resource and energy assessment for siting purposes.

The wind speed profile is strongly affected by topographic features, such as escarpments, hills and ridges. According to Ngoa and Letchford (2008), these features modify the flow over them acting as obstructions to the boundary layer accelerating the wind near the ground.

According to Fraenkel *et al.* (1993) and Loureiro *et al.* (2005), a change in topography causes an immediate response of the boundary layer in the acceleration of flow over the crest of the hill, to about twice the original surface wind speed. This phenomenon which is known as the speed-up factor, is associated with deceleration of the wind and turbulence on the leeward side (Fig. 2.2).

Taking cognizance of this, Freris (1990) has stated that siting on top of hills takes advantage of the higher wind speeds that generally prevail there. Conversely, Fraenkel *et al.* (1993) stated that valleys are not suitable for siting, unless aligned with the prevailing winds. Generally, valleys are typically characterised by lower and more variable wind speeds than on flat ground or surrounding hills.

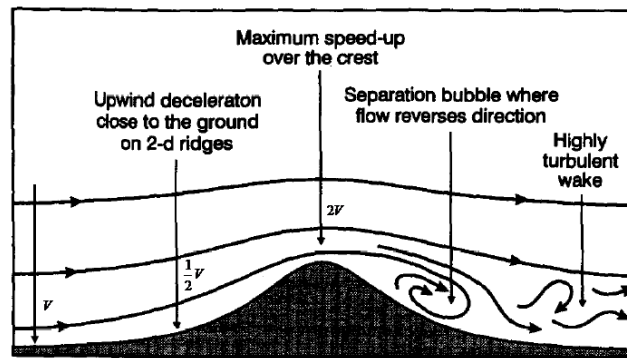


Figure 2. 2: Acceleration of air flow over a hill [Source: Raupach and Finnigan, 1997].

2.5.2 The effect of surface roughness

The surface boundary layer (SBL), about 100 m from the ground, which has a negligible (roughly constant) shear stress (Freris, 1990; Crasto, 2007) is the lower layer of the atmospheric boundary layer (ABL) (Fig. 2.3). According to Crasto (2007), the friction and pressure gradient are the only important forces, therefore the roughness of the ground is the more significant parameter and affects both the velocity profile and the angle of incidence of wind at the ground.

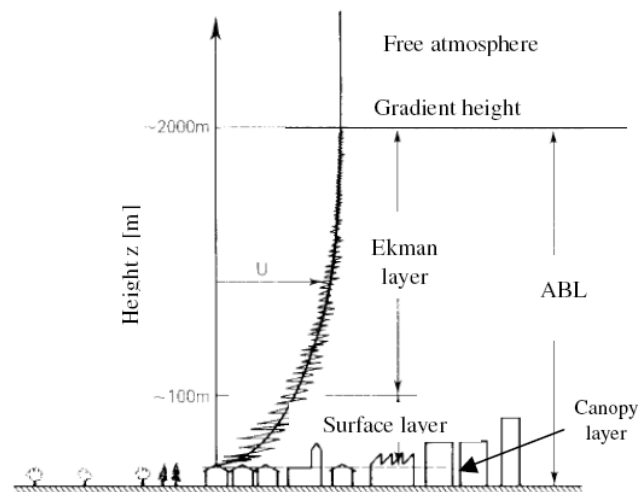


Figure 2. 3: The atmospheric boundary layer (ABL) shear profile [Source: Crasto, 2007].

The roughness of an area often changes with the season of the year due to foliation, vegetation and snow-cover, and then, according to Petersen *et al.* (1997) and Freris (1990), the roughness length must be considered as a climatic parameter. Mortensen *et al.* (1991) and Mortensen *et al.* (2007) have noted how the roughness of different surface affects the retardation of the wind and the wind profile. Figure 2.4 shows that the higher roughness of a city results in greater retardation of the wind in the lower layers and that the effects of roughness extend through a deeper layer.

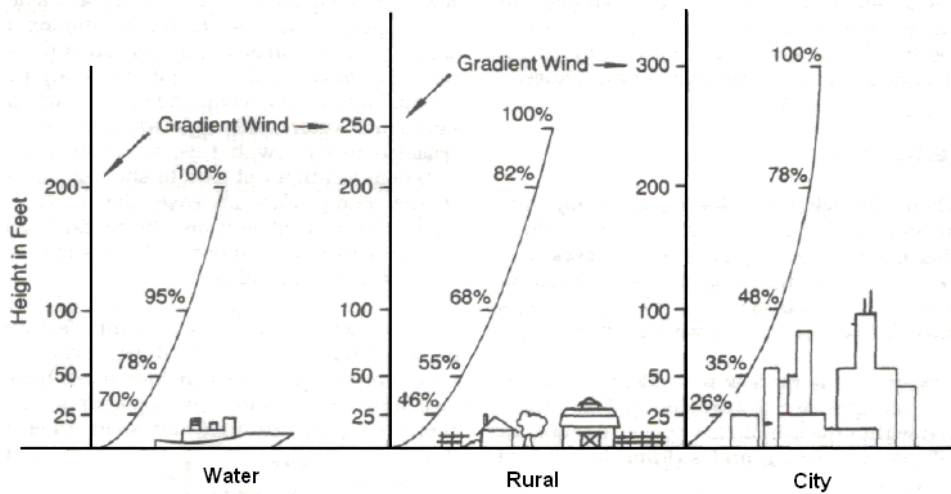


Figure 2. 4: The surface roughness and the change of wind speed with height [Source Fraenkel *et al.*, 1993].

In the ABL wind is retarded by surface roughness (Lipman *et al.*, 1982; Wortman, 1983; Freris, 1990). The friction between the surface and air flow, which generally happens in the first few tens of meters above the surface (Fraenkel *et al.*, 1993; SADC, 1996) weakens the lower layers of wind above them and as a result a change of mean wind speed occurs with height (Lipman *et al.*, 1982; Freris, 1990).

This effect, known as wind shear or vertical wind profile (WMO, 1981; Walker and Jenkins, 1997; Gipe, 2004; Twidell and Weir, 2006), according to Freris (1990) is almost nil above the gradient height typically about 2 000 to 2 500 m, where the wind speeds are dependent only upon the pressure field and altitude.

According to Freris (1990) and Crasto (2007), in the surface layer, the variation of mean wind speed with height, can be adequately represented by the Prandtl logarithmic law model in neutral² conditions,

$$U_0(z) = \frac{u_*}{k} \ln\left(\frac{z}{z_0}\right) \quad (2.6)$$

where u_* is the friction velocity, k is the Von Karman constant (about 0.4), $U_0(z)$ is the mean wind speed at height z and z_0 is the aerodynamic roughness length or just roughness length (Freris, 1990; Crasto, 2007).

The Prandtl logarithmic law model is the basic underlying assumption of the WA^{SP} roughness change method which assumes that within the surface or atmospheric boundary layer (Troen and Petersen, 1989; Freris, 1990), the wind speed grows logarithmically with height (Giebel and Gryning, 2004), and the upwind terrain must be reasonably homogeneous, otherwise a unique surface roughness length to the terrain cannot be assigned (Troen and Petersen, 1988).

The modified Prandtl logarithmic law model that results from eliminating the unknown friction velocity u_* yields the log-law (Freris, 1990) given as,

$$\frac{v}{v_0} = \frac{\ln\left(\frac{h}{z_0}\right)}{\ln\left(\frac{h_0}{z_0}\right)} \quad (2.7)$$

² When the thermal effects are negligible.

where, v_0 and v are the wind speeds at reference height ($h_0 = 10$ m) and new height h , respectively and z_0 is the roughness length. The log-law is approximately applicable up to heights of a few hundred meters (Freris, 1990).

The power law given by $v/v_{\text{avg}}(H) = (h/H)^\alpha$ (Justus *et al.*, 1976; Doran and Verholek, 1978; Spera and Richards, 1979; Lipman *et al.*, 1982; Walker and Jenkins, 1997; Freris, 1990; Gipe, 2004; Shata and Hanitsch, 2006) is an empirical model which is used when simple estimates of the distribution of mean wind speed with height are required. Here v_{avg} and v are the average wind speeds at reference height ($H=10$ m) and new height (h), respectively (Freris, 1990), and α is the wind shear exponent. The wind shear exponent depends on the surface roughness, the range of height and varies with the time of the day, season and stability of the atmosphere (Justus *et al.*, 1976; Spera and Richards, 1979; Gipe, 2004; Hrayshat, 2007).

The variation of the exponent α with surface roughness, and typical values (Table 2.2), is given approximately by,

$$z_0 = 15.25 \exp\left(-\frac{1}{\alpha}\right) \quad (2.8)$$

Freris (1990) stated that despite there being no physical basis for the use of the power law model unlike the log-law model for which there is a theoretical basis, it is widely used and give reasonable good predictions.

Table 2. 2: Typical values of surface roughness length z_0 and power law exponent, α , for various types of terrain [Source: Freris, 1990].

Type of terrain	Z_0 (m)	α
Mud flats, ice	10^{-5} to 3.10^{-5}	
Smooth sea	2.10^{-4} to 3.10^{-4}	
Sand	2.10^{-4} to 10^{-3}	0.1
Snow surface	10^{-3} to 6.10^{-3}	
Mown grass	10^{-3} to 10^{-2}	0.13
Low grass, steppe	10^{-2} to 4.10^{-2}	
Fallow field	2.10^{-2} to 3.10^{-2}	
High grass	4.10^{-2} to 10^{-1}	0.19
Palmetto	10^{-1} to 3.10^{-1}	
Forest and woodland	10^{-1} to 1	
Suburb	1 to 2	0.32
City	1 to 4	

2.5.3 The effect of obstacles

Obstacles such as trees and buildings upwind of the reference (meteorological station) or siting site (turbine site), interrupt the air flow and cause turbulence in their wake (Fig. 2.5) (Fraenkel *et al.*, 1993). The strong effect of obstacles is the decrease of the wind speed, known as the shelter effect.

According to Mortensen *et al.* (1991) the shelter effect extends vertically to approximately three times the height of the obstacle. Fraenkel *et al.* (1993) stated that the turbulent region extends downwind to about 15 to 20 times the height and this effect is more severe for buildings because they present a sharper barrier to the wind and have a higher solidity.

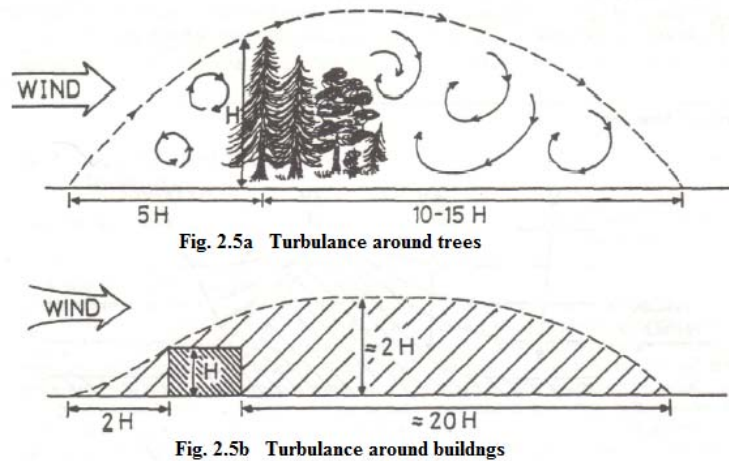


Figure 2. 5: The effect of trees and buildings on the air flow [Source Fraenkel *et al.*, 1993].

Different solidity of the obstacles can be characterized by their porosity, which is the ratio of the area of the windbreak's pores to its total area (Mortensen *et al.*, 1991). According to Troen and Petersen (1989) and Mortensen *et al.* (1991), the porosity (dimensionless) is set to zero for buildings and about 0.5 for trees and 0.33 for a row of similar buildings with a separation between them of $1/3$ their length. Such information must be set up at the obstacle description stage in the modelling.

The wind assessment either for wind data collection or the siting of turbines, must consider the obstacle effect in two different situations: when the point of interest is inside the range mentioned by Mortensen *et al.* (1991), the sheltering must be taken into account, whereas if the point of interest is outside that range the obstacle must be treated as a roughness element (Mortensen *et al.*, 1991).

The shelter effect at a specific site depends upon five characteristics: the height of the point of interest H [m], the distance from the obstacle to the site x [m], the height h [m], the length L [m], and the porosity P of the obstacle (Troen and Mortensen, 1989; Mortensen *et al.*, 1991).

2.5.4 The effect of local winds

The local winds generally are a result of two main factors, namely, thermal and orographic effects. The differential heating of the land and water causes a change in wind flow, which results in the occurrence of land-sea-breezes.

The change of surface roughness influenced by the low roughness of water and the long unobstructed fetch that the wind travels over the water, results in more frequent strong winds along the shores of lakes and coastal zones (Fraenkel *et al.*, 1993, Gipe, 2004). The sea-breeze diminishes rapidly inland and is insignificant more than 3.0 km from the beach (Gipe, 2004). This is related to the high roughness of the inland surface.

The reversal of the wind flow between the two different surfaces, land and water, has a meaningful effect on the wind climatology, and is caused by the differences in thermal properties of the two surfaces. A similar phenomenon occurs in valleys and in mountainous regions resulting in anabatic and katabatic winds. During the day, warmer air rises up into the heated slopes (anabatic winds) and at night the cooler, heavier air descends into the valleys (katabatic winds) (Cheremisnoff, 1978; Fraenkel *et al.*, 1993; Gipe, 2004). This thermal contrast also generates the valley and mountain breezes, which blow up and down the longitudinal axes of valleys respectively.

Both the local thermal and topographically-induced winds can have a significant influence on wind energy applications by enhancing the gradient winds.

2.6 Numerical modelling of wind energy

Wind field simulation models are widely available and can be subdivided into two main groups: the diagnostic (equations with no time-dependent terms) and prognostic models (full time-dependent equations), and both are summarized in four main classes by Finardi *et*

al. (1997) as linearized models, mass consistent models, hydrostatic models and non-hydrostatic models.

The linearized models, of which the WA^sP model is an example, stem from the original work of Jackson-Hunt (Walmsley *et al.*, 1990; Mortensen *et al.*, 1991; Finardi *et al.*, 1997; Mortensen *et al.*, 2007). They are based on linearized solutions of the dynamic equations for the boundary-layer perturbed by terrain under conditions of neutral atmospheric stability.

The advantage of linearized models is their very limited computer requirements. They can normally run on personal computers (PC), and are fast and easy to use. They require a very small amount of input data such as topography and roughness length description in raster format (2-D arrays of data) or vectorial format (isopleths), a time series of wind speed and direction data at a given height or wind and temperature vertical profiles (Finardi *et al.*, 1997).

The main drawbacks of these models are their inability to describe the flow in the lee region of a hill where turbulent wakes and separation develop, and they also cannot be applied over mountains where slopes are too steep and the topography too complex (Finardi *et al.*, 1997).

Another limitation of this class of models is the usual hypothesis of a horizontally uniform oncoming wind and topography that has to be flat or periodic at model domain boundaries due to the Fourier transformation technique which is applied to solve the differential equations (Finardi *et al.*, 1997).

The mass-consistent models, examples of which are the WINDS (Wind-field interpolation by non-divergent schemes) and NOABL (Numerical Objective Analysis of Boundary Layer) models (Finardi *et al.*, 1997; Gallino *et al.*, 1998) are widely used in applied problems like air pollution and wind energy (Finardi *et al.*, 1997).

According to Finardi *et al.* (1997) and Burlando *et al.* (2007), these models reconstruct 3-D wind fields from vertical profiles and near-ground wind measurements, through the interpolation of wind observations to the computational mesh, which is adjusted to satisfy mass conservation by the least amount of modification. In these kind of models the wind data interpolation method is crucial to determine the final wind field features. For local scale applications, the incompressible form of the continuity equation, $\partial u/\partial x + \partial v/\partial y + \partial w/\partial z = 0$ (Wallace and Hobbs, 1977) is normally used.

Some advantages of these models are their intrinsic simplicity, which means they have no theoretical application limits and, therefore, can be applied to any kind of terrain and they are able to describe effectively and clearly the main features of a wind field over complex terrain (Finardi *et al.*, 1997). They can run on a PC, and can be used in applications dealing with very long time periods and large computational meshes (Finardi *et al.*, 1997).

The main drawbacks, according to Finardi *et al.* (1997), are their dependence on the availability of good site input data that is relatively more than linearized models. The data required are namely: topography and roughness length data over the computational domain, wind speed and direction from a number of surface stations, vertical wind profiles and/or upper air data, as well as surface and upper air temperature data.

The hydrostatic models, of which the MM4 (Fourth-Generation NCAR/Penn State Mesoscale Model) is an example, use a simplification of the vertical equation of motion that consists of neglecting the vertical acceleration and considering only the pressure gradient and the gravitational terms. This implies that the vertical scale of motion has to be smaller than the horizontal scale (Finardi *et al.*, 1997).

Previous studies (Finardi *et al.*, 1997) stated that hydrostatic models can describe thermal circulations like land/sea breezes, as well as stable stratified flow over complex terrain of moderate steepness (less than 45°).

They should not be applied to sites characterized by very complex terrain or in the local to micro-scale range (grid size less than 1-3 km). In addition, their applicability depends not only on the geometry of the wind field, but also strongly on the vertical stability and therefore on the time of day and season (Finardi *et al.*, 1997). They require variable computer resources and can run on a workstation if a real-time forecast is not needed.

The non-hydrostatic models, of which the KAMM (Kalsruhe Atmospheric Mesoscale Model) and MM5 (Fifth-Generation NCAR/Penn State Mesoscale Model) are examples, are considered the new generation models in the framework of applied studies. They use the full set of equations describing atmospheric motions (Finardi *et al.*, 1997).

The advantages of these kind of models are that they have no direct limitations due to terrain slopes or scales and are the most suitable models to describe the atmospheric flow over complex terrain. Their main drawbacks are the large computer resources and long periods of time taken for simulations. The model simulations have to be performed on super-computers or parallel machines, while only short-time simulations can be run on workstations (Finardi *et al.*, 1997).

The input data for both hydrostatic and non-hydrostatic models are the vertical profiles of wind, temperature, humidity and gridded meteorological fields provided by large-scale models (Finardi *et al.*, 1997).

2.6.1 Background to the WA^sP model

The Wind Atlas Analysis and Application Program (WA^sP) is a PC program that performs the horizontal and vertical extrapolation of wind data from meteorological stations considering the roughness, sheltering effect of obstacles and terrain height variation (orography) effects to calculate the regional wind climate at a reference site and thereafter to predict the wind resources for the prediction sites. It also identifies the best sites for wind turbine siting.

The model provides a user with the means to correct the wind climate data measured at a specific point (meteorological station) to site specific conditions. It also offers tools for the detailed siting of wind turbines (Mortensen *et al.*, 1991).

Its development is ascribed to the Danish wind atlas group who presented the basic surface wind statistics, together with detailed procedures for estimating the wind speed distribution at a particular site and height (Mortensen *et al.*, 1991).

Worldwide, WA^SP has been used for wind power assessment and siting (Troen and Petersen, 1989; Dube, 1994; Mortensen *et al.*, 2003; Esteves, 2004; Bowen and Mortensen, 2004; Migoya *et al.*, 2007; DNER, 2008), as well as the validation of assessments performed by other models (Mortensen *et al.*, 2005; Palma *et al.*, 2008; Narayana, 2008).

2.6.1.1 The principles of the WA^SP model

Generally the WA^SP model is implemented in four modules (Mortensen *et al.*, 1991), which can be summarized in three main applications.

1. Analysis with two modules:
 - Firstly, an option of the analysis of raw data enables an analysis of any time-series of wind measurements to provide a statistical summary of the observed, site-specific wind climate into a velocity frequency distribution and in Weibull parameters (Mortensen *et al.*, 1991; Mortensen *et al.*, 2007). This output table summary is known as the observed wind climate (OWC) and the data are the meteorological data input to WA^SP. The analysis is implemented in separate sub-routines: the Observed Wind Climate (OWC) Wizard or the WA^SP Climate Analyst (Mortensen *et al.*, 2007).

- Secondly, an option allows the generation of the wind atlas data. In this option, the OWC can be converted into the regional wind climate (RWC) or wind atlas data sets (WADS). At this stage, the wind observations are cleaned or corrected with respect to site-specific conditions and reduced to some standard conditions. The WADS are therefore site-independent and the wind distributions have been reduced into four standard roughness classes and five standard heights a.g.l. (Troen and Petersen, 1989; Mortensen *et al.*, 1991; Mortensen *et al.*, 2007).
2. Application with two modules:
- The first module permits the wind climate estimation. It uses a wind atlas calculated by WA^{SP} to estimate the wind climate at any specific point, performing the inverse calculation to that used to generate the wind atlas. By introducing descriptions of the terrain around the predicted site, the models can predict the actual expected wind climate at this site (Troen and Petersen, 1989; Mortensen *et al.*, 1991; Mortensen *et al.*, 2007). The wind climate is estimated in terms of the Weibull parameters and the sector-wise distribution of the wind.
 - The second module enables the estimation of the wind power potential. This option of WA^{SP} calculates the total energy content of the mean wind. In addition, an estimate of the actual, annual mean power production of a turbine can be obtained by inputting the power curve of the wind turbine in question (Troen and Petersen, 1989; Mortensen *et al.*, 1991; Mortensen *et al.*, 2007).
3. Wind farm application as a single module:
- This module enables one to calculate the wind farm production. This option of WA^{SP} estimates the wake losses for each turbine on a farm and thereby the annual energy production of each wind turbine and of the entire farm by inputting the thrust coefficient curve of the wind turbine and the wind farm layout (Mortensen *et al.*, 1991; Mortensen *et al.*, 2007). This module also enables one to map the wind and energy resource potential for the selected domain.

2.6.1.2 The sub-models of WA^sP

The functioning of WA^sP is integrated into five distinct sub-models (Fig. 2.6):

(1) The roughness change sub-model

According to Mortensen *et al.* (1991), this model operates by considering that downstream of the change in surface roughness, an internal boundary layer develops and the wind profile slowly adjusts to the new surface (Fig. 2.7). In addition, this sub-model can take into account up to ten consecutive changes in surface roughness in each wind directional sector analysed.

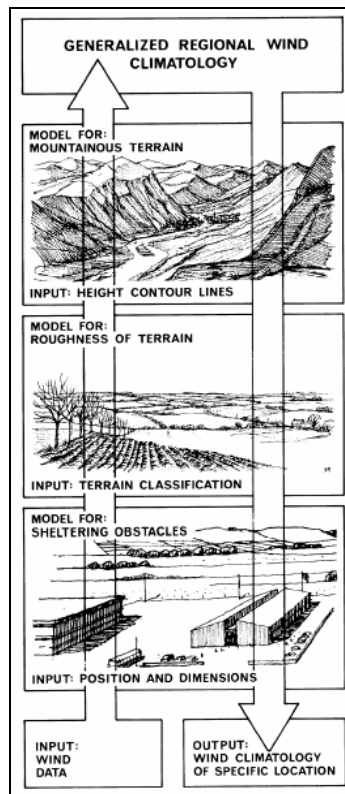


Figure 2. 6: The wind atlas methodology [Source: Mortensen *et al.*, 2007].

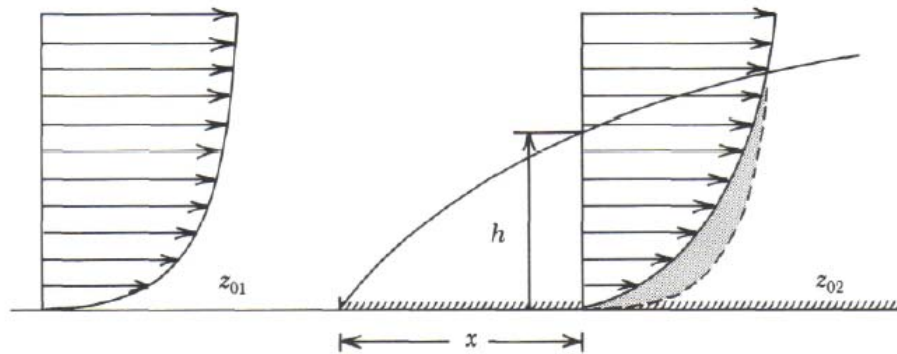


Figure 2. 7: Ideal flow with a change of roughness class and the modified profile with the height of the internal boundary layer h as function of x [Source: Troen and Petersen 1989].

The roughness of the surface is determined by the size and distribution of the roughness elements it contains (Troen and Petersen, 1989; Mortensen *et al.*, 1991, Mortensen *et al.*, 2007). For example, the roughness of the terrain is commonly parameterized by a length scale called the roughness length, z_0 (Table 2.3).

(2) The shelter sub-model

This sub-model can handle up to fifty obstacles at the same time (Mortensen *et al.*, 1991). Mortensen *et al.* (2007) states that investigations done by Taylor and Salmon in 1993 indicate that the shelter model of WA^sP is likely to overestimate the shelter provided by 3-dimensional obstacles.

Most anemometers that are often used for wind energy assessment, are meteorological stations which are sited at one standard height, 10 m a.g.l. (Ahmed and Abouzeid, 2001; Twidell and Weir, 2006; Hrayshat, 2007; Carta *et al.*, 2008) and are often sited close to buildings. Therefore, the shelter effect is potentially important in the analysis of wind data acquired from these stations.

Table 2. 3: Roughness length, surface characteristics and roughness class according to the European wind atlas [Source: Troen and Petersen, 1989; Mortensen *et al.*, 1991].

Z ₀ [m]	Terrain surface characteristics	Roughness class
1.00	City	3
0.80	Forest	
0.50	Suburbs	
0.40		
0.30	Shelter belts	2
0.20	Many trees and /or bushes	
0.10	Farmland with close appearance	1
0.05	Farmland with open appearance	
0.03	Farmland with very few buildings, trees etc.	0
0.02	Airports areas with buildings and trees	
0.01	Airport runway areas	
0.008	Mown grass	
0.005	Bare soil (smooth)	
0.004		
0.003		
0.002		
0.001	Snow surface (smooth)	
0.0007		
0.0005		
0.0003	Sand surface (smooth)	
0.0002		
0.0001	Water areas (lakes, fjords, open sea)	

Mortensen *et al.* (1991) stated that in order to decide whether to include obstacles in the terrain as sheltering obstacles or as roughness elements, WA^sP requires that if the point of interest (anemometer or wind turbine) is closer than 50 obstacle heights to the obstacle and closer than about three obstacle heights to the ground, the object should be included as an obstacle. In this case the obstacle cannot, at the same time, be considered as a roughness element. But if the point of interest is further away than about 50 obstacle heights or higher than about three obstacle heights, the obstacle should be included in the roughness description.

The sheltering or shadowing effects sometimes are known quantitatively from measurements at the site. Such knowledge must be supplied directly to WA^sP through the site description at the site visit stage (Table 2.4). An aerial photograph or a detailed map of the point of interest might be helpful, if available.

Table 2. 4: Porosity of obstacles [Source: Troen and Petersen, 1989; Mortensen *et al.*, 1991].

Porosity P	Obstacles and Windbreak appearance
>0.5	Open
≈ 0.5	Trees
0.35–0.5	Dense
<0.3	Very dense
0.33	Row of similar buildings (separated between them of 1/3 the length of the building)
0	Solid (Wall/buildings)

(3) The orographic sub-model

This sub-model, according to Troen and Petersen (1989), calculates firstly the potential flow perturbation induced by the terrain. In addition, Mortensen *et al.* (1991) described the orographic model³ as a high resolution flow model, the so-called Bessel Expansion on a Zooming Grid model (BZ-model), for flow in complex terrain. It is a linearized spectral model based on the Jackson-Hunt theory (Walmsley *et al.*, 1990).

The BZ-model employs a polar computational grid and calculates the wind velocity perturbations induced by orographic features such as single hill or more complex terrain only at the centre point (Mortensen *et al.*, 1991; Walmsley *et al.*, 1990). This model, instead of calculating the Fourier coefficient (Walmsley *et al.*, 1990), which is the typical analysis methodology and transformation employed by linearized models (Finardi *et al.*, 1997), computes the coefficient of Fourier-Bessel expansion for the potential flow perturbation on the polar grid with 100 radius and 72 azimuths (5° intervals) (Walmsley *et al.*, 1990).

According to Mortensen *et al.* (1991), the BZ-model was developed for the specific purpose of wind energy siting. It was designed to directly accept arbitrarily-chosen contour lines as input and to integrate the estimation of grid-point values and the numerical integrations into one process with the following features:

- Firstly, it employs a high-resolution, zooming, polar grid. This is coupled with a map analysis routine, in order to calculate the potential flow perturbation profile at the central point of the model;
- Secondly, it integrates the roughness conditions of the terrain surface into the spectral or scale decomposition. The inner layer structure is calculated using a balanced condition between surface stress, advection and the pressure gradient; and

³ The map size can have an influence on the sensitivity of WAsP therefore according to Bowen and Mortensen (2004), a minimum area of about 6x6 km² is recommended, depending on site complexity.

- Thirdly, it uses an atmospheric boundary layer thickness of about 1 km to force the large-scale flow around high resolution areas.

Mortensen *et al.* (1991) and Mortensen *et al.* (2007) have stated that for complex terrain, the effect of the flow must be taken into account and the height variations around the site must be described as well. In such a case, the input to the model is the height of the terrain at each grid point and it is more convenient to represent the terrain heights by contour lines given on the standard topographic map in meters.

Special care is recommended by Mortensen *et al.* (1991) and Mortensen *et al.* (2007) when the site is right at the top of a hill or a ridge. The highest contour line should enclose the site and, in this way, it defines the hill-top precisely.

(4) The wind atlas analysis sub-model

This sub-model performs wind statistics correction of the observed wind statistics by employing the above-mentioned models. The result is an atlas data of wind climate in the form of Weibull tables, corresponding to the standard azimuth sectors, heights and surface roughness conditions.

According to Mortensen *et al.* (1991), the sub-model uses the empirical relations between the wind over homogeneous terrain and the overlying large-scale synoptic scale wind. The data are extrapolated to yield the geostrophic wind climate for the region of the selected point in a 100 square kilometer domain, which is referred to as upward transformation in the WA^SP model (Fig. 2.6, page 43).

Secondly, the data are analysed in terms of the Weibull distribution function and generate the Weibull parameters which constitute the wind atlas data in the region of the selected point. Mortensen *et al.* (1991) also state that this sub-model can use either surface data or upper-air data as input to generate a wind atlas data in WA^SP.

(5) The wind atlas application sub-model

This sub-model performs the inverse calculation employed by the wind atlas analysis sub-model (downward transformation in Figure 2.6, page 43), which estimates the actual wind climate at a specific site and standard height over an surface roughness. It generates outputs in terms of the Weibull parameters and the sector-wise distribution of the wind.

The predicted wind and power potential and wind farm production are outputs of the wind atlas applications sub-model. The first estimates the wind climate at a turbine site and the predicted power production, also known as annual energy production (AEP) is based on the regional wind climate (RWC), the site description and power curve of a typical wind turbine.

The second calculates the wind farm production and estimates the wake losses for each turbine on farm land, and thereby the total annual energy production, given the thrust coefficient curves of the wind turbine and the wind farm layout.

The wind and energy resource grid is also another application of the wind atlas application sub-model. This enables one to calculate a spatial summary prediction of the wind climate for a selected rectangular domain for a spatial representation pattern of wind and energy resources (mean annual wind speeds, power density and annual energy production) by specifying the location of the grid and the spatial resolution (Mortensen *et al.*, 2009).

The wind power potential from a given wind turbine at a given site is estimated by using the wind turbine power curve $P(v)$. This is the power produced as a function of the wind speed at hub height, as well as the probability density (or distribution) function (PDF) $P_r(v)$ of the wind speed at hub height, which gives the frequency of occurrence of a given wind speed.

The product of these two functions, $P(v)$ and PDF, gives the power density curve, which is an integral of the mean power production (Troen and Petersen, 1989; Mortensen *et al.*, 2007). This integral according to Mortensen *et al.* (2007) is evaluated by WA^sP in terms of

the Weibull distribution parameters by approximating the power curve to a piecewise linear function.

Troen and Petersen (1989) stated that for a power curve $P(v)$ that is measured for a wind turbine, the mean power production P [MWh] can be estimated. It is known as the PDF of the wind speed at hub height which can be determined by measurements or a siting procedure such as:

$$P = \int_0^{\infty} P_r(v)P(v)dv \quad (2.9)$$

In that case the PDF is determined by a siting procedure, then it is given as a Weibull function and therefore the expression of the mean power production becomes (Troen and Petersen, 1989; Mortensen *et al.*, 2007):

$$P = \int_0^{\infty} \left(\frac{k}{c}\right) \left(\frac{v}{c}\right)^{k-1} \exp\left[-\left(\frac{v}{c}\right)^k\right] P(v)dv \quad (2.10)$$

The power production of a wind turbine is a function of the available wind that strikes the rotor and is calculated for the interval of wind speed between the cut-in and the cut-out speeds.

According to Troen and Petersen (1989) and Mortensen *et al.* (2007), if the wind speed is less than the cut-in speed, the turbine cannot produce power, but when the wind speed is higher than the cut-in speed, the power output $P(U)$ increases with increasing wind speed to a maximum value (the rated power) and thereafter the output is almost constant. At wind speeds higher than the cut-out speed, the wind turbine is stopped to prevent structural failures.

2.6.3 Application of WA^sP model in wind energy assessment

The WA^sP model has been implemented successfully for wind power assessment and sitting in various partes of the world. Troen and Petersen (1989) implemented the WA^sP model to generate the European Wind Atlas, which also gives a theoretical background of the WA^sP implementation methodology.

In South Africa, WA^sP model has been implemented successfully by Jury and Diab (1989) and Botha (1989). Diab and Killick (1991) implemented the WA^sP to model windflow at Saldanha Bay area, and the results have shown that are comparable with those derived from NOABL and UVMM models. Denison (1990), in a study in Soetanyberg at Cape Town, has shown that the results of the model compare weel with field data. Diab *et al.* (1992), in the demonstration of wind energy project at Mabibi Primary School, used wind data from a station situated at Mission Rocks to model wind speeds at Mabibi using WA^sP model. Dube (1994) implemented the WA^sP model to assess the wind energy potential in Maputaland. The study findings were that the coastal plain which is relatively flat is characterized by higher mean wind speeds of between 4.8 and 6.1 ms⁻¹ at sites adjacents to the coast, while inland sites had mean wind speeds closer to 4.5 ms⁻¹.

Mortensen and Petersen (1997) explored the influence of terrain ruggedness and characteristics of the topographical input data in the accuracy of WA^sP predictions in rugged and mountainous terrain using data from northern Portugal and France. The study found that WA^sP may give accurate results outside its operational limits, provided that the difference in ruggedness indices between the reference and predicted sites is small and the topographical input data are adequate and reliable.

Lange and Højstrup (2001), using the WA^sP model, validated modeled data at the offshore sites in the Danish Baltic sea region where the wind resources estimated from measurements were compared to WA^sP predictions and they agreed well. Esteves (2004) developed a GIS data base for wind power potential in Portugal implementing WA^sP and MM5 models to generate the wind power potential resource maps.

Mortensen *et al.* (2005) used the WA^SP and KAMM models to produce the wind atlas of Egypt. Migoya *et al.* (2007) implemented the WA^SP model to assess the wind energy resource in the Madrid region and as a result of the successful application of the model, four wind farms with a capacity of 94 MW were licensed.

In Mozambique, DNER (2008) with support of Danida with RISO as technical consultant was implemented the WA^SP model to support for wind power development in Mozambique. The assessment findings based on wind data for Mozambique from the global meteorological database provided by NCEP/NCAR, was that the best wind resources in Mozambique is expected to be found along the coastline in the south of Mozambique and the wind resources is expected to decrease with the distance from the sea, but this has neither been verified nor quantified. The study revealed also that the wind resources along the coastline in the south of country correspond to annual wind power generation of 2 to 2.5 GWh per MW installed wind power capacity. In addition, the costs estimated in 2008 revealed that the total investment for large-scale wind power are estimated at €2 million per MW of installed wind power at 100 to 200 €/MWh generation. Narayana (2008) validated the wind resource assessment model (WRAM) map of Sri Lanka using measured data to evaluated the wind power generation potential through WA^SP model.

2.7 Summary

This chapter has given a background on wind energy and the factors that have an influence on the wind climate such as topography, roughness, obstacles, and local winds. The most widely used models for the estimation of wind speed and energy potential and the extrapolation of wind data over space considering the aforementioned effects were also outlined. A brief overview of the different techniques employed in wind energy assessment studies, as well as a detailed discussion of the WA^SP model used in this study, is highlighted. The application of the WA^SP model in different studies and assessment of wind

energy in various parts of the world is briefly outlined as evidence that it is one most widely used tool for wind energy assessment in the world.

CHAPTER THREE

DATA AND RESEARCH METHODOLOGY

3.1 Data

3.1.1 Introduction

A brief overview is provided of all meteorological stations in Mozambique which collect wind data, with the aim of justifying the selection of the potential meteorological stations to be used as input for modelling. Mean annual wind speeds and mean seasonal and mean diurnal wind speed patterns are presented and analyzed with respect to an annual mean reference threshold wind speed of 3.0 ms^{-1} (Sahin, 2004).

3.1.2 Wind data and data quality

Meteorological Services (NMS) in Mozambique have two classes of meteorological stations which collect wind data: Class 1 (synoptic) and Class 2 (climatological). The meteorological stations that collect and provide hourly averaged wind data sets are the synoptic stations (or Class 1). The ideal distance between such stations averages 150 to 200 km (WMO, 1970). Class 2 or climatological stations collect and provide wind data at three hourly intervals and the ideal average distance between such stations is 50 to 60 km (WMO, 1970).

The data series used in this study (Table 3.1) are the data sets of both wind speed and direction collected by the Instituto Nacional de Meteorologia (INAM) at 10 Class 1 meteorological stations. All data are measured at a height of 10 m above ground level (a.g.l.). In addition, data are available from the National Department of New and Renewable Energy (DNER) from two meteorological masts (Ponta de Ouro and Tofinho), sited for the specific purpose of wind energy assessment data collection. At these two

stations, wind data are measured at three different heights, *viz.* 10 m, 20 m and 30 m a.g.l. (Plate 3.1).

Data from the INAM stations were only available in hard copy format. For the purpose of this study, data were transferred to electronic format for a period of two years. It was not possible to extend the period due to the considerable effort involved in converting the data.

Table 3. 1: Meteorological stations that collect hourly wind speed.

Station Name	Designation	Data period	Period	Long(°)	Lat (°)	Alt (m)
Beira	Class1	2 years	2006-2007	34°54′	-18° 48′	8
Inhambane	Class1	2 years	2001-2002	35° 23′	-23° 52′	14
Lichinga	Class1	2 years	2006-2007	35° 14′	-13° 18′	136
Maputo Mavalane	Class1	2 years	2006-2007	32° 34′	-25° 55′	39
Nampula	Class1	2 years	2006-2007	36° 53′	-17° 53′	6
Pemba	Class1	2 years	2006-2007	40° 32′	-12° 59′	101
Ponta de Ouro	ME-Mast	1 year	2007/2008	32° 53′	-26° 44′	30
Quelimane	Class1	2 years	2006-2007	36° 53′	-17° 53′	6
Tete	Class1	2 years	2006-2007	33° 35′	-16° 11′	149
Tofinho	ME-Mast	1 year	2007/2008	35° 33′	-23° 52′	30
Vilankulo	Class1	2 years	2002-2003	35° 19′	-22° 00′	20
Xai-Xai	Class1	2 years	2006-2007	33° 38′	-25° 03′	4



Plate 3. 1: Ponta do Ouro meteorological mast looking towards the east [Source: DNER, 2008; Photo by Risø, 2007].

Most of the meteorological stations (7) are located in the coastal zone, with the exception of Tete, Lichinga and Nampula, which are situated in the interior. Quelimane is located about 20 km from the coast (Fig. 3.1). Furthermore, 90% of Class 1 meteorological stations are situated at the main airports of the provincial capitals.

The wind speed is captured by a cup anemometer and the mean wind speed and direction are recorded every 10 minutes and averaged on an hourly basis at the INAM stations. These data are stored as hourly values.

The majority of the INAM stations still use the anemography of R. Fuess (Fig. 3.2a), which measures the wind velocity and gust. Some are automatic weather stations (AWS) and use the VAISALA anemometer WAA151 (Fig. 3.2b), with a measuring range between 0.4 and 75 ms^{-1} , a starting threshold of 0.5 ms^{-1} and accuracy within 0.4 - 60 $\pm 0.17\text{ms}^{-1}$ (VAISALA, 2002). Most of the AWS are situated at the main airports alongside runways (Plate 3.2).

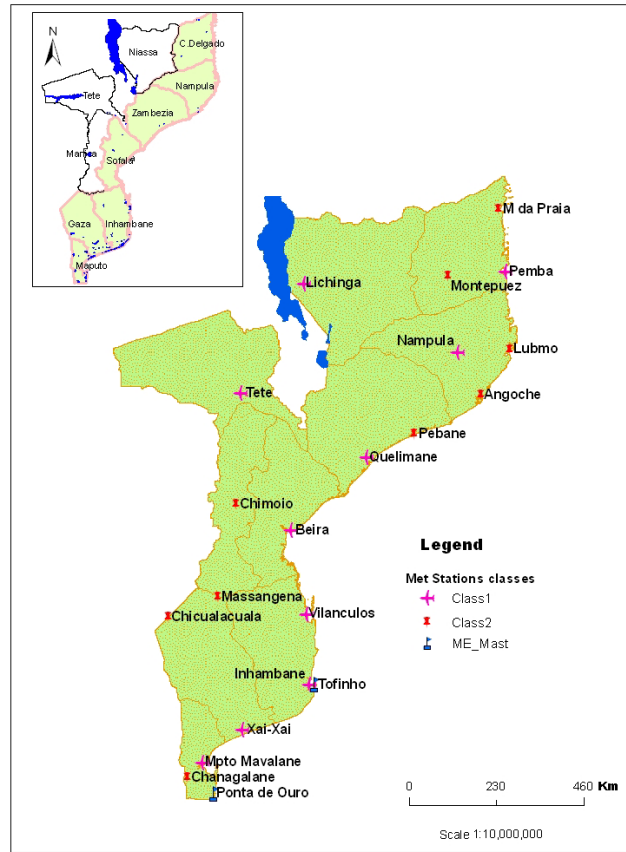


Figure 3. 1: Geographic location of stations collecting wind data.



Figure 3. 2a: Anemography Universal 82a [Source: Fuess, 1956].

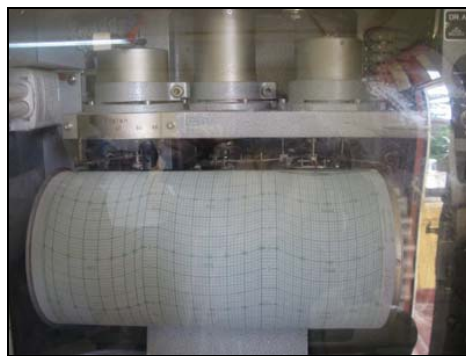


Figure 3. 2b: Anemometer WAA151 [Source: VAISALA, 2002].



Plate 3. 2: Mavalane anemometer viewed towards the east (E) [Photo: Author, 2009].

All the data were checked visually for quality control and to verify missing data, which may have been due to instrument failure or other technical reasons related to human error or local operational procedures where the meteorological staff office is located. From this procedure, it was found that there were no observations recorded at Inhambane from 22:00 to 04:00, which represented 13.6% of zero and 31.3% of missing observations for the whole period of analysis.

At Vilankulo, a district airport, 15.6% of the observations were missing and 20.5% exhibited zero readings. The zero values of both speed and direction were also found mostly from 01:00 to 07:00, most likely because it is not a full-time operational airport. Therefore, at both the Vilankulo and Inhambane stations (Plate 3.3), the mean and prevailing wind direction might not be the expected, due to zero, and missing, observations.

At Tofinho, 19.73% of the data was also found to be missing. This figure represented 38 consecutive days between the end of October and the beginning of December in 2007 when no recording was done as the data logger was off.

Data availability for all twelve stations that collect hourly wind speed and direction, are summarized in Table 3.2. From this it is noted that data availability varies between 67% at Inhambane and 100% at Pemba, Nampula, Quelimane and Ponta de Ouro.



Plate 3. 3: Inhambane meteorological station (left) and Vilankulo anemometer (right) [Photo: INAM, 2008].

Table 3. 2: Summary statistics of wind speed at the synoptic stations.

Station	Period (year)	Fr (%)		Total n° of Hours	Mean annual speed (ms ⁻¹)	Peak time (hour)
		Calm speed	Data Availability			
Beira	2006	6.5	96	8,760	3.50	15:00
	2007	8.6	98	8,760		
	All	7.6	97	17,520		
Inhambane	2001	14.9	71	8,760	3.35	12:00
	2002	12.4	67	8,760		
	All	13.7	69	17,520		
Lichinga	2006	2.5	99	8,760	3.90	11:00
	2007	2.1	99	8,760		
	All	2.3	99	17,520		
Maputo Mavalane	2006	8.5	92	8,760	4.31	15:00
	2007	8.6	88	8,760		
	All	8.6	90	17,520		
Nampula	2006	0.1	100	8,760	3.00	11:00
	2007	0.2	100	8,760		
	All	0.2	100	17,520		
Pemba	2006	1.4	100	8,760	3.70	16:00
	2007	2.4	99	8,760		
	All	1.9	100	17,520		
Ponta de Ouro	2007/08	16.7	100	8,829	4.91	16:00
Quelimane	2006	23.4	99	8,760	2.40	12:00
	2007	26.4	100	8,760		
	All	22.9	100	17,520		
Tete	2006	56.5	99	8,760	1.51	13:00
	2007	56.6	98	8,760		
	All	56.5	98	17,520		
Tofinho	2007/08	0.4	80	8,796	6.58	17:00
Vilankulo	2002	16.2	73	8,760	3.25	9:00
	2003	15.1	98	8,760		
	All	15.6	85	17,520		
Xai-Xai	2006	35.6	99	8,760	2.09	12:00
	2007	36.1	99	8,760		
	All	35.8	99	17,520		

3.1.3 Wind observations

It is well known that the wind speed varies with time of the day, the season of the year, from year to year and with height above the ground (Jamil *et al.*, 1995; Walker and Jenkins, 1997; Gipe, 2004; Himri *et al.*, 2008). Therefore, the mean annual (Table 3.2), mean

diurnal (Fig. 3.3) and mean monthly wind speeds for the meteorological stations recording hourly wind data were calculated.

All the meteorological stations, except Quelimane, Tete and Xai-Xai, have an annual mean wind speed of 3.0 ms^{-1} or higher. The inland location of two meteorological stations (Nampula and Tete), as well as likely sheltering effects at Quelimane, and Xai-Xai might be the reason for the low mean wind speeds.

Tofinho and Ponta de Ouro have higher mean hourly wind speeds of between 3.5 and 6.0 ms^{-1} (Ponta de Ouro) and between 6.0 and 7.3 ms^{-1} (Tofinho) throughout the day (Fig. 3.3). The mean monthly wind speed is between 4.0 and 8.0 ms^{-1} throughout the year (Fig. 3.4).

Figure 3.3 illustrates the mean diurnal wind speed profile, where Beira, Lichinga, Maputo Mavalane, Pemba and Vilankulo have a significant number of hours with wind speeds greater than or equal to 3.0 ms^{-1} . Figure 3.4 shows the variation in mean monthly wind speeds for all stations. Generally, mean monthly wind speeds vary by less than 2.0 ms^{-1} from the lowest to the highest, although Tofinho shows relatively greater variability.

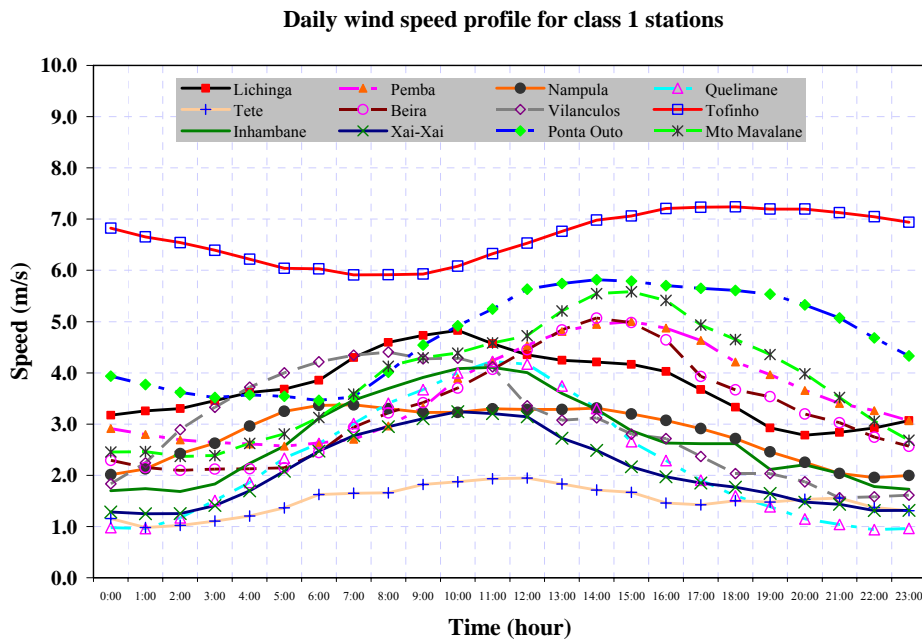


Figure 3. 3: Mean diurnal wind speeds for Class 1 meteorological stations.

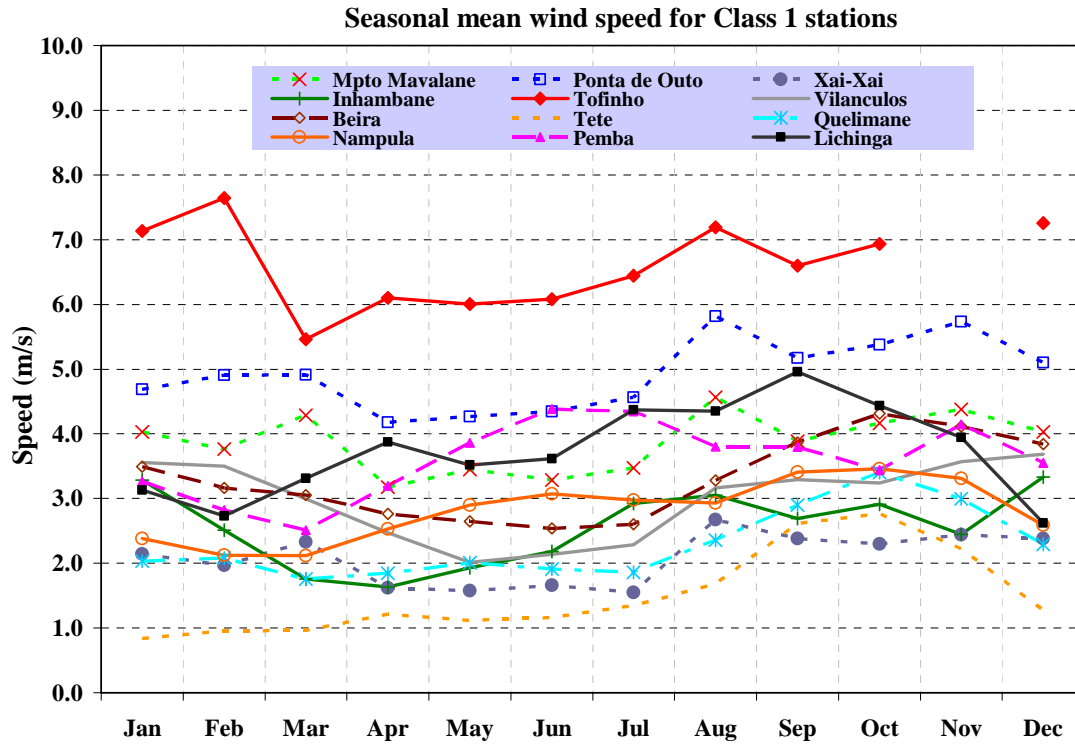


Figure 3. 4: Mean monthly wind speeds for Class 1 meteorological stations.

The estimates of the world-wide wind energy resource distribution published many years ago (WMO, 1981) revealed that for Mozambique there was more wind and wind energy potential in the coastal zone. However, this should not lead to the conclusion that the wind resource in the interior of the country is inadequate. On the contrary, Lichinga and Nampula meteorological stations are examples of interior stations with annual mean winds speed above 3.0 ms^{-1} .

From Figure 3.3 and Figure 3.4, is clear that the coastal meteorological stations represent sites with relatively greater wind resources that could be harnessed for wind power generation. This concurs with the results of WMO (1981) for Mozambique that estimated wind speeds of about 4.4 ms^{-1} at a 10 m height and about 5.6 ms^{-1} at a 50 m height a.g.l. throughout the coastal zone of the country.

3.1.4 Meteorological station selection criteria for modelling

The starting point for this study was an overview of the wind observations in Mozambique. Only twelve meteorological stations throughout the country were collecting hourly wind data sets (Table 3.2). These data sets were evaluated in terms of their quality (absence of zero and missing observations) and calculated annual mean wind speeds as well as their the monthly and diurnal mean wind distributions.

Three stations (Xai-Xai, Tete, an Quelimane) were excluded as candidate sites due to their low mean annual wind speeds; they were below the threshold of 3.0 ms^{-1} . Inhambane was excluded as a result of poor data availability ($< 70\%$) and sheltering by obstacles (trees and buildings around).

Of the eight remaining stations, all had a minimum one and two year data record and all were checked in terms of their anemometry siting; *viz*, well-exposed anemometer, distance from buildings and other obstacles. All were candidate potential sites.

Finally, it was decided to focus the modeling on two regions of Mozambique; the southern region where mean wind speeds were the highest (Ponta de ouro, Mavalane, Tofinho and Vilankulo) and the northern region (Nampula, Pemba and Lichinga) where relatively little research has been conducted. The central region encompassing Beira was eliminated and left for further studies.

3.1.5 Summary

A background has been given of the kind of meteorological data sets, the height at which they are collected, the class of meteorological stations that collect it and their geographical location.

The selection criteria of the potential modelling stations were based on a reference threshold annual mean wind speed of 3.0 ms^{-1} or higher, and with more than one third ($1/3$)

to half of the day with consecutive hours and wind speeds above the same threshold. Data availability was also an important factor.

It was found that at the northern region of Mozambique Lichinga, Nampula (interior areas) and Pemba (coastal area), Vilankulo, Tofinho Mavalane and Ponta de Ouro (coastal areas) at the southern region are potential stations suitable for modelling.

3.2 Research methodology

3.2.1 Introduction

The wind is a very local characteristic, influenced by the topography and by change of the surface roughness. Its measurement takes a long time to obtain a climatological estimate and is costly to carry it out. This limitation is also accompanied by the low density of meteorological stations, particularly in remote inland areas.

However, the rising interest in renewable energy, with special reference to fast-growing wind energy technology and improvements in wind turbine technology, has forced the development of a number of techniques to overcome this limitation by providing a means of predicting the wind climate at specific sites without measurements at those sites (Petersen *et al.*, 1997).

This section discusses the methodology based on the WAsP, model that was implemented in this study to overcome the shortcomings of the measured data.

3.2.2 Technique of wind energy assessment

There are many techniques that are employed in wind energy assessment studies, ranging from inferential techniques to sophisticated techniques that involve modelling the wind.

Statistical modelling techniques of wind speed for wind energy estimates have been undertaken, and the most successful one is the Weibull distribution model (Justus *et al.*, 1976; Hennessey, 1977; Lun and Lam, 2000; Gipe, 2004; Twidell and Weir, 2006; Zaharim *et al.*, 2009a).

Nevertheless, with the rising interest in renewable energy resources, the use of numerical models in recent wind energy studies has become popular due to the fact that models provide an objective method by including the characteristics and effects of terrain (shape, roughness, and slope) on airflow to interpolate wind data from sites where measurements do exist, to locations where measurements do not exist (Petersen *et al.*, 1997).

The WA^SP model is one such example most often used and it is considered the standard method for wind resource prediction on land (onshore) and offshore (Lange and Højstrup, 2001; Ackermann and Söder, 2002; Esteves, 2004; Sahin, 2004; Bowen and Mortensen, 2004; Mortensen *et al.*, 2007).

In the present study, the modelling and the evaluation of the wind power potential for the selected meteorological stations was done by employing the WA^SP model. Figure 3.5 shows a schematic diagram summarizing the WA^SP modelling methodology.

All wind data input to the model were collected and the data quality checked (Fig. 3.5). The geographic location of the stations were converted to World Geodetic system (WGS 84) and projected to Universal Transverse Mecator (UTM). The wind data sets of the selected meteorological stations were input to the model and the site-specific wind climate summary or OWC generated. The wind data set was then represented as a velocity frequency distribution (table, graph and wind rose) and Weibull parameters.

The subsets of digital elevation model (DEM) with spatial coverage of 60 x 60 km (Abrams *et al.*, 2005) from Advanced Spaceborne Thermal Emission and Reflection Radiometer (ASTER) which covered the study areas to generate the topographical map were aquired (from <https://wist.echo.nasa.gov/api>) and the topography data at 10 m contour intervals

were generated for an area approximately 6 km radius from the meteorological station using a GlobalMapper software, then exported to WA^SP format and projected to UTM.

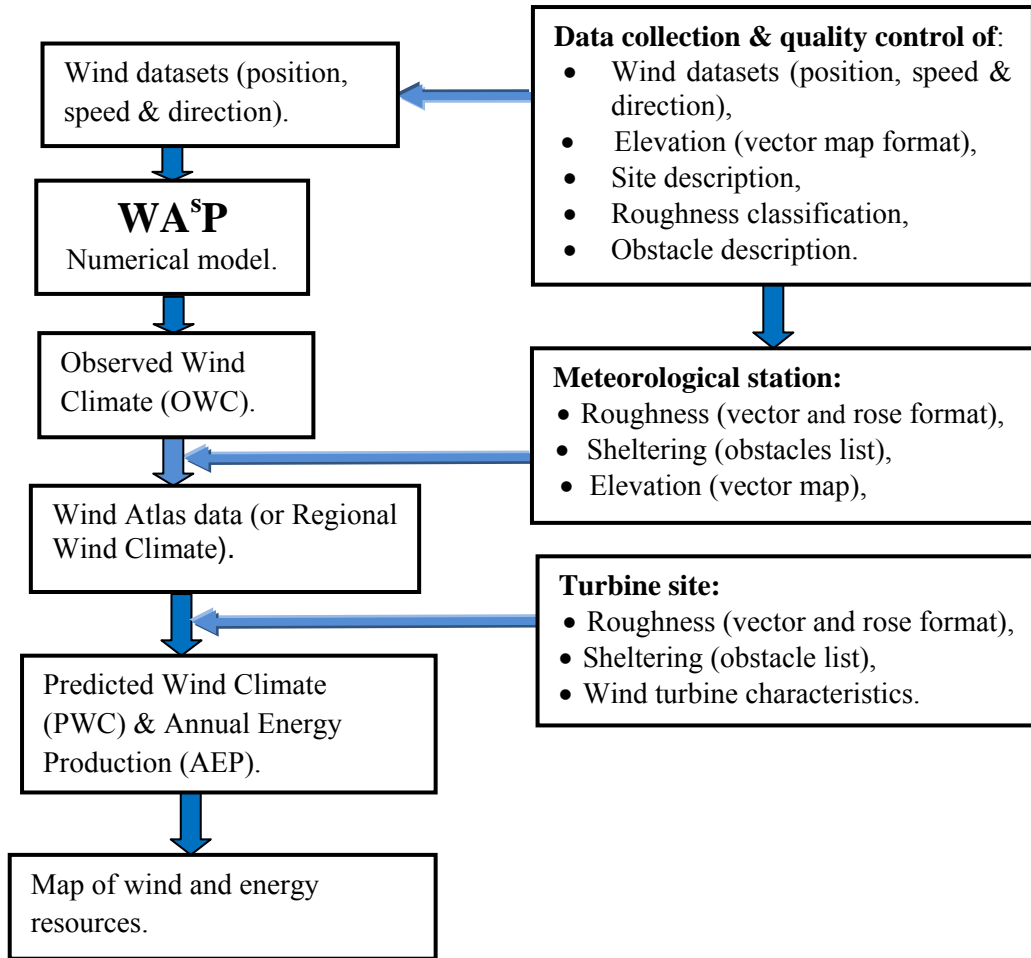


Figure 3. 5: A schematic representation of the WA^SP modeling methodology.

The roughness length and terrain surface characteristics classification around the meteorological stations and turbine sites was determined (Table A4, Appendix A) based on the European Wind Atlas (Troen and Petersen, 1989); and WMO (1981). Site visits (only at Mavalane meteorological station), the topographic maps from Direccção Nacional de Geografia e Cadastro (DINAGECA) and Google Earth satellite imagery (land-use/cover) of sufficient quality (Fig. 3.6) were used for roughness analysis, classification and collection

and the roughness rose was generated for each meteorological station and turbine site through the WA^{SP} roughness rose window.

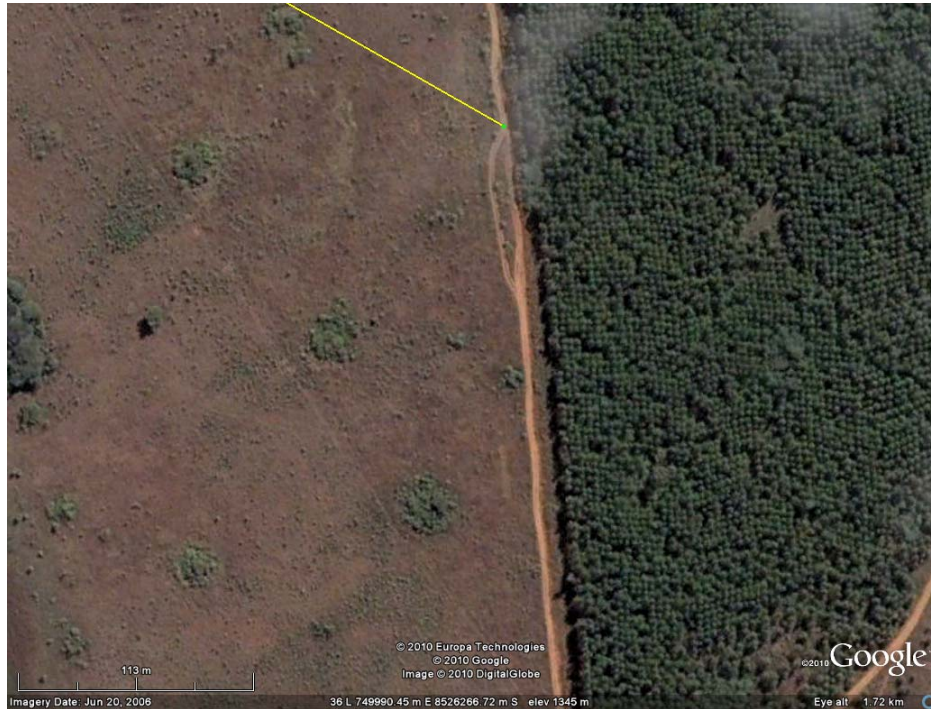


Figure 3. 6: A typical Google Earth image of land-use/cover at potential turbine site 1 in the Lichinga area used for roughness classification and collection.

The obstacle description method was employed based on European Wind Atlas method (Troen and Petersen, 1989; Mortensen *et al.*, 1991). The obstacles were collected for each meteorological station and turbine site. The centre was the meteorological station (or turbine site), and a list of obstacles was generated considering the height (h), depth (d), porosity (P) of the obstacles and was assigned α_1 and α_2 values (the angles in degrees from North to the first and second corner), R_1 and R_2 values (the radial distances to the first and second corner, of each obstacle, in meters). The obstacle collection was based on Google Earth satellite imagery (Fig. 3.7) by implementing the WA^{SP} obstacle group window. Considering the source from which data were collected, the height (h) and depth (d) of the obstacles are approximate values.

Obstacle and roughness data were collected for a 9 km radius from the meteorological station and turbine sites (Troen and Petersen, 1989; Mortensen *et al.*, 1991) for the twelve azimuth sectors of 30 degrees each. In Appendices C and D, the obstacle lists and roughness data respectively, are depicted.

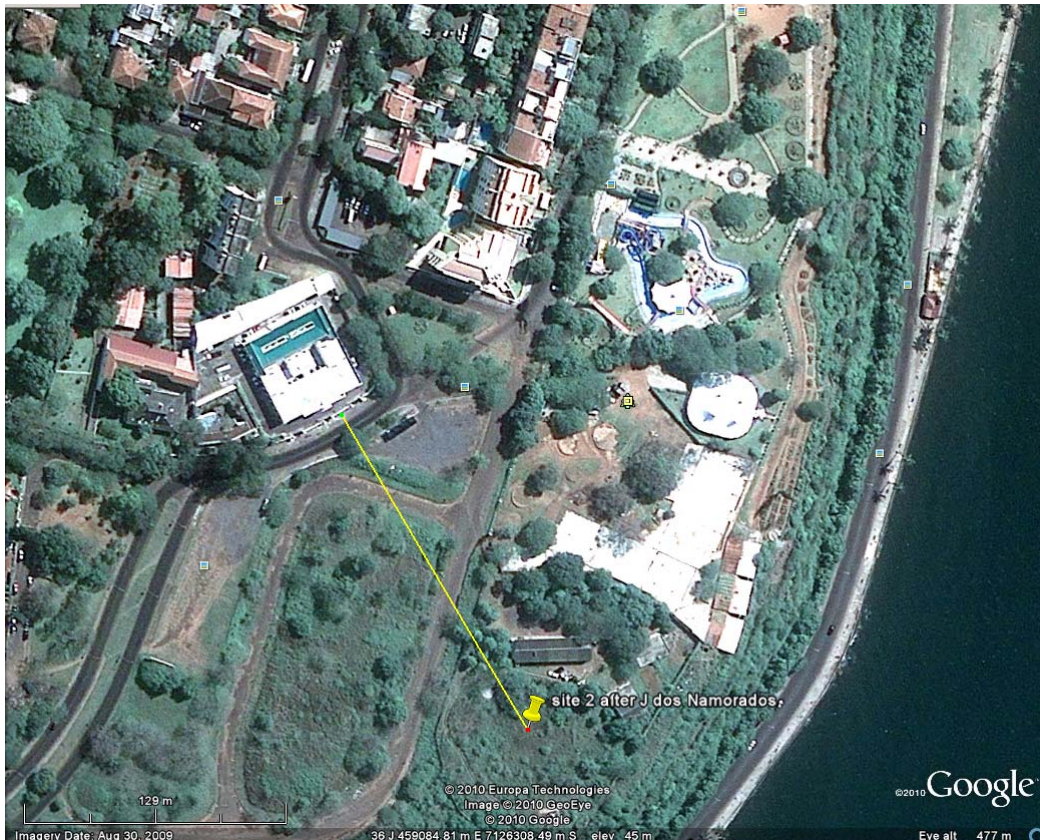


Figure 3. 7: A typical Google Earth image at potential turbine site 1 in the Mavale area used for obstacles collection.

The wind atlas for each meteorological station selected for modeling was implemented with the integration of the OWC and meteorological station UTM coordinates, a topographical map, the roughness rose and obstacle list into the WA^SP model.

Most of the meteorological stations selected for modelling (Ponta de Ouro, Mavalane, Tofinho, Vilankulo, Nampula, Pemba and Lichinga) have a mean annual wind speed of

about 4 ms^{-1} or higher. Therefore, a Vestas (V52-850kW) wind turbine, the characteristics of which are given in Figure 3.8 and Table 3.3, was selected for modeling. It was also one of the turbines for which full information on the turbine characteristics was available from the manufacturer.

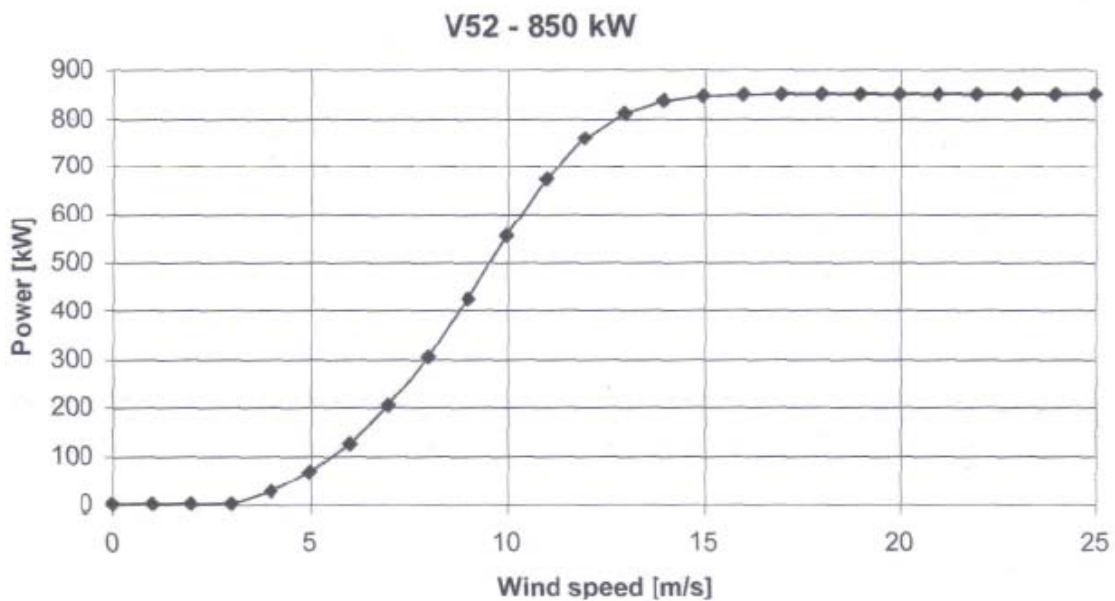


Figure 3. 8: The Vestas V52 power curve [Source: Vestas Wind Systems A/S, 2008].

Table 3. 3: Specifications and performance of V52-850 kW wind turbine. [Source: Vestas Wind Systems A/S, 2008].

Rotor	Description
Diameter	52.0 m
Swept area	2 124 m ²
Rated rotor speed	26.0 Rotations Per Minute (RPM)
Rotor speed range	14.0 - 31.4 RPM
Tilt angle	6°
Number of blades	3
Weight	10 000 Kg (Rotor) & 22 000 Kg (Nacelle)
Yaw system and gears	
Yawing speed	<0.5°/s
Motor	2.2 KW, 6 – pole asynchronous with electrical brake
Gear box	
Type	1 planetary stage/2 helical stages
Ratio	1:62 at 50 Hertz (Hz) - 1:74.4 at 60 Hz
Generator	
Type	Asynchronous with wound rotor. slip ring and Vestas Converter System (VCS)
Rated power	850 kW
Voltage	690 Volts Alternate current (VAC)
Number of poles	4
Rated speed	1620 RPM (50 Hz) and 1944 RPM (60 Hz)
Rated current	711 A
Control unity	
Voltage	3x690 VAC - 50/60 Hz
Power supply for lighting - Standard	1x10 A - 230 VAC - 50/60 Hz
Power supply for outlets - Standard	1x13 A - 230 VAC - 50/60 HZ
Environmental conditions	
Ambient temperature	Between - 20° and +40° C
Noise level - Standard	104.2 dB (A)
Hub height	
40.0 m	39.0 t/3.0 m
44.0 m	43.0 t/3.0 m
49.0 m	51.0 t/3.3 m
55.0 m	58.0 t/3.3 m
60.0 m	70.0 t/3.6 m
65.0 m	77.0 t/3.6 m
74.0 m	95.0 t/4.0 m

The WA^sP application modules were implemented to estimate the wind power potential at predicted sites. The turbine sites were chosen randomly and the predicted wind climate (PWC) and the extractable wind energy based on the Vestas (V52-850kW) wind turbine was determined at the default wind turbine height (55 m a.g.l.), and then the wind resource grid sub-model was implemented and the wind resource map generated. Different runs were performed with randomly chosen predicted sites around the study area defined by the topographic map over the meteorological station and the outputs were visually compared.

This procedure was repeated for all study areas and then the potential turbine sites were selected based on this analysis. Furthermore, the selected wind turbine sites were checked visually by means of Google Earth satellite imagery (land-use/cover) to their proximity to a road (about 2 to 3 km) to facilitate the transport of goods for installation and maintenance; to nearby obstacles and the surrounding topography due to its effect on the retardation or acceleration of wind speed. Open areas or open areas with relief were therefore potentially optimum sites.

A number up to three potential wind turbine sites were selected in the vicinity of each meteorological station and their coordinates are illustrated in Appendix B (Table B4). At each potential wind turbine site, the roughness and obstacle characteristics were determined using the same procedure as described above. The predicted wind climate (PWC), including extractable wind energy, for five heights (10, 25, 40, 50 and 60 m a.g.l) was determined based on the Vestas (V52-850kW) wind turbine. Thereafter, a wind resource map for each area with spatial resolution of 100 meters was generated implementing the WAsP wind resource grid sub-model.

3.2.3 Summary

In this chapter the criteria for selection of the meteorological stations for modelling were highlighted. The WA^sP model was selected from amongst others, as the best tool for the study because it is one of the most widely used and is considered the standard method for

wind resource assessment on land (onshore) and offshore. It forms the basis of most wind atlases around the world. It is also suitable for use in data scarce regions, particularly relevant for Mozambique, and has the facility to incorporate the characteristics of a particular wind turbine to predict the extractable wind energy at specific sites, giving a spatial representation of wind and energy resources in a given spatial domain. Furthermore, it has very limited computer requirements; it is fast and easy to use and it requires a very small amount of input data.

CHAPTER FOUR

RESULTS AND DISCUSSION

4.1 Introduction

This chapter presents the results of the modeling undertaken for the three different study areas. The procedure adopted for each modeling domain was to first describe the observed wind data at the meteorological station. Secondly, the wind atlas analysis sub-model was applied at the same site to generate the cleaned wind data that takes account of topography, roughness and obstacles at the site. Topography data at 10 m contour intervals were generated for an area approximately 6 km radius from the meteorological station from the Digital Elevation Model (DEM). Obstacle and roughness data were collected for a 9 km radius from the meteorological station and turbine sites using Google Earth land use imagery.

A number (up to three) potential wind turbine sites were selected in the vicinity of each meteorological station. At each potential wind turbine site, the roughness and obstacle characteristics were determined using the same procedure as described above. The predicted wind climate, including extractable wind energy, for five heights (10, 25, 40, 50 and 60 m a.g.l.) was determined based on the Vestas (V52-850kW) wind turbine and thereafter, a wind resource map for each area was generated.

4.2 Results for Mavelane

4.2.1 Observed wind data

The Mavalane meteorological station has a mean annual wind speed of 4.38 ms^{-1} and an available wind energy of 87 Wm^{-2} for all azimuth sectors. Figure 4.1 shows the observed wind rose and wind speed frequency distribution at Mavalane.

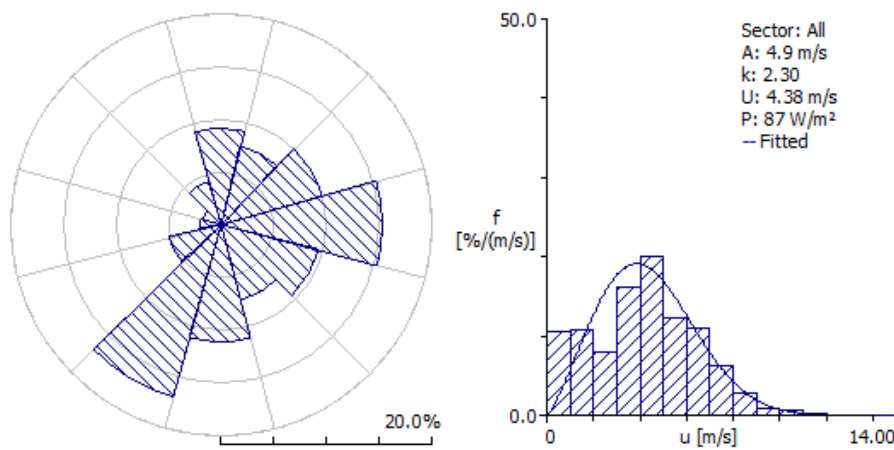


Figure 4. 1: Observed wind rose and wind speed frequency distribution at Mavalane meteorological station.

The most frequent winds are from the 210° (16.8%) and 90° (15.3 %) sectors (Figs. 4.1 and 4.2). Highest mean wind speeds and available wind energy are associated with the 180° (4.81 ms^{-1} ; 109 Wm^{-2}) and 90° (4.75 ms^{-1} ; 100 Wm^{-2}) sectors.

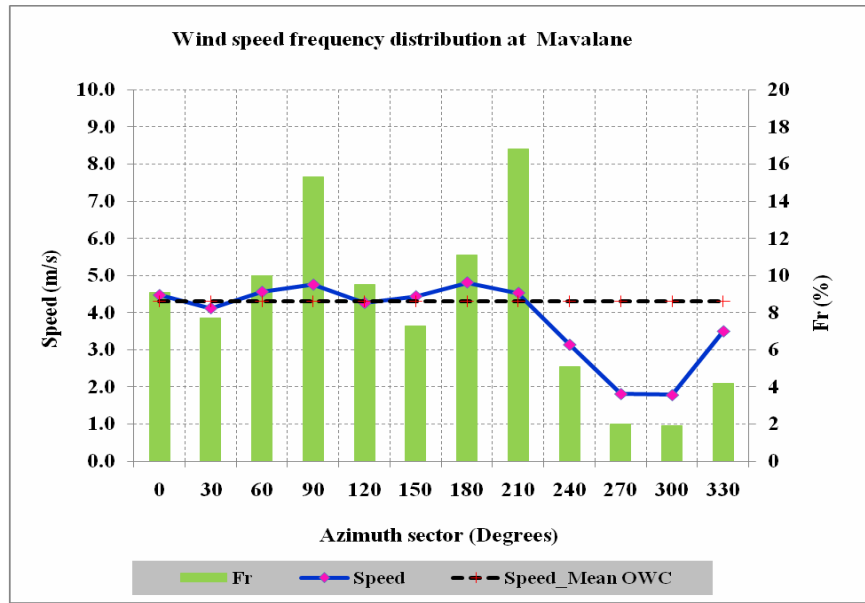


Figure 4. 2: Wind speed frequency distribution and mean wind speed by directional sector at Mavalane.

4.2.2 Wind atlas data at Mavalane

After application of the wind atlas analysis sub-model, the relevant wind data for Mavalane are presented in Table 4.1. The data are cleaned of the influence of obstacles and are presented for four roughness classes (0.0, 0.03, 0.1, and 0.4 m) and four standard heights. Figure 4.3 represents the mean wind speed for three roughness classes (Z_{00} to Z_{02} representing roughness values of 0.00, 0.03 and 0.10 m respectively) and for the first three standard heights (10, 25 and 50 m). The results show clearly that relatively higher wind speeds are associated with lower roughness and with greater heights a.g.l. Highest wind speeds are associated with the 120° directional sector (Fig. 4.3).

Table 4. 1: Wind atlas data at Mavalane, where A = Weibull scale factor; k = Weibull shape factor; v = mean wind speed; and E = Available wind energy (or power density).

Height [m]	Parameter	Roughness-class			
		0.00 m	0.030 m	0.10 m	0.40 m
10	A [ms^{-1}]	7.7	5.4	4.7	3.7
	k	2.15	1.88	1.89	1.90
	v [ms^{-1}]	6.8	4.8	4.1	3.3
	E [Wm^{-2}]	346	134	88	42
25	A [ms^{-1}]	8.3	6.4	5.8	4.8
	k	2.18	2.00	1.99	2.00
	v [ms^{-1}]	7.4	5.7	5.1	4.3
	E [Wm^{-2}]	435	214	155	92
50	A [ms^{-1}]	8.8	7.4	6.7	5.8
	k	2.20	2.19	2.16	2.14
	v [ms^{-1}]	7.8	6.5	6.0	5.2
	E [Wm^{-2}]	509	300	229	150
100	A [ms^{-1}]	9.3	8.7	8.0	7.0
	k	2.10	2.35	2.37	2.38
	v [ms^{-1}]	8.2	7.7	7.1	6.2
	E [Wm^{-2}]	616	462	354	242

Immediately evident from Figure 4.3 is a shift in the maximum speed directional sector from 90° to 120° . It is also evident that the observed wind peak associated with the 210° sector has disappeared, leading to the conclusion that it was most likely due to speed up or channeling of winds due to obstacles.

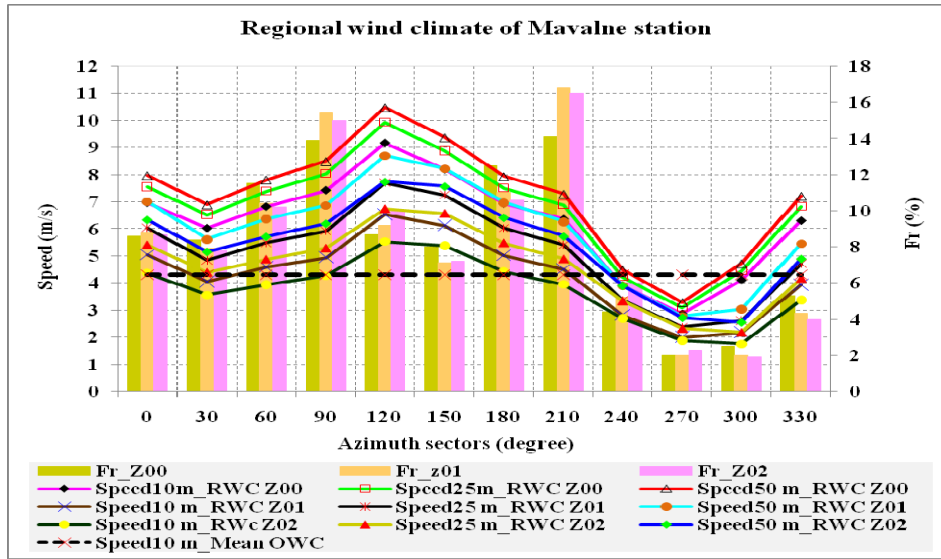


Figure 4. 3: Regional wind climate of Mavalane meteorological station.

4.2.3 Predicted wind climate for the Mavalane area

The predicted wind climate (PWC) was calculated for three potential wind turbine sites located on the coastal plain at distances of less than 7 km from the meteorological station and less than 400 m from the shoreline (Fig. 4.4).

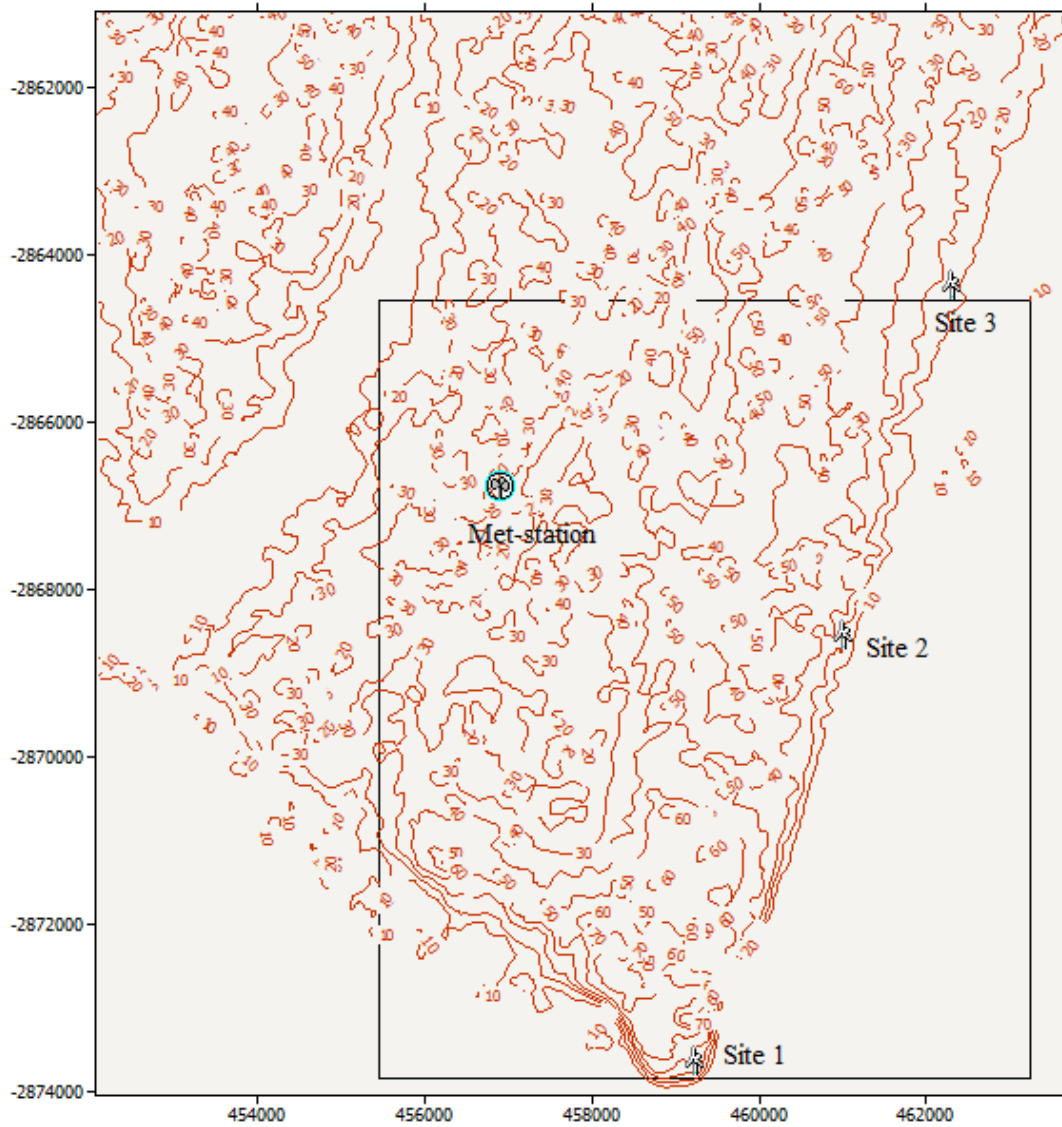


Figure 4. 4: Map showing the location of the three potential wind turbine sites (🌪️) and the location of the Mavalane meteorological station (📍) and the selected area for wind resource maps.

The predicted mean annual wind speeds and extractable energy at the three potential wind turbine sites are presented in Figure 4.5 for five heights a.g.l. The mean annual wind speed is lowest at site 3, but exceeds 4.5 ms^{-1} at 10 m a.g.l. Highest mean annual wind speeds are found at site 1, where values approach 8.0 ms^{-1} at higher levels (50 and 60 m). Site 1 shows

evidence of a relatively steep rise in terrain which could account for the higher wind speeds. Available wind energy at 60 m a.g.l. ranges between 334 and 533 Wm^{-2} at the three different sites.

A similarity of the predicted wind climate (PWC) to the regional wind climate (RWC) is found for the roughness class 0 ($Z_{00}=0.000$ m) and class 1 (0.030 m).

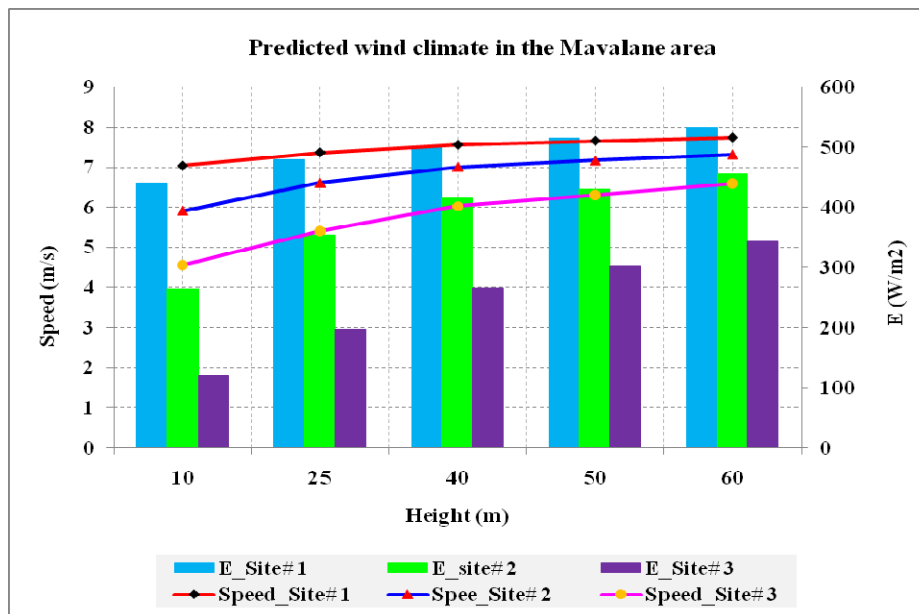


Figure 4. 5: Predicted mean wind speed and available wind energy at three potential wind turbine sites in the Mavalane area.

Figure 4.6 illustrates the predicted wind rose and wind speed frequency distribution at sites 1, 2 and 3 in the Mavalane area. It is noted that the winds are predominantly from the 210° and 90° with a secondary contribution from the 60° and 180° sectors. Highest wind speeds are associated with the 120° directional sector (Fig. 4.7).

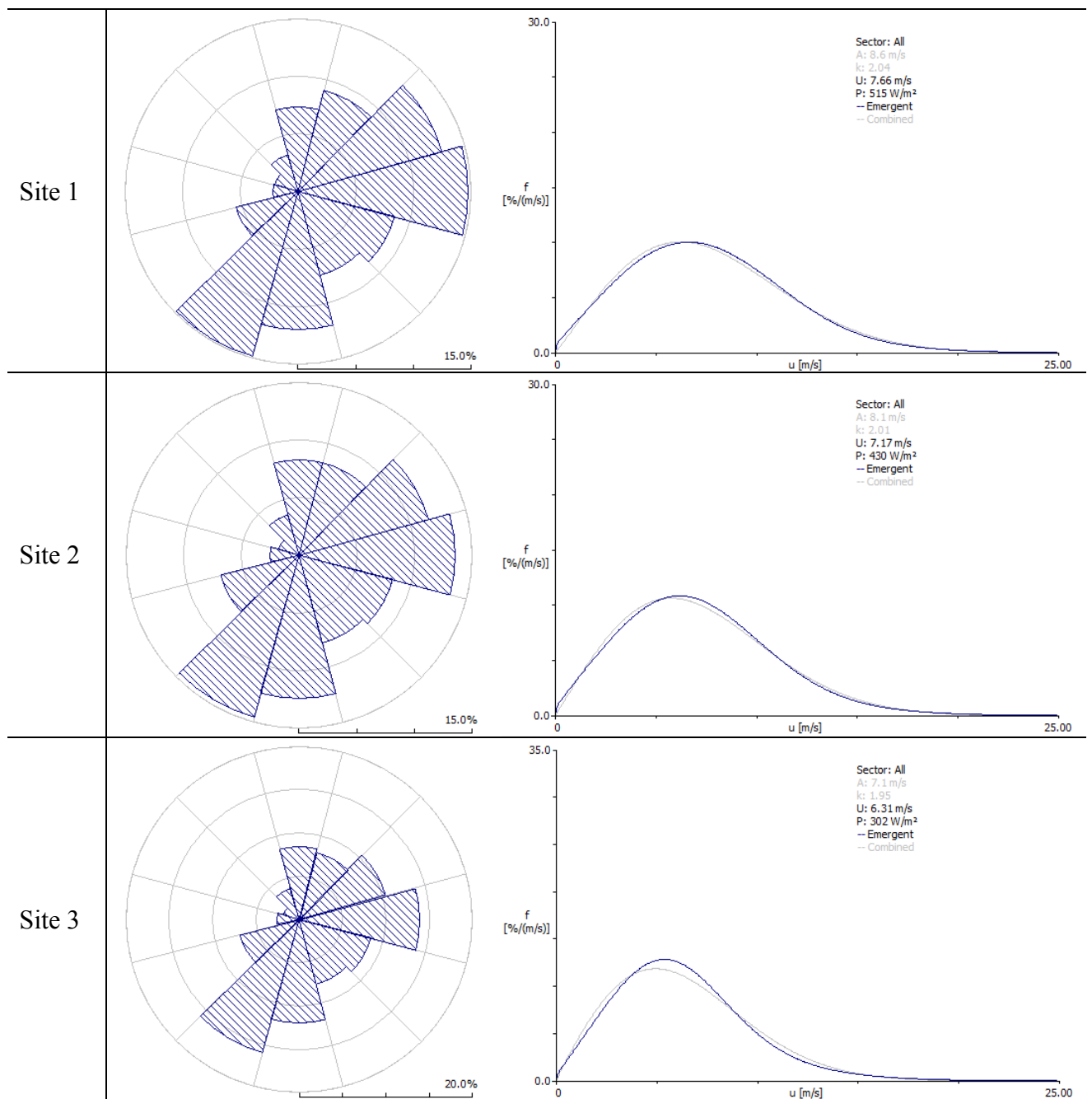


Figure 4. 6: Predicted wind rose and wind speed frequency distribution at wind turbine sites in the Mavalane area.

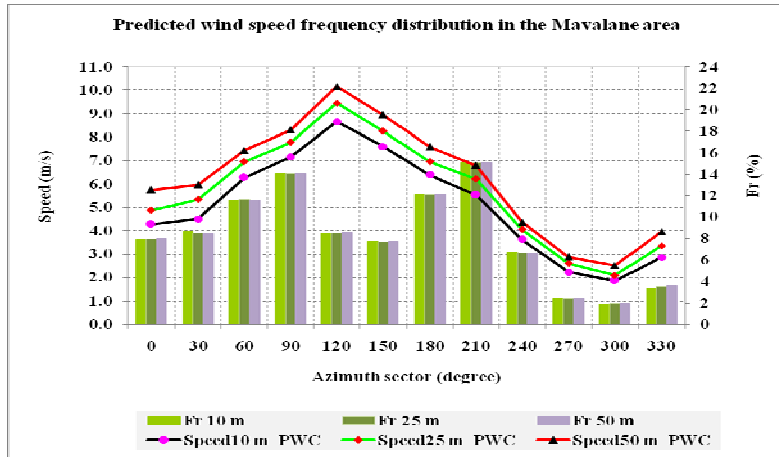


Figure 4. 7: Predicted wind speed frequency distribution for 3 standard heights (10, 25 and 50 m a.g.l.) at turbine sites in the Mavalane area.

The annual energy production or extractable wind energy (AEP) in the Mavalane area is above 2 000 MWh for heights greater than 25 m a.g.l. and between 870 and 2 400 MWh for a 10 m a.g.l. hub height. Figure 4.8 illustrates the extractable wind energy at the three potential wind turbine sites in the Mavalane area.

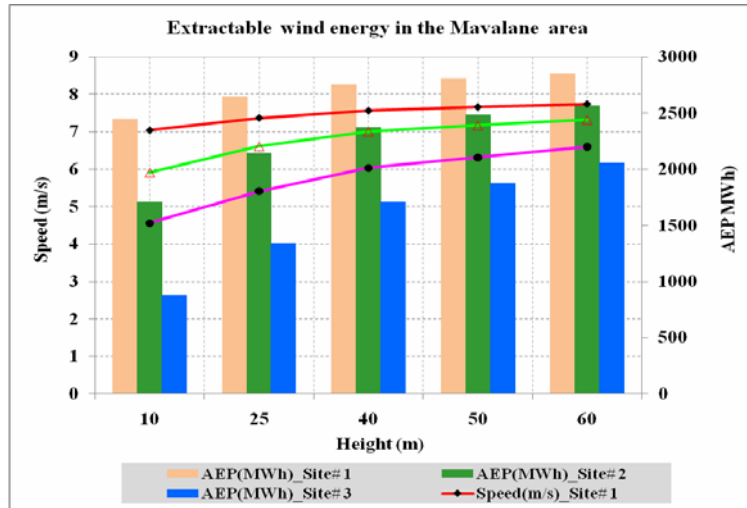


Figure 4. 8: The extractable wind energy at three potential wind turbine sites in the Mavalane area.

The highest extractable wind energy is from the 90° and 120° azimuth sectors. Figure 4.9 depicts the extractable average wind energy by azimuth sector for three standard heights (10, 25 and 50 m a.g.l.) at potential turbine sites in the Mavalane area, while Figure 4.10 illustrates the extractable energy rose and energy frequency distribution at 50 m a.g.l. at site 2 in the Mavalane area.

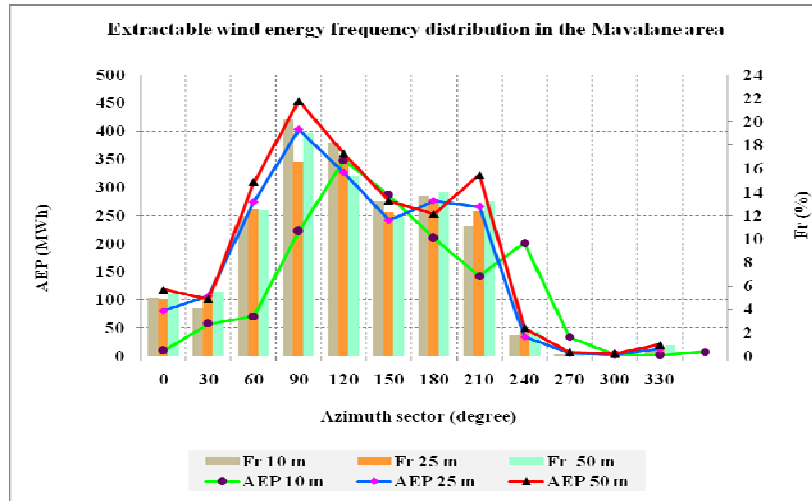


Figure 4. 9: Extractable wind energy by azimuth sector for 3 standard heights (10, 25, and 50 m a.g.l.) at site 2 in the Mavalane area.

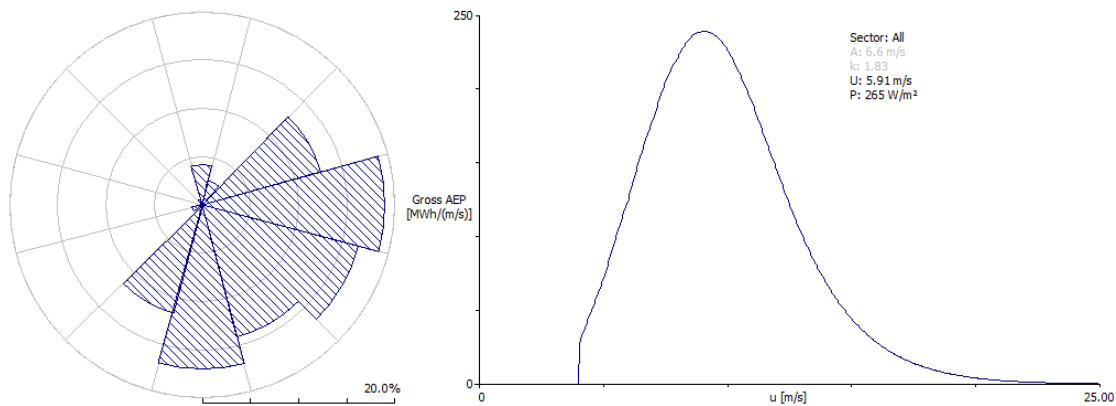


Figure 4. 10: Extractable energy rose and energy frequency distribution at 50 m a.g.l. for site 2 in the Mavalane area.

The speed-up (down) due to roughness change and orography at the lowest level (10 m a.g.l.) was between -8.4 and 13.5% and -3.1 to 6%, while at highest level (50 m a.g.l.) it was between -3.5 and 4.7% and -2.8 to 2.7% respectively. The turning effect due to orography was between -1.9° and 3.5° at 10 m a.g.l. and -1.4° to 1.9° at 50 m a.g.l.

4.2.4 Wind resource maps

The wind resource maps (Fig. 4.11) illustrate the spatial distribution of wind speed and energy resource in the Mavalane area at a height of 55 m a.g.l.

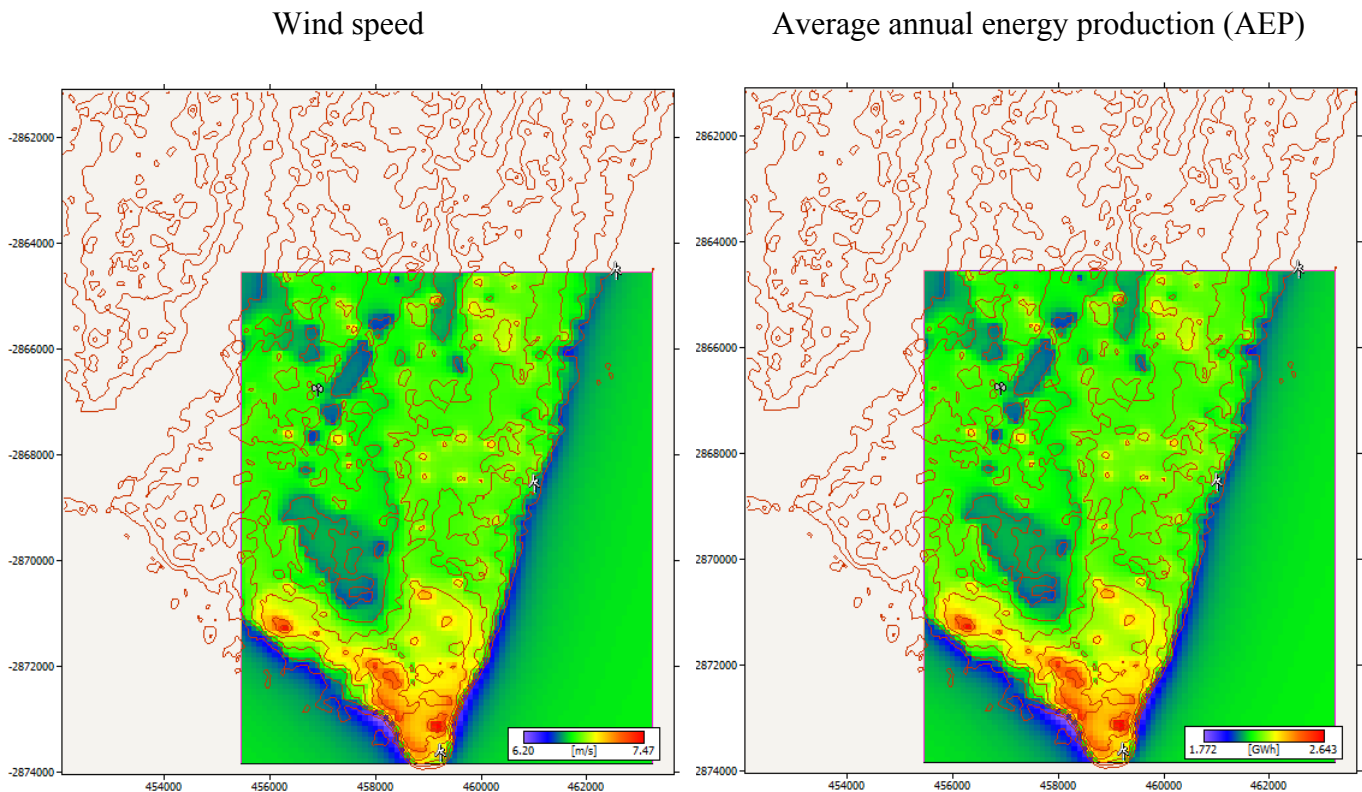


Figure 4. 11: Wind and energy resource maps in the Mavalane area.

The maps show an average wind speed over the domain of 6.72 ms^{-1} and average annual energy production (AEP) of 2 130 MWh. Highest wind energy potential is found in the southernmost section of the modeling domain, near Maputo Bay facing Catembe village, where the mean wind speed reaches 7.47 ms^{-1} with an AEP of 2 643 MWh. The site with the highest wind speeds and the greatest wind power potential has UTM coordinates of 459200; -2873100.

4.3 Results for Ponta de Ouro

4.3.1 Observed wind data

The Ponta de Ouro meteorological station has a mean annual observed wind speed of 4.9 ms^{-1} and an available wind energy of 116 Wm^{-2} for all azimuth sectors. Figure 4.12 shows the observed wind rose and wind speed frequency distribution at Ponta de Ouro.

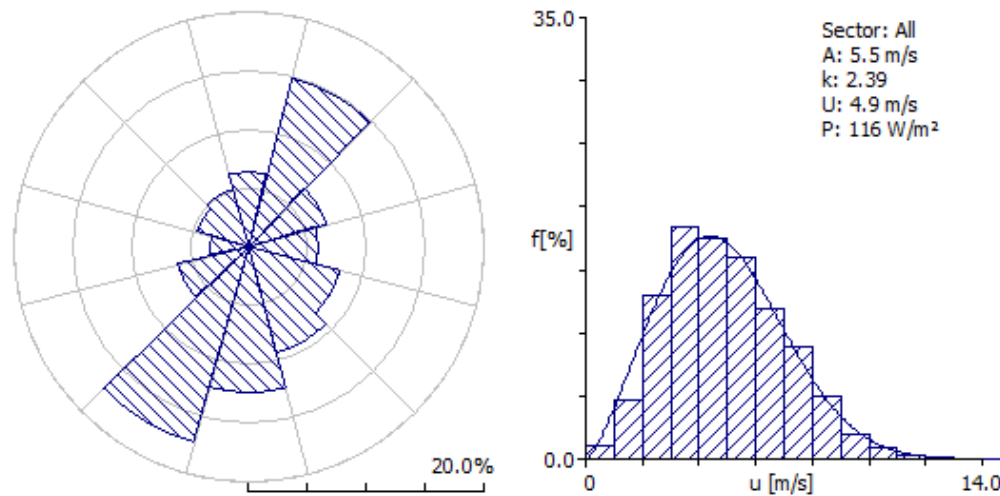


Figure 4. 12: Observed wind rose and wind speed frequency distribution at Ponta de Ouro meteorological station.

The most frequent winds are from the 210° (17%) and 30° (15%) sectors (Figs. 4.12 and 4.13). Highest mean wind speeds and available wind energy are associated with the 180° (6.7 ms⁻¹; 259 Wm⁻²) and 30° (6.4 ms⁻¹; 186 Wm⁻²) sectors. The double maximum is a feature that was also observed at Mavalane further to the north.

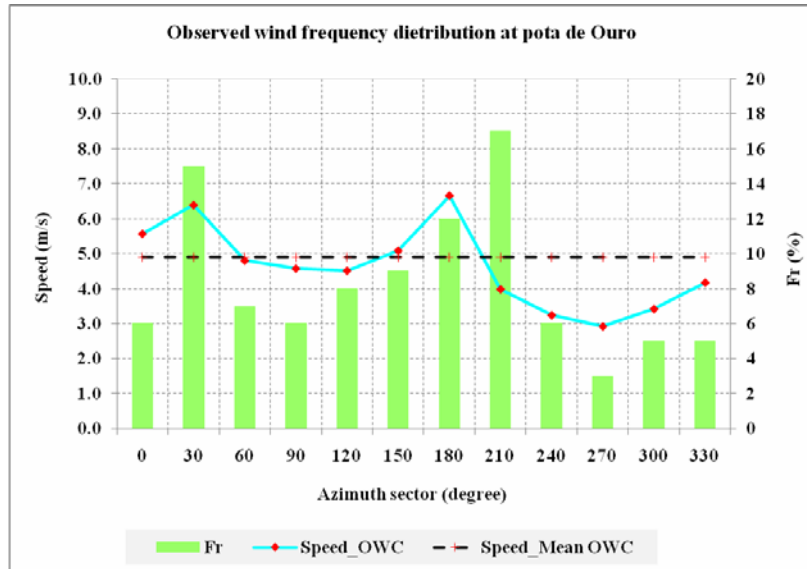


Figure 4.13: Wind speed frequency distribution and mean wind speed by directional sector at Ponta de Ouro.

4.3.2 Wind atlas data at Ponta de Ouro

After application of the wind atlas analysis sub-model, the relevant wind data for Ponta de Ouro are presented in Table 4.2. The data are cleaned of the influence of obstacles and are presented for four roughness classes (0.00, 0.03, 0.10, and 0.40 m) and four standard heights. Figure 4.14 depicts the mean wind speed for three roughness classes (Z_{00} to Z_{02} representing roughness values of 0.00, 0.03 and 0.10 m respectively) and for the first three standard heights (10, 25 and 50 m a.g.l.). The results show clearly that relatively higher wind speeds are associated with lower roughness and with greater heights a.g.l. Highest wind speeds are associated with the 0°-60° and 180° directional sectors (Fig. 4.14).

Table 4. 2: Wind atlas data at Ponta de Ouro, where A = Weibull scale factor; k = Weibull shape factor; v = mean wind speed; and E = Available wind energy (or Power density).

Height [m]	Parameter	Roughness-class			
		0.00 m	0.03 m	0.10 m	0.40 m
10	A [ms^{-1}]	7.9	5.5	4.8	3.8
	k	2.68	2.34	2.32	2.30
	v [ms^{-1}]	7.0	4.9	4.2	3.3
	E [Wm^{-2}]	319	119	78	38
25	A [ms^{-1}]	8.6	6.6	5.9	4.9
	k	2.72	2.50	2.46	2.43
	v [ms^{-1}]	7.6	5.9	5.2	4.4
	E [Wm^{-2}]	402	194	140	83
50	A [ms^{-1}]	9.0	7.6	6.9	6.0
	k	2.74	2.76	2.69	2.62
	v [ms^{-1}]	8.0	6.8	6.1	5.3
	E [Wm^{-2}]	472	281	213	138
100	A [ms^{-1}]	9.5	9.0	8.2	7.2
	k	2.59	2.90	2.90	2.90
	v [ms^{-1}]	8.5	8.0	7.3	6.4
	E [Wm^{-2}]	568	456	346	232

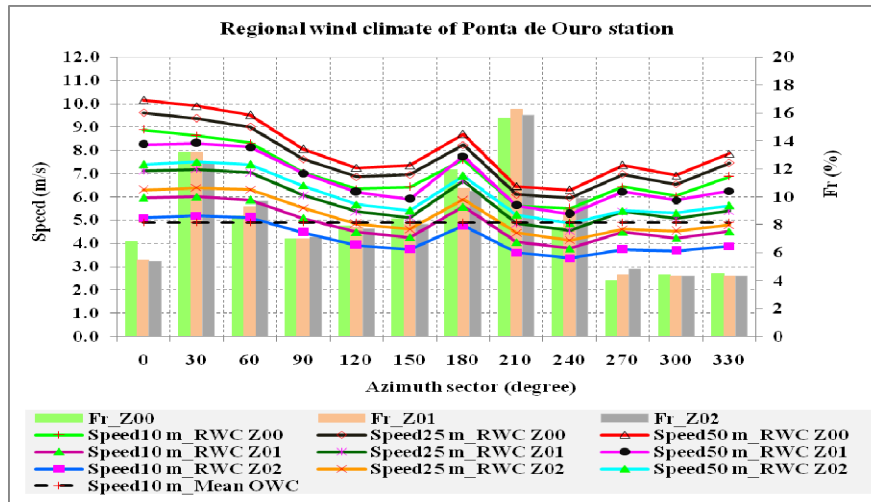


Figure 4. 14: Regional wind climate of Ponta de Ouro meteorological station.

4.3.3 Predicted wind climate for the Ponta de Ouro area

The predicted wind climate (PWC) was calculated for two potential wind turbine sites located to the north-west of the meteorological station at distances of 3 and 6 km from the meteorological station to site 2 and site 1 respectively (Fig. 4.15).

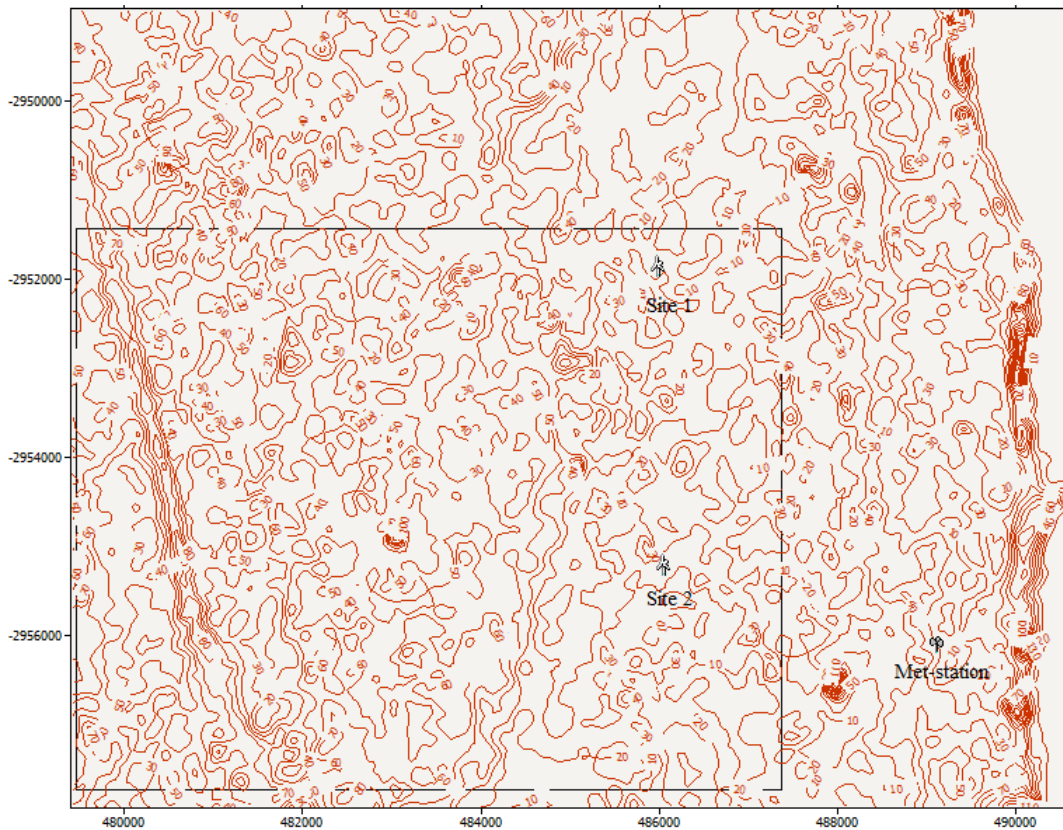


Figure 4. 15: Map showing the location of the two potential wind turbine sites (🌳) and the location of the Ponta de Ouro meteorological station (🌳) and the selected area for wind resource maps.

The predicted mean annual wind speeds and extractable energy at the two potential wind turbine sites are presented in Figure 4.16 for five heights a.g.l. The mean annual wind speed is greater than 5.0 ms^{-1} at 10 m a.g.l. Highest mean annual wind speeds are found at higher

levels (50 and 60 m) where values approach 8.0 ms^{-1} at the two sites. Available wind energy at 60 m a.g.l. ranges between 333 and 418 Wm^{-2} at the two different sites.

A similarity of the predicted wind climate (PWC) to the regional wind climate (RWC) is found for the roughness class 0 ($Z_{00}=0.00 \text{ m}$) at higher levels, class 1 and class 2 ($Z_{01}=0.030, Z_{02}=0.10 \text{ m}$) at lower levels (10 and 25 m a.g.l.).

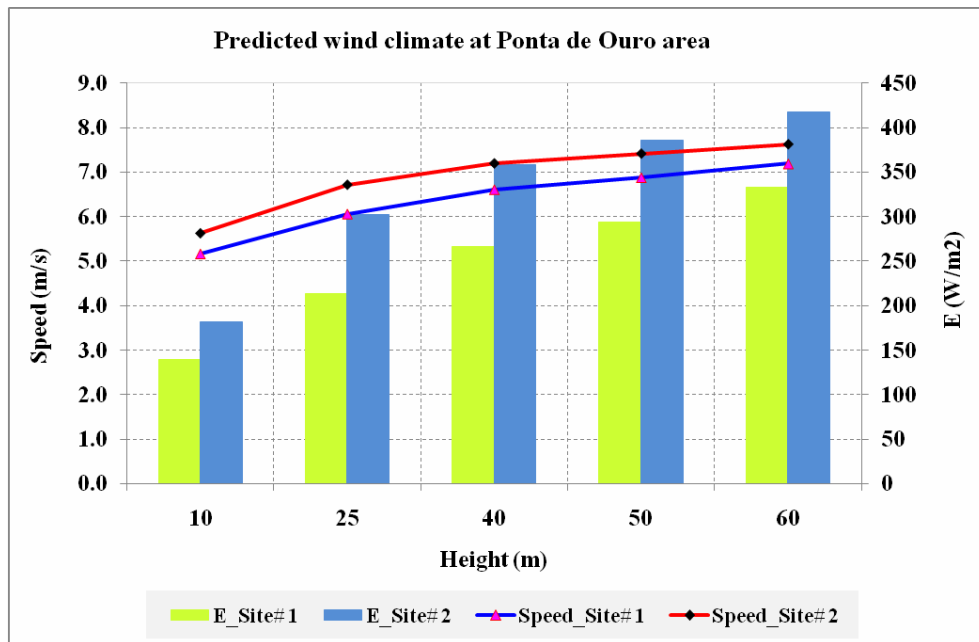


Figure 4. 16: Predicted mean wind speed and available wind energy at two potential wind turbine sites in the Ponta de Ouro area.

Figure 4.17 illustrates the predicted wind rose and wind speed frequency distribution at sites 1 and 2 in the Ponta de Ouro area. It is noted that the winds are predominantly from the 210° and 30° sectors. Highest predicted wind speeds are associated with the $30^\circ - 60^\circ$ and 180° directional sectors (Fig. 4.18).

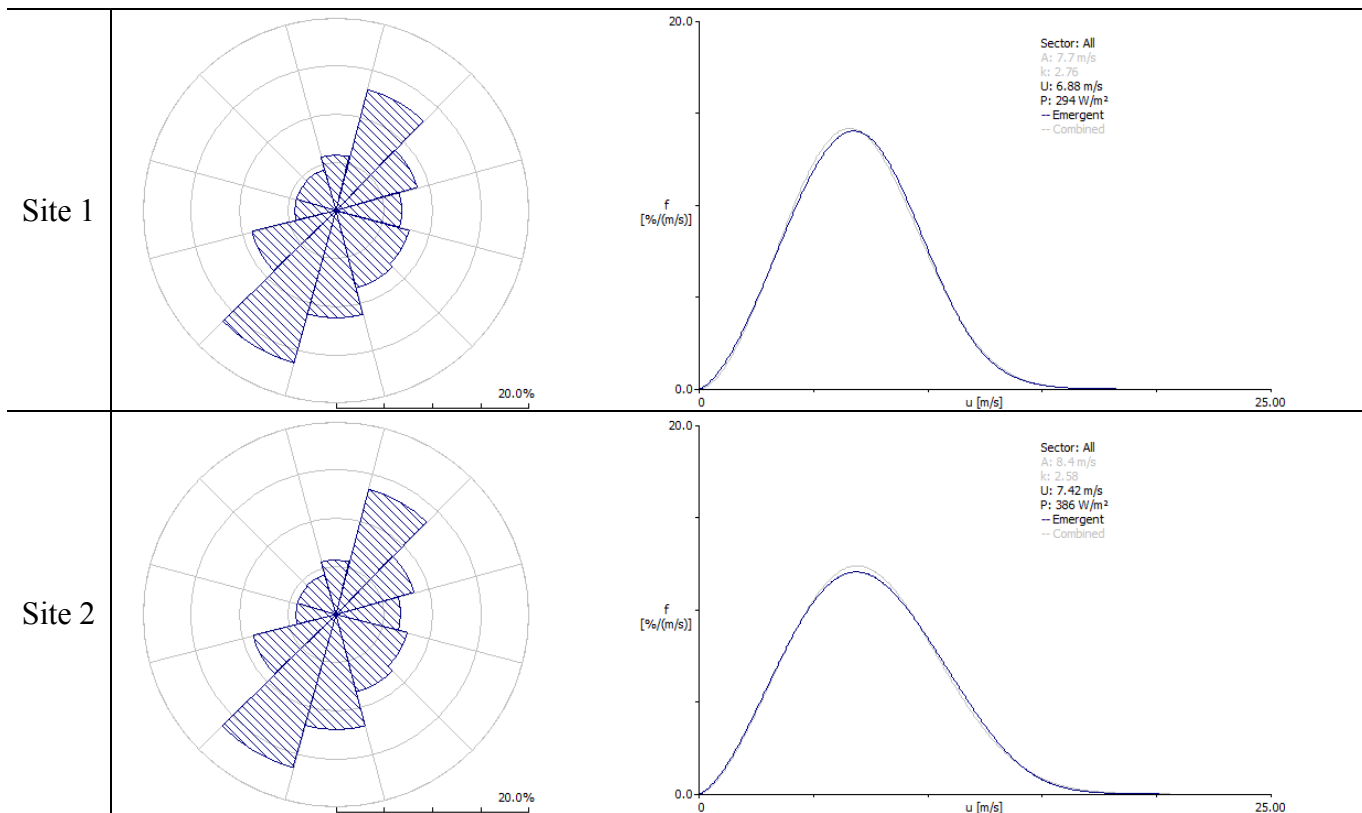


Figure 4. 17: Predicted wind rose and wind speed frequency distribution at potential wind turbine sites in the Ponta de Ouro area.

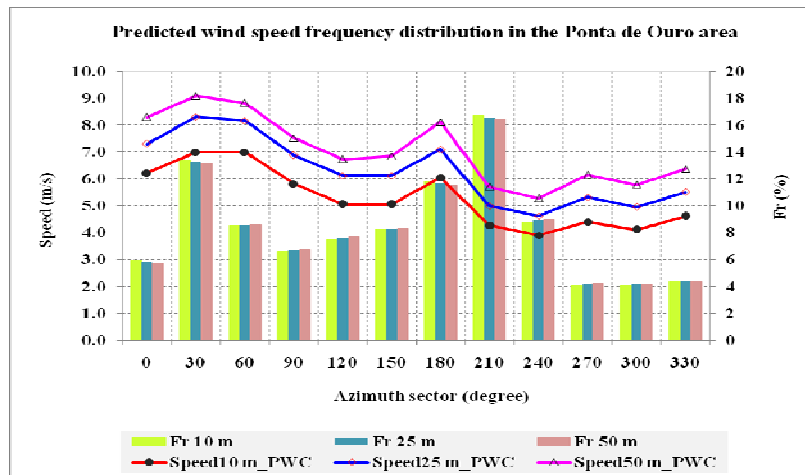


Figure 4. 18: Predicted wind speed frequency distribution for 3 standard heights (10, 25 and 50 m a.g.l.) at potential wind turbine sites in the Ponta de Ouro area.

The annual energy production or extractable wind energy (AEP) in the Ponta de Ouro area is between 2 000 and 2 800 MWh for heights greater than 25 m a.g.l. and below 1 500 MWh for a 10 m a.g.l. hub height. Figure 4.19 illustrates the extractable wind energy at the two potential wind turbine sites in the Ponta de Ouro area.

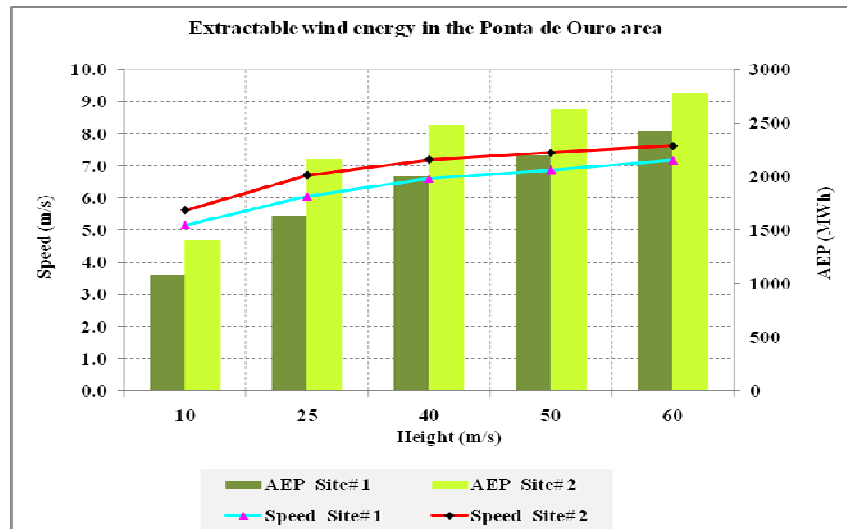


Figure 4. 19: The extractable wind energy at two potential wind turbine sites in the Ponta de Ouro area.

The highest extractable wind energy is from the 30° and 180° azimuth sectors. Figure 4.20 depicts the extractable average wind energy by azimuth sector for three standard heights (10, 25 and 50 m a.g.l.) at potential turbine sites in the Ponta de Ouro area, while Figure 4.21 illustrates the extractable energy rose and energy frequency distribution at 50 m a.g.l. at site 2 in the Ponta de Ouro area.

The speed-up (down) due to roughness change and orography at the lowest level (10 m a.g.l.) was between -12.9 and 1.1% and -3.3 to 5.8%, while at the highest level (50 m a.g.l.), it was between -4.4 and 1.5% and -1.9 to 2.7% respectively. The turning effect due to orography was between -2.7° and 2.7° at 10 m a.g.l. and -1.4° to 1.3° at 50 m a.g.l.

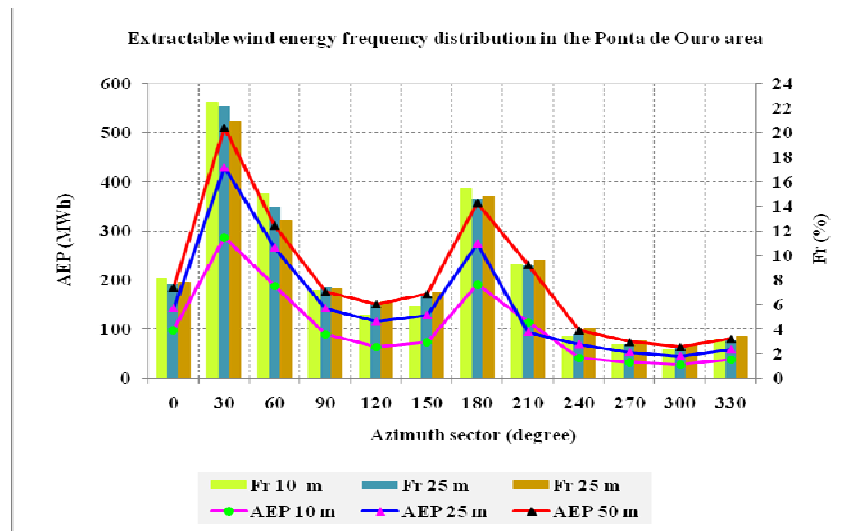


Figure 4.20: Extractable average wind energy by azimuth sector for 3 standard heights (10, 25 and 50 m a.g.l.) at potential wind turbine sites in the Ponta de Ouro area.

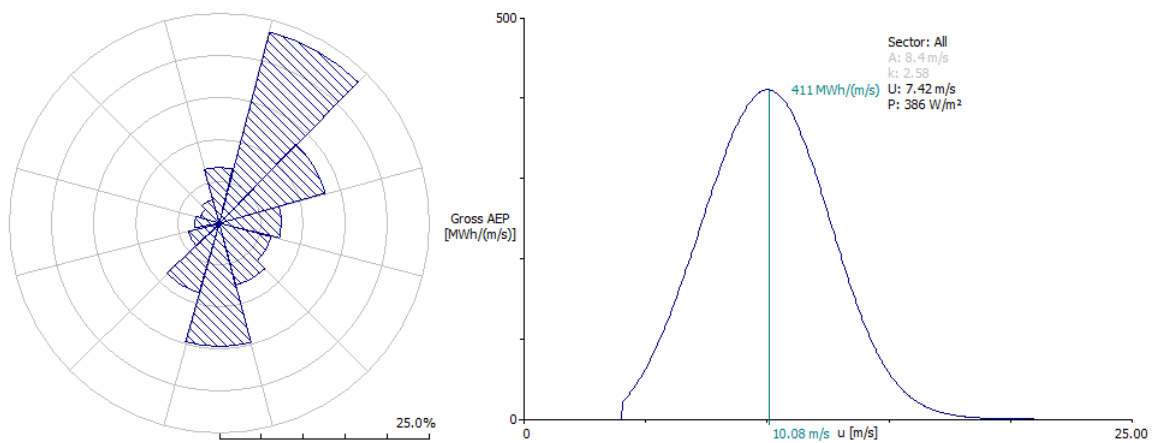


Figure 4.21: Extractable energy rose and energy frequency distribution at 50 m a.g.l. at site 2 in the Ponta de Ouro area.

4.3.4 Wind resource maps

The wind resource maps illustrate the spatial distribution of wind speed (Fig. 4.22) and energy (Fig. 4.23) in the Ponta de Ouro area at a height of 55 m a.g.l. The average wind speed is 6.8 ms^{-1} and average annual energy production (AEP) is 2 116 MWh. Highest wind energy potential is found in the western highland areas, inland from sites 1 and 2 and in a narrow NW to S valley that leads to Maputo Bay, where the mean wind speed reaches 8.3 ms^{-1} with an AEP of 3 240 MWh. Clearly, proximity to the coast, where wind speeds are traditionally higher due to lower roughness values over the ocean, and channeling of winds are factors accounting for the modeled maxima. The site with UTM coordinates of 483015; -2954883 is the site with the highest wind energy potential.

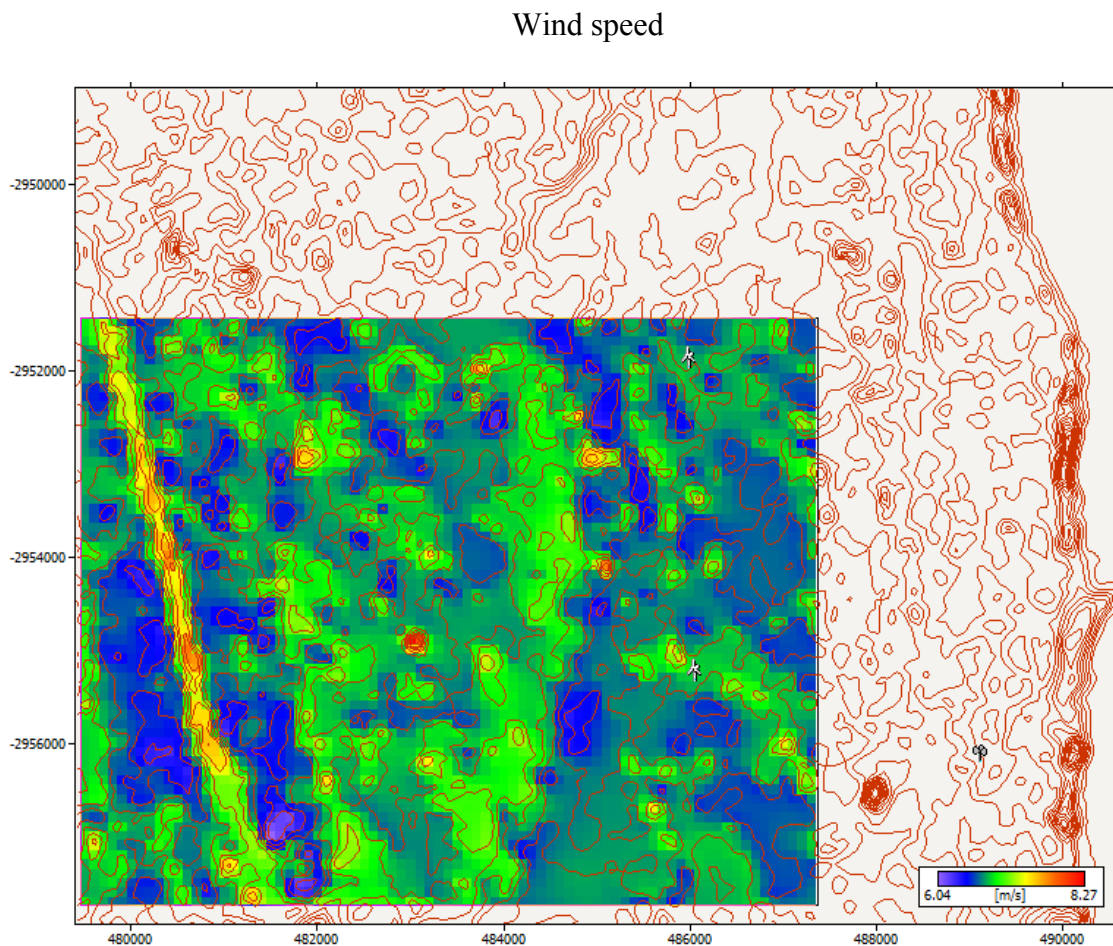


Figure 4. 22: Wind speed resource map in the Ponta de Ouro area.

Average annual energy production (AEP)

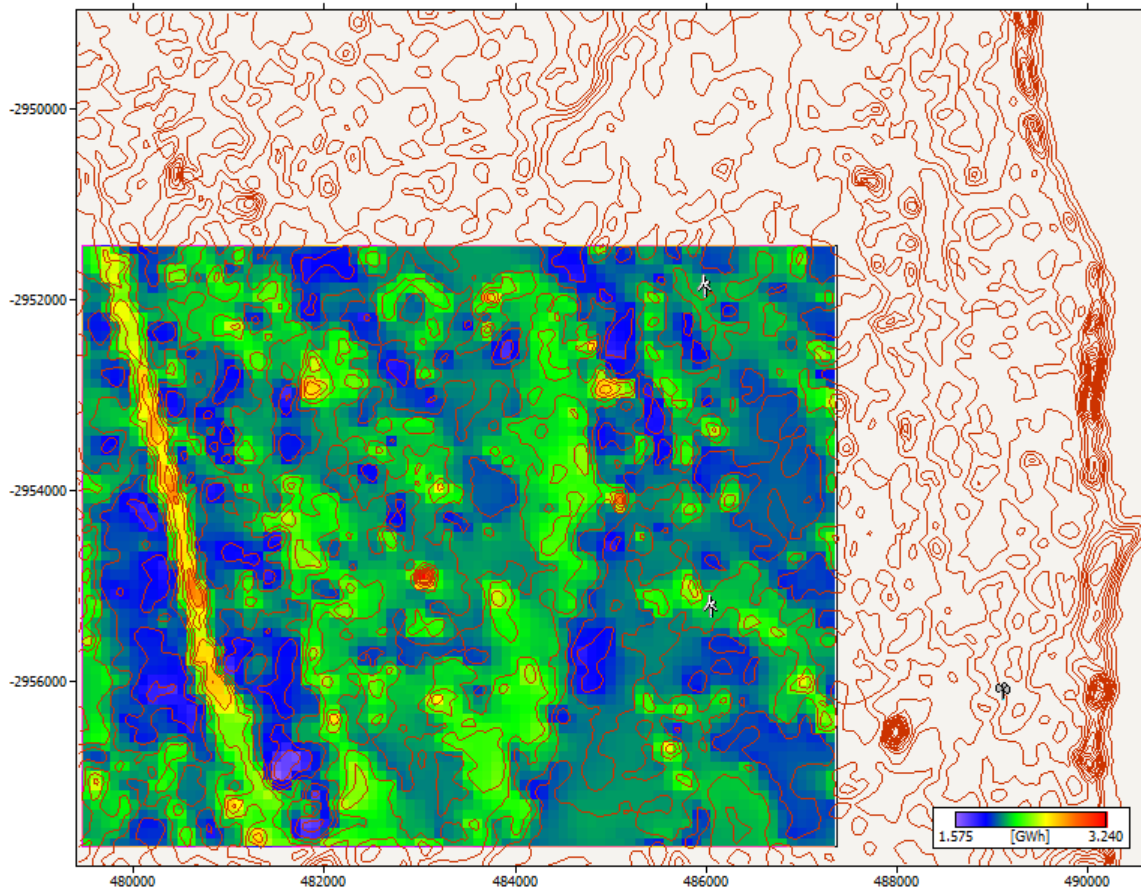


Figure 4. 23: Wind energy resource map in the Ponta de Ouro area.

4.4 Results for Tofinho

4.4.1 Observed wind data

The Tofinho meteorological station has a mean annual observed wind speed of 6.5 ms^{-1} (the highest value of all the meteorological stations) and an available wind energy of 291 Wm^{-2} for all azimuth sectors. Figure 4.24 shows the observed wind rose and wind speed frequency distribution at Tofinho.

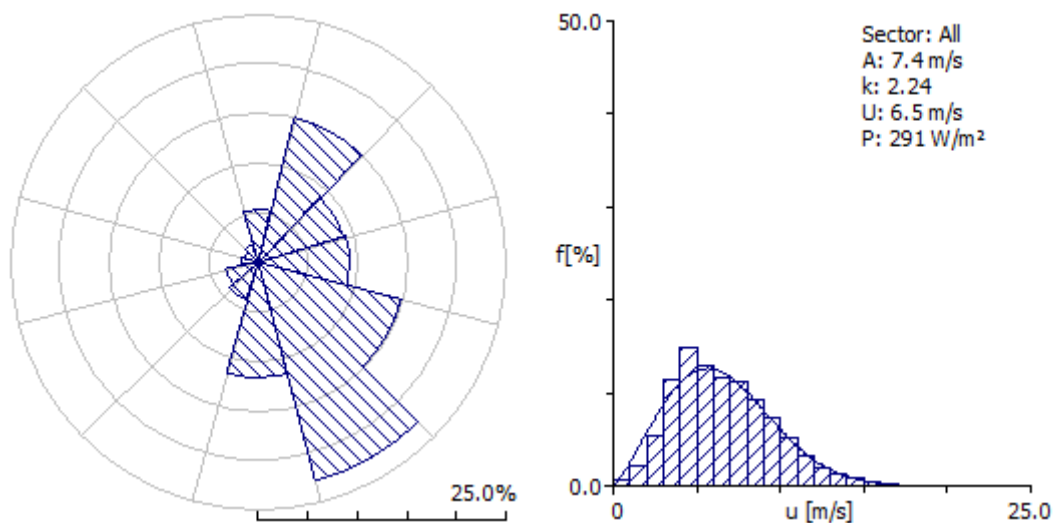


Figure 4. 24: Observed wind rose and wind speed frequency distribution at Tofinho meteorological station.

The most frequent winds are from the 150° (22.6%) sector, with a secondary maximum from the 30° (15%) sector (Figs. 4.24 and 4.25). The orientation of coastline accounts for winds from a more SE sector than a SW sector as was the case in the two former stations. High mean wind speeds and available wind energy are associated with the 180° (8.65 ms^{-1} ; 562 Wm^{-2}) and 0° (8.64 ms^{-1} ; 519 Wm^{-2}) sectors.

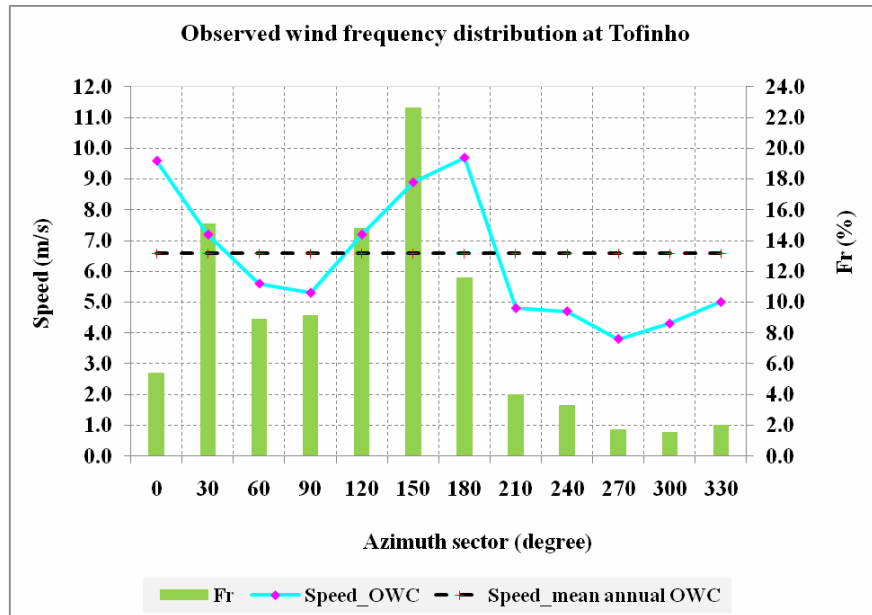


Figure 4.25: Wind speed frequency distribution and mean wind speed by directional sector at Tofinho.

4.4.2 Wind atlas data at Tofinho

After application of the wind atlas analysis sub-model, the relevant wind data for Tofinho are presented in Table 4.3. The data are cleaned of the influence of obstacles and are presented for four roughness classes (0.00, 0.03, 0.10, and 0.40 m) and four standard heights. Figure 4.26 depicts the mean wind speed for three roughness classes (Z_{00} to Z_{02} representing roughness values of 0.00, 0.03 and 0.10 m respectively) and for the first three standard heights (10, 25 and 50 m). The results show clearly that relatively higher wind speeds are associated with lower roughness and with greater heights a.g.l. Highest wind speeds are associated with the 180°, 150° and 0° directional sectors (Fig. 4.26).

Table 4. 3: Wind atlas data at Tofinho, where A = Weibull scale factor; k = Weibull shape factor; v = mean wind speed; and E = Available wind energy (or Power density).

Height [m]	Parameter	Roughness-class			
		0.00 m	0.03 m	0.10 m	0.40 m
10	A [ms ⁻¹]	7.8	5.4	4.7	3.7
	k	2.37	2.07	2.06	2.07
	U [ms ⁻¹]	6.9	4.8	4.2	3.3
	E [Wm ⁻²]	326	124	82	39
25	A [ms ⁻¹]	8.4	6.5	5.8	4.8
	k	2.40	2.20	2.18	2.18
	U [ms ⁻¹]	7.4	5.7	5.1	4.3
	E [Wm ⁻²]	410	200	145	85
50	A [ms ⁻¹]	8.9	7.5	6.8	5.9
	k	2.42	2.42	2.37	2.34
	U [ms ⁻¹]	7.9	6.6	6.0	5.2
	E [Wm ⁻²]	481	285	218	141
100	A [ms ⁻¹]	9.3	8.8	8.1	7.1
	k	2.31	2.56	2.57	2.59
	U [ms ⁻¹]	8.3	7.8	7.2	6.3
	E [Wm ⁻²]	580	452	346	233

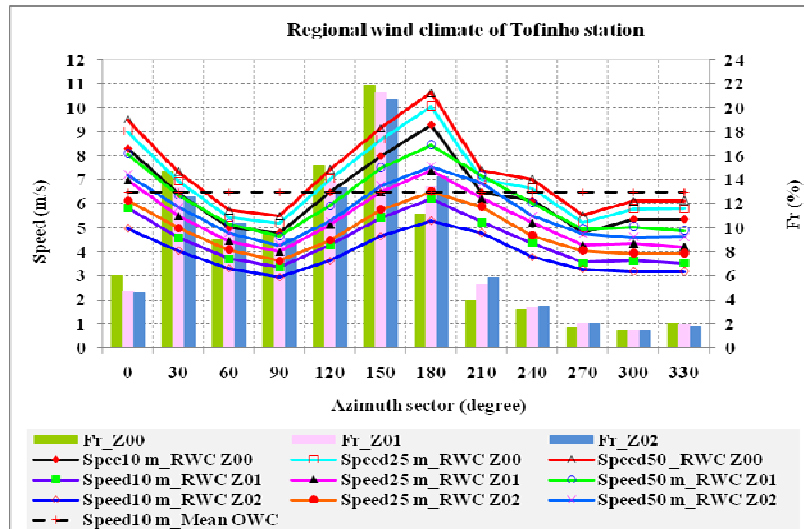


Figure 4. 26: Regional wind climate of Tofinho meteorological station.

4.4.3 Predicted wind climate for the Tofinho area

The predicted wind climate (PWC) was calculated for two potential wind turbine sites located on the south-westward of meteorological station at distances between 3 and 4.5 km from the meteorological station to site 2 and site 1 respectively (Fig. 4.27).

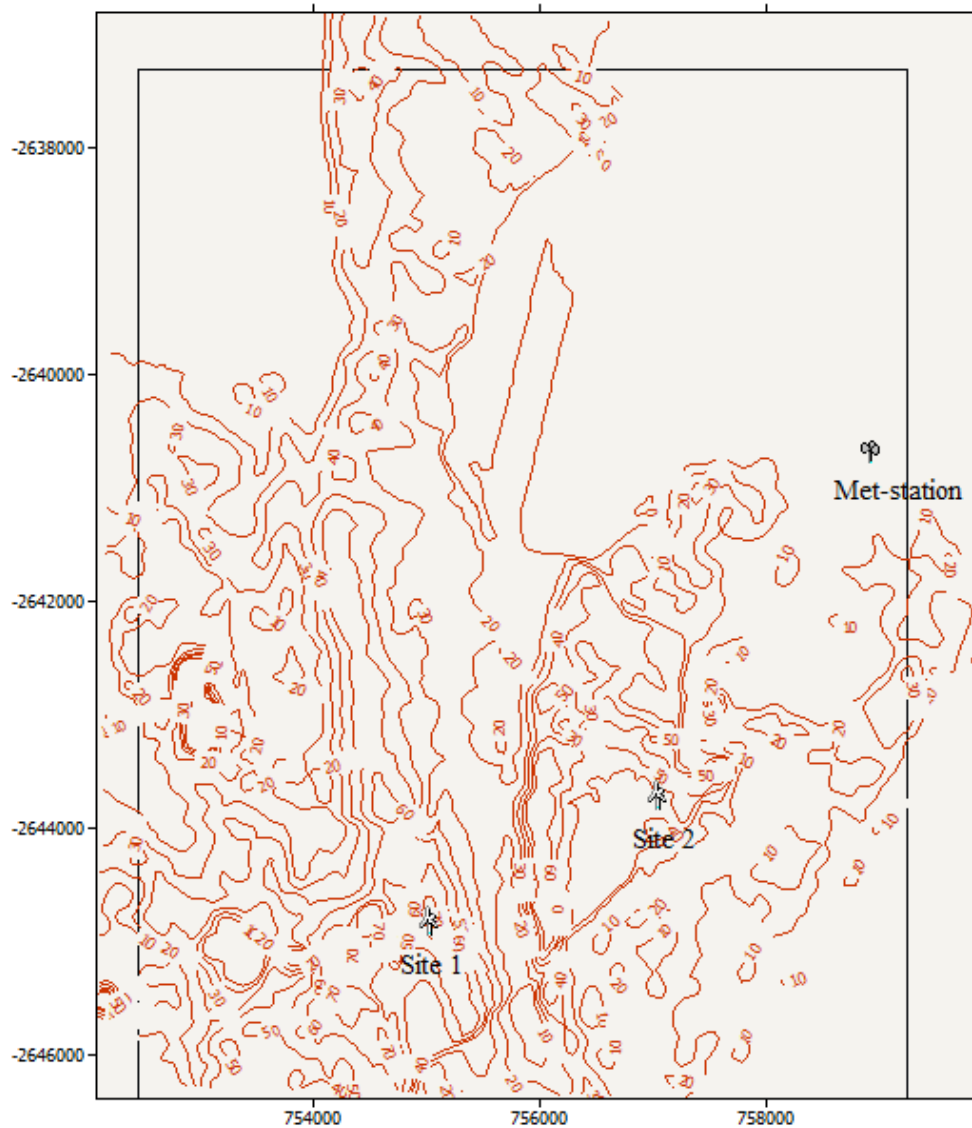


Figure 4. 27: Map showing the location of the two potential wind turbine sites (★) and the location of the Tofinho meteorological station (⊕) and the selected area for wind resource maps.

The predicted mean annual wind speeds and extractable energy at the two potential wind turbine sites are presented in Figure 4.28 for five heights a.g.l. The mean annual wind speed is about 6.0 ms^{-1} at 10 m a.g.l. Higher mean annual wind speeds are found at higher levels (50 and 60 m) where values approach 8.0 ms^{-1} at the two sites. Available wind energy at 60 m a.g.l. ranges between 441 and 504 Wm^{-2} at the two different sites. In general, the wind resource in the vicinity of Tofinho is good.

A similarity of the predicted wind climate (PWC) to the regional wind climate (RWC) is found for the roughness class 0 ($Z_{00}=0.00 \text{ m}$) at higher levels (above 25 m) and roughness class 1 and class 2 ($Z_{01}=0.030$, $Z_{02}=0.10 \text{ m}$) at lower levels (10 - 25 m a.g.l.).

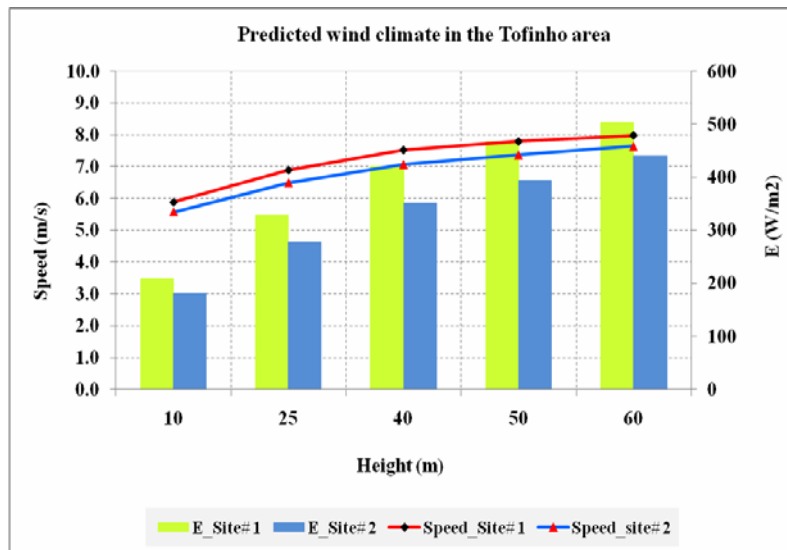


Figure 4. 28: Predicted mean wind speed and available wind energy at two potential wind turbine sites in the Tifinho area.

Figure 4.29 illustrates the predicted wind rose and wind speed frequency distribution at sites 1 and 2 in the Tofinho area. It is noted that the winds are predominantly from the 150° and 30° sectors. Highest predicted wind speeds are associated with the 180° and 150° and 0° to 30° directional sectors (Fig. 4.30).

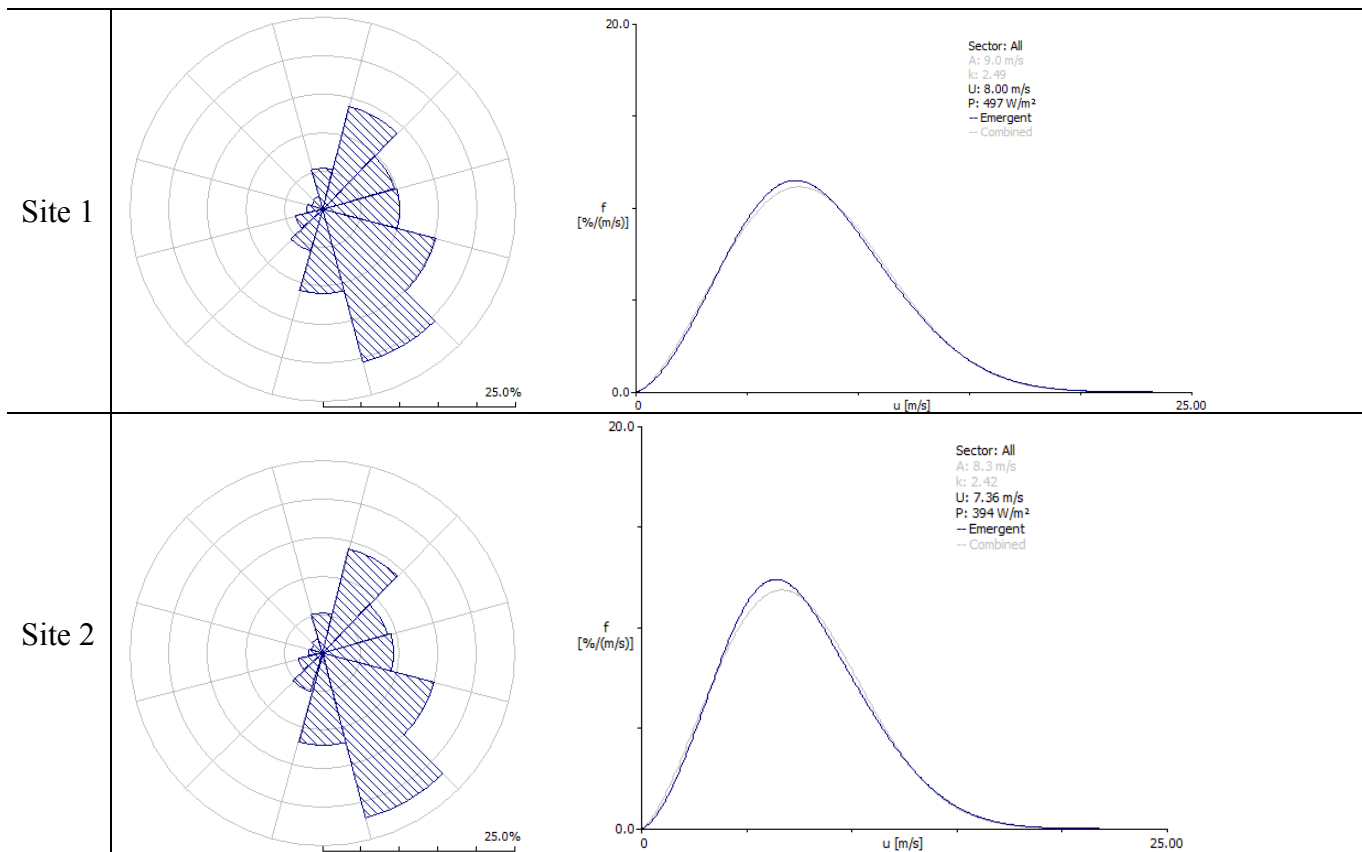


Figure 4. 29: Predicted wind rose and wind speed frequency distribution at potential wind turbine sites in the Tofinho area.

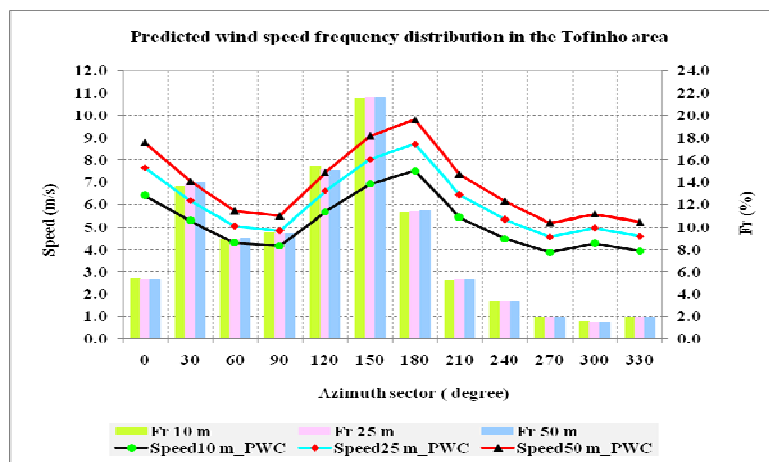


Figure 4. 30: Predicted wind speed frequency distribution for 3 standard heights (10, 25 and 50 m a.g.l.) at potential wind turbine sites in the Tofinho area.

The annual energy production or extractable wind energy (AEP) in the Tofinho area is between 2 359 and 2 990 MWh for heights greater than 25 m a.g.l. and less than 1 600 MWh for 10 m a.g.l. hub height. Figure 4.31 illustrates the extractable wind energy in two sites in the Tofinho area.

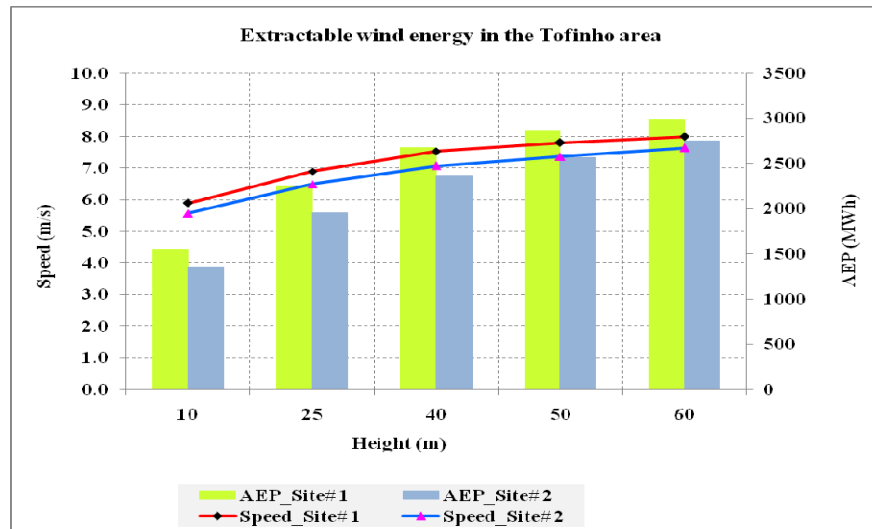


Figure 4. 31: The extractable wind energy at two potential wind turbine sites in the Tofinho area.

The highest extractable wind energy is from the 150° and 180° azimuth sectors. Figure 4.32 depicts the extractable wind energy by azimuth sector for three standard heights (10, 25 and 50 m a.g.l.) at potential turbine sites in the Tofinho area, while Figure 4.33 illustrates the extractable energy rose and wind energy frequency distribution at 50 m a.g.l. at site 1 in the Tofinho area.

The speed-up (down) due to roughness change and orography at the lowest level (10 m a.g.l.) was between -16.0 and 0.0% and 3.8 to 10.0%, while at highest level (50 m a.g.l.) it was between -7.7 and 0.0% and 2.8 to 5.5% respectively. The turning effect due to orography was between -1.4° and 1.5° at 10 m a.g.l. and -0.7° to 0.7° at 50 m a.g.l.

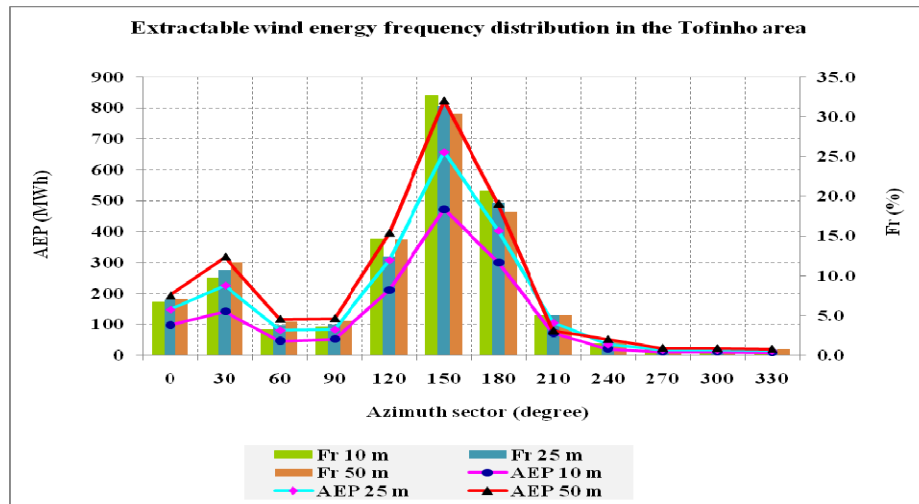


Figure 4. 32: Extractable average wind energy by azimuth sector for 3 standard heights (10, 25 and 50 m a.g.l.) at potential wind turbine sites in the Tofinho area.

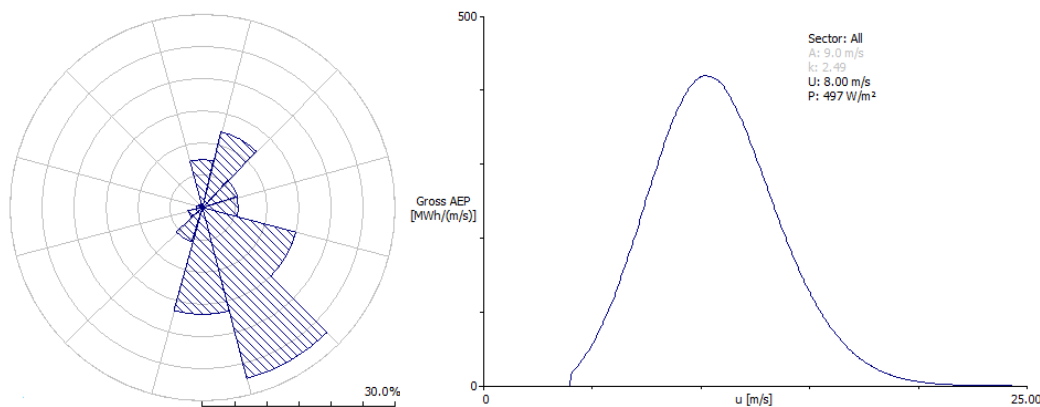


Figure 4. 33: Extractable energy rose and energy frequency distribution at 50 m a.g.l. at site 1 in the Tofinho area.

4.4.4 Wind resource maps

The wind resource maps (Fig. 4.34) illustrate the spatial distribution of wind speed and energy resource in the Tofinho area at a height of 55 m a.g.l. The average wind speed over the domain is 6.6 ms^{-1} and the mean annual energy production (AEP) is 2 031 MWh. Highest wind energy potential is in the south-western highland areas inland of the meteorological station area, around sites 1 and 2 and towards the north-west, where the

mean wind speed reaches 7.5 ms^{-1} with an AEP of 2 633 MWh. The SE (150°) - S-SW (210°) and N sectors are these with higher magnitude of mean wind speed ($6.3 - 7.5 \text{ ms}^{-1}$) and AEP (2 000 – 2 633 MWh). The site with UTM coordinates of 752996; -2642558 is the site with the highest wind energy potential.

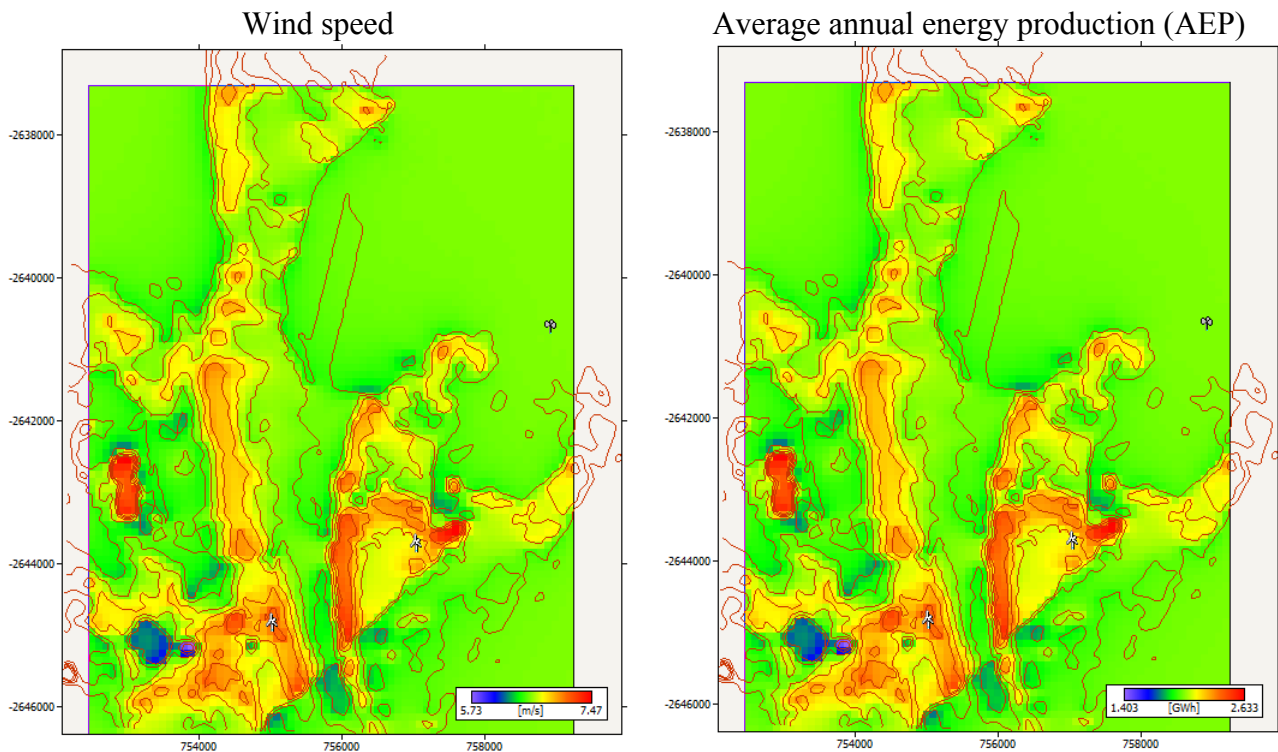


Figure 4. 34: Wind speed and energy resource maps in the Tofinho area.

4.5 Results for Vilankulo

4.5.1 Observed wind data

The Vilankulo meteorological station has a mean annual observed wind speed of 3.3 ms^{-1} and an available wind energy of 45 Wm^{-2} for all azimuth sectors. Figure 4.35 shows the observed wind rose and wind speed frequency distribution at Vilankulo.

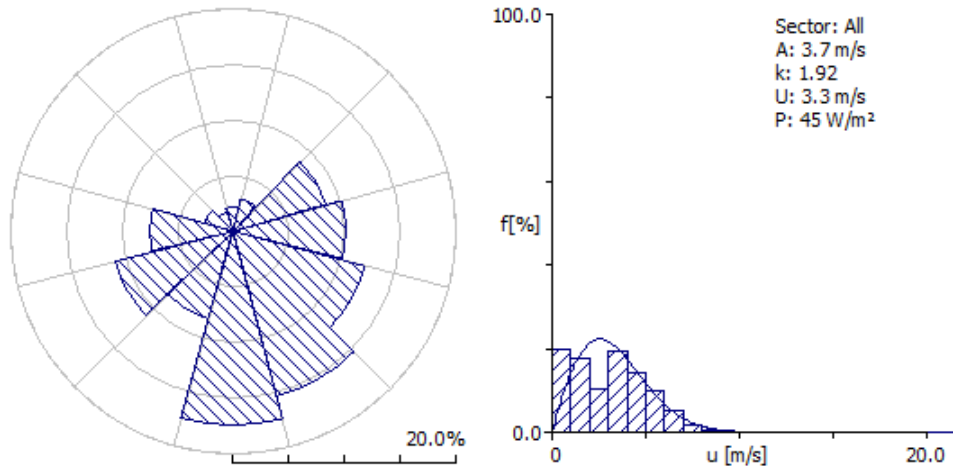


Figure 4.35: Observed wind rose and wind speed frequency distribution at Vilankulo meteorological station.

The most frequent winds are from the 180° (17.5%) to 150° and 120° (15.2 and 12%) sectors (Figs. 4.35 and 4.36). High mean wind speeds and available wind energy are associated with the 180° (4.62 ms⁻¹; 86 Wm⁻²) sector.

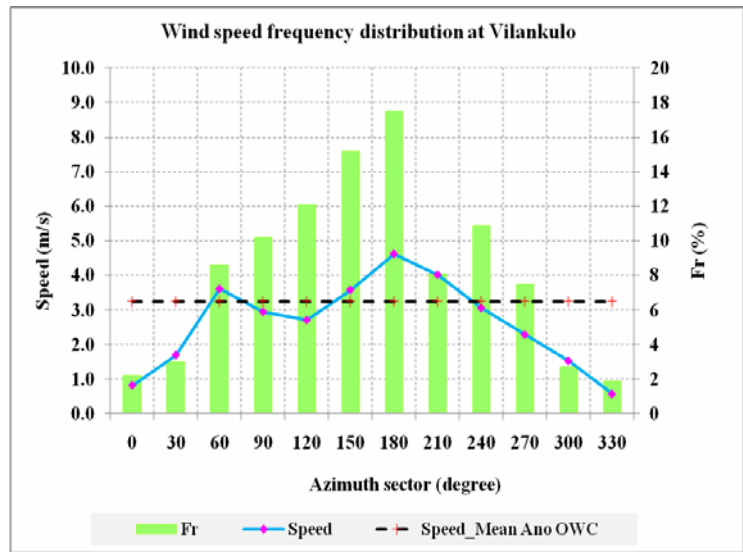


Figure 4.36: Wind speed frequency distribution and mean wind speed by directional sector at Vilankulo.

4.5.2 Wind atlas data at Vilankulo

After application of the wind atlas analysis sub-model, the relevant wind data for Vilankulo are presented in Table 4.4. The data are cleaned of the influence of obstacles and are presented for four roughness classes (0.00, 0.03, 0.10, and 0.40 m) and four standard heights. Figure 4.37 depicts the mean wind speed for three roughness classes (Z_{00} to Z_{02} representing roughness values of 0.00, 0.03 and 0.10 m respectively) and for the first three standard heights (10, 25 and 50 m). The results show clearly that relatively higher wind speeds are associated with lower roughness and with greater heights a.g.l. Highest wind speeds are associated with the 180° and 150° directional sector (Fig. 4.37).

Table 4. 4: Wind atlas data at Vilankulo, where A = Weibull scale factor; k = Weibull shape factor; v = mean wind speed; and E = Available wind energy (or Power density).

Height [m]	Parameter	Roughness-class			
		0.00 m	0.03 m	0.10 m	0.40 m
10	A [ms^{-1}]	5.1	3.6	3.1	2.5
	K	1.86	1.64	1.63	1.65
	U [ms^{-1}]	4.6	3.2	2.8	2.2
	E [Wm^{-2}]	120	48	31	15
25	A [ms^{-1}]	5.6	4.3	3.8	3.2
	K	1.89	1.75	1.72	1.73
	U [ms^{-1}]	4.9	3.8	3.4	2.9
	E [Wm^{-2}]	150	76	55	33
50	A [ms^{-1}]	5.9	5.0	4.5	3.9
	K	1.90	1.90	1.87	1.85
	U [ms^{-1}]	5.2	4.4	4.0	3.5
	E [Wm^{-2}]	175	106	81	54
100	A [ms^{-1}]	6.2	5.9	5.4	4.8
	K	1.81	2.00	2.00	2.03
	U [ms^{-1}]	5.5	5.2	4.8	4.2
	E [Wm^{-2}]	214	169	129	87

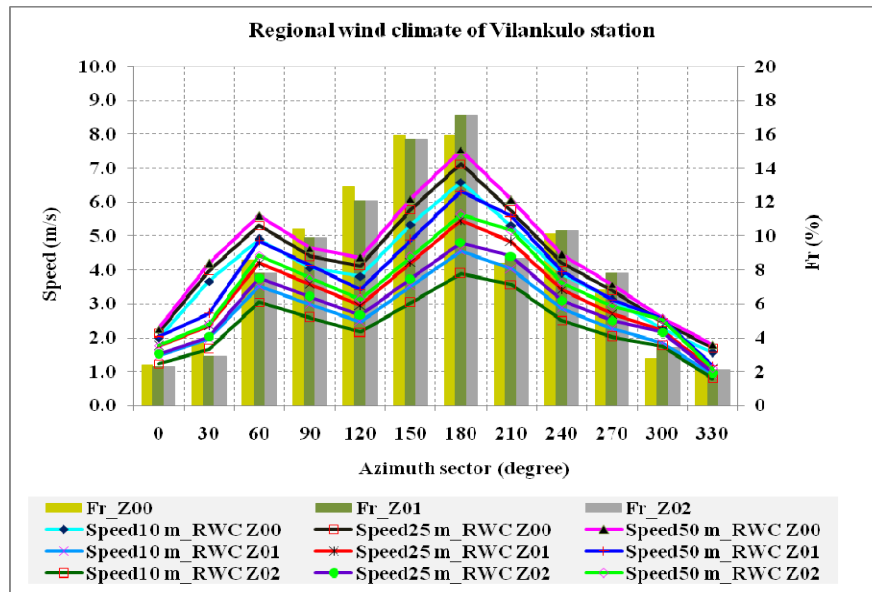


Figure 4. 37: Regional wind climate of Vilankulo meteorological station.

4.5.3 Predicted wind climate for the Vilankulo area

The predicted wind climate (PWC) was calculated for two potential wind turbine sites located on the south-westward of meteorological station at distances between 2 and 7 km from the meteorological station to site 2 and site 1 respectively (Fig. 4.38).

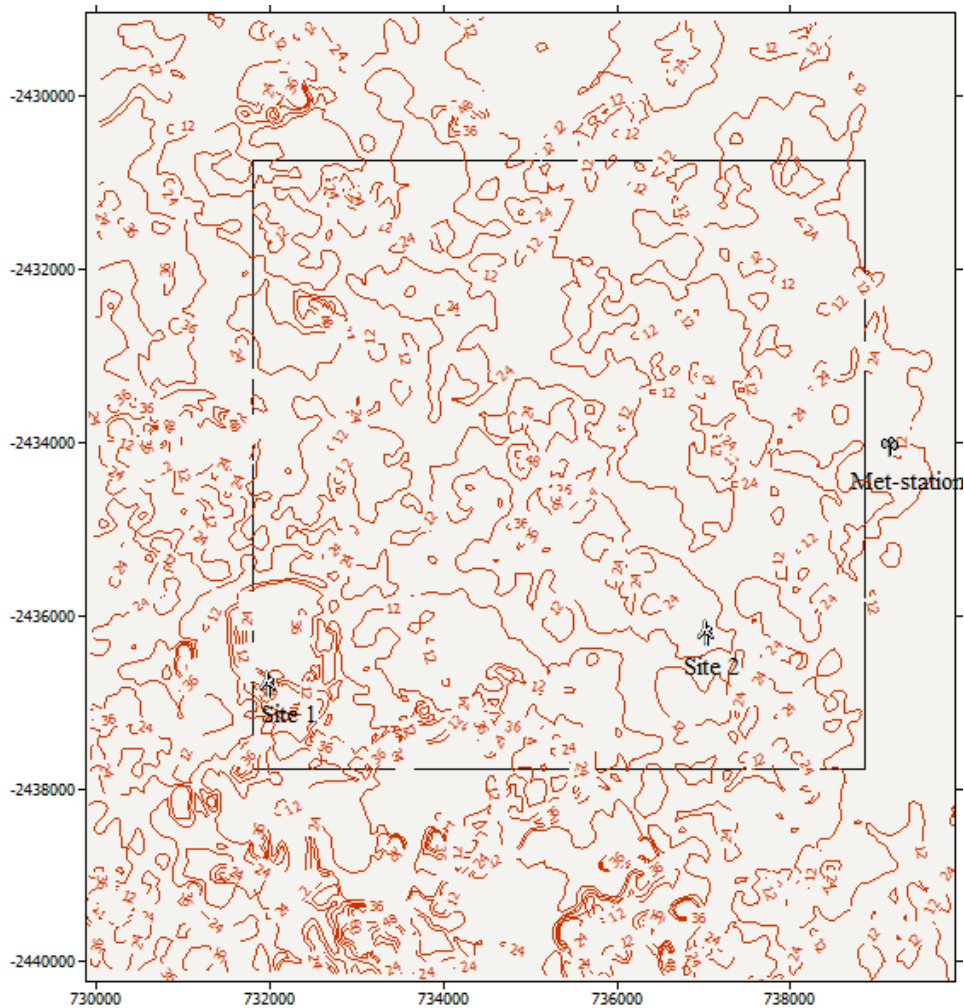


Figure 4. 38: Map showing the location of the two potential wind turbine sites (🌪️) and the location of the Vilankulo meteorological station (🌤️) and the selected area for wind resource maps.

The predicted mean annual wind speeds and extractable energy at the two potential wind turbine sites are presented in Figure 4.39 for four heights a.g.l. The mean annual wind speed is greater than 3.5 ms^{-1} at 10 m a.g.l. The higher mean annual wind speeds are found at higher levels (40 and 50 m a.g.l.) where values approach 4.99 ms^{-1} at the two sites. Available wind energy at 50 m a.g.l. ranges between 138 and 145 Wm^{-2} at the two different sites.

A similarity of the predicted wind climate (PWC) to the regional wind climate (RWC) is found for the roughness class 0 ($Z_{00}=0.00$ m) at higher levels and class 1 ($Z_{01}=0.030$ m) at lower levels (10 and 25 m a.g.l.).

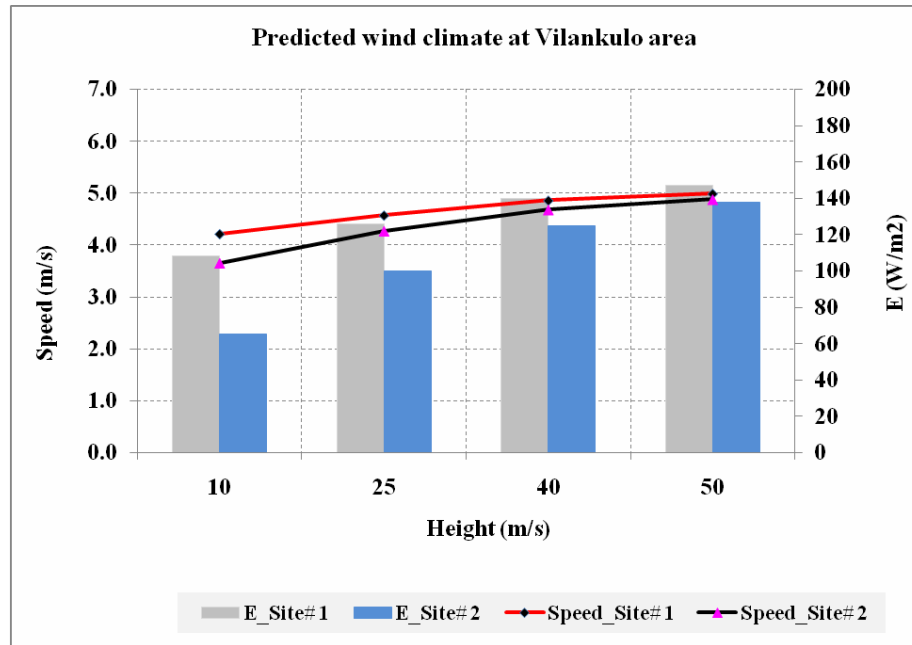


Figure 4.39: Predicted mean wind speed and available wind energy at two potential wind turbine sites in the Vilankulo area.

Figure 4.40 illustrates the predicted wind rose and wind speed frequency distribution at sites 1 and 2 in the Vilankulo area. It is noted that the winds are predominantly from the 180° , 150° and 120° sectors with a secondary contribution from the 90° and 240° sectors. Highest predicted wind speeds are associated with the 180° , 120° and 60° directional sectors (Fig. 4.41).

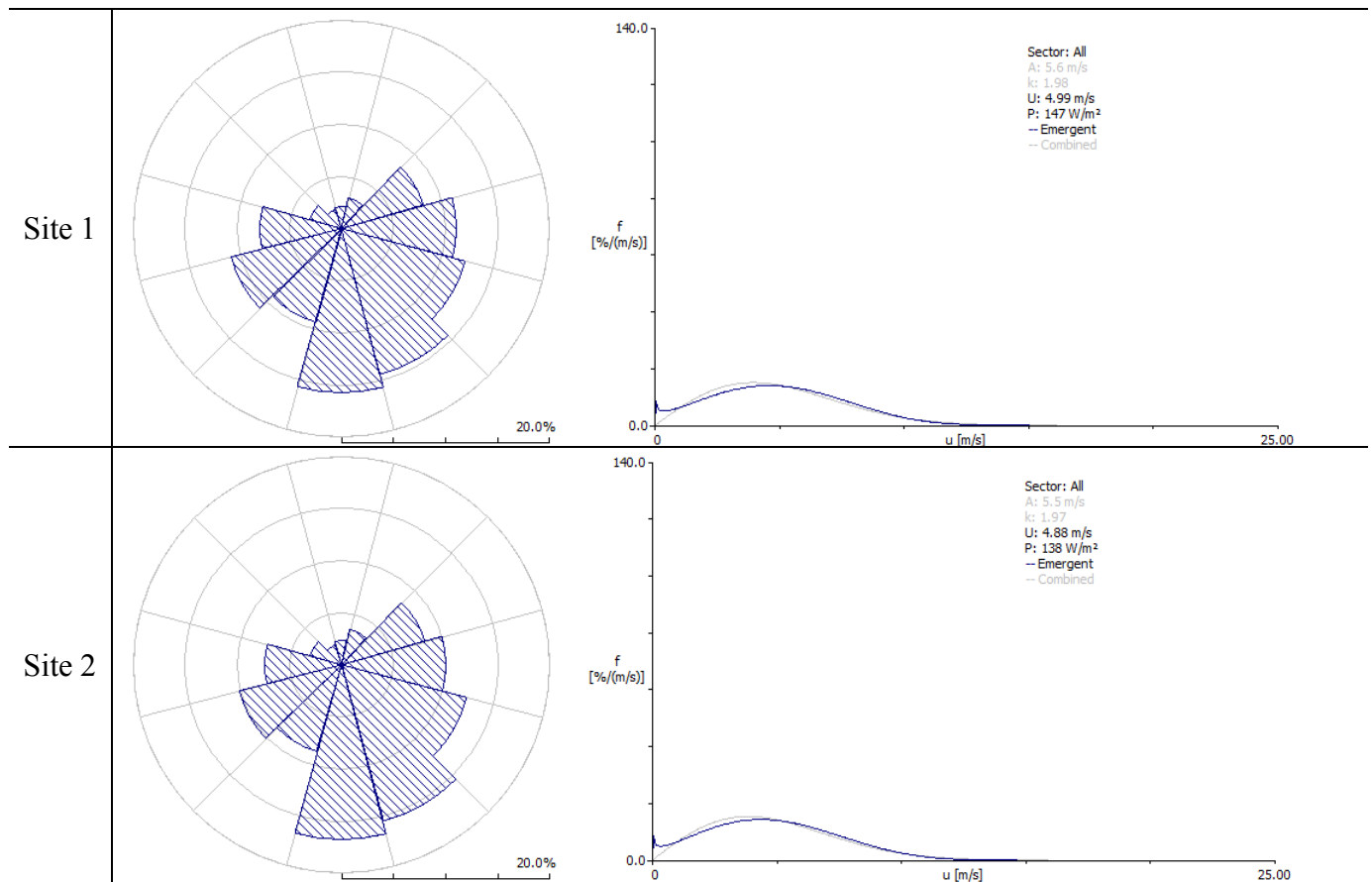


Figure 4. 40: Predicted wind rose and wind speed frequency distribution at potential wind turbine sites in the Vilankulo area.

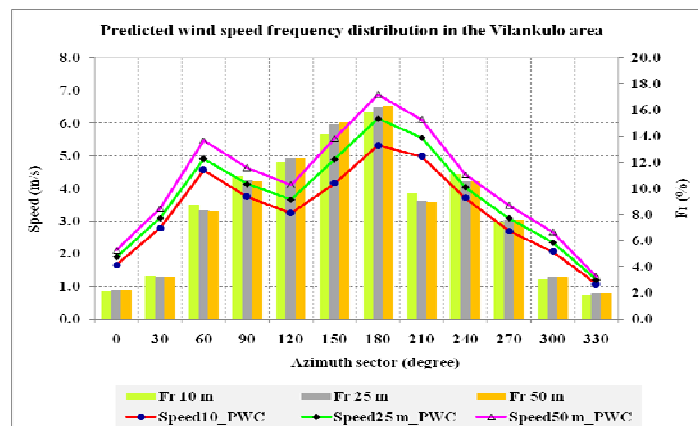


Figure 4. 41: Predicted wind speed frequency distribution for 3 standard heights (10, 25 and 50 m a.g.l.) at potential wind turbine sites in the Vilankulo area.

The annual energy production or extractable wind energy (AEP) in the Vilankulo area is between 936 and 1040 MWh for heights greater than 25 m a.g.l. and about 800 MWh for 10 m a.g.l. hub height. Figure 4.42 illustrates the extractable wind energy in two sites in the Vilankulo area.

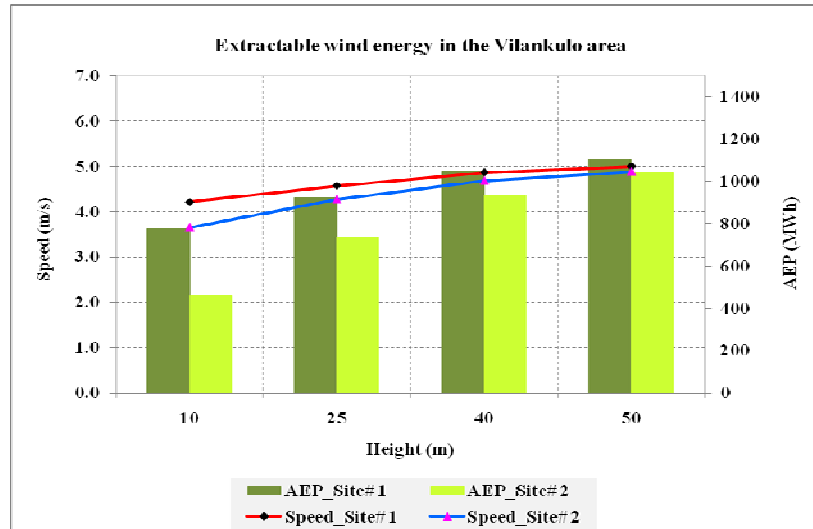


Figure 4. 42: The extractable wind energy at two potential wind turbine sites in the Vilankulo area.

The azimuth sectors with greater frequency of extractable wind energy are S-SW-SE (180° , 210° and 150°). Figure 4.43 depicts the average extractable wind energy by azimuth sector for three standard heights (10, 25, and 50 m a.g.l.) at turbine sites in the Vilankulo area while Figure 4.44 illustrates the extractable energy rose and wind energy frequency distribution at 50 m a.g.l. at site 2 in the Vilankulo area.

The speed-up (down) due to roughness change and orography at the lower level (10 m a.g.l.) was between -7.1 and 9.3% and 0.6 to 15.1%, while at higher level (50 m a.g.l.) it was between -3.4 and 1.4% and 1.9 to 7.4% respectively. The turning effect due to orography was between -3.6° and 3.3° at 10 m a.g.l. and -1.5° to 1.5° at 50 m a.g.l.

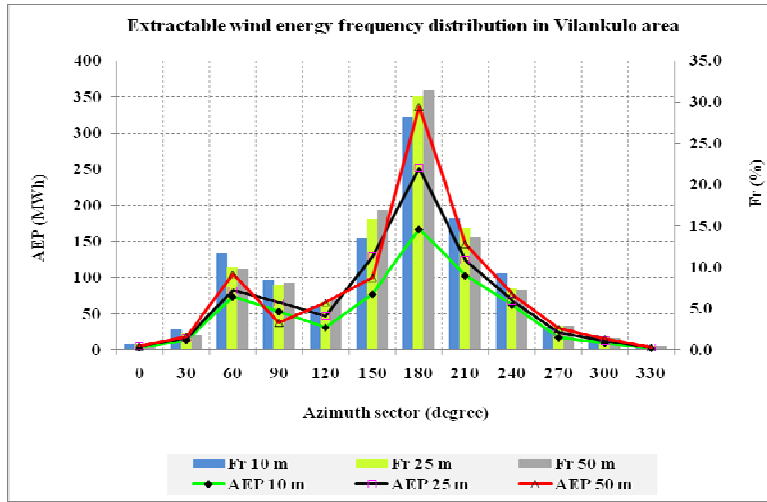


Figure 4. 43: Extractable average wind energy by azimuth sector for 3 standard heights (10, 25 and 50 m a.g.l.) at potential wind turbine sites in the Vilankulo area.

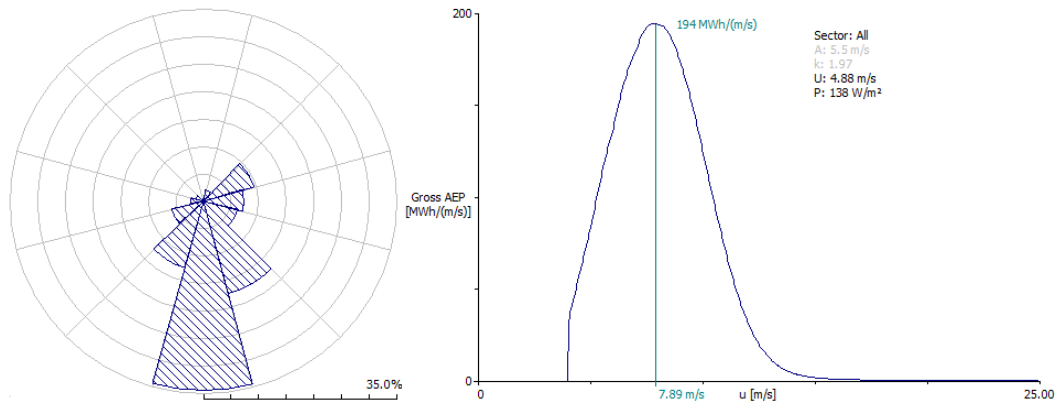


Figure 4. 44: Extractable energy rose and energy frequency distribution at 50 m a.g.l. at site 2 in the Vilankulo area.

4.5.4 Wind resource maps

The wind resource maps illustrate the spatial distribution of wind speed (Fig. 4.45) and energy resource (Fig. 4.46) in the Vilankulo area at a height of 55 m a.g.l. The map gives an average wind speed of 4.42 ms^{-1} and a mean annual energy production (AEP) of

793 MWh. The higher potential wind energy potential is found on south-west side of meteorological station and in the vicinity of site 2 towards the NW where the mean wind speed reaches 4.7 ms^{-1} with an AEP of 980 MWh. The site with UTM coordinates of 732486; -2432454 is the site with the highest wind energy potential.

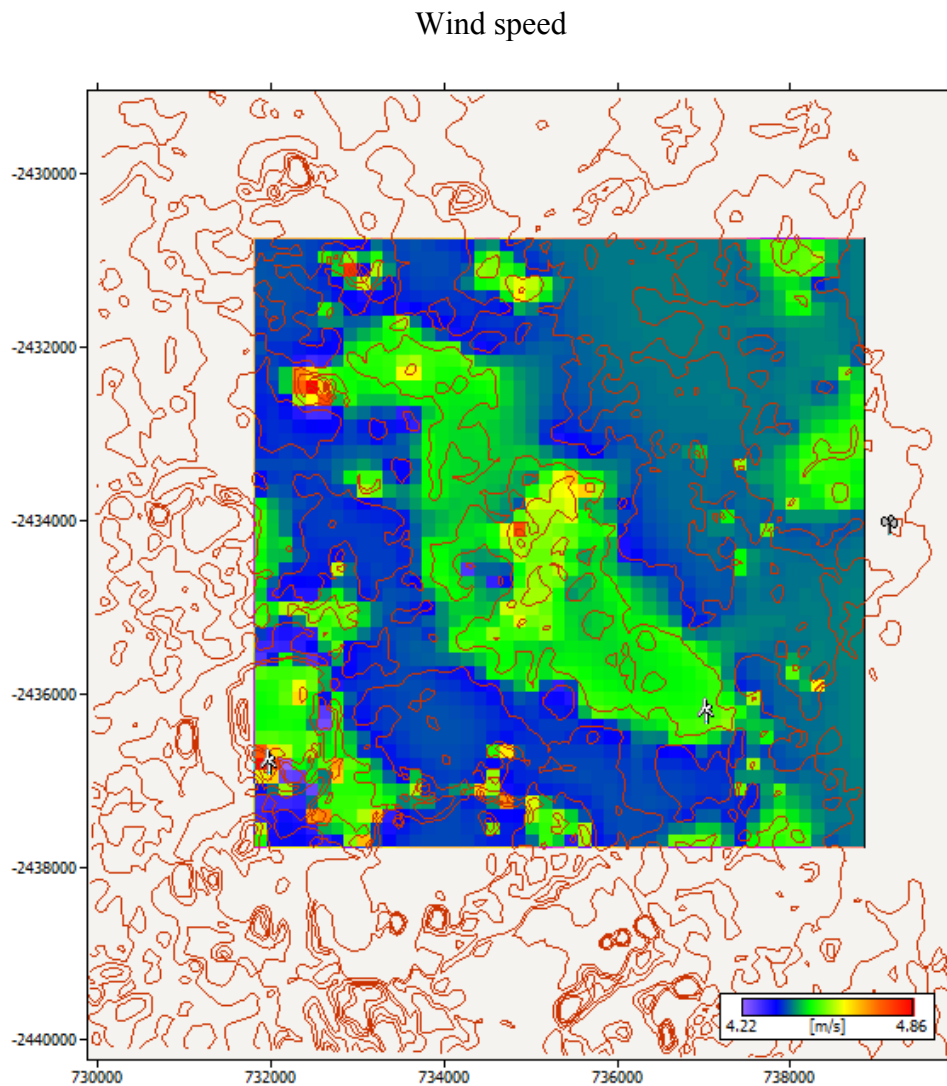


Figure 4. 45: Wind speed resource map in the Vilankulo area.

Average annual energy production (AEP)

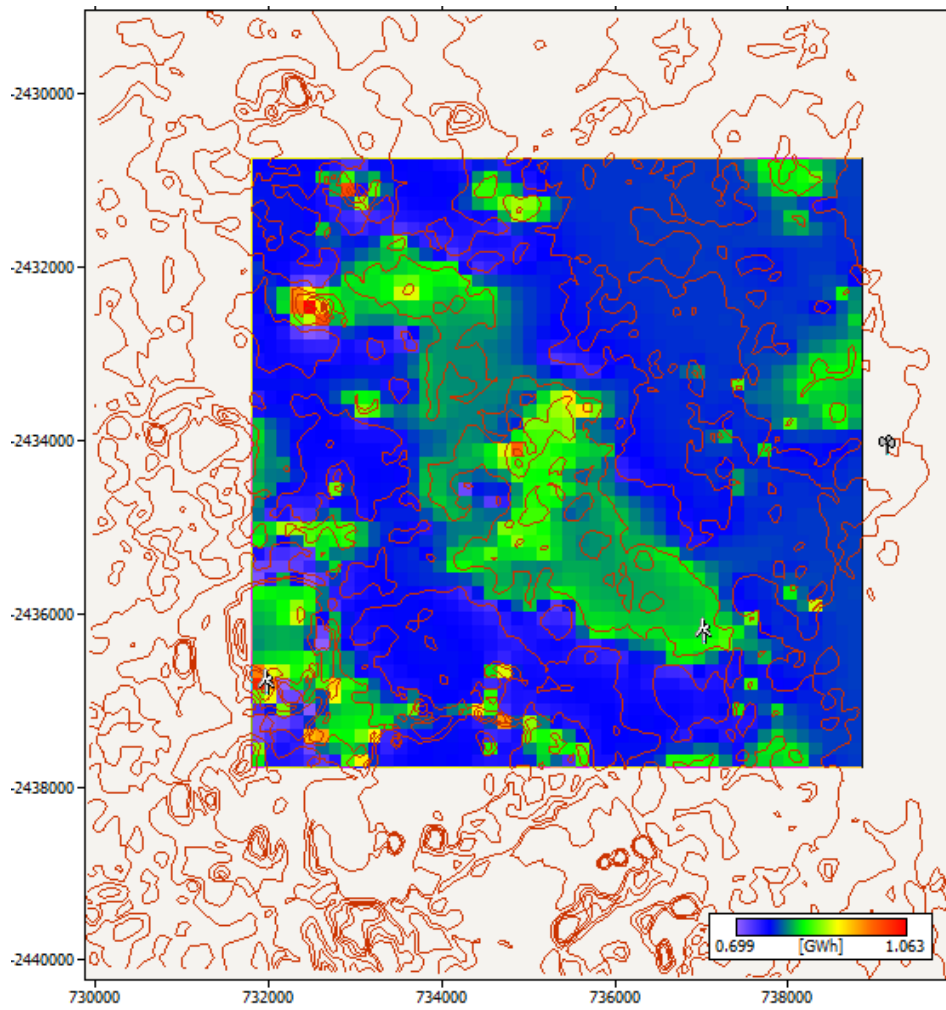


Figure 4. 46: Wind energy resource map in the Vilankulo area.

4.6 Results for Pemba

4.6.1 Observed wind data

The Pemba meteorological station has a mean annual observed wind speed of 3.7 ms^{-1} and an available wind energy of 57 Wm^{-2} for all azimuth sectors. Figure 4.47 shows the observed wind rose and wind speed frequency distribution at Pemba.

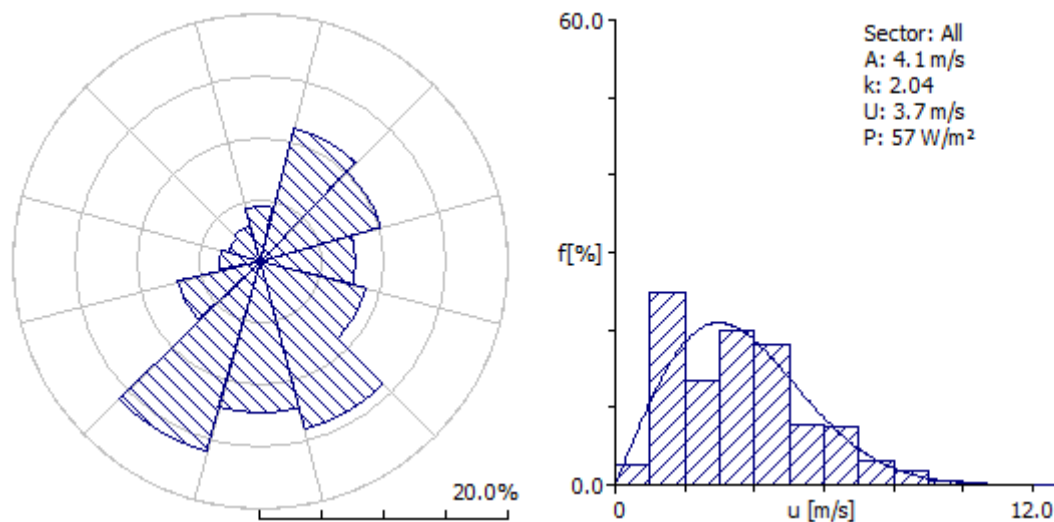


Figure 4.47: Observed wind rose and wind speed frequency distribution at Pemba meteorological station.

The most frequent winds are from the 210° (16.0%) and 150° to 180° (14% and 12.2%) sectors (Figs. 4.47 and 4.48). Highest mean wind speeds and available wind energy are associated with the 150° and 180° (4.65 and 4.55 ms^{-1} ; 102 and 93 Wm^{-2}) with a secondary maximum from the 30° (4.18 ms^{-1} ; 69 Wm^{-2}) sectors.

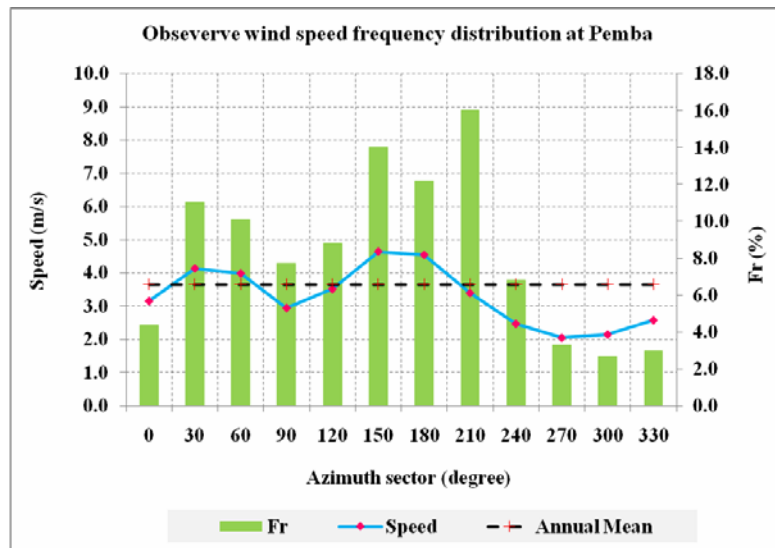


Figure 4.48: Wind speed frequency distribution and mean wind speed by directional sector at Pemba.

4.6.2 Wind atlas data at Pemba

After application of the wind atlas analysis sub-model, the relevant wind data for Pemba are presented in Table 4.5. The data are cleaned of the influence of obstacles and are presented for four roughness classes (0.0, 0.03, 0.1, and 0.4 m) and four standard heights. Figure 4.49 depicts the mean wind speed for three roughness classes (Z_{00} to Z_{02} representing roughness values of 0.00, 0.03 and 0.10 m respectively) and for the first three standard heights (10, 25 and 50 m a.g.l.). The results show clearly that relatively higher wind speeds are associated with lower roughness and with greater heights a.g.l. Highest wind speeds are associated with the 150° directional sector (Fig. 4.49).

Table 4. 5: Wind atlas data at Pemba, where A = Weibull scale factor; k = Weibull shape factor; and E = Available wind energy (or Power density).

Height [m]	Parameter	Roughness-class			
		0.00 m	0.03 m	0.10 m	0.40 m
10	A [ms ⁻¹]	4.8	3.3	2.9	2.2
	k	2.01	1.74	1.77	1.75
	V [ms ⁻¹]	4.2	2.9	2.5	2.0
	E [Wm ⁻²]	87	34	22	11
25	A [ms ⁻¹]	5.2	3.9	3.5	2.9
	k	2.04	1.86	1.87	1.84
	V [ms ⁻¹]	4.6	3.5	3.1	2.6
	E [Wm ⁻²]	108	53	39	23
50	A [ms ⁻¹]	5.4	4.6	4.2	3.6
	k	2.06	2.04	2.04	1.98
	V [ms ⁻¹]	4.8	4.0	3.7	3.2
	E [Wm ⁻²]	127	75	57	37
100	A [ms ⁻¹]	5.7	5.4	5.0	4.3
	k	1.96	2.15	2.19	2.18
	V [ms ⁻¹]	5.1	4.8	4.4	3.8
	E [Wm ⁻²]	155	120	91	61

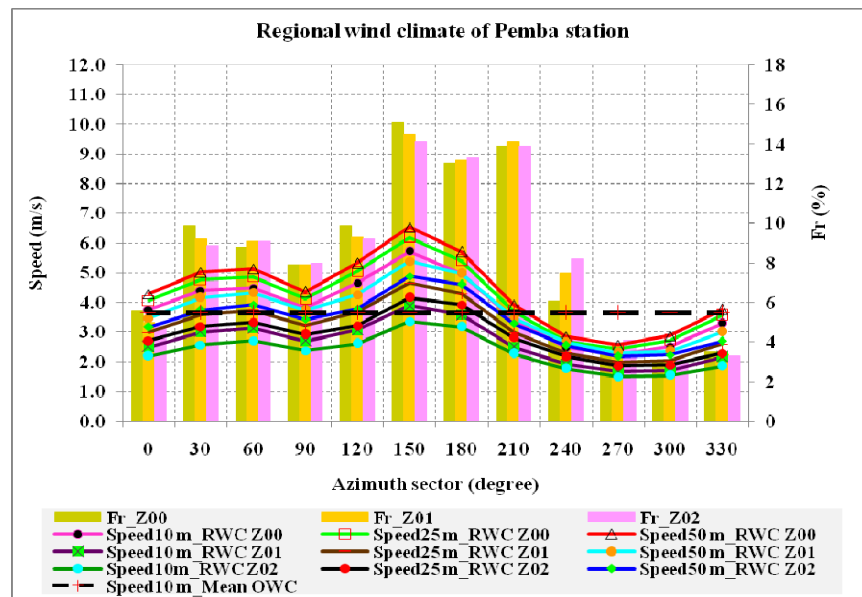


Figure 4. 49: Regional wind climate of Pemba meteorological station.

4.6.3 Predicted wind climate for the Pemba area

The predicted wind climate (PWC) was calculated for three potential wind turbine sites located on the east and south-eastward of the meteorological station at distances of 3 and 6 km from the meteorological station to site 1 and site 2 respectively, and 4 km to site 3 (Fig. 4.50).

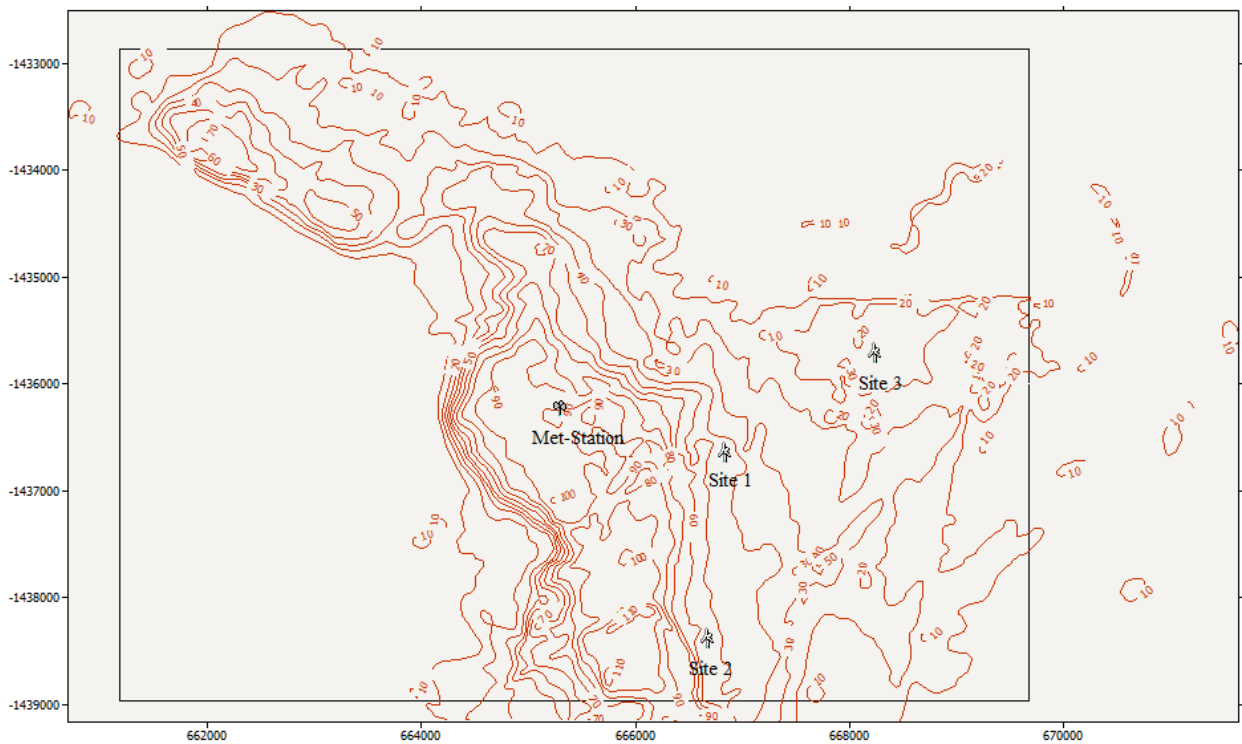




Figure 4. 50: Map showing the location of the three potential wind turbine sites () and the location of the Pemba meteorological station () and the selected area for wind resource maps.

The predicted mean annual wind speeds and extractable energy at the three potential wind turbine sites are presented in Figure 4.51 for five heights a.g.l. The mean annual wind speed is lower than the mean annual observed wind speed (3.7 ms^{-1}) at 10 m a.g.l. Highest mean annual wind speeds is almost similar for the three sites, where values approach 4.6 ms^{-1} at

higher levels (60 m a.g.l.). Available wind energy at 60 m a.g.l. ranges between 97 and 110 Wm^{-2} at the three different sites.

A similarity of the predicted wind climate (PWC) to the regional wind climate (RWC) is found for the roughness class 0 ($Z_{00}=0.00$ m) and class 1 ($Z_{01}=0.03$ m) for the higher levels (above 25 m a.g.l.) and to class 2 ($Z_{02}=0.10$ m) for the lower level (10 m a.g.l.).

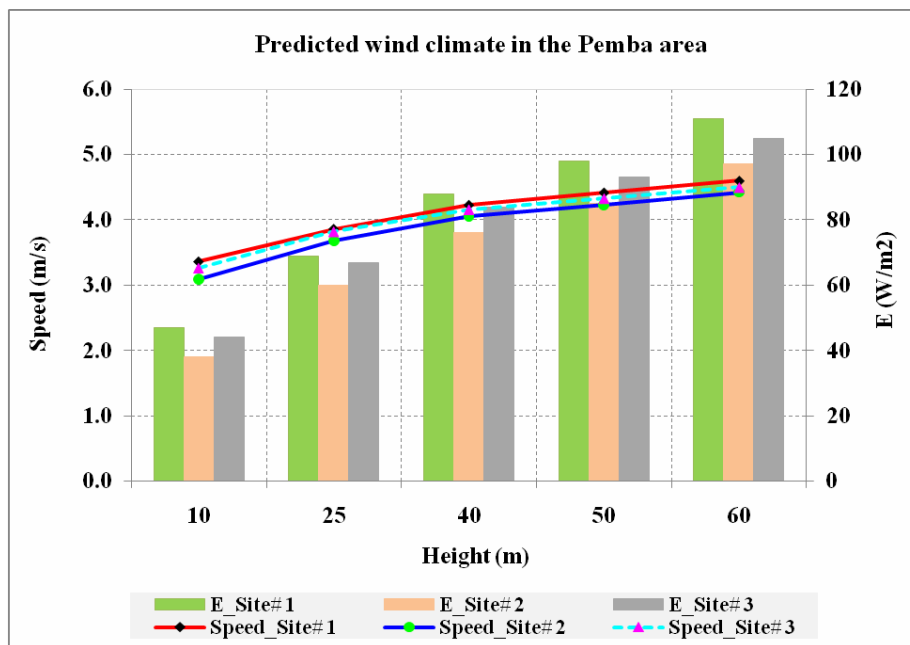


Figure 4.51: Predicted mean wind speed and available wind energy at three potential wind turbine sites in the Pemba area.

Figure 4.52 illustrates the predicted wind rose and wind speed frequency distribution at sites 1, 2 and 3 in the Pemba area. It is noted that the winds are predominantly from the 150°, 180° and 210° sectors. Highest predicted wind speeds are associated with the 150° and 180° directional sector (Fig. 4.53).

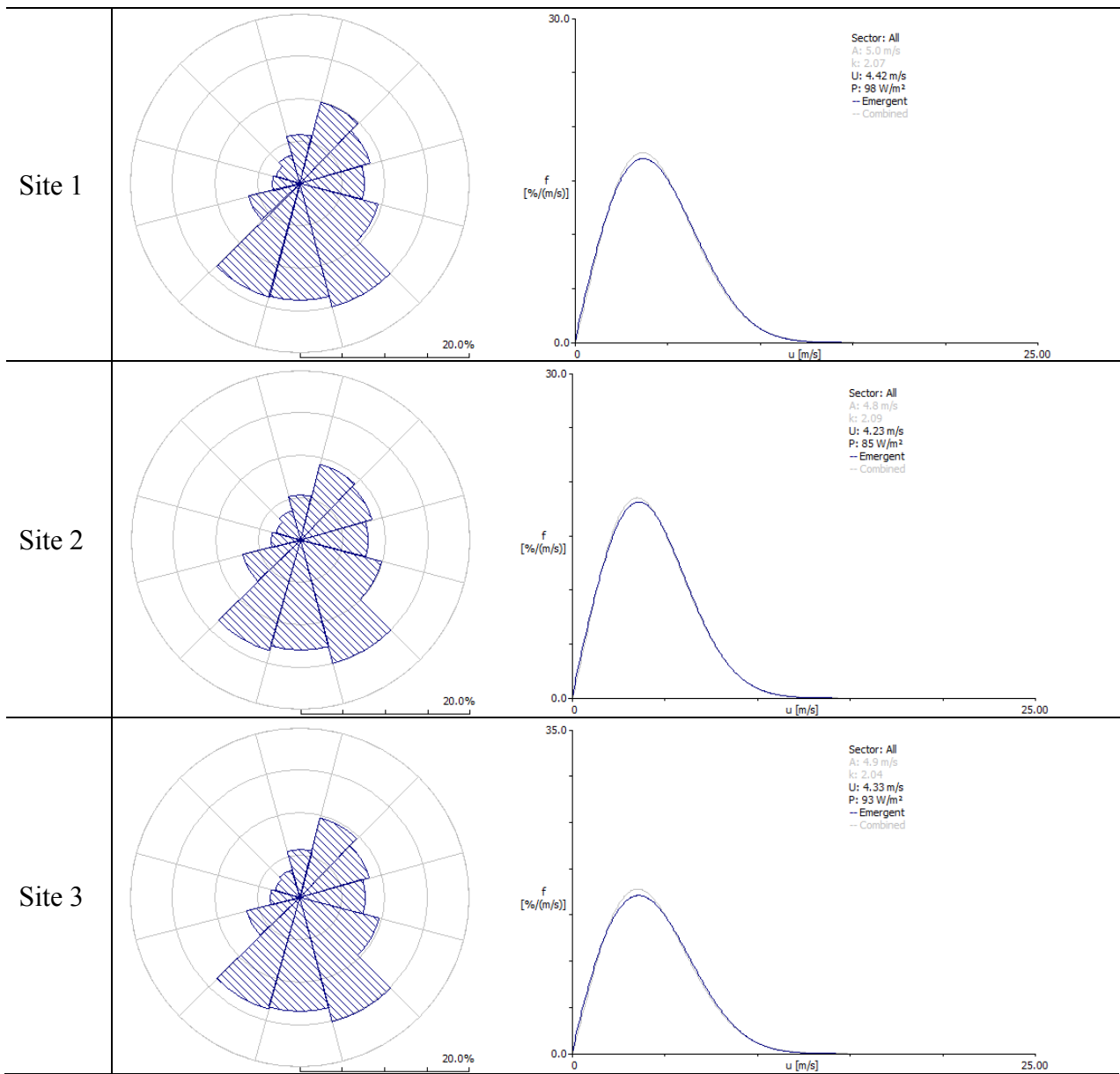


Figure 4. 52: Predicted wind rose and wind speed frequency distribution at potential wind turbine sites in the Pemba area.

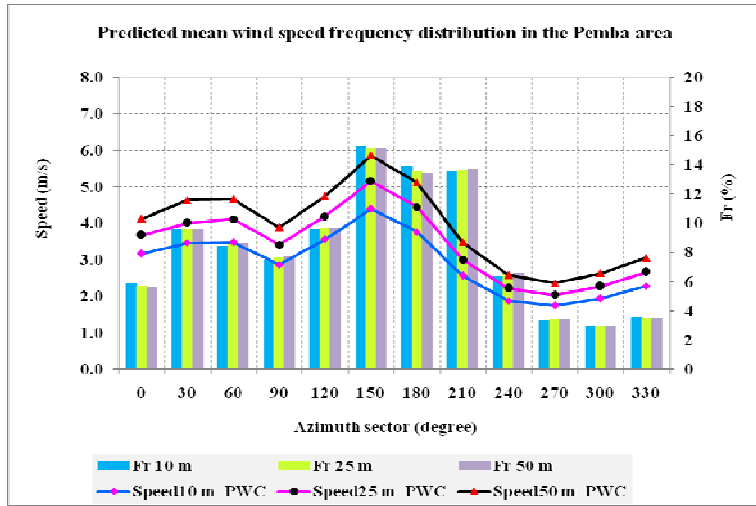


Figure 4. 53: Predicted wind speed frequency distribution for 3 standard heights (10, 25 and 50 m a.g.l.) at potential wind turbine sites in the Pemba area.

The annual energy production or extractable wind energy (AEP) in the Pemba area is between 600 and 900 MWh for heights greater than 25 m a.g.l. and less than 350 MWh for a 10 m hub height. Figure 4.54 illustrates the extractable wind energy at the three potential wind turbine sites in the Pemba area.

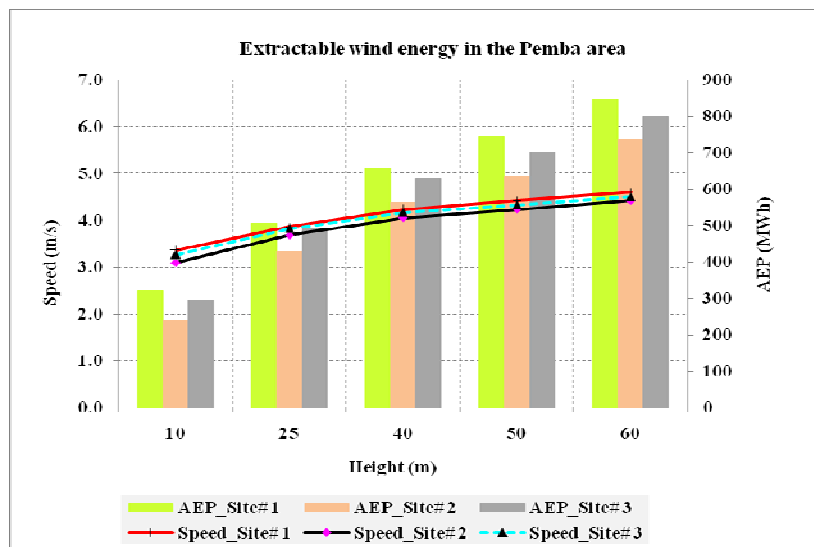


Figure 4. 54: The extractable wind energy at three potential turbine sites in the Pemba area.

The highest extractable wind energy is from the 150° and 180° azimuth sectors. Figure 4.55 depicts the average extractable wind energy by azimuth sector for three standard heights (10, 25 and 50 m a.g.l.) at potential turbine sites in the Pemba area, while Figure 4.56 illustrate the extractable energy rose and energy frequency distribution at 50 m a.g.l. at site 2 in the Pemba area.

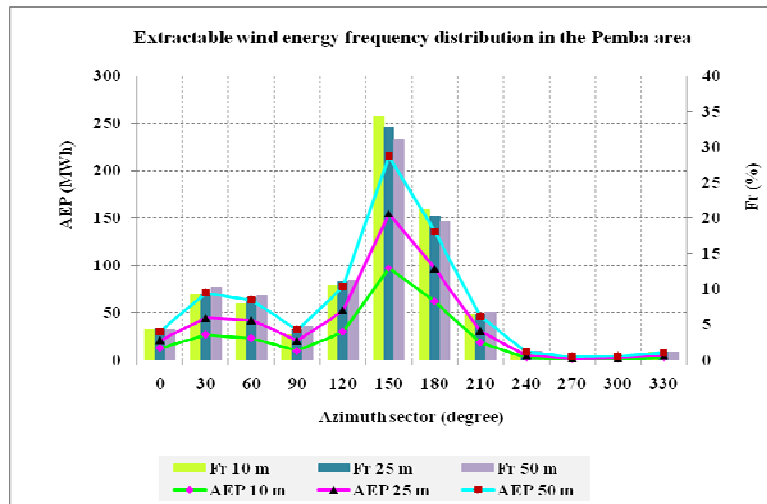


Figure 4. 55: Extractable average wind energy by azimuth sector for 3 standard heights (10, 25 and 50 m a.g.l.) at potential wind turbine sites in the Pemba area.

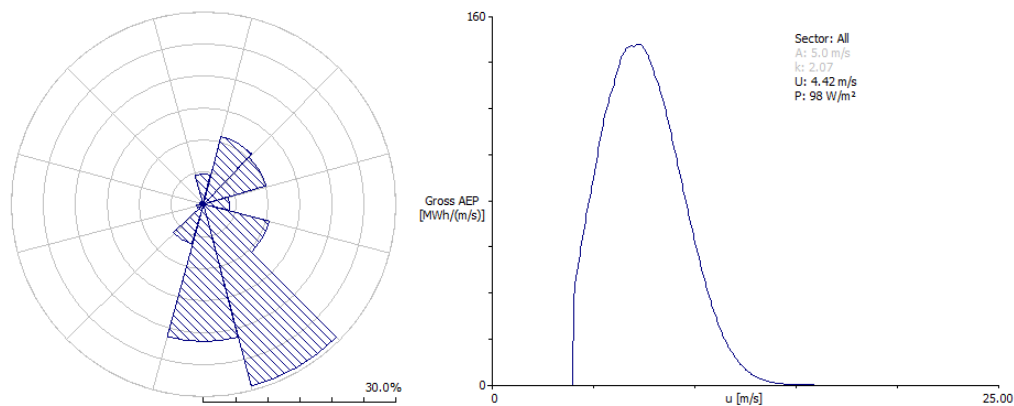


Figure 4. 56: Extractable energy rose and energy frequency distribution at 50 m a.g.l. at site 2 in the Pemba area.

The speed-up (down) due to roughness change and orography at the lowest level (10 m a.g.l.) was between -14 and 0.0% and -3.9 to 3.9%, while at highest level (50 m a.g.l.) it was between -6.3 and 0.0% and -1.7 to 2.3% respectively. The turning effect due to orography was between -2.5° and 2.5° at 10 m a.g.l. and -1.1° to 1.1° at 50 m a.g.l.

4.6.4 Wind resource maps

The wind resource maps illustrate the spatial distribution of wind speed (Fig. 4. 57) and energy resource (Fig. 4. 58) in the Pemba area at a height of 55 m a.g.l. The maps show an average wind speed of 4.10 ms^{-1} and a mean annual energy production (AEP) of 563 MWh. The highest wind energy potential is found around the meteorological station, as well as S and NW of meteorological station on the west side of Pemba Bay where the mean wind speed reaches 4.63 ms^{-1} with an AEP of 868 MWh. The site with UTM coordinates of 664427; -1436313 is the site with the highest wind energy potential.

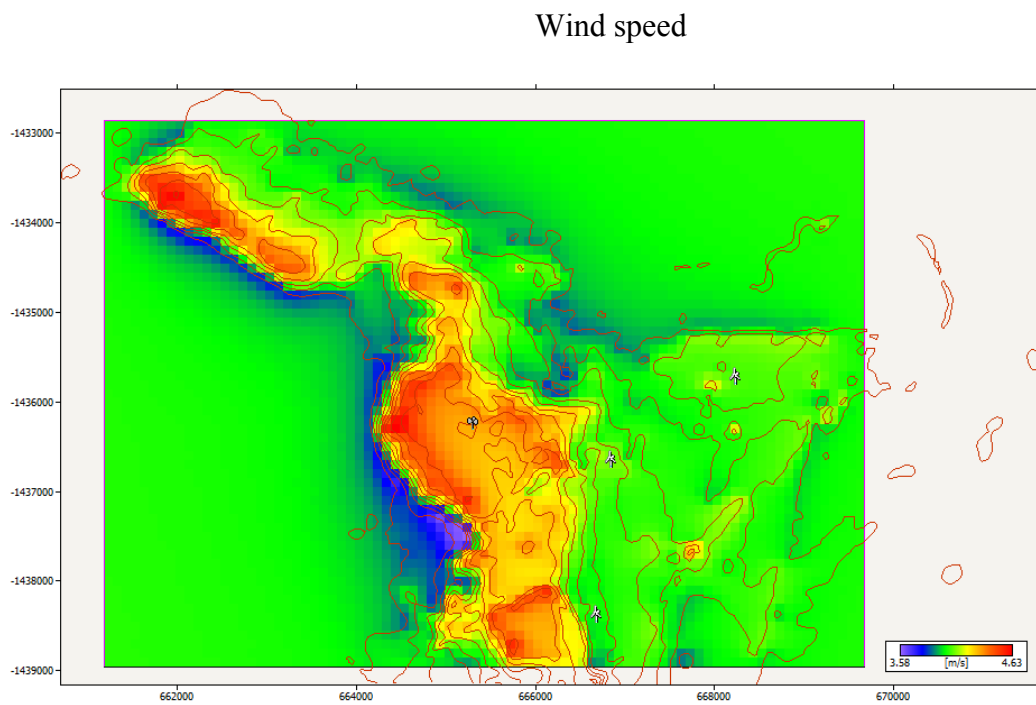


Figure 4. 57: Wind speed resource map in the Pemba area.

Average annual energy production (AEP)

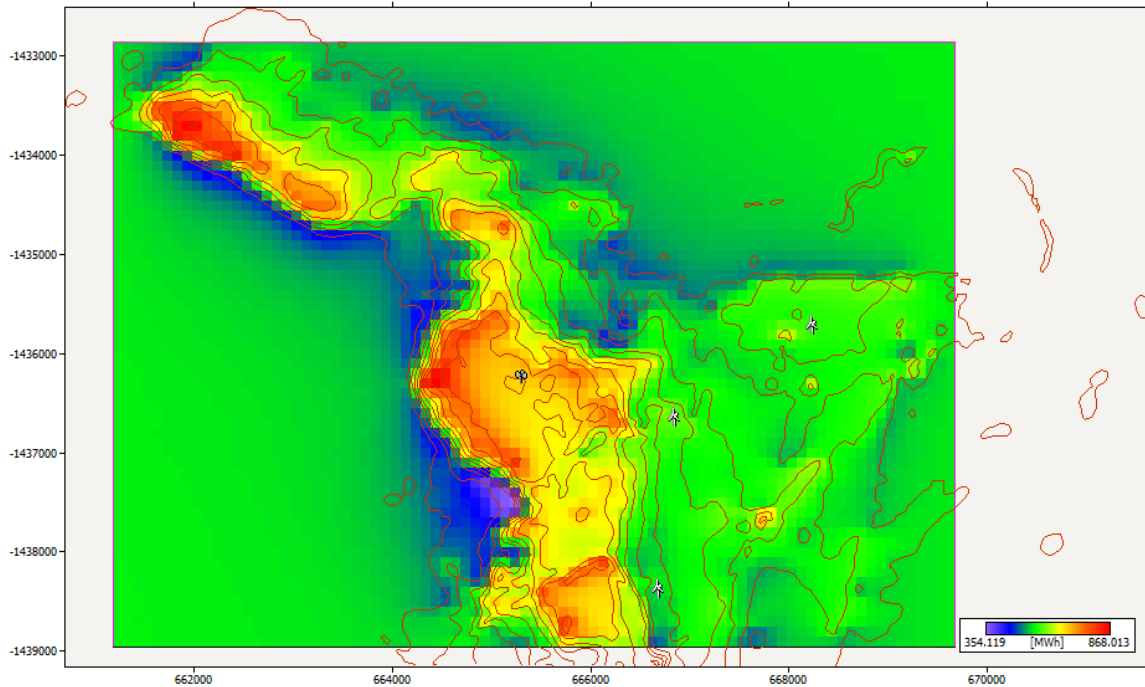


Figure 4. 58: Wind energy resource map in the Pemba area.

4.7 Results for Nampula

4.7.1 Observed wind data

The Nampula meteorological station has a mean annual observed wind speed of 3.0 ms^{-1} and an available wind energy of 30 Wm^{-2} for all azimuth sectors. Figure 4.59 shows the observed wind rose and wind speed frequency distribution at Nampula.

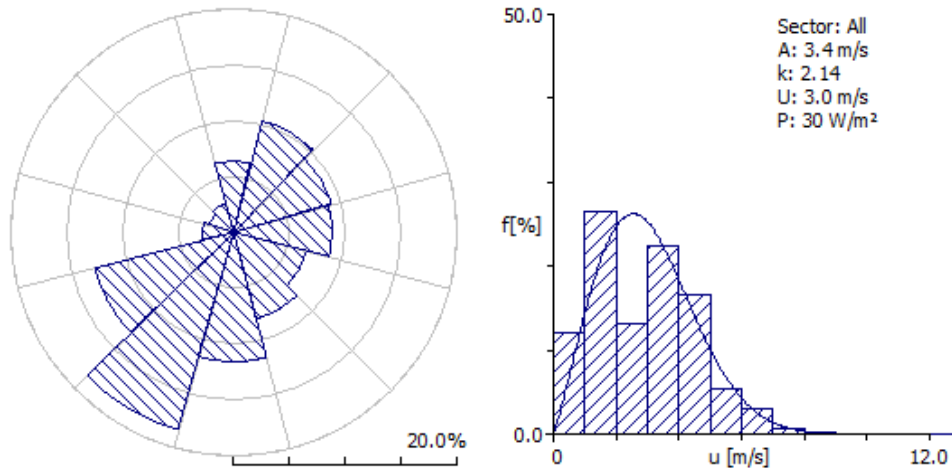


Figure 4.59: Observed wind rose and wind speed frequency distribution at Nampula meteorological station.

The most frequent winds are from the 210° (18.0%) to 240° (13%) with a secondary contribution from the 180° (12%) sectors (Figs. 4.59 and 4.60). Highest mean wind speeds and available wind energy are associated with the 210° (3.5 ms⁻¹; 38 Wm⁻²) sector.

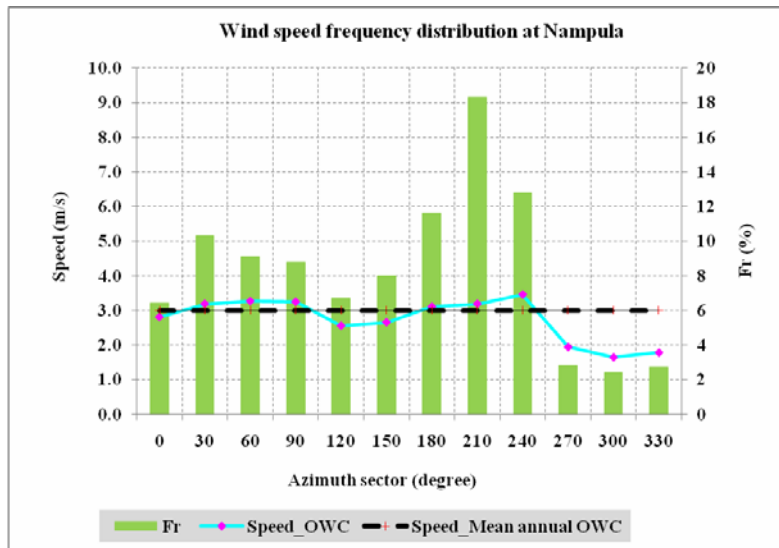


Figure 4.60: Wind speed frequency distribution and mean wind speed by directional sector at Nampula.

4.7.2 Wind atlas data at Nampula

After application of the wind atlas analysis sub-model, the relevant wind data for Nampula are presented in Table 4.6. The data are cleaned of the influence of obstacles and are presented for four roughness classes (0.00, 0.03, 0.10, and 0.40 m) and four standard heights. Figure 4.61 depicts the mean wind speed for three roughness classes (Z_{00} to Z_{02} representing roughness values of 0.00, 0.03 and 0.10 m respectively) and for the first three standard heights (10, 25 and 50 m a.g.l.). The results show clearly that relatively higher wind speeds are associated with lower roughness and with greater heights a.g.l. Highest wind speeds are associated with the 240° and 210° directional sector (Fig. 4.61).

Table 4. 6: Wind atlas data at Nampula, where A = Weibull scale factor; k = Weibull shape factor; v = mean wind speed; and E = Available wind energy (or Power density).

Height [m]	Parameter	Roughness-class			
		0.00 m	0.03mm	0.10 m	0.40 m
10	A [ms^{-1}]	4.6	3.2	2.7	2.2
	k	2.37	1.99	1.95	2.04
	U [ms^{-1}]	4.1	2.8	2.4	2.0
	E [Wm^{-2}]	67	26	17	8
25	A [ms^{-1}]	5.0	3.8	3.4	2.9
	k	2.41	2.13	2.08	2.15
	U [ms^{-1}]	4.4	3.4	3.0	2.6
	E [Wm^{-2}]	84	42	30	18
50	A [ms^{-1}]	5.2	4.4	4.0	3.5
	k	2.42	2.38	2.29	2.34
	U [ms^{-1}]	4.6	3.9	3.5	3.1
	E [Wm^{-2}]	99	59	45	30
100	A [ms^{-1}]	5.5	5.2	4.7	4.2
	k	2.28	2.52	2.49	2.62
	U [ms^{-1}]	4.9	4.6	4.2	3.8
	E [Wm^{-2}]	120	95	71	50

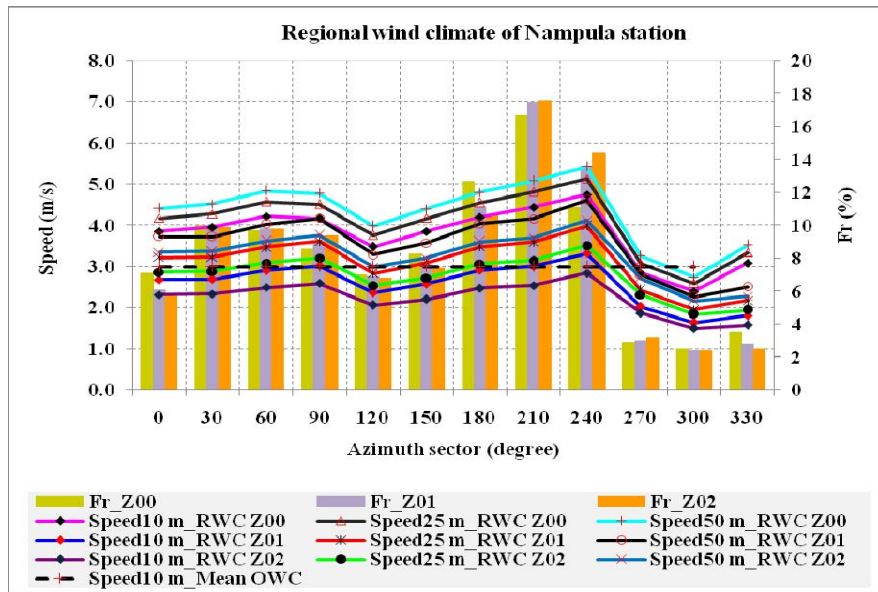


Figure 4. 61: Regional wind climate of Nampula meteorological station.

4.7.3 Predicted wind climate for the Nampula area

The predicted wind climate (PWC) was calculated for two potential wind turbine sites located to the north-east of the meteorological station at distances of 6 and 8 km from the meteorological station to site 1 and site 2 respectively (Fig. 4.62).

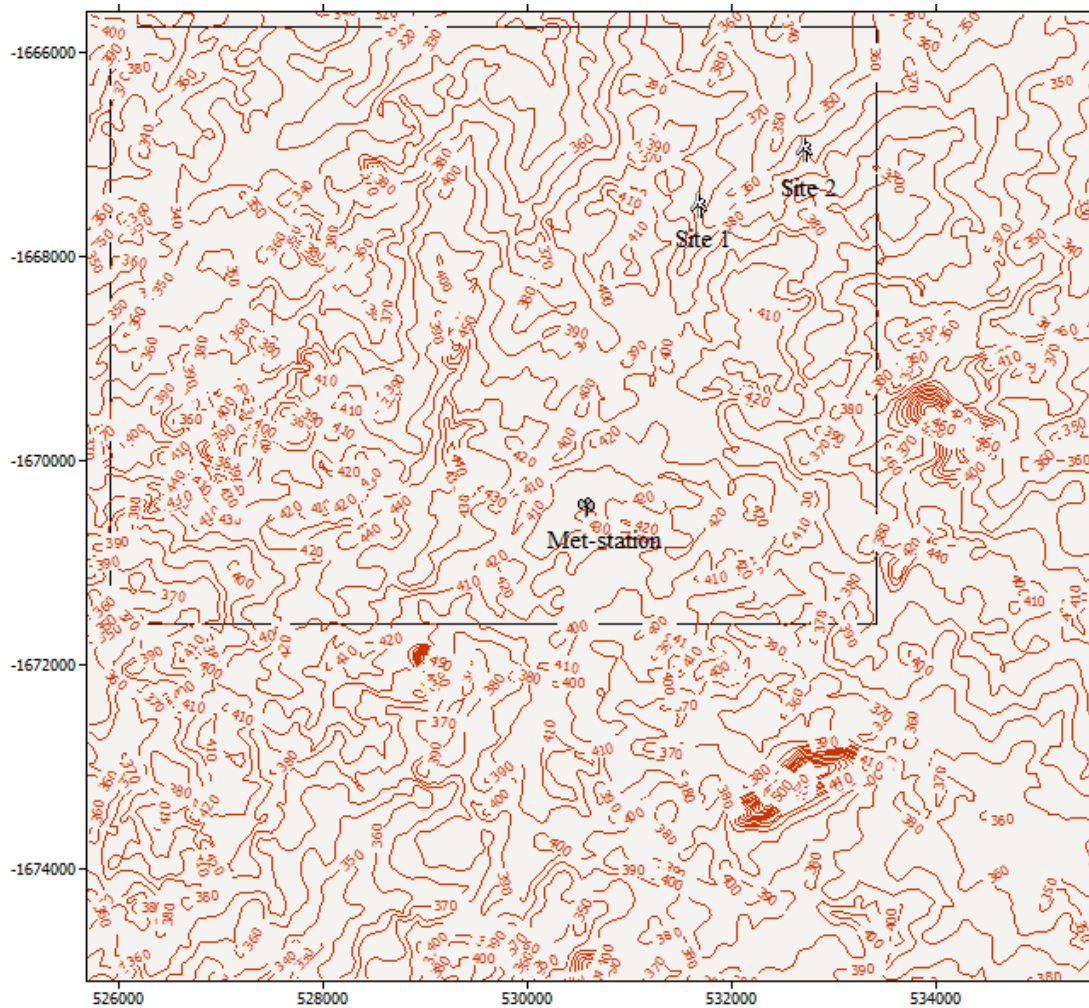


Figure 4. 62: Map showing the location of the two potential wind turbine sites (🌪️) and the location of the Nampula meteorological station (🌤️) and the selected area for wind resource maps.

The predicted mean annual wind speeds and extractable energy at the two potential wind turbine sites are presented in Figure 4.63 for five heights a.g.l. The mean annual wind speed is lower than the mean annual observed wind speed (3.0 ms^{-1}) at 10 m a.g.l. Higher mean annual wind speeds are found at higher levels (60 m a.g.l.) where values approach 4.0 ms^{-1} at the two sites. Available wind energy at 60 m a.g.l. ranges between 60 and 65 Wm^{-2} at the two different sites.

A similarity of the predicted wind climate (PWC) to the regional wind climate (RWC) is found for the roughness class 1 ($Z_{01}=0.03$ m) and class 2 ($Z_{02}=0.10$ m).

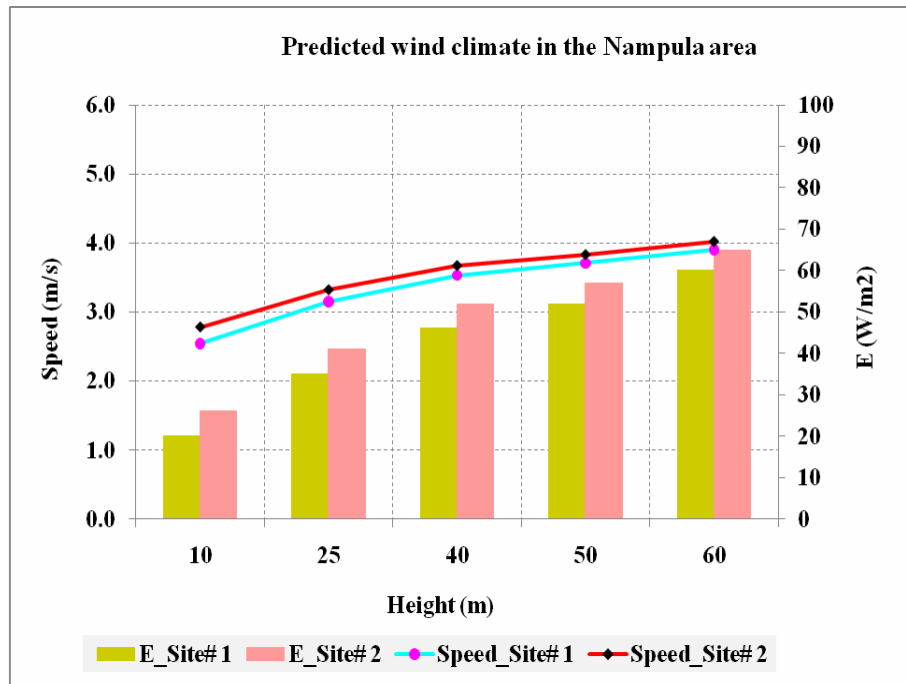


Figure 4. 63: Predicted mean wind speed and available wind energy at two potential wind turbine sites in the Nampula area.

Figure 4.64 illustrates the predicted wind rose and wind speed frequency distribution at sites 1 and 2 in the Nampula area. It is noted that the winds are predominantly from the 210° , 240° and 180° with a secondary contribution from the 30° and 60° sectors. Highest predicted wind speeds are associated with the 240° and 90° directional sectors (Fig. 4.65).

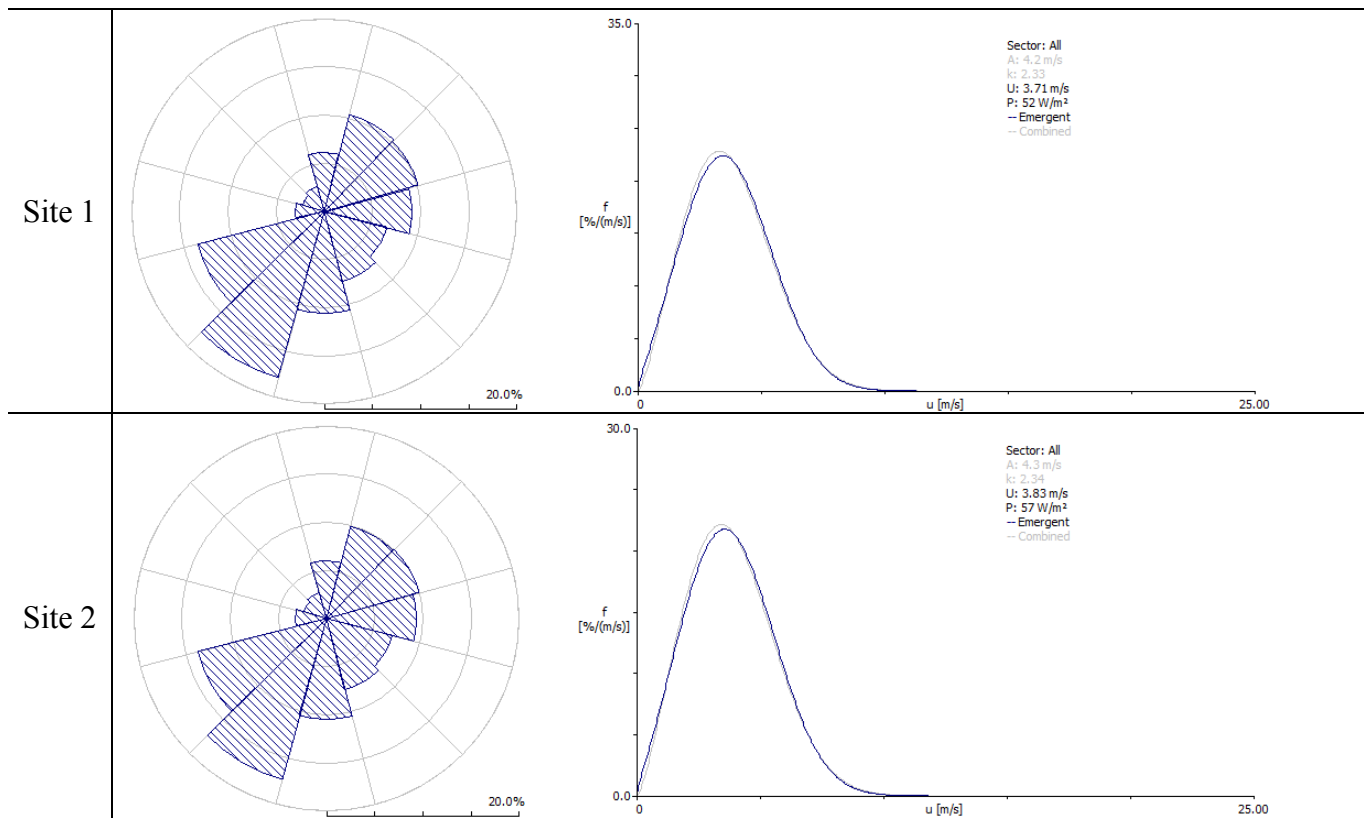


Figure 4. 64: Predicted wind rose and wind speed frequency distribution at potential wind turbine sites in the Nampula area.

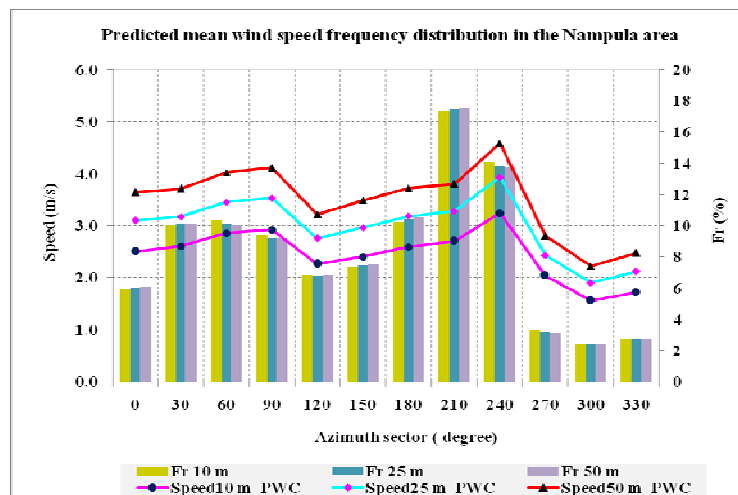


Figure 4. 65: Predicted wind speed frequency distribution for 3 standard heights (10, 25 and 50 m a.g.l.) at potential wind turbine sites in the Nampula area.

The annual energy production or extractable wind energy (AEP) in the Nampula area is between 300 and 470 MWh for heights greater than 25 m a.g.l. and below 140 MWh for a 10 m a.g.l. hub height. Figure 4.66 illustrates the extractable wind energy at the two potential wind turbine sites in the Nampula area.

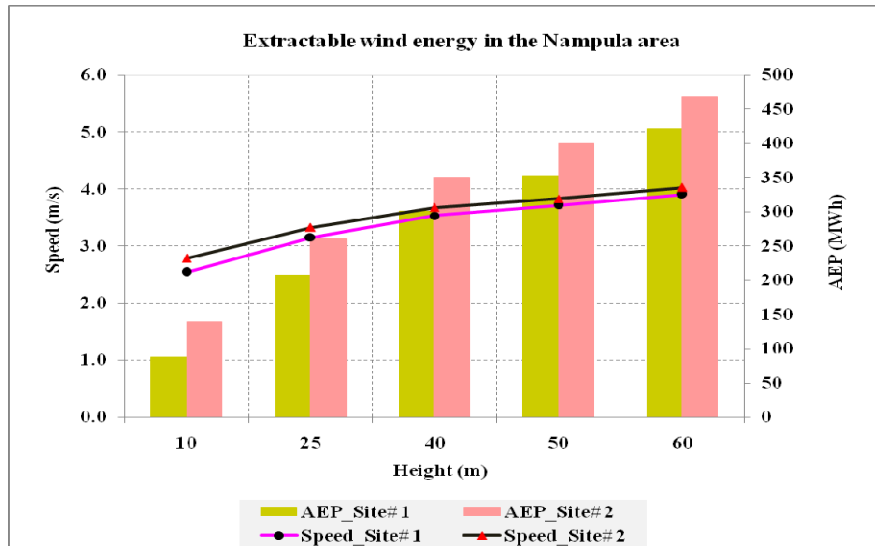


Figure 4.66: The extractable wind energy at two potential wind turbine sites in the Nampula area.

The highest extractable wind energy is from the 240° to 210° and 60° to 90° azimuth sectors. Figure 4.67 depicts the average extractable wind energy by azimuth sector for three standard heights (10, 25 and 50 m a.g.l.) at potential turbine sites in the Nampula area, while Figure 4.68 illustrates the extractable energy rose and energy frequency distribution at 50 m a.g.l. at site 2 in the Nampula area.

The speed-up (down) due to roughness change and orography at the lowest level (10 m a.g.l.) was between 12 and 17.8% and -8.1 to 2.4%, while at highest level (50 m a.g.l.) it was between 5.7 and 6.9% and -3.5 to 0.9% respectively. The turning effect due to orography was between -1.7° and 1.8° at 10 m a.g.l. and -0.8° to 0.8° at 50 m a.g.l.

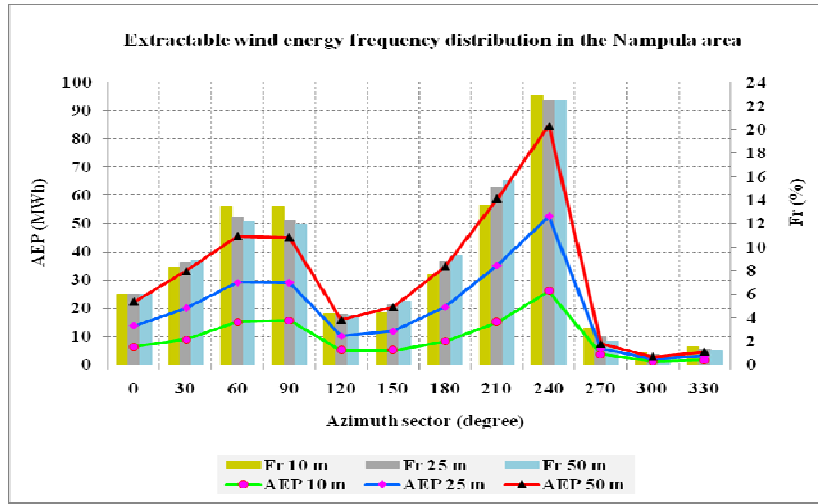


Figure 4. 67: Extractable average wind energy by azimuth sector for 3 standard heights (10, 25 and 50 m a.g.l.) at potential wind turbine sites in the Nampula area.

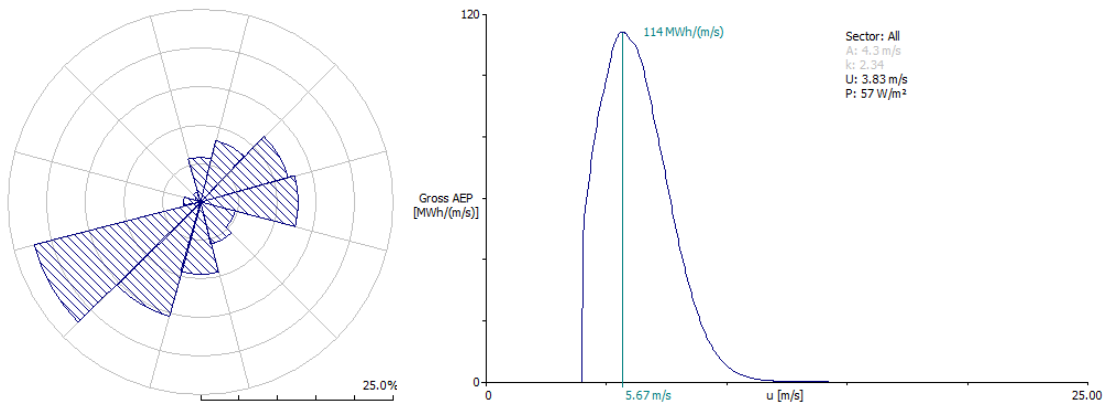


Figure 4. 68: Extractable energy rose and energy frequency distribution at 50 m a.g.l. at site 2 in the Nampula area.

4.7.4 Wind resource maps

The wind resource maps illustrate the spatial distribution of wind speed (Fig. 4.69) and energy resource (Fig. 4.70) in the Nampula area at a height of 55 m a.g.l. The maps show an average wind speed of 3.93 ms^{-1} and an average annual energy production (AEP) of

432 MWh. Highest potential is found on the E and W side of meteorological station area, where the mean wind speed reaches 4.72 ms^{-1} with an AEP of 825 MWh. The site with UTM coordinates of 529300; -1668836 is the site with the highest wind energy potential.

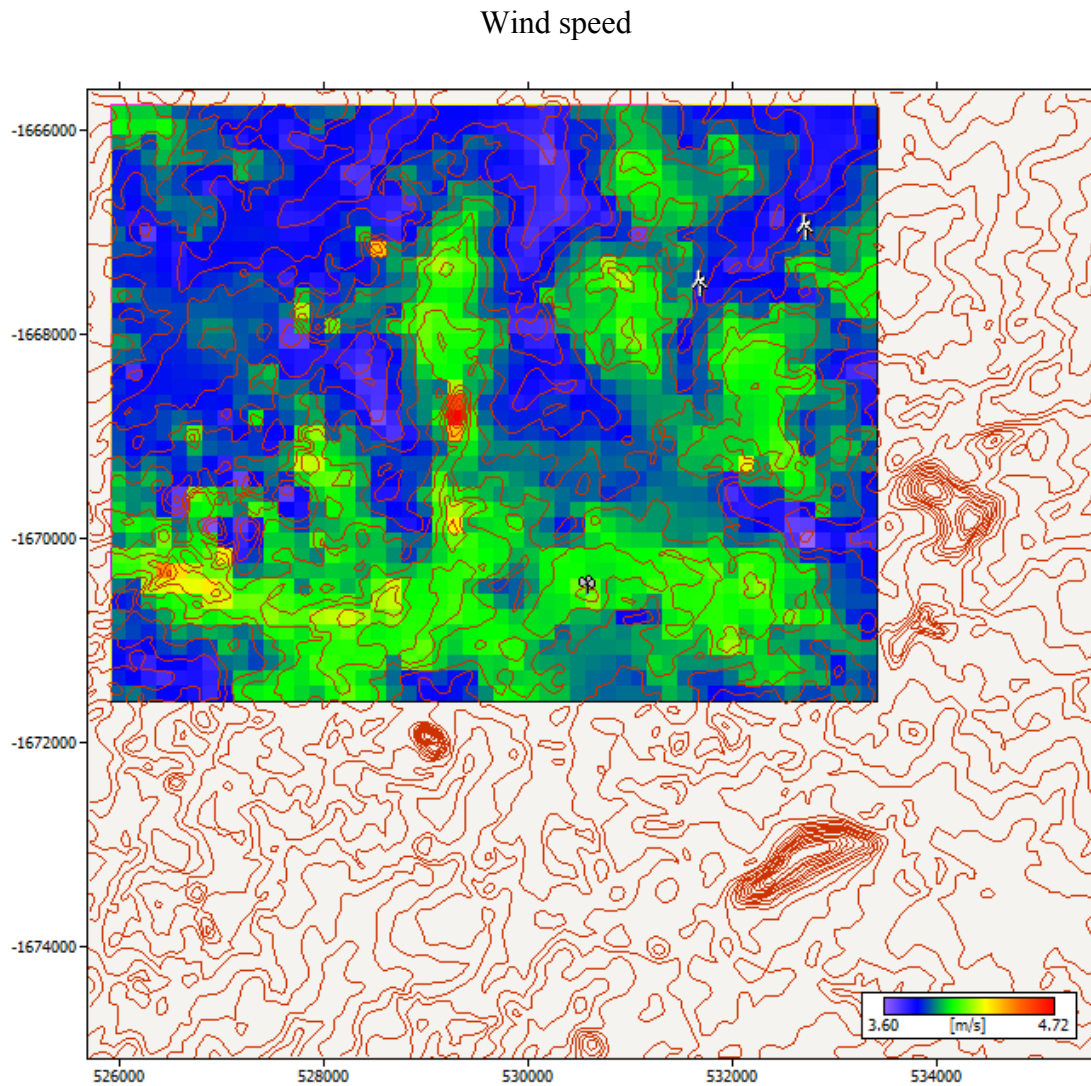


Figure 4. 69: Wind speed resource map in the Nampula area.

Average annual energy production (AEP)

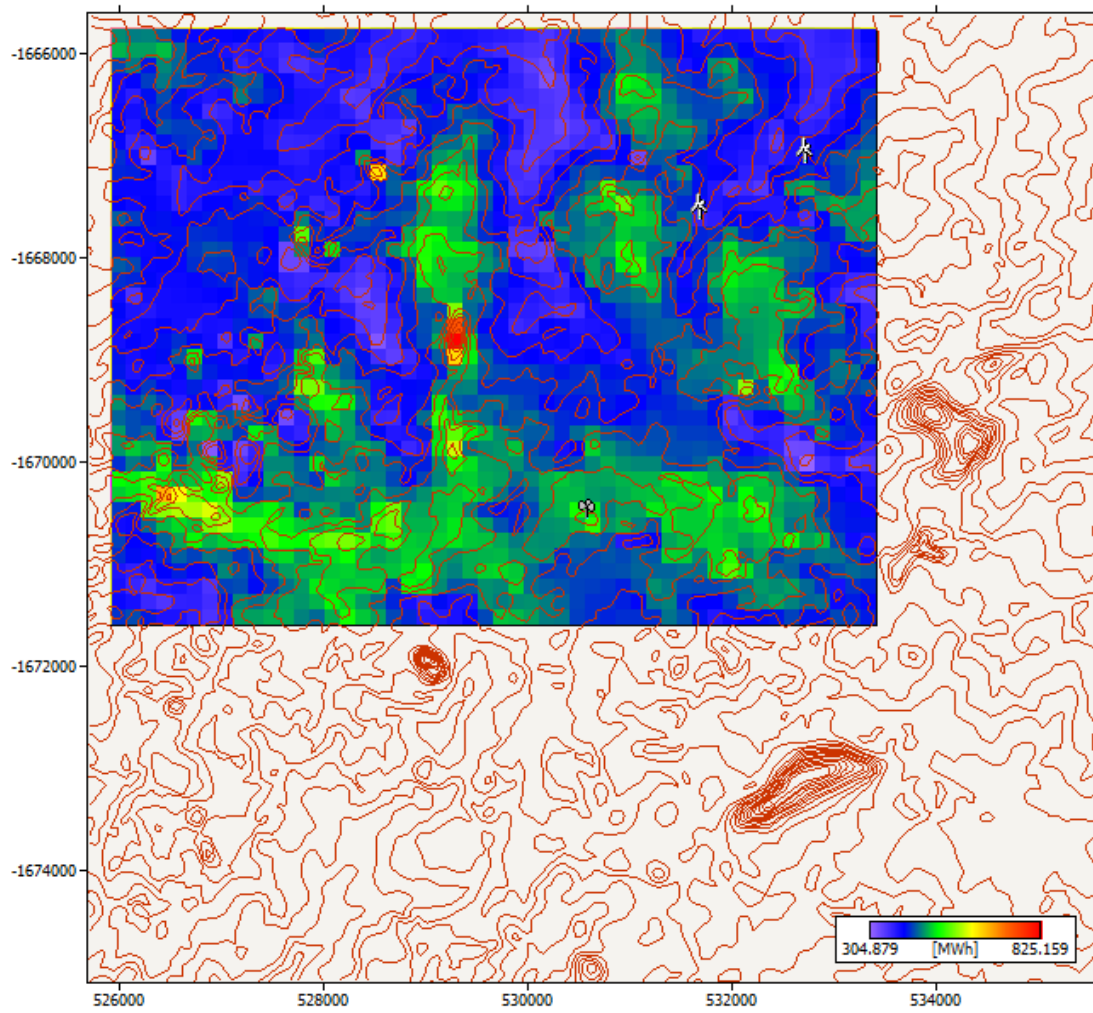


Figure 4. 70: Wind energy resource map in the Nampula area.

4.8 Results for Lichinga

4.8.1 Observed wind data

The Lichinga meteorological station has a mean annual observed wind speed of 3.9 ms^{-1} and an available wind energy of 65 Wm^{-2} for all azimuth sectors. Figure 4.71 shows the observed wind rose and wind speed frequency distribution at Lichinga.

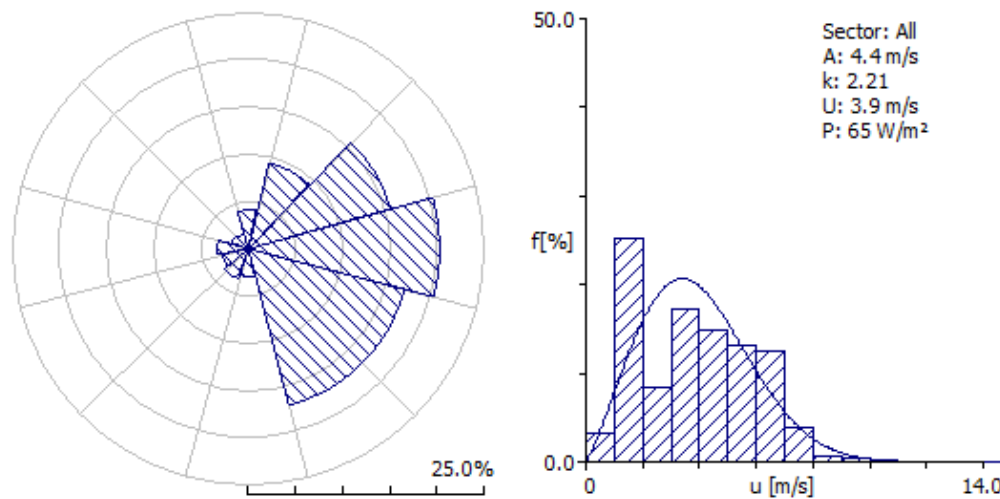


Figure 4.71: Observed wind rose and wind speed frequency distribution at Lichinga meteorological station.

The most frequent winds are from the 90° (20.3%), 120° and 150° (17.0%) and 60° (15.70%) sectors (Figs. 4.71 and 4.72). Highest mean wind speeds and available wind energy are associated with the 120° and 150° (4.8 and 4.25 ms^{-1} ; 100 and 82 Wm^{-2}) and 90° (4.25 ms^{-1} ; 71 Wm^{-2}) sectors.

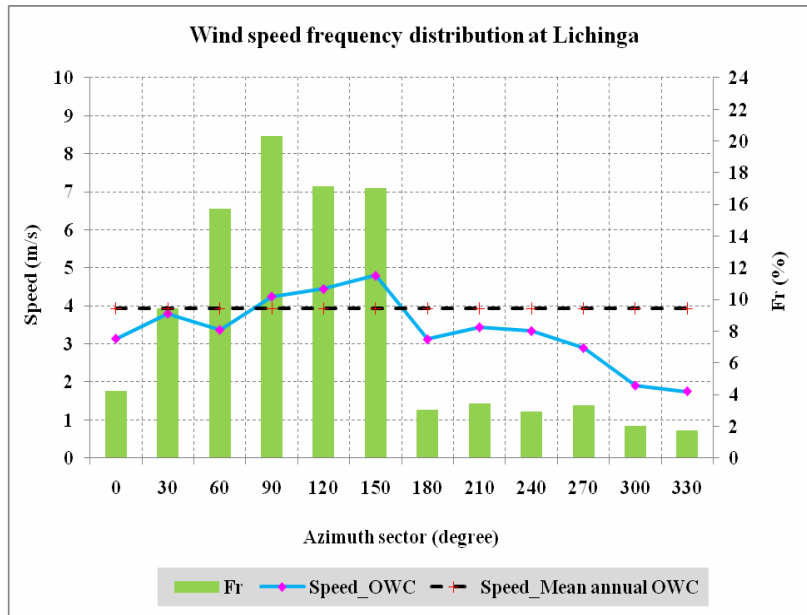


Figure 4. 72: Wind speed frequency distribution and mean wind speed by directional sector at Lichinga.

4.8.2 Wind atlas data at Lichinga

After application of the wind atlas analysis sub-model, the relevant wind data for Lichinga are presented in Table 4.7. The data are cleaned of the influence of obstacles and are presented for four roughness classes (0.0, 0.03, 0.1, and 0.4 m) and four standard heights. Figure 4.73 depicts the mean wind speed for three roughness classes (Z_{00} to Z_{02} representing roughness values of 0.00, 0.03 and 0.10 m respectively) and for the first three standard heights (10, 25 and 50 m a.g.l.). The results show clearly that relatively higher wind speeds are associated with lower roughness and with greater heights a.g.l. Highest wind speeds are associated with the 120° and 150° directional sector (Fig. 4.73).

Table 4. 7: Wind atlas data at Lichinga, where A = Weibull scale factor; k = Weibull shape factor; v = mean wind speed; and E = Available wind energy (or Power density).

Height [m]	Parameter	Roughness-class			
		0.00 m	0.03 m	0.10 m	0.40 m
10	A [ms^{-1}]	6.0	4.2	3.6	2.9
	k	2.54	2.18	2.16	2.21
	U [ms^{-1}]	5.4	3.7	3.2	2.5
	E [Wm^{-2}]	146	55	36	17
25	A [ms^{-1}]	6.5	5.0	4.5	3.8
	k	2.58	2.33	2.29	2.33
	U [ms^{-1}]	5.8	4.4	4.0	3.3
	E [Wm^{-2}]	183	88	64	38
50	A [ms^{-1}]	6.9	5.8	5.2	4.5
	k	2.60	2.58	2.51	2.52
	U [ms^{-1}]	6.1	5.1	4.6	4.0
	E [Wm^{-2}]	215	127	96	63
100	A [ms^{-1}]	7.3	6.8	6.2	5.5
	k	2.46	2.73	2.72	2.8
	U [ms^{-1}]	6.4	6.1	5.5	4.9
	E [Wm^{-2}]	261	205	155	104

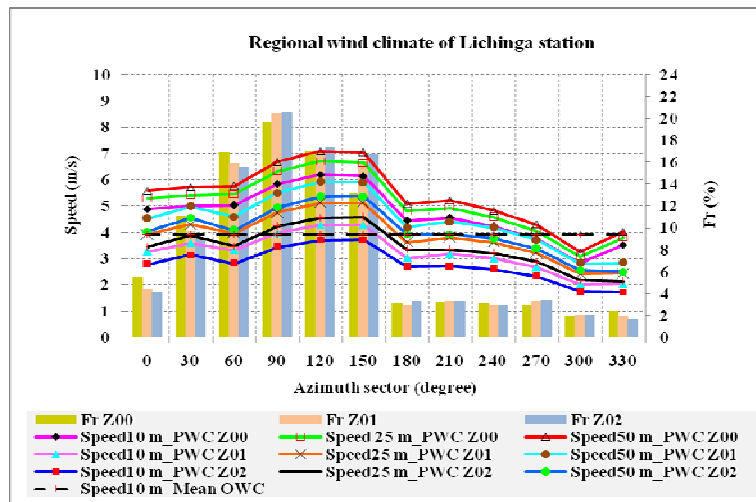


Figure 4. 73: Regional wind climate of Lichinga meteorological station.

4.8.3 Predicted wind climate for the Lichinga area

The predicted wind climate (PWC) was calculated for three potential wind turbine sites located near the dam to the south-east of meteorological station at distances of 4 and 6 km from the meteorological station to site 2 and site 3 respectively, and less than 9 km from Lichinga city in the west (Fig. 4.74).

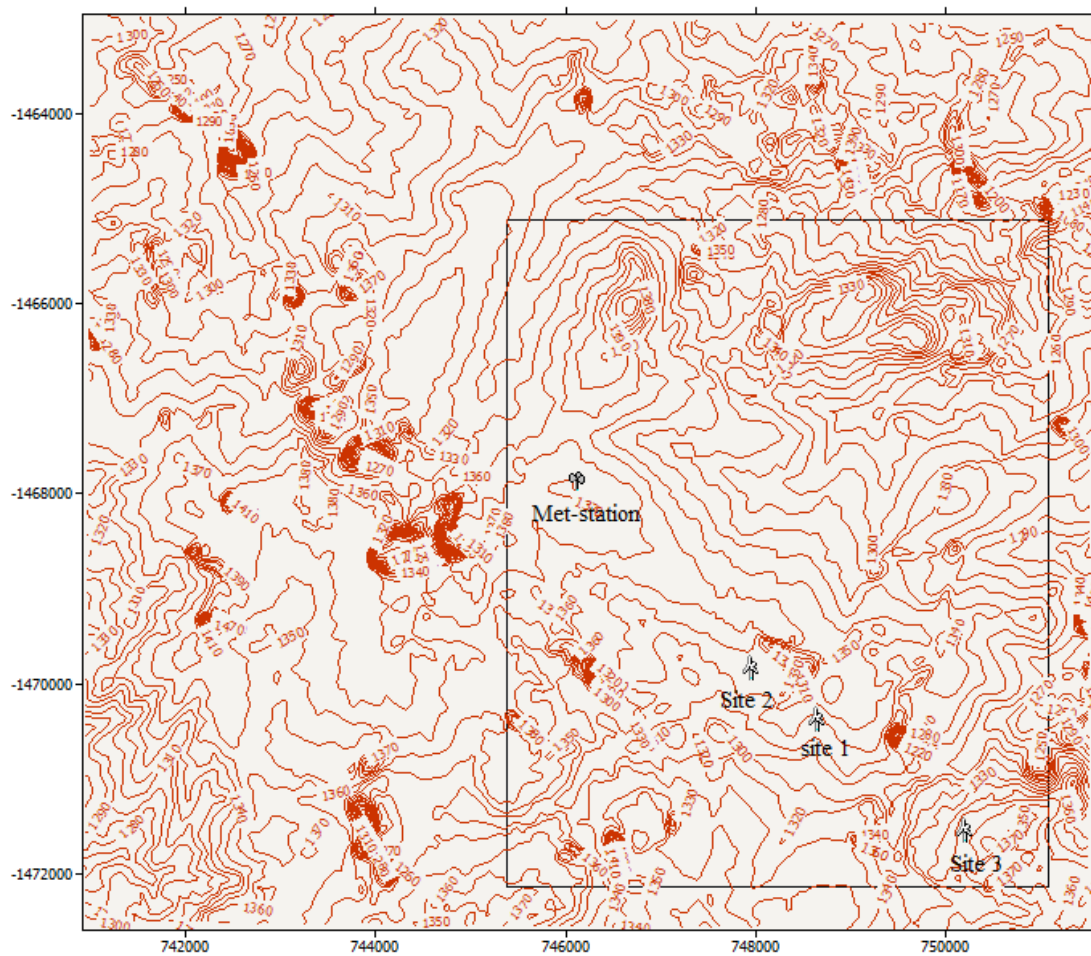


Figure 4. 74: Map showing the location of the three potential wind turbine sites (⚙) and the location of the Lichinga meteorological station (⚙) and the selected area for wind resource maps.

The predicted mean annual wind speeds and extractable energy at the three potential wind turbine sites are presented in Figure 4.75 for five heights a.g.l. Wind speeds on site 1 and 2 are similar probably due to close proximity of these sites. The mean annual wind speed is lower at site 1 and 2 than at site 3, but equal to the mean annual observed wind speed of 3.9 ms^{-1} at 10 m a.g.l. Highest mean annual wind speeds are found at site 3, where values approach 6.0 ms^{-1} at 60 m a.g.l. Available wind energy at 60 m a.g.l. ranges between 142 and 184 Wm^{-2} at the three different sites.

A similarity of the predicted wind climate (PWC) to the regional wind climate (RWC) is found for the roughness class 1 ($Z_{01}=0.03 \text{ m}$) and class 2 ($Z_{02}=0.10 \text{ m}$).

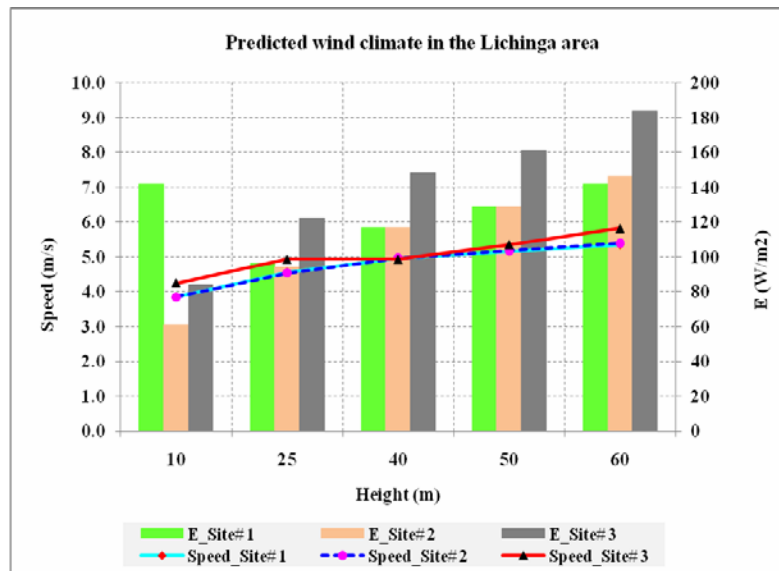


Figure 4. 75: Predicted mean wind speed and available wind energy at three potential wind turbine sites in the Lichinga area.

Figure 4.76 illustrates the predicted wind rose and wind speed frequency distribution at sites 1, 2 and 3 in the Lichinga area. It is noted that the winds are predominantly from the 90° and 120° , with a secondary contribution from the 30° and 150° sectors. Highest predicted wind speeds are associated with the 150° and 120° directional sector (Fig. 4.77).

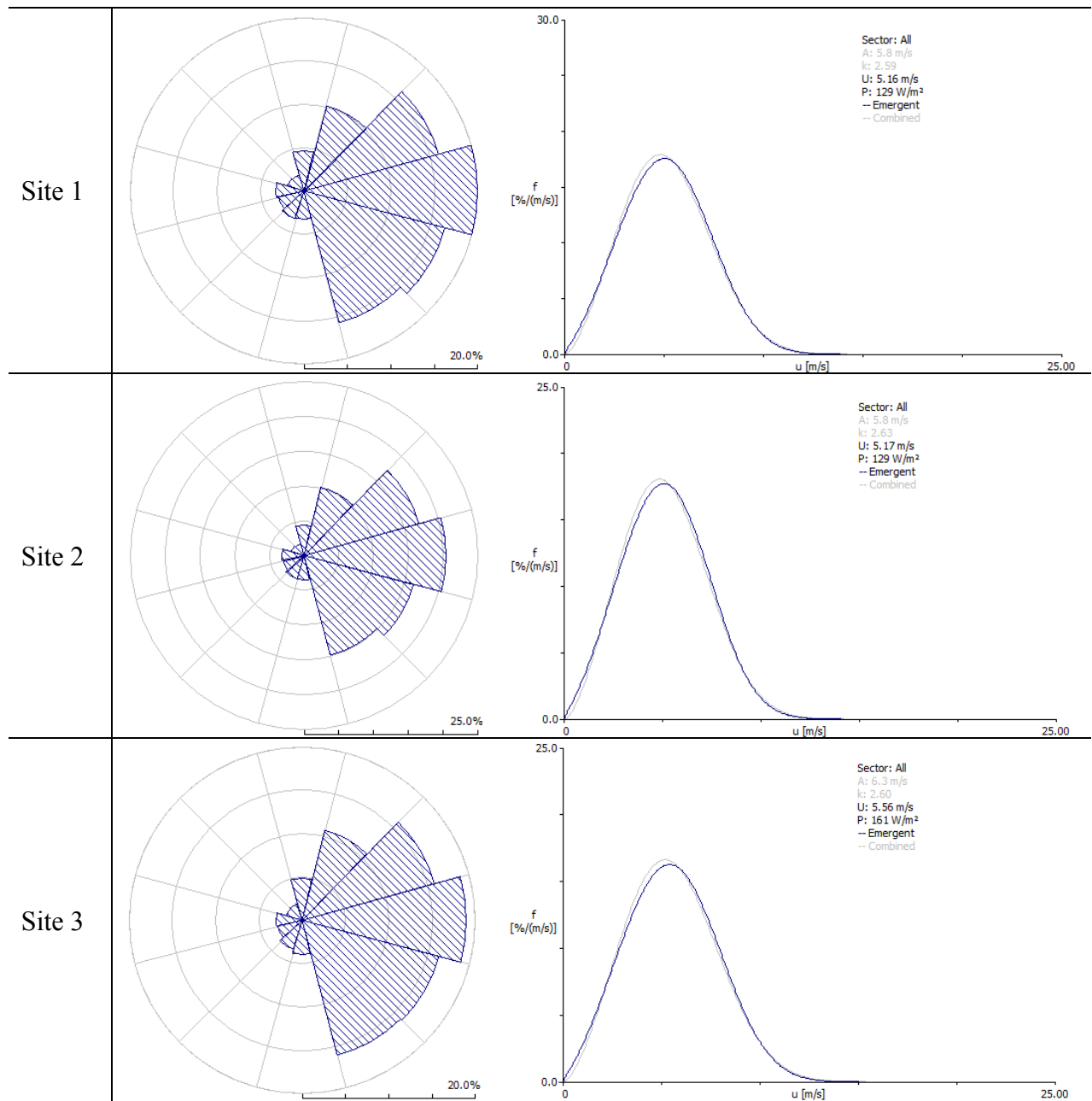


Figure 4. 76: Predicted wind rose and wind speed frequency distribution at potential wind turbine sites in the Lichinga area.

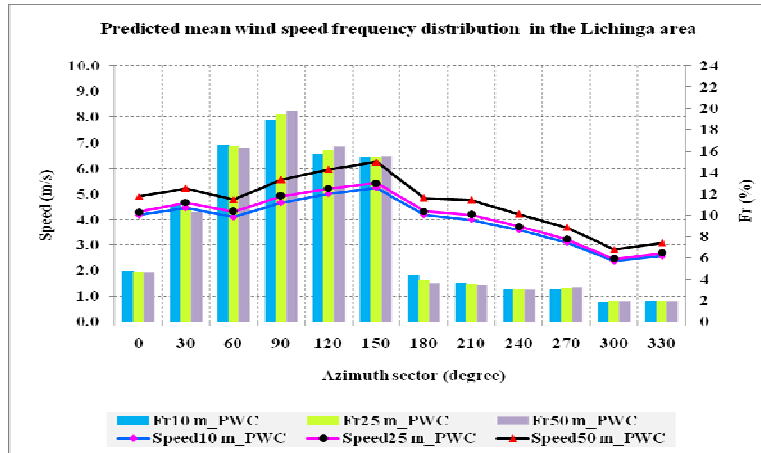


Figure 4. 77: Predicted wind speed frequency distribution for 3 standard heights (10, 25 and 50 m a.g.l.) at potential wind turbine sites in the Lichinga area.

The annual energy production or extractable wind energy (AEP) in the Lichinga area is above 900 MWh for heights greater than 25 m a.g.l. and below 650 MWh for a 10 m a.g.l. hub height. Figure 4.78 illustrates the extractable wind energy at the three potential wind turbine sites in the Lichinga area.

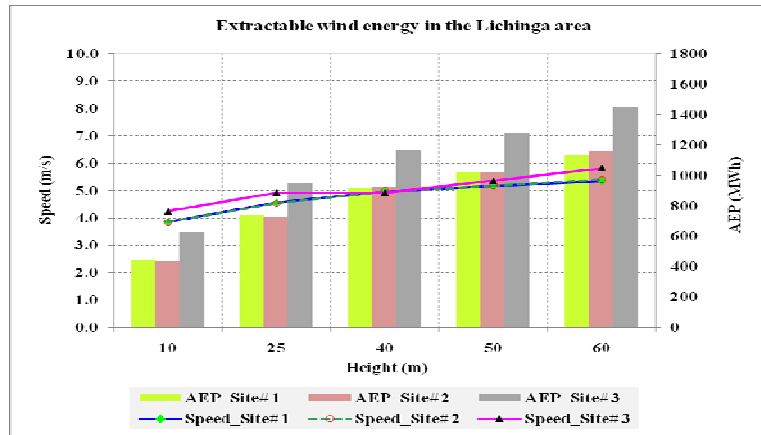


Figure 4. 78: The extractable wind energy at three potential wind turbine sites in the Lichinga area.

The highest extractable wind energy is from the 150° and 120° to 90° azimuth sectors. Figure 4.79 depicts the average extractable wind energy by azimuth sector for three standard heights (10, 25, 50 m a.g.l.) at potential turbine sites in the Lichinga area, while Figure 4.80 illustrates the extractable energy rose and energy frequency distribution at 50 m a.g.l. at site 2 in the Lichinga area.

The speed-up (down) due to roughness change and orography at the lowest level (10 m a.g.l.) was between -0.1 and 2.8% and -1.6 to 10.1%, while at highest level (50 m a.g.l.) it was between -2.7 and 0.2% and -0.1 to 5.1% respectively. The turning effect due to orography was between -3.4° and 3.2° at 10 m a.g.l. and -1.4° to 1.4° at 50 m a.g.l.

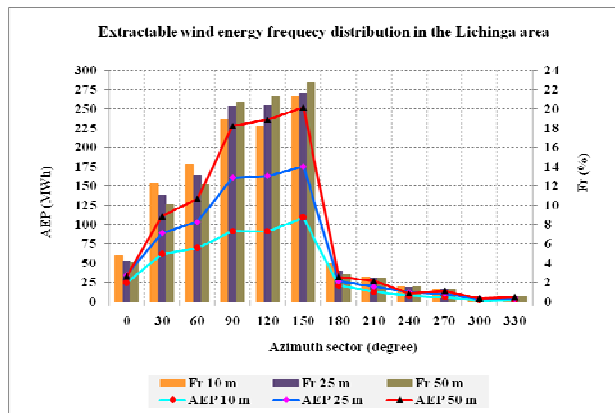


Figure 4. 79: Extractable average wind energy by azimuth sector for 3 standard heights at potential wind turbine sites in the Lichinga area.

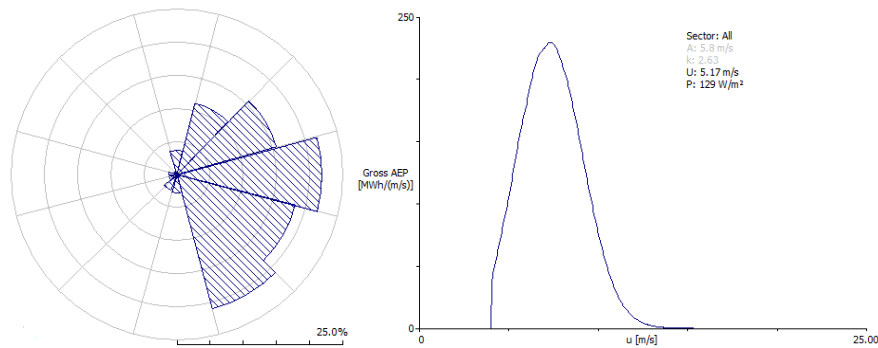


Figure 4. 80: Extractable energy rose and energy frequency distribution at 50 m a.g.l. at site 2 in the Lichinga area.

4.8.4 Wind resource maps

The wind resource maps illustrate the spatial distribution of wind speed (Fig. 4.81) and energy resource (Fig. 4.82) in the Lichinga area at a height of 55 m a.g.l. The maps show an average wind speed of 5.2 ms^{-1} and an average annual energy production (AEP) of 1 021 MWh. The highest wind energy potential is found in the highland areas situated to the NE and SE of the meteorological station where the mean wind speed reaches 6.95 ms^{-1} with an AEP of 2 292 MWh. The site with UTM coordinates of 746527; -1466678 is the site with the highest wind energy potential. These sites are on the north and north-east side of the meteorological station upward the river which runs north-east-southward down to the dam by the Chiulugo settlement.

Wind speed

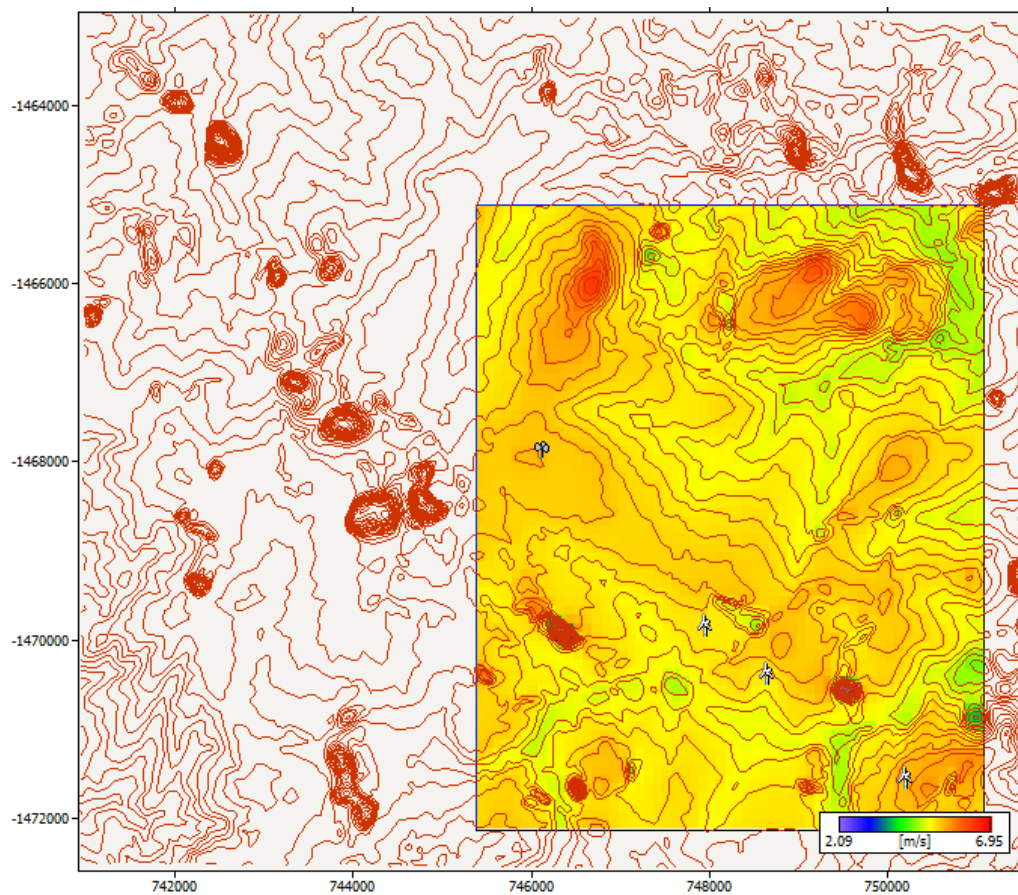


Figure 4. 81: Wind speed resource map in the Lichinga area.

Average annual energy production (AEP)

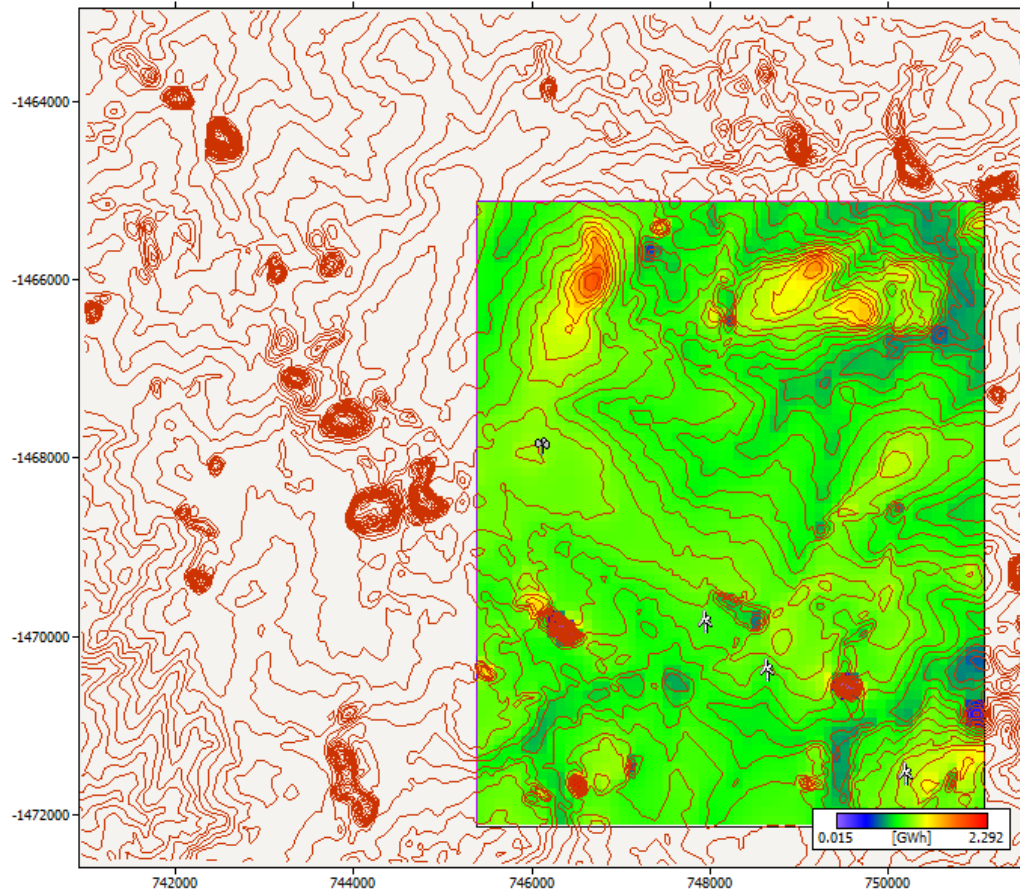


Figure 4. 82: Wind energy resource map in the Lichinga area.

4.9 General discussion

The predicted results revealed that at the lowest level (10 m a.g.l.), the coastal sites of Ponta de Ouro, Mavalane and Tofinho have relatively higher mean wind speeds ranging between 4.5 - 6.0 ms⁻¹ and an AEP value up to 1 600 MWh, while Vilankulo and Pemba have mean wind speeds below 4.0 ms⁻¹ and AEP up to 900 MWh. The potential wind turbine sites in the interior in the vicinity of Nampula area have mean annual wind speeds below 3.0 ms⁻¹ and AEP values below 150 MWh. Potential wind turbine sites in the vicinity of Lichinga have slightly higher mean annual wind speeds approximately 3.9 ms⁻¹ at 10 m a.g.l. and AEP value up to 800 MWh.

At the highest levels (50 - 60 m), the coastal areas in the vicinity of Pemba and Vilankulo have mean annual wind speeds below 5.0 ms⁻¹ and AEP up to 1000 MWh), whereas the coastal areas of Ponta de Ouro, Mavalane and Tofinho areas have relatively greater wind energy potential (mean annual wind speed of about 8.0 ms⁻¹ and AEP up to 3 000 MWh). The interior site of Nampula area has the lowest mean wind speeds (3.9 ms⁻¹) and AEP (below 500 MWh) compared with potential wind turbine sites at Lichinga area (mean annual wind speeds of about 6.0 ms⁻¹ and AEP up to 1 200 MWh).

The poor observed wind data quality (15.5% missing data and 20.5% zero observations) at the Vilankulo meteorological station may have caused an underestimate of the wind energy potential as described above. The poor wind energy resource at Pemba, which was expected to have a good resource similar to that of the Mavalane area, might be due to its geographic location. It is located alongside a runway at an elevation of 194 m above sea level (a.s.l.), near the coast but on the west side of the Bay of Pemba, in contrast to locations on the east side of the bay where there is a low friction and more undisturbed free flow of wind from the coast.

In addition, the lower annual wind speeds and extractable wind energy at these two coastal areas (Vilankulo and Pemba) might be exacerbated by poor anemometry siting. With the exception of Tofinho (150 m from the sea) and Ponta de Ouro (about 500 m from the sea) which were explicitly sited for wind energy resource evaluation at coastal

areas, the other meteorological stations are at airport locations, and are located in protected, rather than exposed areas. As such, this might result in an underestimate of the wind energy resource at these locations.

The achievement of this study is the finding that both interior and coastal areas are suitable for wind energy exploitation in the form of small and medium scale power systems to generate electricity although the coastal area possesses higher wind resources, concurring with the published estimates by the WMO in 1981 and DNER in 2008.

The wind and energy resource maps show average mean annual wind speed and AEP in the vicinity of Ponta de Ouro and Vilankulo, mean annual wind speeds and AEP at Pemba, Tofinho and Mavalane, and are relatively higher values in the interior areas (Nampula).

The geographic location of the Lichinga meteorological station area (above 1350 m a.s.l.), the low roughness change (at both reference and predicted sites) and almost no obstacles around the meteorological station might account for the high wind energy potential which is almost comparable to the Vilankulo area which is a coastal area. This finding is a good indication that there are some interior areas suited to wind power generation.

At Nampula the potential wind turbine sites possess the least wind energy potential (mean wind speed of about 4.0 ms^{-1} and annual energy production less than or equal to 450 MWh). Despite the good observed wind data quality (almost no missing observations) and the similarity of instrumentation, its interior location might be indicative of the fact that some interior regions do not have a sufficient wind energy resource. This result concurs with the estimates published by the WMO (1981) which revealed poor wind and energy resource potential in inland areas.

The short climatic data series used for the analysis (one to 2 years), according to a study published by Lange and Højstrup in 2001, might influence the high value of the Weibull-A parameter, which exceeds the mean annual wind speed by a magnitude of 1.1 ms^{-1} . In addition, the WAS^P analysis procedure which forces the measured data to fit the standard Weibull frequency distribution, according to the study published by Bowen

and Mortensen (2004) might be also another possible reason that accounts for Weibull-A parameter in excess of the mean annual wind speed.

Mozambique is in a trade winds belt, hence the Weibull-k parameter (shape factor) of between 1.63 and 2.90 found in this study, concurs with previous studies for similar areas (Gipe, 2004; Knecht, 2004).

4.10 Summary

The results of the WAsP model simulations indicate that there is sufficient wind energy potential in most areas, particularly Ponta de Ouro, Mavelane, and Tofinho areas, where the mean annual wind speed is above 5.0 ms^{-1} at the 10 m level and about 8.0 ms^{-1} at the highest levels (50 - 60 m). The lowest mean annual wind speed and consequently wind energy is found in the Nampula area.

CHAPTER FIVE

CONCLUSION

5.1 Summary

The purpose of this study was to evaluate the wind energy potential for the purpose of electricity generation in Mozambique. It was established that wind energy is a viable option.

The selected study areas (coastal and interior areas) revealed that for the two main heights (10 m and 50 m a.g.l.) that were used as reference heights, in accordance with thresholds determined by the WMO (1981), there is a sufficient wind energy resource that can be harnessed for both water pumping and electrical power generation.

The results of the present study found that coastal areas of the country are more suited for wind power exploitation which concurs with the estimate published by the WMO in 1981 and the study conducted by DNER in 2008. However, some inland areas, such as Lichinga, are also determined to be suitable for wind power generation, a finding that was not evident from both the WMO and DNER studies.

The wind resource maps from this study are a valuable tool for wind energy development planning, *viz.* siting instrumentation for wind data collection at different heights, wind turbines for water pumping and wind power production in the vicinity of the identified potential sites.

Despite the infrastructural and economic constraints that Mozambique is experiencing, the exploitation of wind energy can be a viable option. The exploitation of this renewable energy resource can bring some advantages, such as, increased provision of electricity that can improve access to electricity in the country and at the same time reduce pressure on the environment through the reduction of biomass fuel consumption.

5.2 Limitations of the study

The present study was conducted with limited climatic data series (2 years) which is not ideal from a climatological perspective to account for the wind resource availability of a region. However, although limited in the number of years of data, the seasonality was captured by having a full annual cycle.

Furthermore, the data used for modeling were hourly mean wind velocities which do not give details of extreme winds (gusts) that are also important for the evaluation of the wind resource and particularly important when it comes to siting considerations.

One of most important components of an evaluation of wind and energy resources, using the methodology employed in this study, are the field site visits used to verify roughness characteristics and presence of obstacles. For logistical reasons (funds) it was only possible to visit one of the reference stations, *viz.* Mavalane. It is acknowledged that better site characteristics could have been obtained if further site visits had been undertaken.

5.3 Recommendations

This research was intended to provide a general overview of the potential that Mozambique possesses for the exploitation of wind as a source of energy. Due to some of the limitations of this study, the following recommendations for future investigations are made:

1. The selected potential wind turbine sites used for the model simulations were not all included in the field survey. In this regard, it is recommended that subsequent studies must ensure that site visits are undertaken to determine detailed site characteristics in order to improve accuracy and achieve better results. Precise descriptions of the obstacles and roughness elements that impact on wind flow and which cannot be seen from a satellite image will improve results.

2. The possibility of using strategically located Vodacom, Mozambique Cellular (Mcel) or Mozambique's Telecommunications (TDM) masts spread throughout the country to install anemometers for wind velocity data collection should be explored.
3. To accomplish the aforementioned wind velocity data collection, the Ministry of Energy (ME) through the National Department of New and Renewable Energy (DNER) and the National Energy Fund (FUNAE), in collaboration with a number of organizations and institutions such as INAM, UEM, the Mozambican Confederation of Economic Association (CTA) and relevant non-governmental organizations, should promote this initiative by seeking funds and potential investors for wind data collection and wind energy exploitation.
4. Some areas which appear to have good wind power potential (i.e. they have mean monthly wind speeds above 3.0 ms^{-1}) based on data from second class meteorological stations must be prioritized. These include the coastal areas of Mocimboa da Praia and Angoche, as well as the interior region of Chicualacuala.
5. Further detailed investigations are required at Vilankulo, Pemba and Nampula, in order to verify that the wind energy resource at these locations is insufficient, as determined by this study.
6. Considering the interest in renewable energy, particularly wind energy, in the country, INAM should promote the digitization of historical wind data collected from previous years, adding the data to the official database.

7. It is also recommended that INAM should co-operate with all governmental and private institutions that collect wind data to integrate all wind observations into a single database that could be made available to any users, particularly those from the scientific community.

8. A similler study should be carried out at the central region coastal and interior of the country. To ensure good results, reliable wind velocity data should be collected at coastal and interior areas of Sofala, Manica, Tete and Zambézia provinces. Furthermore, the Niassa Province, from which the Lichinga area showed, in this study, a good indication of wind power potential, should be more fully investigared, particularly in the Niassa Lake area.

9. A ground-truthed survey, which would comprise data collection at different heights around the identified potential sites should be conducted to validade the results of this study.

REFERENCES

Abdeladim, K., Romeo, R. and Magrí, S., 1996: Wind Mapping of a Region in the North-east of Algeria. World Renewable Energy Congress Renewable Energy, Energy Efficiency and the Environment, 789–793.

Abrams, M., Hook, S. and Ramachandran, B., 2005: ASTER User Handbook, Version 2. Jet Propulsion Laboratory, California Institute of technology, 1-135.

Ackermann, T. and Söder, L., 2002: An overview of wind energy-status. Renewable and Sustainable Energy Reviews, 6, 67–128.

Ahmed, H. K. and Abouzeid, M., 2001: Utilization of wind energy in Egypt at remote areas. Renewable Energy, 23, 595–604.

Ayoade, J. O., 1983: Introduction to Climatology for the Tropics. John Wiley & Sons, Chichester, England, 56-75, 98-99, 125-132, 175-202.

Botha, C. P., 1989: The siting of wind turbines. Unpublished MSc (Eng.) thesis, University of Cape Town.

Bowen, A. J. and Mortensen, N. G., 2004: WAsP prediction errors due to site orography. Risø National Laboratory, Roskilde, Denmark, 1-65.

Burlando, M., Carassale, L., Georgieva, E., Ratto, C. F., and Solari, G., 2007: A simple and efficient procedure for the numerical simulation of wind fields in complex terrain. Boundary Layer Meteorology, 125, 417–439.

Carta, J. A., Ramírez, P. and Velázquez, S., 2008: Influence of the level of fit of a density probability function to wind-speed data on the WECS mean power output estimation. Energy Conservation and Management, 49, 2647-2655.

Chambal, H., 2010: Energy Security in Mozambique. International Institute for Sustainable Development, Winnipeg, Canada, 1-28.

- Cheremisinoff, N. P., 1978: Fundamentals of Wind Energy. Ann Arbor Science Publisher inc., USA, 1–127.
- Crasto, G., 2007: Numerical simulations of the atmospheric boundary layer. Unpublished PhD thesis in Industrial Engineering, Università degli Studi di Cagliari, Italy, 1-182.
- Da Mata, L. A., 1962: Clima – Conforto humano – Habitação, Generalidades (Climate – human comfort – habitation, generalizes). Separata do Boletim da Sociedade de Estudos de Moçambique, 33 (141), 86-106.
- Denison, J., 1990: The siting of a wind turbine using the WA^SP numerical model and its validation by comparison with field data. Unpublished MSc. (Eng.) thesis, University of Cape Town.
- Diab, R. D. and Killick, S. E., 1991: Windflow modelling in the Saldanha Bay area. South African Geographical Journal, 73, 14 - 21.
- Diab, R. D., Ligoff, D., Viljoen, R. and Kidgell, U., 1992: The Mabibi wind energy: Part I. Journal of Energy R & D in Southern Africa, 3 (2), 13-17.
- DNER (Direção Nacional de Energias Novas e Renováveis), 2008: Support for wind power development in Mozambique-Final report (Draft), DNER, Maputo, 1-90.
- Doran, J. C. and Verholek, M. G., 1978: A note in vertical extrapolation formulas for Weibull velocity distribution parameters. Journal of Applied Meteorology, 17, 410-412.
- Dube, L. T. N, 1994: Wind energy potential in Maputaland. Unpublished MSocSc thesis, University of Natal, 1-105.
- EDM (Electricidade de Moçambique), 2007: Relatório anual de estatística (Annual statistical report), Maputo, 1-80.
- ENM (Editora Nacional de Moçambique), 2009: Atlas de Moçambique (Atlas of Mozambique). ENM, Maputo, 1-81.

- Erdogdu, E., 2008: On the wind energy in Turkey. Renewable and Sustainable Energy Reviews, 1-11.
- Esteves, Teresa M. V. N. S., 2004: Base de dados do potencial energético do vento em Portugal – Metodologia e desenvolvimento (Data base for wind power potential in Portugal – Methodology and development). Unpublished MSc (Land Eng.) thesis, Universidade de Lisboa, 1–93, http://enggeografica.fc.ul.pt/documentos/tese_teresa_simoes.pdf, accessed in February, 2009.
- Faria, J. M. R. and Gonçalves, C. A., 1968: Cartas de isopletas dos valores médios de alguns elementos climáticos e classificação climática de Köppen em Moçambique por Distritos (Maps of some climatic elements average and Mozambique Köppen climatic classification by district). Serviço Meteorológico de Moçambique, Lorneço Marques, 38, (36), 1–13.
- Fraenkel, P., Barlow, R., Crick, F., Derrick, A. and Bokalders, V., 1993: Windpumps a Guide for Development Workers. Intermediate Technology Publications Ltd, London, 1-156.
- Freris, L. L., 1990: Wind Energy Conversion Systems. Prentice Hall International Ltd, UK, 1-2, 14-18, 27-32.
- Finardi, S., Morselli, M. G. and Jeannet, P., 1997: Wind flow models over complex terrain for dispersion calculations. COST 710 Working Group4, 1-49.
- FUESS, R., 1956: Instrument de precision de mesure et de controle pur les Sciences et L'ndustre – Prospectus 214. F, Anémographe 82 a, Berlin, 1-12.
- Gallino, S., Mazzino, A., Ratto, C. F., 1998: A simple procedure to account for non-kinematic effects in a mass-consistent wind model. Journal of Wind Engineering and Industrial Aerodynamics, 74-76, 229-237.
- Garcia, A., Torres, J. L., Prieto, E. and De Francisco, A., 1998: Fitting wind speed distributions: A case study. Solar Energy, 62, (2), 139–144.

Gipe, P., 2004: Wind Power. James & James (Science Publishers) Ltd, London, 8-12; 30-46; 50-67; 400-403.

Giebel, G. and Gryning, S-E., 2004: Shear and stability in high met masts and how WA^SP treats it. AWEA special topic conference “The Science of Making Torque from Wind”, Delft (NL), 19-21.

GovM (Government of Mozambique), 2006a: Plano de Acção para a redução da Pobreza Absoluta (PARPA II) (in Portuguese), Maputo, Mozambique, 1-4, 122-124.

GovM (Government of Mozambique), 2005b: Resolução n° 16/2005, 11 de Maio (in Portuguese) Bolentim da Republica n° 19, 1ª Série.

Gronau, D, 2003: Why is the gamma function so as it is. Teaching Matheamtics and Computer Science, 1 (1), 43-53, University of Debrecen.

Hankins, M., 2009: A Renewable Energy Plan for Mozambique. Justiça Ambiental (JÁ), Maputo, Moçambique, 7-60.

Hastenrath, S., 1985: Climate and Circulation of the Tropics. D. Reidel Publishing Company, Dordrecht, Holand, 56-68, 120-121, 123-129, 147-149, 160, 173-188.

Himri, Y., Rehman, S., Draoui, B. and Hemri, S., 2008: Wind power potential assessment for three locations in Algeria. Renewable & Sustainable Energy Review, 12, 2495-2504.

Hennessey, J. P. JR., 1977: Some aspects of wind power statistics. Journal of Applied Meteorology, 16, (2), 119-128.

Hrayshat, E. S., 2007: Wind resource assessment of the Jordanian southern region. Renewable Energy, 32, 1948-1960.

INE (Instituto Nacional de Estatística), 1998: Anuário estatístico de 1998, (Mozambique National Institute of Statistics: Statistical yearbook for 1998). INE, Maputo, 1-133.

IMF (International Monetary Fund), 2007: Republic of Mozambique: Poverty Reduction Strategy Paper, IMF country Report. International Monetary Fund Publication Services, 07/37, 1-164, Washington, DC, (<http://www.imf.org>; Accessed 4 on October, 2010).

Jamil, M., Parsa, S. and Majidi, M., 1995: Wind power statistics and evaluation of wind energy density. Renewable Energy, 6, (5-6), 623-628.

Jaramillo, O. A., Borja, M. A., 2004: Wind speed analysis in La Ventosa, Mexico: a bimodal probability distribution case. Renewable Energy, 29, 1613-1630.

Jury, M. R. and Diab, R., 1989: Wind energy potential in Cape coastal belt. South African Geographical Journal, 71, 1, 3-11.

Justus, C. G., Hargraves, W. R. and Yalcin, A., 1976: Nationwide wide assessment of potential output from wind-powered generators. Journal of Applied Meteorology, 15, (7), 673-678.

Knecht, K., 2004: Wind Regimes of Africa - Comparative evaluation of wind data from selected countries. InWEnt Division-Environment, Energy and Water, Berlin, Germany, 1-73.

Lange, B. and Højstrup, J., 2001: Evaluation of the wind-resource estimation program WAsP for offshore applications. Journal of Wind Engineering and Industrial Aerodynamics, 89, 271-291.

Leite, L. M. and Filho, J. S. V., 2006: Evaluation of average speed and predominant direction of wind in Ponta Grossa-PR. Revista Brasileira de Agrometeorologia, 14, (2), 157-167.

Lipman, N. H., Musgrove, P. J. and Pontin, G. W. W., 1982: Wind Energy for the Eighties. Peter Peregrinus Ltd, Stevenage, UK, 1-372.

Loureiro, J. B. R., Soares, D. V., Rodrigues, J. L. A. F., Pinho, F. T. and Freire, A. P. S., 2005: Investigation of turbulent flow over steep hill using laser dopler anemometer. 18th International Congress of Mechanical Engineering, Ouro Preto, MG, Brazil, 6-11.

Lun, I. Y. F. and Lam, J. C., 2000: A study of Weibull parameters using long – term wind observations. Renewable Energy, 20, 145–153.

Matos, M. L. S. A. and Ramalho, M. H. R., 1989: A Terra, planeta dinâmico (The Earth, dynamic planet), Edições ASA, Portugal, 227-229. Martyn, D., 1992; Developments in Atmospheric Science, 18 - Climates of the World. Polish Scientific Publishers PWN Ltd, Warszawa, 201-214, 246-256.

McGregor, G. R. and Nieuwolt, S., 1998: Tropical Climatology: An Introduction to the Climates of Low Latitudes. John Wiley & Sons Ltd, Second Edition, Chichester, England, 65-96, 119-141, 244-250.

Migoya, E., Crespo, A., Jiménez, A., García, J., Manuel, F., 2007: Wind energy resource assessment in Madrid region. Renewable Energy, 32, 1467–1483.

ME (Ministério de Energia), 2007: Boletim estatístico de energia (Ministry of Energy, Statistical bulletin of energy). ME, Maputo, 1, 5-31.

MINED (Ministério da Educação), 1986: Atlas geográfico (Ministry of Education: Geographic atlas). MINED, Maputo, 1, (14); 16-17.

Mortensen, N. G., Landberg, L., Troen, I. and Petersen, E. L., 1991: Wind Atlas Analysis and Application Program (WA^{SP}) User Guide, version 3.2. Risø National Laboratory, Roskilde, Denmark, 1-130.

Mortensen, N. G. and Petersen, E., 1997: Influence of topographical input data on the accuracy of wind flow modeling in complex terrain. Proceedings of the 1997 European Wind Energy Conference and Exhibition, Dublin, Ireland, 317-320.

Mortensen, N. G., Said, U. S., Frank; H.P., Georgy, L., Hasager, C. B., Akmal, M., Hansen, J. C. and Salam, A. A., 2003. Wind Atlas for the Gulf of Suez. Measurements

and Modelling. New and Renewable Energy Authority, Cairo, and Risø National Laboratory, Roskilde, 1-196.

Mortensen, N. G., Hansen, J. C., Badger, J., Jørgensen, B. H., Hasager, C. B., Youssef, L. G., Said, U. S., Moussa, A. A. E. S., Mahmoud, M. A., Yousef, A. E. S., Awad, M. A. M., Ahmed, M. A. E. R. A., Sayed; M. A. M., Korany, M. H., Tarad, M. A. E. B., 2005. Wind Atlas for Egypt, Measurements and Modelling. New and Renewable Energy Authority, Egyptian Meteorological Authority and Risø National Laboratory. 1-258.

Mortensen, N. G., Myllerup, L., Landberg, L., Rathmann, O., Mortensen, S. S., Heathfield, D., Drummond, R., 2007: WAsP 9 Help Facility and On-line Documentation. Risø National Laboratory, Roskilde, Denmark.

Mortensen, N. G., Heathfield, D. N., Rathmann, O. and Nielsen, M., 2009: Wind Atlas Analysis and Application Program: WAsP 10 Help Facility. Risø National Laboratory for Sustainable Energy, Technical University of Denmark, Roskilde, Denmark. 1-356 topics.

Mulder, P. and Tembe, J., 2008: Rural electrification in an imperfect world: A case study from Mozambique. Energy Policy, 36, 2785-2794.

Narayana, M., 2008: Validation of wind resource assessment model (WRAM) map of Sri Lanka, using measured data, and evaluation of wind power generation potential in the country. Energy for Sustainable Development, XII (1), 64-68.

NAP (National Academy Press), 1991: Assessment of research needs for wind turbine rotor materials technology. NAP, Washington D.C., 1-107 (www.nap.edu/catalog/1824.html, accessed in October 2008).

Ngoa, T. and Letchford, C., 2008: A comparison of topographic effects on gust wind speed. Journal of Wind Engineering and Industrial Aerodynamics, 96, 2273–2293.

- O'Brien, K. and Vogel, C., 2003: Coping with climate variability—The use of seasonal climate forecast in Southern Africa. Ashgate Publishing Limited, Gower House, England, 135-150.
- Palma, J. M. L., Castro, F. A., Ribeiro, L. F., Rogrigues, A. H. and Pinto, A. P., 2008: Linear and nonlinear models in wind resource assessment and wind turbine micro-siting in complex terrain. Journal of Wind Engineering and Industrial Aerodynamics, 96, 2308-2326.
- Petersen, E. L., Mortensen, N. G., Landberg, L., Højstrup, J. and Frank., H., 1997: Wind power meteorology. Risø National Laboratory, Roskilde, Denmark, 1-46.
- Raupach, M. R. and Finnigan, J. J., 1997: The influence of topography on meteorological variables and surface-atmosphere interactions. Journal of Hydrology, 190, 182-213.
- Sahin, A. D., 2004: Progress and recent trends in wind energy. Progress in Energy and Combustion Science, 30, 501–543.
- Shata, A. S. A. and Hanitsch, R., 2006: The potential of electricity generation on the east coast of Red Sea in Egypt. Renewable Energy, 31, 1597–1615.
- SADC (Southern Africa Development Community) Project AAA 5.17, 1996: Rural energy planning and environmental management training program. SADC Energy Sector Technical and Administrative Unit, Luanda, 1-26.
- Souza, A. and Granja, S. C., 1997: Estimate of the parameters C and K of Weibull model and of the wind speed direction to Campo Grande and Douras/MS, Brazil. Revista Brasileira de Agrometeorologia, Santa Maria, 5 (1), 109-114.
- Spera, D. A. and Richards, T. R., 1979: Modified power law equations for vertical wind profiles. U.S. Department of Energy-Energy Technology Distributed Solar Technology Division, Washington D.C. 20545, 1-10.

Takle, E. S. and Brown, J. M., 1978: Note on use of Weibull statistics to characterize wind-speed data. Journal of Climate and Applied Meteorology, 17, 556-559.

Troen, I. and Petersen, E. L., 1988: Siting of wind turbines. European Community wind energy conference and exhibition. Risø National Laboratory, Roskilde, Denmark, 21-31.

Troen, I. and Petersen, E. L., 1989: European wind atlas. Risø National Laboratory, Roskilde, Denmark, 1-656.

Tuller, S. E. and Brett, A. C., 1994: The characteristics of wind velocity that favor the fitting of a Weibull distribution in wind speed analysis. Journal of Climate and Applied Meteorology, 23, 124-134.

Twidell, J. and Weir, T., 2006: Renewable Resources. Second Edition, Taylor & Francis Group, 2 - 25; 263 - 319.

Tyson, P. D. and Preston-Whyte, R. A., 2000: The Weather and Climate of Southern Africa. Second Edition, Oxford University Press, South Africa, 109-127, 151-175, 191-209.

VAISALA, 2002: Anemometer WAA151–User Guide M210293en-A, Finland, 1-27.

Van Heerden, J. and Hurry, L., 1987: Southern Africa's Weather Patterns-An Introductory Guide. Acaia Books, South Africa, 9-29, 72-80.

VESTAS Wind systems A/S, 2008: General specification Vestas V 52-850 kW 50/60Hz OptiSpeed[®] -wind Turbine. Vestas, Denmark, 946506 (10), 1-21.

Vinh, N. V. and Ngoc, N. P. N., 2009: An Inequality for the Gamma function. International Mathematics Forum, 4 (28), 1379-1382.

Walker, J. F. and Jenkins, N., 1997: Wind Energy Technology. John Wiley & Sons, England, 1-34, 75-87.

Wallace, J. M. and Hobbs, P. V., 1977: Atmospheric Science-An Introductory Survey. Academic Press, Inc, 396-407.

Walmsley, J. L., Troen, I. B., Lalas, D. P. and Mason, P. J., 1990: Surface-Layer flow in complex terrain: comparison of models and full-scale observations. Boundary Layer Meteorology, 52, 258-281.

Wells, N., 1986: The Atmosphere and Ocean-A Physical Introduction. Taylor & Francis Ltd, London, 126-132, 161-168, 176-185.

WMO (World Meteorological Organization), 1970: The planning of meteorological station networks. WMO Technical, Technical Note (111), 1-35.

WMO (World Meteorological Organization), 1981: Meteorological aspects of the utilization of wind as an energy source. WMO Technical, Technical Note (175), 1-133.

Wortman, A. J., 1993: Introduction to Wind Turbine Engineering. Butterworth Publishers, Woburn, MA 01801, Boston U.S.A., (chp1) 1-5, (chp2) 7-12, (chp3) 3-5.

Zaharim, A., Razali, A. M., Abidin, R. Z. and Sopian, K., 2009a: Fitting of Statistical Distribution to Wind speed data in Malaysia. European Journal of Scientific Research, 26, (1), 6-12.

Zaharim, A., Najid, S, K., Razali, A. M. and Sopian, K., 2009b: Wind speed analysis in East coast of Malaysia. European Journal of Scientific Research, 32, (2), 208-215.

APPENDICES

APPENDIX A Roughness length and terrain surface characteristics used for modelling

Table A4: Roughness length (Z_0), terrain surface characteristics and roughness classes used for modeling in WA³P [After Troen and Petersen 1989].

Z_0 (m)	Terrain surface characteristics	Roughness class
0.0000	Water	0
0.0070	Wetland	0
0.0050	Bore soil (smooth)	0
0.0100	Airport Runway area	1
0.0500	Cultivated land/Open land	1
0.2000	Many trees/Plantation or bushes	2
0.5000	Suburbs	3
1.0000	City	3
Observed two or more roughness		
0.0085	Marshes and open land	0
0.0150	Marshes and cultivated land/trees/water	1
0.0200	Airport Areas with few Buildings/ trees or plantation	1
0.0250	Open land with grass/very few buildings and some trees	1
0.0300	Cultivated Land with few buildings /trees or plantation	1
0.0400	Cultivated Land with open appearance and trees/plantation	1
0.0600	Cultivated Land with closed appearance	1
0.0750	Open land and trees	1
0.1000	Land and trees with closed appearance	2
0.150	Residential area with open appearance and very few buildings	2
0.4000	Residential area with trees/plantation	3
0.6000	Trees /plantation with open appearance	3
0.7500	Plantation and trees with closed appearance	3
0.8000	Forest	3

APPENDIX B Coordinates of the meteorological station and predicted sites

Table B4: Coordinates in UTM of the meteorological stations and potential wind turbine sites used for modeling.

Area	Turbine site	Coordinates UTM		Elevation [m]
		x [m]	y [m]	
Mavalane	Turbine site 1	459261.5	-2873788.0	30.0
	Turbine site 2	461035.0	-2868682.0	17.0
	Turbine site 3	462589.3	-2864656.0	10.0
	Mavalane meteorological station	456937.0	-2866906.0	27.0
Ponta de Ouro	Turbine site 1	486010.1	-2951959.0	40.0
	Turbine site 2	486065.9	-2955304.0	21.0
	Ponta de Ouro meteorological station	489129.7	-2956178.0	21.0
Tofinho	Turbine site 1	755044.6	-2644929.0	61.0
	Turbine site 2	757067.9	-2643824.0	40.0
	Tofinho meteorological station	758946.3	-2640778.0	12.0
Vilankulo	Turbine site 1	731993.2	-2436900.0	41.0
	Turbine site 2	737048.5	-2436315.0	24.0
	Vilankulo meteorological station	739168.0	-2434156.0	12.0
Nampula	Turbine site 1	531710.4	-1667606.0	372.0
	Turbine site 2	532732.5	-1667056.0	371.0
	Nampula meteorological station	530606.8	-1670549.0	430.0
Pemba	Turbine site 1	666856.1	-1436712.0	43.0
	Turbine site 2	666690.6	-1438450.0	55.0
	Turbine site 3	668248.9	-1435789.0	21.0
	Pemba meteorological station	665311.1	-1436298.0	90.0
Lichinga	Turbine site 1	748662.0	-1470473.0	1327.0
	Turbine site 2	747968.5	-1469932.0	1332.0
	Turbine site 3	750216.1	-1471644.0	1366.0
	Lichinga meteorological station	746146.9	-1467952	1368

APPENDIX C Obstacle description

Table C4 List of obstacles around the selected met stations.

a) Mavalane

Object ID	α_1 [°]	R_1 [m]	α_2 [°]	R_2 [m]	Height[m]	Depth[m]	Porosity
1	111.41	190.0	155.58	260.0	14.0	43.92	0
2	158.24	270.0	159.57	280.0	25.0	40.83	0
3	167.48	404.64	174.6	397.1	18.0	00.46	0
4	104.84	254.28	118.85	256.51	16.0	139.53	0
5	301.07	686.65	305.05	673.97	12.75	46.0	0
6	296.36	808.69	300.09	830.89	6.0	38.68	0
7	227.89	987.58	229.37	967.37	6.0	45.34	0
8	346.39	581.54	351.84	592.0	12.75	31.0	0
9	338.29	712.74	340.0	729.76	12.75	26.69	0
10	240.03	1013.47	242.03	1007.23	8.5	38.1	0
11	182.07	768.27	192.09	826.31	6.5	50.0	0
12	329.78	651.23	334.36	631.2	12.75	15.23	0
13	314.58	666.07	318.34	664.07	12.75	39.08	0
14	258.14	744.72	261.37	710.75	12.75	13.6	0
15	270.37	712.62	273.75	718.59	12.75	15.56	0
16	252.05	1006.46	253.86	1007.24	5.0	31.14	0.5

b) Ponta de Ouro

Object ID	Angle1[°]	Radius1[m]	Angle2[°]	Radius2[m]	Height[m]	Depth[m]	Porosity
1	42.71	1405.74	135.02	1118.86	110.0	285.92	0.30
2	32.83	2054.51	40.58	1476.21	80.0	290.47	0.30
3	148.88	1952.65	170.46	2985.75	120.0	190.82	0.30
4	8.41	4448.81	10.78	3883.21	120.0	300.95	0.30
5	10.94	3827.27	18.84	2002.02	70.0	305.88	0.30
6	169.64	2935.47	188.51	3397.18	80.0	185.79	0.35
7	250.30	1021.32	265.23	1175.67	130.0	348.39	0.35

c) Tofinho

Object ID	Angle1[°]	Radius1[m]	Angle2[°]	Radius2[m]	Height[m]	Depth[m]	Porosity
1	292.16	33.00	312.06	29.49	5.50	13.45	0.50
2	281.89	68.82	292.07	64.63	6.50	11.72	0.50
3	260.11	112.75	269.64	102.05	6.00	11.89	0.50
4	202.71	67.87	219.28	64.28	12.49	12.49	0.40
5	212.98	163.89	216.44	156.45	7.50	7.07	0.00
6	230.88	180.38	233.91	176.94	5.00	11.14	0.00
7	191.06	181.06	193.76	173.92	7.50	6.80	0.00
8	174.41	238.87	174.82	250.14	7.50	7.00	0.00

d) Vilankulo

Object ID	Angle1[°]	Radius1[m]	Angle2[°]	Radius2[m]	Height[m]	Depth[m]	Porosity
1	124.81	41.07	141.13	36.54	5.00	11.80	0.00
2	129.62	71.90	148.60	63.89	6.50	40.09	0.00
3	85.15	27.53	109.18	30.98	4.50	9.12	0.50
4	1.15	61.80	9.46	60.34	6.50	13.78	0.50
5	348.27	64.44	355.74	64.16	5.00	23.88	0.50
6	6.38	123.77	357.49	73.72	5.00	26.60	0.00
7	347.98	123.77	353.38	126.69	5.50	26.59	0.00
8	90.41	252.82	95.46	253.38	8.00	19.34	0.50

e) Nampula

Obstacle ID	Angle 1 [°]	Radius 1 [m]	Angle 2 [°]	Radius 2 [m]	Height [m]	Depth [m]	Porosity
1	73.01	445.33	75.37	414.17	5.50	23.99	0.00
2	64.77	624.13	68.59	520.83	5.50	22.75	0.00
3	65.98	601.67	66.32	594.71	7.00	7.19	0.00
4	62.88	702.60	64.71	630.45	4.50	21.24	0.00
5	71.06	518.26	71.22	501.75	3.50	67.27	0.00
6	69.48	493.04	71.53	486.01	3.50	5.07	0.00
7	109.86	257.03	115.42	245.60	3.00	11.37	0.00

f) Pemba

Obstacle ID	Angle 1 [°]	Radius 1 [m]	Angle 2 [°]	Radius 2 [m]	Height [m]	Depth [m]	Porosity
1	64.45	201.14	67.71	200.30	3.00	13.06	0.00
2	117.92	275.98	120.25	266.37	3.00	18.46	0.00
3	117.97	323.40	120.32	315.43	3.00	13.87	0.00
4	130.59	367.11	132.18	362.08	3.50	20.78	0.00
5	124.13	428.46	126.15	417.53	3.50	12.83	0.00
6	128.56	350.88	130.44	343.64	3.50	18.38	0.00

g) Lichinga

Obstacle ID	Angle 1 [°]	Radius 1 [m]	Angle 2 [°]	Rradius 2 [m]	Height [m]	Depth [m]	Porosity
1	54.56	60.92	56.25	47.61	3.50	7.60	0.00
2	343.17	34.93	0.540	36.33	4.50	80.97	0.33
3	261.59	191.65	310.20	52.32	4.50	10.07	0.33
4	248.05	164.45	248.37	140.53	3.50	20.58	0.00
5	314.12	86.92	318.17	44.74	4.50	11.71	0.33
6	66.91	173.46	69.96	173.02	3.50	23.5	0.00
7	63.92	238.15	69.74	237.16	3.50	20.51	0.00

APPENDIX D Roughness description

Table D4: Roughness length and change assigned to the surrounding meteorological station at:

a) Ponta de Ouro

Sector	Z_{01} [m]	X_1 [m]	Z_{02} [m]	X_2 [m]	Z_{03} [m]	X_3 [m]	Z_{04} [m]	X_4 [m]	Z_{05} [m]	X_5 [m]	
1	0°	0.007	0.00	0.600	972.20						
2	30°	0.007	0.00	0.600	663.26	0.0085	1 084.57	0.750	1 537.02	0.000	2 230.28
3	60°	0.007	0.00	0.750	686.18	0.000	1 273.64				
4	90°	0.007	0.00	0.750	685.99	0.000	979.06				
5	120°	0.007	0.00	0.750	878.49	0.000	1 066.12				
6	150°	0.007	0.00	0.025	1 941.92	0.000	2 092.88				
7	180°	0.007	0.00	0.600	2 638.48	0.000	5 917.09				
8	210°	0.007	0.00	0.0085	1 433.78	0.600	3 480.81	0.025	4 867.93	0.007	4 867.91
9	240°	0.007	0.00	0.0085	4 168.12	0.600	6 447.05				
10	270°	0.007	0.00	0.600	235.94	0.600	1 146.36				
11	300°	0.007	0.00	0.600	163.63	0.600	429.11				
12	330°	0.007	0.00	0.600	238.62	0.600	1 274.61				

b) Tofinho (Inhambane)

Sector	Z_{01} [m]	X_1 [m]	Z_{02} [m]	X_2 [m]	Z_{03} [m]	X_3 [m]	Z_{04} [m]	X_4 [m]	Z_{05} [m]	X_5 [m]	
1	0°	0.007	0.00	0.000	39.72						
2	30°	0.007	0.00	0.000	37.74						
3	60°	0.007	0.00	0.000	37.31						
4	90°	0.007	0.00	0.000	51.11						
5	120°	0.007	0.00	0.000	98.87						
6	150°	0.007	0.00	0.000	168.29						
7	180°	0.007	0.00	0.000	559.93						
8	210°	0.025	0.00	0.007	528.86						
9	240°	0.025	0.00	0.030	650.48						
10	270°	0.025	0.00	0.030	969.96	0.000	8 160.23				
11	300°	0.025	0.00	0.007	1 272.24	0.060	2 450.09	0.000	6 916.10		
12	330°	0.007	0.00	0.000	56.16	0.025	577.70	0.000	1 684.47	0.600	8 168.62

c) Mavalane

Sector		[Z ₀₁][m]	[X ₁][m]	[Z ₀₂][m]	X ₂ [m]	Z ₀₃ [m]	X ₃ [m]	[Z ₀₄][m]	X ₄ [m]	[Z ₀₅][m]	X ₅ [m]	[Z ₀₆][m]	X ₆ [m]
1	0°	0.20	0.0	0.50	1,133.29	0.75	5,258.13	0.50	7,237.08				
2	30°	0.010	0.0	0.50	4,886.90								
3	60°	0.010	0.0	0.50	1,483.26	0.015	6,188.64						
4	90°	0.020	0.0	0.50	810.55	0.015	5,386.37	0.50	6,276.28	0.0	6,831.89		
5	120°	0.020	0.0	0.50	641.23	1.00	4,395.88	0.00	5,336.38				
6	150°	0.020	0.0	0.50	871.81	1.00	3,544.19	0.60	5,553.95	0.0	5,684.01		
7	180°	0.020	0.0	0.50	864.34	1.00	3,700.68	0.0	6,090.08				
8	210°	0.010	0.0	0.50	1,216.88	1.00	3,581.25	0.00	5,061.70	0.007	6,820.45	0.05	8,165.06
9	240°	0.02	0.0	0.50	1,300.13	0.00	4,593.33						
10	270°	0.020	0.0	0.50	1,087.01	0.015	2,937.28	0.50	6,287.78				
11	300°	0.010	0.0	0.50	820.56	0.015	2,548.71	0.50	3,213.80				
12	330°	0.02	0.0	0.50	1,133.89	0.015	2,880.59	0.50	3,652.27				

d) Vilankulo

Sector		Z ₀₁ [m]	X ₁ [m]	Z ₀₂ [m]	X ₂ [m]	Z ₀₃ [m]	X ₃ [m]	Z ₀₄ [m]	X ₄ [m]	Z ₀₅ [m]	X ₅ [m]	Z ₀₆ [m]	X ₆ [m]	Z ₀₇ [m]	X ₇ [m]
1	0°	0.020	0.0	0.40	159.39	0.007	961.80	0.40	1 286.93	0.0	4 260.92	0.075	7 013.39		
2	30°	0.020	0.0	0.40	73.35	0.007	539.53	0.40	607.87	0.0	1 900.21				
3	60°	0.020	0.0	0.40	60.44	0.007	404.45	0.40	511.02	0.0	849.18				
4	90°	0.020	0.0	0.40	65.59	0.007	395.33	0.75	535.89	0.0	679.81				
5	120°	0.020	0.0	0.40	251.26	0.005	376.06	0.007	524.92	0.005	583.96	0.0	667.58		
6	150°	0.010	0.0	0.40	446.59	0.007	845.23	0.10	949.50	0.0	1 340.50				
7	180°	0.010	0.0	0.075	961.81	0.007	8 097.66	0.075	8 204.29						
8	210°	0.010	0.0	0.075	497.56	0.0	3 614.47	0.075	4 549.33						
9	240°	0.010	0.0	0.075	660.53	0.0	4 520.98	0.075	7 754.46						
10	270°	0.010	0.0	0.075	592.20	0.0	4 937.77	0.075	7 969.37						
11	300°	0.010	0.0	0.15	722.03	0.0	7 146.46	0.075	8 221.68						
12	330°	0.010	0.0	0.40	831.78	0.075	3 291.59	0.0	6 023.25	0.075	7 121.19	0.0	8 541.35	0.075	8 931.99

e) Nampula

Sector		Z ₀₁ [m]	X ₁ [m]	Z ₀₂ [m]	X ₂ [m]	Z ₀₃ [m]	X ₃ [m]	Z ₀₄ [m]	X ₄ [m]	Z ₀₅ [m]	X ₅ [m]
1	0°	0.01	0.0	0.15	45.00	0.050	2096.00				
2	30°	0.01	0.0	0.40	1126.00	0.050	1 724.00				
3	60°	0.01	0.0	0.05	2065.00						
4	90°	0.01	0.0	0.40	553.00	0.050	1724.00				
5	120°	0.01	0.0	0.40	573.0	0.05	3 009.00				
6	150°	0.01	0.0	0.40	266.00	0.075	4 651.00				
7	180°	0.01	0.0	0.40	296.00	0.075	4 068.00				
8	210°	0.01	0.0	0.40	464.00	0.075	3 563.00				
9	240°	0.01	0.0	0.50	796.00	0.075	4 718.00				
10	270°	0.01	0.0	0.50	438.00	0.075	6 899.00				
11	300°	0.01	0.0	0.50	319.00	0.075	1665.00	0.40	2287.00	0.075	3726.00
12	330°	0.01	0.0	0.50	314.00	0.050	2 411.00				

f) Pemba

Sector		Z ₀₁ [m]	X ₁ [m]	Z ₀₂ [m]	X ₂ [m]	Z ₀₃ [m]	X ₃ [m]	Z ₀₄ [m]	X ₄ [m]	Z ₀₅ [m]	X ₀₆ [m]
1	0°	0.01	0.0	0.5	947.00	0.005	2 836.00	0.00	2997.00		
2	30°	0.01	0.0	0.5	424.00	0.005	2 281.00	0.00	2 516.00		
3	60°	0.01	0.0	0.5	328.00	0.03	4 791.00	0.00	4911.00		
4	90°	0.01	0.0	0.5	346.00	0.075	1962.00	0.00	6724.00		
5	120°	0.01	0.0	0.02	259.00	0.5	498.00	0.075	1410.00	0	6 355.00
6	150°	0.01	0.0	0.075	1 547.00	0.0	7 684.00				
7	180°	0.01	0.0	0.075	920.00	0.0	6 700.00				
8	210°	0.01	0.0	0.075	838.00	0.0	2 200.00				
9	240°	0.01	0.0	0.075	759.00	0.0	1 215.00				
10	270°	0.01	0.0	0.075	851.00	0.0	1 123.00				
11	300°	0.01	0.0	0.07	920.00	0.0	1636.00				
12	330°	0.01	0.0	0.07	764.00	0.5	1 444.00	0.00	4742.00		

g) Lichinga

	Sector	Z ₀₁ [m]	X ₁ [m]	Z ₀₂ [m]	X ₂ [m]	Z ₀₃ [m]	X ₃ [m]	Z ₀₄ [m]	X ₄ [m]
1	0°	0.01	0.0	0.075	129.00	0.1	461.00		
2	30°	0.01	0.0	0.03	144.00	0.075	768.00		
3	60°	0.02	0.0	0.05	415.00				
4	90°	0.01	0.0	0.05	415.00				
5	120°	0.01	0.0	0.05	627.00	0.6	5 236.00		
6	150°	0.01	0.0	0.05	3 188.00	0.05	3 280.00		
7	180°	0.01	0.0	0.05	592.00	0.06	2 494.00	0.5	4 332.00
8	210°	0.01	0.0	0.02	856.00	0.5	1 519.00	0.04	5 512.00
9	240°	0.01	0.0	0.5	1 989.00	0.05	3 711.00		
10	270°	0.01	0.0	0.05	2152.00				
11	300°	0.02	0.0	0.05	178.00				
12	330°	0.02	0.0	0.075	130.00				

APPENDIX E The wind speed and Weibull-k frequency distribution

Table E4.1: The sector-wise wind speed and Weibull-k parameter frequency distribution by roughness class and height at Mavalane.

a) Mavalane roughness class $Z_0=0.0002$ m

Height [m]	0°	30°	60°	90°	120°	150°	180°	210°	240°	270°	300°	330°
10.0	7.9	6.8	7.7	8.4	10.4	9.3	7.8	7.2	4.4	3.1	4.6	7.2
	2.49	2.63	3.02	2.49	2.25	2.22	2.55	2.61	1.73	1.24	1.49	2.31
25.0	8.7	7.5	8.4	9.2	11.3	10.1	8.6	7.9	4.8	3.4	5.1	7.9
	2.57	2.72	3.12	2.56	2.28	2.28	2.63	2.69	1.78	1.28	1.54	2.38
50.0	9.3	8.0	9.0	9.9	12.1	10.8	9.2	8.5	5.2	3.7	5.4	8.4
	2.64	2.79	3.20	2.63	2.34	2.34	2.70	2.76	1.83	1.31	1.58	2.44
100.0	10.1	8.7	9.8	10.7	12.9	11.7	10.0	9.2	5.6	4.0	5.9	9.2
	2.55	2.70	3.10	2.55	2.31	2.29	2.62	2.67	1.77	1.27	1.53	2.37
200.0	11.2	9.6	10.9	11.9	13.9	12.7	11.1	10.2	6.2	4.3	6.5	10.1
	2.42	2.56	2.93	2.41	2.24	2.20	2.48	2.53	1.68	1.21	1.45	2.24
Fr[%]	8.6	8.4	11.5	13.9	8.7	8.0	12.5	14.1	4.4	2.0	2.5	5.3

b) Mavalane roughness class $Z_{01}=0.030$ m

Height [m]	0°	30°	60°	90°	120°	150°	180°	210°	240°	270°	300°	330°
10.0	5.7	4.6	5.2	5.6	7.4	6.9	5.7	5.1	3.1	2.1	2.2	4.4
	2.15	2.14	2.48	2.32	2.02	2.01	2.22	2.22	1.51	1.09	0.99	1.78
25.0	6.8	5.5	6.2	6.7	8.7	8.2	6.8	6.1	3.7	2.5	2.7	5.3
	2.32	2.31	2.68	2.50	2.10	2.10	2.40	2.40	1.63	1.17	1.06	1.93
50.0	7.9	6.3	7.1	7.7	9.8	9.3	7.8	7.0	4.4	3.0	3.2	6.2
	2.61	2.60	3.02	2.81	2.22	2.26	2.70	2.70	1.83	1.31	1.18	2.17
100.0	9.3	7.5	8.5	9.1	11.2	10.7	9.3	8.3	5.2	3.6	3.9	7.3
	2.78	2.76	3.21	3.00	2.39	2.43	2.87	2.87	1.94	1.39	1.25	2.31
200.0	11.6	9.3	10.5	11.3	13.0	12.6	11.5	10.4	6.5	4.5	4.8	9.1
	2.65	2.64	3.06	2.86	2.32	2.35	2.74	2.74	1.86	1.33	1.20	2.20
Fr[%]	8.8	7.9	10.4	15.4	9.2	7.1	11.0	16.8	5.2	2.0	2.0	4.3

c) Mavalane roughness class $Z_{02}=0.100$ m

Height [m]	0°	30°	60°	90°	120°	150°	180°	210°	240°	270°	300°	330°
10.0	5.0	4.0	4.5	4.8	6.2	6.0	5.0	4.5	3.0	2.0	1.7	3.8
	2.16	2.09	2.42	2.43	1.98	2.01	2.22	2.23	1.54	1.18	0.93	1.79
25.0	6.1	5.0	5.5	5.9	7.6	7.4	6.1	5.5	3.7	2.5	2.2	4.7
	2.31	2.23	2.58	2.60	2.06	2.10	2.38	2.39	1.65	1.26	0.99	1.92
50.0	7.2	5.8	6.4	6.9	8.7	8.5	7.2	6.4	4.4	3.0	2.6	5.5
	2.56	2.47	2.86	2.88	2.17	2.23	2.63	2.65	1.82	1.39	1.08	2.13
100.0	8.5	6.9	7.6	8.2	10.1	9.9	8.5	7.7	5.2	3.6	3.2	6.6
	2.81	2.72	3.15	3.16	2.37	2.45	2.90	2.91	2.00	1.52	1.18	2.34
200.0	10.5	8.5	9.4	10.2	11.8	11.7	10.6	9.5	6.5	4.4	3.9	8.2
	2.69	2.60	3.01	3.03	2.30	2.37	2.77	2.78	1.91	1.46	1.13	2.24
Fr[%]	8.7	7.8	10.2	15.0	10.0	7.2	10.6	16.5	6.0	2.3	1.9	4.0

d) Mavalane roughness class $Z_{03}=0.400$ m

Height [m]	0°	30°	60°	90°	120°	150°	180°	210°	240°	270°	300°	330°
10.0	3.8	3.2	3.5	3.8	4.7	4.8	4.0	3.6	2.7	1.8	1.6	2.9
	2.14	2.04	2.38	2.46	1.92	2.03	2.20	2.30	1.65	1.38	1.06	1.67
25.0	5.1	4.3	4.6	4.9	6.1	6.2	5.2	4.7	3.5	2.4	2.1	3.8
	2.27	2.16	2.52	2.61	1.99	2.10	2.33	2.44	1.75	1.46	1.12	1.76
50.0	6.1	5.2	5.5	5.9	7.2	7.4	6.3	5.7	4.3	3.0	2.6	4.6
	2.46	2.35	2.74	2.84	2.09	2.21	2.53	2.65	1.90	1.58	1.21	1.92
100.0	7.3	6.2	6.6	7.1	8.5	8.8	7.6	6.8	5.1	3.6	3.2	5.5
	2.81	2.68	3.12	3.23	2.28	2.41	2.88	3.02	2.16	1.80	1.37	2.18
200.0	9.0	7.6	8.1	8.7	10.1	10.4	9.3	8.3	6.3	4.4	3.9	6.8
	2.71	2.58	3.01	3.11	2.28	2.41	2.78	2.91	2.08	1.74	1.32	2.10
Fr[%]	8.1	7.9	9.9	14.4	10.7	7.4	10.1	15.7	7.3	2.7	1.9	3.8

Table E4.2: The sector-wise wind speed and Weibull-k parameter and frequency distribution by roughness class and height at Ponta de Ouro.

a) Ponta de Ouro roughness class $Z_0=0.0002$ m

Height [m]	0°	30°	60°	90°	120°	150°	180°	210°	240°	270°	300°	330°
10.0	9.8	9.5	9.3	7.9	7.0	7.2	8.9	6.5	6.3	7.3	6.8	7.7
	4.08	4.46	3.24	3.01	3.30	2.92	2.67	2.40	2.50	2.14	2.11	2.49
25.0	10.7	10.3	10.2	8.6	7.7	7.9	9.7	7.1	6.9	8.0	7.5	8.5
	4.21	4.59	3.35	3.11	3.41	3.01	2.76	2.47	2.58	2.21	2.18	2.57
50.0	11.5	11.1	10.9	9.2	8.2	8.5	10.4	7.6	7.4	8.6	8.0	9.1
	4.31	4.71	3.44	3.19	3.50	3.09	2.83	2.54	2.65	2.27	2.23	2.64
100.0	12.5	12.0	11.9	10.0	8.9	9.2	11.3	8.3	8.0	9.3	8.7	9.9
	4.18	4.56	3.33	3.09	3.39	2.99	2.74	2.46	2.57	2.19	2.16	2.56
200.0	13.8	13.3	13.2	11.1	9.9	10.2	12.5	9.2	8.9	10.3	9.6	10.9
	3.96	4.33	3.15	2.92	3.21	2.83	2.60	2.33	2.43	2.08	2.05	2.42
Fr [%]	6.7	13.2	8.7	7.0	7.9	8.3	11.8	15.7	7.9	4.0	4.3	4.4

b) Ponta de Ouro roughness class $Z_{01}=0.030$ m

Height [m]	0°	30°	60°	90°	120°	150°	180°	210°	240°	270°	300°	330°
10.0	6.6	6.5	6.6	5.7	5.0	4.7	6.5	4.6	4.3	5.1	4.7	5.0
	2.95	3.90	2.83	2.55	2.70	3.01	2.46	1.97	2.12	1.87	1.77	1.97
25.0	7.9	7.8	7.8	6.8	5.9	5.6	7.7	5.6	5.2	6.1	5.7	6.0
	3.19	4.22	3.06	2.76	2.92	3.25	2.65	2.13	2.29	2.01	1.91	2.13
50.0	9.1	9.0	9.0	7.8	6.8	6.5	8.9	6.4	6.0	7.0	6.6	7.0
	3.58	4.73	3.44	3.10	3.28	3.66	2.98	2.39	2.57	2.26	2.15	2.39
100.0	10.8	10.6	10.7	9.2	8.1	7.6	10.5	7.6	7.1	8.3	7.8	8.3
	3.81	5.03	3.66	3.30	3.49	3.89	3.18	2.55	2.74	2.41	2.29	2.55
200.0	13.4	13.2	13.3	11.5	10.1	9.5	13.1	9.5	8.8	10.4	9.7	10.3
	3.64	4.81	3.49	3.15	3.33	3.72	3.03	2.43	2.62	2.30	2.19	2.43
Fr [%]	5.4	13.2	9.5	7.0	7.8	7.9	10.6	16.3	9.3	4.5	4.3	4.2

c) Ponta de Ouro roughness class $Z_{02}=0.100$ m

Height [m]	0°	30°	60°	90°	120°	150°	180°	210°	240°	270°	300°	330°
10.0	5.7	5.7	5.7	5.0	4.4	4.1	5.5	4.1	3.8	4.2	4.1	4.3
	2.86	3.72	2.86	2.54	2.62	3.00	2.40	1.94	2.18	1.78	1.75	1.93
25.0	7.0	7.0	7.0	6.2	5.4	5.1	6.8	5.1	4.7	5.2	5.1	5.4
	3.06	3.98	3.06	2.72	2.81	3.21	2.56	2.08	2.34	1.90	1.87	2.06
50.0	8.2	8.1	8.2	7.2	6.3	5.9	7.9	6.0	5.5	6.1	6.0	6.3
	3.39	4.40	3.38	3.01	3.11	3.56	2.84	2.30	2.59	2.11	2.07	2.28
100.0	9.7	9.6	9.7	8.5	7.4	7.0	9.4	7.1	6.6	7.3	7.1	7.5
	3.72	4.83	3.72	3.31	3.41	3.90	3.12	2.53	2.84	2.31	2.28	2.51
200.0	12.0	11.9	12.0	10.6	9.2	8.7	11.7	8.8	8.1	9.0	8.8	9.2
	3.56	4.62	3.56	3.17	3.27	3.74	2.99	2.42	2.72	2.22	2.18	2.40
Fr [%]	5.4	12.5	9.8	7.2	7.7	7.9	10.4	15.8	10.0	4.9	4.3	4.3

d) Ponta de Ouro roughness class $Z_{03}=0.400$ m

Height [m]	0°	30°	60°	90°	120°	150°	180°	210°	240°	270°	300°	330°
10.0	4.3	4.4	4.5	4.0	3.5	3.3	4.2	3.4	3.0	3.2	3.3	3.4
	2.72	3.55	2.97	2.53	2.54	2.95	2.29	1.97	2.13	1.76	1.76	1.93
25.0	5.7	5.8	5.9	5.3	4.5	4.3	5.5	4.5	4.0	4.2	4.3	4.5
	2.88	3.77	3.15	2.69	2.69	3.13	2.43	2.08	2.26	1.87	1.87	2.04
50.0	6.9	7.0	7.0	6.3	5.5	5.1	6.6	5.4	4.8	5.0	5.2	5.4
	3.13	4.09	3.42	2.92	2.92	3.40	2.64	2.26	2.46	2.03	2.03	2.22
100.0	8.2	8.4	8.4	7.6	6.6	6.2	8.0	6.5	5.8	6.1	6.3	6.5
	3.56	4.65	3.90	3.33	3.33	3.87	3.01	2.58	2.80	2.31	2.31	2.53
200.0	10.1	10.3	10.3	9.3	8.0	7.6	9.7	7.9	7.0	7.4	7.7	7.9
	3.44	4.49	3.76	3.21	3.21	3.73	2.90	2.49	2.70	2.23	2.22	2.44
Fr [%]	5.2	11.6	10.4	7.4	7.5	7.8	10.1	15.0	11.0	5.4	4.2	4.3

Table E4.3: The sector-wise wind speed and Weibull-k parameter frequency distribution by roughness class and height at Tofinho.

a) Tofinho roughness class $Z_0=0.0002$ m

Height [m]	0°	30°	60°	90°	120°	150°	180°	210°	240°	270°	300°	330°
10.0	9.3	7.2	5.6	5.4	7.3	9.0	10.4	7.4	6.8	5.4	6.1	6.1
	3.25	2.92	2.97	2.37	2.52	2.99	2.90	2.17	4.13	1.65	1.86	2.24
25.0	10.2	7.9	6.2	5.9	8.0	9.8	11.4	8.1	7.5	6.0	6.6	6.6
	3.35	3.01	3.06	2.44	2.60	3.08	2.97	2.24	4.26	1.71	1.92	2.31
50.0	10.9	8.5	6.6	6.4	8.6	10.5	12.2	8.7	8.0	6.4	7.1	7.1
	3.44	3.09	3.14	2.51	2.67	3.16	3.05	2.30	4.37	1.75	1.97	2.37
100.0	11.8	9.2	7.2	6.9	9.3	11.4	13.1	9.4	8.7	6.9	7.7	7.7
	3.33	2.99	3.04	2.42	2.58	3.06	2.98	2.23	4.24	1.69	1.91	2.29
200.0	13.1	10.2	7.9	7.6	10.3	12.7	14.3	10.4	9.6	7.6	8.5	8.5
	3.15	2.83	2.88	2.29	2.44	2.90	2.87	2.11	4.01	1.61	1.81	2.17
Freq [%]	6.0	14.7	9.0	9.5	15.2	21.9	11.2	4.0	3.2	1.7	1.5	2.1

b) Tofinho roughness class $Z_{01}=0.030$ m

Height [m]	0°	30°	60°	90°	120°	150°	180°	210°	240°	270°	300°	330°
10.0	6.5	5.2	4.2	3.8	4.8	6.1	7.0	5.9	4.9	4.0	4.0	4.0
	2.76	2.38	2.21	2.21	1.99	2.47	2.39	1.92	2.92	1.64	1.49	2.28
25.0	7.8	6.2	5.0	4.5	5.8	7.2	8.3	7.1	5.8	4.8	4.8	4.7
	2.98	2.58	2.38	2.38	2.15	2.67	2.54	2.05	3.15	1.78	1.61	2.46
50.0	9.0	7.1	5.8	5.2	6.6	8.3	9.4	8.1	6.7	5.6	5.7	5.4
	3.35	2.90	2.68	2.68	2.42	3.00	2.77	2.28	3.54	1.99	1.81	2.77
100.0	10.6	8.4	6.8	6.1	7.9	9.9	11.0	9.5	8.0	6.6	6.7	6.4
	3.57	3.08	2.86	2.86	2.57	3.19	2.97	2.43	3.77	2.12	1.92	2.95
200.0	13.2	10.5	8.5	7.7	9.8	12.3	13.3	11.7	9.9	8.3	8.4	8.0
	3.41	2.94	2.73	2.73	2.46	3.05	2.86	2.33	3.60	2.03	1.83	2.82
Freq [%]	4.8	13.4	9.9	9.1	13.9	21.3	13.5	5.3	3.4	2.0	1.5	1.9

c) Tofinho roughness class $Z_{02}=0.100$ m

Height [m]	0°	30°	60°	90°	120°	150°	180°	210°	240°	270°	300°	330°
10.0	5.6	4.5	3.7	3.3	4.1	5.2	5.9	5.4	4.3	3.7	3.5	3.6
	2.63	2.39	2.13	2.25	1.90	2.44	2.36	2.04	2.58	1.88	1.51	2.45
25.0	6.9	5.6	4.6	4.1	5.0	6.4	7.3	6.7	5.3	4.6	4.4	4.4
	2.81	2.56	2.28	2.41	2.04	2.62	2.49	2.15	2.76	2.01	1.62	2.62
50.0	8.0	6.5	5.4	4.8	5.9	7.5	8.4	7.8	6.1	5.4	5.2	5.1
	3.12	2.83	2.53	2.67	2.25	2.90	2.71	2.35	3.06	2.23	1.79	2.90
100.0	9.5	7.8	6.4	5.7	7.0	8.9	9.9	9.1	7.3	6.4	6.2	6.1
	3.42	3.11	2.78	2.93	2.48	3.19	2.97	2.58	3.36	2.45	1.97	3.19
200.0	11.8	9.6	7.9	7.0	8.7	11.0	12.0	11.1	9.0	7.9	7.6	7.5
	3.28	2.98	2.66	2.80	2.37	3.05	2.86	2.48	3.22	2.34	1.88	3.05
Freq [%]	4.6	12.6	10.4	9.1	13.4	20.7	14.4	5.9	3.5	2.1	1.5	1.8

d) Tofinho roughness class $Z_{03}=0.400$ m

Height [m]	0°	30°	60°	90°	120°	150°	180°	210°	240°	270°	300°	330°
10.0	4.3	3.6	3.0	2.6	3.1	4.0	4.5	4.5	3.4	3.0	2.7	2.7
	2.51	2.37	2.10	2.30	1.85	2.40	2.38	2.26	2.50	2.02	1.49	2.03
25.0	5.6	4.8	3.9	3.4	4.1	5.3	5.9	5.9	4.5	3.9	3.6	3.6
	2.66	2.51	2.22	2.44	1.96	2.54	2.51	2.37	2.65	2.14	1.58	2.15
50.0	6.7	5.7	4.8	4.1	5.0	6.3	7.1	7.1	5.4	4.7	4.4	4.3
	2.89	2.73	2.42	2.65	2.13	2.76	2.70	2.54	2.88	2.33	1.71	2.34
100.0	8.1	6.9	5.7	5.0	6.0	7.6	8.5	8.4	6.5	5.7	5.3	5.2
	3.29	3.11	2.75	3.03	2.42	3.15	3.06	2.87	3.28	2.65	1.95	2.66
200.0	9.9	8.4	7.0	6.1	7.3	9.3	10.3	10.2	7.9	6.9	6.5	6.4
	3.18	3.00	2.65	2.92	2.33	3.03	2.96	2.78	3.16	2.55	1.88	2.56
Freq [%]	4.2	11.4	11.1	9.0	12.8	19.9	15.6	6.7	3.6	2.3	1.6	1.8

Table E4.4: The sector-wise wind speed and Weibull-k parameter wind speed frequency distribution by roughness class and height at Vilankulo.

a) Vilankulo roughness class $Z_0=0.0002$ m

Height[m]	0°	30°	60°	90°	120°	150°	180°	210°	240°	270°	300°	330°
10.0	1.8	4.0	5.5	4.6	4.3	6.0	7.4	6.0	4.4	3.5	1.9	1.0
	0.87	1.37	2.28	2.02	2.16	2.65	3.29	2.27	1.99	1.63	0.72	0.56
25.0	2.1	4.4	6.1	5.0	4.7	6.6	8.1	6.6	4.8	3.9	2.0	1.1
	0.89	1.41	2.35	2.09	2.23	2.73	3.40	2.34	2.05	1.69	0.74	0.57
50.0	2.2	4.7	6.5	5.4	5.1	7.0	8.7	7.1	5.2	4.1	2.2	1.1
	0.91	1.45	2.41	2.14	2.29	2.80	3.49	2.40	2.11	1.73	0.75	0.57
100.0	2.4	5.1	7.1	5.8	5.5	7.6	9.4	7.7	5.6	4.5	2.4	1.2
	0.88	1.40	2.33	2.07	2.21	2.71	3.38	2.33	2.04	1.68	0.74	0.57
200.0	2.6	5.6	7.8	6.5	6.1	8.5	10.5	8.5	6.2	4.9	2.5	1.3
	0.85	1.33	2.21	1.96	2.10	2.57	3.20	2.20	1.93	1.59	0.72	0.56
Fr[%]	2.4	3.8	8.6	10.4	12.9	15.9	15.9	8.4	10.1	6.8	2.8	2.1

b) Vilankulo roughness class $Z_{01}=0.030$ m

Height[m]	0°	30°	60°	90°	120°	150°	180°	210°	240°	270°	300°	330°
10.0	1.3	1.8	3.9	3.3	2.8	4.0	5.1	4.6	3.2	2.5	1.6	0.4
	0.78	0.87	1.93	1.73	1.80	2.12	2.83	2.16	1.68	1.51	0.76	0.47
25.0	1.6	2.2	4.7	4.0	3.3	4.7	6.1	5.4	3.8	3.0	2.0	0.5
	0.84	0.94	2.08	1.87	1.94	2.29	3.06	2.33	1.81	1.63	0.81	0.47
50.0	1.9	2.7	5.4	4.6	3.8	5.5	7.0	6.3	4.4	3.5	2.4	0.5
	0.93	1.04	2.35	2.10	2.18	2.58	3.44	2.63	2.04	1.83	0.90	0.48
100.0	2.4	3.3	6.5	5.5	4.5	6.5	8.3	7.5	5.3	4.2	2.9	0.6
	0.98	1.10	2.50	2.24	2.32	2.74	3.65	2.79	2.17	1.95	0.95	0.49
200.0	2.9	4.0	8.0	6.8	5.6	8.1	10.4	9.3	6.6	5.2	3.6	0.7
	0.94	1.05	2.38	2.14	2.22	2.62	3.49	2.67	2.07	1.87	0.91	0.49
Fr[%]	2.3	2.9	7.8	9.9	12.1	15.7	17.1	8.6	10.3	7.8	3.4	2.1

c) Vilankulo roughness class $Z_{02}=0.100$ m

Height[m]	0°	30°	60°	90°	120°	150°	180°	210°	240°	270°	300°	330°
10.0	1.0	1.5	3.4	2.9	2.4	3.4	4.4	4.0	2.8	2.2	1.6	0.4
	0.74	0.85	1.93	1.65	1.73	2.13	2.71	2.21	1.61	1.52	0.86	0.47
25.0	1.3	1.9	4.2	3.6	3.0	4.2	5.4	5.0	3.4	2.8	2.1	0.4
	0.78	0.90	2.07	1.77	1.85	2.28	2.90	2.37	1.72	1.62	0.91	0.47
50.0	1.6	2.4	4.9	4.2	3.5	4.9	6.3	5.8	4.1	3.3	2.5	0.5
	0.85	0.99	2.29	1.96	2.05	2.53	3.22	2.62	1.91	1.79	1.00	0.48
100.0	2.0	2.9	5.9	5.0	4.2	5.8	7.5	6.9	4.9	3.9	3.1	0.6
	0.92	1.08	2.52	2.15	2.26	2.78	3.53	2.88	2.10	1.97	1.09	0.49
200.0	2.4	3.5	7.3	6.2	5.2	7.2	9.2	8.5	6.0	4.8	3.8	0.7
	0.88	1.03	2.41	2.06	2.16	2.66	3.38	2.76	2.01	1.89	1.04	0.50
Fr[%]	2.3	2.8	7.4	9.7	11.9	15.4	17.0	9.4	10.0	8.0	3.8	2.2

d) Vilankulo roughness class $Z_{03}=0.400$ m

Height[m]	0°	30°	60°	90°	120°	150°	180°	210°	240°	270°	300°	330°
10.0	0.5	1.2	2.6	2.3	2.0	2.5	3.4	3.2	2.3	1.9	1.5	0.4
	0.60	0.84	1.79	1.73	1.81	1.97	2.63	2.29	1.69	1.60	0.99	0.52
25.0	0.7	1.6	3.4	3.1	2.6	3.4	4.4	4.2	3.1	2.5	2.0	0.5
	0.62	0.88	1.90	1.83	1.92	2.09	2.79	2.42	1.79	1.70	1.04	0.52
50.0	0.9	2.0	4.1	3.7	3.2	4.0	5.3	5.1	3.7	3.0	2.5	0.6
	0.67	0.96	2.07	1.99	2.08	2.27	3.04	2.63	1.94	1.84	1.13	0.53
100.0	1.2	2.5	5.0	4.5	3.8	4.9	6.4	6.1	4.5	3.6	3.1	0.8
	0.74	1.07	2.36	2.27	2.37	2.58	3.46	3.00	2.21	2.10	1.28	0.55
200.0	1.4	3.0	6.1	5.5	4.7	6.0	7.8	7.5	5.5	4.4	3.7	0.9
	0.71	1.04	2.27	2.19	2.29	2.49	3.33	2.89	2.13	2.02	1.23	0.56
Fr[%]	2.3	2.7	6.8	9.5	11.5	15.1	16.9	10.5	9.7	8.4	4.3	2.3

Table E4.5: The sector-wise wind speed and Weibull-k parameter wind speed frequency distribution by roughness class and height at Nampula.

a) Nampula roughness class $Z_0=0.0002$ m

Height [m]	0°	30°	60°	90°	120°	150°	180°	210°	240°	270°	300°	330°
10	3.9	4	4.2	4.2	3.49	3.86	4.21	4.45	4.75	2.84	2.41	3.09
	2.21	2.50	2.46	2.37	2.13	2.40	2.67	2.90	2.92	1.47	1.37	1.61
25	4.2	4.3	4.6	4.5	3.77	4.18	4.56	4.82	5.14	3.08	2.61	3.35
	2.25	2.54	2.50	2.41	2.17	2.44	2.72	2.96	2.97	1.50	1.40	1.64
50	4.4	4.5	4.8	4.8	3.99	4.41	4.81	5.09	5.43	3.26	2.75	3.53
	2.26	2.56	2.52	2.43	2.19	2.46	2.74	2.98	3.00	1.51	1.41	1.65
100	4.7	4.8	5.1	5	4.19	4.64	5.06	5.35	5.71	3.42	2.89	3.72
	2.12	2.40	2.36	2.28	2.05	2.31	2.56	2.79	2.81	1.42	1.32	1.55
200	4.9	5	5.3	5.3	4.38	4.84	5.28	5.59	5.96	3.57	3.02	3.88
	1.89	2.14	2.10	2.03	1.83	2.05	2.28	2.49	2.50	1.27	1.19	1.38
Fr [%]	7.1	10	9.7	8.6	7	8.3	12.7	16.7	11.1	2.9	2.5	3.5

b) Nampula roughness class $Z_{01}=0.030$ m

Height [m]	0°	30°	60°	90°	120°	150°	180°	210°	240°	270°	300°	330°
10	2.7	2.7	2.9	3	2.37	2.59	2.92	3.01	3.33	2.03	1.64	1.82
	1.76	2.06	2.04	2.07	1.71	1.94	2.19	2.36	2.55	1.24	1.15	1.18
25	3.2	3.2	3.5	3.6	2.84	3.1	3.49	3.6	3.99	2.43	1.96	2.18
	1.90	2.23	2.20	2.24	1.85	2.10	2.37	2.55	2.76	1.33	1.24	1.27
50	3.7	3.7	4	4.2	3.29	3.58	4.04	4.17	4.61	2.81	2.27	2.52
	2.13	2.51	2.47	2.52	2.07	2.36	2.66	2.87	3.10	1.49	1.38	1.42
100	4.4	4.4	4.8	5	3.9	4.25	4.8	4.95	5.48	3.34	2.7	3
	2.28	2.67	2.63	2.68	2.21	2.51	2.83	3.06	3.30	1.59	1.47	1.51
200	5.5	5.5	6	6.2	4.85	5.29	5.97	6.15	6.81	4.15	3.35	3.73
	2.17	2.55	2.51	2.56	2.11	2.40	2.71	2.92	3.15	1.52	1.40	1.44
Fr [%]	6.1	10	9.8	9.1	6.9	7.6	11.1	17.5	13.6	3	2.4	2.8

c) Nampula roughness class $Z_{02}=0.100$ m

Height [m]	0°	30°	60°	90°	120°	150°	180°	210°	240°	270°	300°	330°
10	2.3	2.3	2.5	2.6	2.07	2.21	2.49	2.55	2.85	1.88	1.5	1.58
	1.71	2.09	2.01	2.00	1.74	1.89	2.10	2.26	2.39	1.32	1.22	1.26
25	2.9	2.9	3.1	3.2	2.55	2.73	3.07	3.15	3.52	2.32	1.85	1.95
	1.83	2.24	2.16	2.14	1.86	2.02	2.24	2.42	2.56	1.41	1.30	1.35
50	3.4	3.4	3.6	3.8	2.99	3.21	3.61	3.7	4.13	2.72	2.17	2.29
	2.0	2.5	2.4	2.4	2.1	2.2	2.5	2.7	2.8	1.6	1.4	1.5
100	4	4	4.3	4.5	3.57	3.83	4.31	4.42	4.93	3.24	2.59	2.73
	2.22	2.72	2.62	2.60	2.26	2.46	2.72	2.94	3.11	1.71	1.57	1.63
200	5	5	5.4	5.6	4.43	4.74	5.34	5.48	6.11	4.02	3.21	3.39
	2.12	2.60	2.50	2.49	2.16	2.35	2.60	2.81	2.97	1.63	1.50	1.56
Fr [%]	5.9	9.9	9.8	9.4	6.8	7.4	10.6	17.6	14.4	3.2	2.4	2.5

d) Nampula roughness class $Z_{03}=0.400$ m

Height [m]	0°	30°	60°	90°	120°	150°	180°	210°	240°	270°	300°	330°
10	1.9	1.9	2.0	2.1	1.7	1.8	2.0	2.1	2.3	1.8	1.2	1.2
	1.78	2.09	2.06	2.10	1.85	1.98	2.18	2.35	2.47	1.73	1.24	1.24
25	2.5	2.4	2.6	2.7	2.3	2.4	2.6	2.7	3.0	2.4	1.6	1.6
	1.89	2.22	2.19	2.23	1.96	2.10	2.31	2.49	2.63	1.84	1.31	1.31
50	3.0	3.0	3.1	3.3	2.8	2.8	3.2	3.3	3.6	2.9	2.0	2.0
	2.06	2.43	2.40	2.44	2.14	2.29	2.53	2.72	2.87	2.00	1.43	1.42
100	3.6	3.6	3.8	4.0	3.4	3.4	3.9	4.0	4.4	3.5	2.4	2.4
	2.32	2.74	2.70	2.75	2.41	2.58	2.85	3.07	3.23	2.26	1.60	1.60
200	4.5	4.5	4.7	5.0	4.2	4.3	4.8	4.9	5.4	4.4	3.0	3.0
	2.22	2.62	2.58	2.63	2.31	2.47	2.72	2.94	3.10	2.16	1.53	1.53
Fr [%]	5.5	9.4	9.9	9.4	7.1	7.4	10.2	16.8	14.8	4.5	2.5	2.5

Table E4.6: The sector-wise wind speed and Weibull-k parameter wind speed frequency distribution by roughness class and height at Pemba.

a) Pemba roughness class $Z_0=0.0002$ m

Height [m]	0°	30°	60°	90°	120°	150°	180°	210°	240°	270°	300°	330°
10	3.8	4.4	4.5	3.8	4.6	5.7	5.0	3.5	2.5	2.2	2.5	3.3
	2.24	2.41	2.48	2.27	2.40	2.63	2.43	2.02	1.64	1.51	1.68	1.99
25	4.1	4.8	4.9	4.1	5.0	6.2	5.5	3.7	2.7	2.4	2.7	3.6
	2.29	2.46	2.53	2.31	2.45	2.68	2.48	2.06	1.67	1.54	1.71	2.03
50	4.3	5.1	5.2	4.3	5.3	6.6	5.8	4.0	2.9	2.6	2.9	3.8
	2.31	2.47	2.55	2.33	2.47	2.70	2.50	2.08	1.69	1.55	1.72	2.04
100	4.6	5.4	5.4	4.5	5.6	6.9	6.1	4.2	3.0	2.7	3.0	4.0
	2.16	2.31	2.38	2.18	2.31	2.53	2.34	1.95	1.58	1.46	1.62	1.91
200	4.8	5.6	5.7	4.7	5.8	7.2	6.3	4.3	3.1	2.8	3.1	4.1
	1.92	2.06	2.13	1.94	2.06	2.25	2.08	1.74	1.41	1.30	1.44	1.71
Fr [%]	5.6	10	8.8	7.8	9.8	15.1	13.1	14	6.1	3.3	2.9	3.5

b) Pemba roughness class $Z_{01}=0.030$ m

Height [m]	0°	30°	60°	90°	120°	150°	180°	210°	240°	270°	300°	330°
10	2.5	3.0	3.2	2.7	3.1	3.9	3.6	2.5	1.9	1.7	1.7	2.2
	1.83	2.03	2.10	1.91	1.99	2.19	2.10	1.61	1.44	1.41	1.44	1.54
25	3.0	3.6	3.8	3.2	3.7	4.7	4.3	3.0	2.3	2.0	2.0	2.6
	1.97	2.20	2.26	2.06	2.14	2.36	2.27	1.74	1.55	1.52	1.55	1.67
50	3.5	4.2	4.4	3.7	4.2	5.4	5.0	3.5	2.7	2.3	2.4	3.0
	2.22	2.47	2.54	2.32	2.41	2.66	2.55	1.96	1.74	1.70	1.74	1.87
100	4.2	5.0	5.2	4.4	5.0	6.4	6.0	4.2	3.2	2.7	2.8	3.6
	2.36	2.63	2.71	2.47	2.57	2.83	2.71	2.08	1.85	1.81	1.85	1.99
200	5.2	6.2	6.4	5.5	6.3	8.0	7.4	5.2	4.0	3.4	3.5	4.4
	2.25	2.51	2.59	2.36	2.45	2.70	2.59	1.99	1.77	1.73	1.76	1.90
Fr [%]	5	9.4	9.1	7.8	9.2	14.4	13.3	14.2	7.6	3.8	3	3.3

c) Pemba roughness class $Z_{02}=0.100$ m

Height [m]	0°	30°	60°	90°	120°	150°	180°	210°	240°	270°	300°	330°
10	2.2	2.6	2.7	2.4	2.6	3.4	3.2	2.3	1.8	1.5	1.5	1.9
	1.85	1.94	2.08	1.91	1.92	2.23	2.19	1.66	1.48	1.48	1.56	1.56
25	2.7	3.2	3.4	2.9	3.2	4.2	4.0	2.8	2.2	1.9	1.9	2.3
	1.98	2.08	2.23	2.05	2.06	2.39	2.35	1.78	1.59	1.58	1.67	1.67
50	3.2	3.8	4.0	3.4	3.8	4.9	4.6	3.3	2.6	2.2	2.2	2.7
	2.19	2.31	2.47	2.27	2.28	2.65	2.60	1.97	1.76	1.75	1.85	1.84
100	3.8	4.5	4.7	4.1	4.5	5.8	5.5	4.0	3.1	2.6	2.7	3.2
	2.40	2.53	2.71	2.49	2.50	2.90	2.85	2.16	1.92	1.92	2.03	2.02
200	4.7	5.6	5.8	5.1	5.6	7.2	6.9	4.9	3.8	3.2	3.3	4.0
	2.30	2.42	2.58	2.38	2.38	2.78	2.72	2.06	1.84	1.83	1.94	1.93
Fr [%]	4.8	9	9.2	7.9	9.1	14	13.4	14	8.2	4.1	3	3.3

d) Pemba roughness class $Z_{03}=0.400$ m

Height [m]	0°	30°	60°	90°	120°	150°	180°	210°	240°	270°	300°	330°
10	1.7	2.0	2.1	1.9	2.0	2.6	2.5	1.8	1.4	1.2	1.2	1.5
	1.79	2.00	2.15	2.01	1.95	2.10	2.14	1.61	1.51	1.38	1.40	1.62
25	2.2	2.7	2.8	2.5	2.7	3.4	3.3	2.4	1.9	1.5	1.5	1.9
	1.90	2.13	2.29	2.13	2.07	2.23	2.28	1.71	1.60	1.46	1.48	1.72
50	2.7	3.3	3.4	3.1	3.2	4.1	4.0	2.9	2.3	1.8	1.8	2.3
	2.08	2.32	2.50	2.33	2.26	2.43	2.49	1.86	1.74	1.59	1.61	1.87
100	3.3	4.0	4.1	3.7	3.9	5.0	4.9	3.6	2.8	2.2	2.2	2.8
	2.34	2.62	2.81	2.62	2.54	2.74	2.80	2.10	1.96	1.79	1.81	2.11
200	4.1	4.9	5.2	4.6	4.9	6.2	6.0	4.4	3.5	2.8	2.8	3.5
	2.24	2.51	2.69	2.51	2.44	2.62	2.68	2.01	1.88	1.71	1.74	2.02
Fr [%]	4.6	8.5	9.3	8	8.9	13.4	13.6	13.7	9.2	4.4	3.1	3.3

Table E4.7: The sector-wise wind speed and Weibull-k parameter wind speed frequency distribution by roughness class and height at Lichinga.

a) Lichinga roughness class $Z_0=0.0002$ m

Height [m]	0°	30°	60°	90°	120°	150°	180°	210°	240°	270°	300°	330°
10	4.9	5.0	5.0	5.8	6.2	6.2	4.5	4.6	4.2	3.7	2.8	3.5
	2.21	2.37	2.58	3.12	3.13	3.15	2.35	2.57	2.27	1.81	1.47	1.62
25	5.3	5.4	5.5	6.3	6.7	6.7	4.8	4.9	4.6	4.1	3.1	3.8
	2.26	2.42	2.63	3.17	3.19	3.21	2.40	2.62	2.31	1.85	1.49	1.65
50	5.6	5.7	5.8	6.7	7.1	7.0	5.1	5.2	4.8	4.3	3.3	4.0
	2.28	2.44	2.65	3.20	3.21	3.23	2.42	2.64	2.33	1.86	1.51	1.67
100	5.9	6.0	6.1	7.0	7.5	7.4	5.4	5.5	5.1	4.5	3.4	4.2
	2.13	2.28	2.48	2.99	3.01	3.03	2.26	2.47	2.18	1.74	1.41	1.56
200	6.1	6.3	6.3	7.3	7.8	7.7	5.6	5.7	5.3	4.7	3.6	4.4
	1.90	2.04	2.21	2.67	2.68	2.69	2.02	2.21	1.94	1.56	1.26	1.40
Fr [%]	5.5	11.1	16.9	19.7	17.0	13.1	3.1	3.2	3.1	3.0	1.9	2.4

b) Lichinga roughness class $Z_{01}=0.030$ m

Height [m]	0°	30°	60°	90°	120°	150°	180°	210°	240°	270°	300°	330°
10	3.3	3.6	3.3	4.0	4.3	4.3	3.0	3.2	3.0	2.7	2.0	2.1
	1.78	2.04	2.06	2.60	2.59	2.69	1.90	2.17	2.01	1.57	1.26	1.31
25	3.9	4.3	4.0	4.8	5.1	5.1	3.6	3.8	3.6	3.2	2.4	2.5
	1.92	2.21	2.23	2.81	2.80	2.91	2.06	2.35	2.18	1.70	1.35	1.40
50	4.5	5.0	4.6	5.5	5.9	5.9	4.2	4.4	4.2	3.7	2.8	2.8
	2.16	2.48	2.51	3.15	3.15	3.27	2.31	2.64	2.45	1.91	1.52	1.58
100	5.4	5.9	5.5	6.5	7.0	7.0	5.0	5.2	5.0	4.4	3.3	3.4
	2.30	2.64	2.67	3.36	3.35	3.48	2.46	2.81	2.61	2.03	1.61	1.67
200	6.7	7.4	6.8	8.1	8.7	8.7	6.2	6.5	6.2	5.5	4.1	4.2
	2.20	2.52	2.55	3.21	3.20	3.32	2.35	2.68	2.49	1.94	1.54	1.60
Fr [%]	4.4	9.7	15.9	20.4	17.1	16.1	3.0	3.3	3.0	3.3	2.0	1.9

c) Lichinga roughness class $Z_{02}=0.100$ m

Height [m]	0°	30°	60°	90°	120°	150°	180°	210°	240°	270°	300°	330°
10	2.8	3.2	2.8	3.4	3.7	3.7	2.7	2.7	2.6	2.3	1.8	1.7
	1.72	2.05	1.97	2.59	2.61	2.68	1.85	2.08	1.98	1.57	1.23	1.42
25	3.4	3.9	3.5	4.2	4.6	4.6	3.4	3.4	3.2	2.9	2.2	2.1
	1.83	2.20	2.12	2.77	2.79	2.87	1.99	2.23	2.12	1.68	1.31	1.51
50	4.0	4.6	4.1	5.0	5.4	5.4	3.9	3.9	3.8	3.4	2.6	2.5
	2.03	2.43	2.35	3.07	3.10	3.18	2.20	2.47	2.35	1.86	1.45	1.67
100	4.8	5.5	4.9	5.9	6.4	6.4	4.7	4.7	4.5	4.0	3.1	3.0
	2.23	2.67	2.57	3.37	3.40	3.49	2.41	2.71	2.57	2.03	1.58	1.83
200	6.0	6.8	6.0	7.3	7.9	8.0	5.8	5.8	5.6	5.0	3.8	3.7
	2.13	2.55	2.46	3.22	3.24	3.33	2.31	2.59	2.46	1.94	1.51	1.75
Fr [%]	4.1	9.1	15.6	20.5	17.3	16.7	3.3	3.3	2.9	3.4	2.0	1.7

d) Lichinga roughness class $Z_{03}=0.400$ m

Height [m]	0°	30°	60°	90°	120°	150°	180°	210°	240°	270°	300°	330°
10	2.2	2.5	2.3	2.6	2.9	2.9	2.4	2.2	2.1	1.9	1.6	1.5
	1.72	2.05	2.03	2.52	2.56	2.67	2.14	2.13	2.08	1.72	1.58	1.65
25	2.8	3.3	3.0	3.5	3.8	3.8	3.2	2.8	2.8	2.5	2.2	2.0
	1.83	2.18	2.16	2.67	2.72	2.84	2.27	2.26	2.21	1.83	1.68	1.76
50	3.4	3.9	3.6	4.2	4.6	4.6	3.9	3.4	3.3	3.1	2.6	2.4
	1.99	2.38	2.36	2.92	2.97	3.10	2.48	2.47	2.42	1.99	1.83	1.92
100	4.2	4.8	4.4	5.1	5.6	5.6	4.7	4.2	4.0	3.7	3.2	2.9
	2.25	2.68	2.66	3.29	3.35	3.49	2.79	2.78	2.72	2.25	2.06	2.16
200	5.2	6.0	5.4	6.4	6.9	7.0	5.9	5.2	5.0	4.6	3.9	3.6
	2.15	2.57	2.54	3.15	3.21	3.35	2.67	2.66	2.61	2.15	1.97	2.06
Fr [%]	3.8	8.6	14.8	20.0	17.7	16.7	4.8	3.3	3.0	3.3	2.2	1.8